Studies on Transition Metal Complexes of Flexible Polydentate Schiff Base Ligands

Ph.D. Thesis

By

MRIGANKA DAS

DISCIPLINE OF CHEMISTRY

INDIAN INSTITUTE OF TECHNOLOGY INDORE

JULY 2017

Studies on Transition Metal Complexes of Flexible Polydentate Schiff Base Ligands

A THESIS

Submitted in partial fulfillment of the requirements for the award of the degree of

DOCTOR OF PHILOSOPHY

by

MRIGANKA DAS

DISCIPLINE OF CHEMISTRY

INDIAN INSTITUTE OF TECHNOLOGY INDORE

JULY 2017

INDIAN INSTITUTE OF TECHNOLOGY INDORE

CANDIDATE'S DECLARATION

I hereby certify that the work which is being presented in the thesis entitled **Studies on Transition Metal Complexes of Flexible Polydentate Schiff Base Ligands** in the partial fulfillment of the requirements for the award of the degree of **DOCTOR OF PHILOSOPHY** and submitted in the **Discipline of Chemistry, Indian Institute of Technology Indore**, is an authentic record of my own work carried out during the time period from **July 2012** to **July 2017** under the supervision of **Dr. Suman Mukhopadhyay**, Associate Professor, Discipline of Chemistry, Indian Institute of Technology Indore.

The matter presented in this thesis has not been submitted by me for the award of any other degree of this or any other institute.

Signature of the student with date
(MRIGANKA DAS)

This is to certify that the above statement made by the candidate is correct to the best of my/our knowledge.

Signature of Thesis Supervisor with date
(DR. SUMAN MUKHOPADHYAY)

MR. MRIGANKA DAS has successfully given his/her Ph.D. Oral Examination held on

Signature of Chairperson (OEB) Date:	Signature of External Examiner Date:	Signature(s) of Thesis Supervisor(s) Date:
Signature of PSPC Member #1 Date:	Signature of PSPC Member #2 Date:	Signature of Convener, DPGC Date:

Signature of Head of Discipline
Date:

ACKNOWLEDGEMENTS

It is my great pleasure to express my deep sense of gratitude to my PhD thesis supervisor, Dr. Suman Mukhopadhyay for his constant guidance, encouragement and help throughout the whole course of the thesis work. I am greatly indebted to him for his support, motivation and guidance. His vision and dedication in developing the thesis injected a remarkable impact on my academic career. His assurance and encouragement during the hard times when research plans did not work are gratefully acknowledged. I am thankful to my PSPC committee members, Dr. Anjan Chakraborty and Dr. Amod C. Umarikar for their valuable suggestions and guidance. I wish to express my gratitude to Prof. Pradeep Mathur, Director, IIT Indore for his continuous support in every aspect. I would like to thank IIT Indore and SIC, IIT Indore for providing financial support and instrumentation facility, respectively. I am thankful also to Ms. Indrani Choudhury, Dr. Biswarup Pathak, Dr. Sheikh. M. Mobin, Mr. Ritudhwaj Tiwari, Dr. Debasis Nayak, Dr. Rakesh Ganguly, Dr. Adilia Charmier, Dr. G. Udayabhanu and Mr. Amartya Biswas for their active support in various research projects. I would also like to thank all the faculty members of Discipline of Chemistry, IIT Indore for their guidance and help during the course of the thesis work. I personally extend my heartiest gratitude to Dr. Rajender Nasani and Dr. Manideepa Saha for their constant guidance, help and support at all the ups and downs in those initial days of the PhD programme. I convey my deep thanks to my dear group members, Ms. Poulami Mandal, Ms. Novina Malviya, Mr. Bidyut Kundu, Ms. Chanchal Sonkar, Ms. Rao Jyoti Sultania, Ms. Vaishali Chhabra and Dr. Komal Vyas for their selfless co-operation and help to make my work successful. I would also like to thank Ms. Sarita Batra, Mr. Kinny Pandey, Dr. Ravinder Kumar, Mr. Ghanshyam Bhavsar, Mr. Manish Kushwaha and Ms. Vinita Kothari for their technical support without which it would not be possible to continue my work. I would also like to thank Ms. Anjali Bandiwadekar, Mr. Rajesh Kumar, Mr. Lala Ram Ahirwar, Mr. Gati Krushna Nayak, Mr. Ranjit Raghuwanshi, Mr. Pallab Pradhan, Mr. Nitesh Singh Powar and other library staffs for their constant support, whenever

required. I would like to thank all my co-researchers at IIT Indore. I would like to acknowledge all the technical and non-technical staffs of IIT Indore for their assistance and service. It has been a wonderful experience to work with many friends during my Ph.D. who really helped me in many aspects. I would like to record my thanks to Dr. Anupam Das, Dr. Surajit Chatterjee, Mr. Arpan Bhattacharya, Mr. Arup Mahata, Mr. Sagar Bisaws, Mr. Sagnik Sengupta, Mr. Biju Majumder, Mr. Soumen Biswas, Debashis Majee, and many more in my friend circle.

Most importantly, it would have been almost impossible for me to reach here without the support, care and love of my family. I express my respect, love and gratitude to my beloved parents (Mr. Mrinal Kanti Das and Mrs. Banisree Das).

There are many more who have directly or indirectly contributed in making this journey successful. I wish I could thank them all but time and space compel me to stop here.

MRIGANKA DAS

IIT INDORE

Dedicated to
My Motherland

ABSTRACT

Utility of transition metal complexes in different sphere of life is one of the pertinent research field which has been extensively explored since the time of Werner who has put forward his theory to understand the structure and bonding for this class of compound. Inorganic chemists have also taken clue from the natural phenomena where transition metal complexes have been widely used in several biological processes, to understand the underlying principles of functionality, which eventually helps to develop different structural and more importantly improved functional model systems. The role of different ligand systems to bring out the necessary function has been gradually understood and different kind of ligand systems have been experimented to obtain better results. Schiff base ligands have shown remarkable advantages to stabilize the transition metal complexes which could be advantageous to generate a robust system with effective applications. With the time it has been perceived that metal complexes can be useful not only in biological processes but it can play crucial role in developing new materials and chemicals with diverse properties (Table 1).

Properties of transition metal Schiff base complexes important for their applicability

Biological	Chemical	Material
➢ **Biomacromolecule interaction study** • DNA binding and nuclease activity • Protein binding and protease activity ➢ **Cytotoxic activity** ➢ **Antimicrobial activity** ➢ **Antioxidant activity** ➢ **Anti-inflamatory activity *etc.***	➢ **Catalysis for organic transformations** ➢ **Enzyme catalysis** • Catecholase activity • Glycosidase activity ➢ **Dye degradation** ➢ **Chemical separation *etc.***	➢ **Electrochemical property** • Corrosion inhibition property ➢ **Gas absorption** ➢ **Sensing application** ➢ **Solar cell application** ➢ **Non-linear optics** ➢ **Fluorescent and electronic materials *etc.***

Table 1. *Various properties of transition metal Schiff base complexes.*

With the aim of development of improved Schiff-base ligands for effective application, introduction of flexibility of the ligands have been explored which paved the way of remarkable adaptability in the metal complex which can be utilized to tune it effectively as per desired properties. However, this type of

study has not been explored so far exhaustively and there are ample opportunities to look further into it for the better effectiveness of these kind of systems in terms of applicability. Although there are large scope of applications of metallo-Schiff base complexes which grasps wide and differentiated subjects containing immense territories of coordination chemistry, but this thesis mainly deals with the structure-activity relationship between flexibility of Schiff bases in metal complexes and certain special properties with an emphasis on

(i) DNA / Protein binding and cleavage property: which is a key research field to develop new therapeutic metallodrug.

(ii) Antiproliferative property: for damaging the cancer cell lines.

(iii) Antimicrobial activity: a new way to inhibit the growth of microorganisms like bacteria, fungi, *etc*.

(iv) Catecholase activity: where the polymerization of the oxidized product affords the formation of melanin, which protects damaged tissues against pathogens or insects.

(v) Glycosidase activity: Which catalyze the hydrolysis of glycosidic linkages to mimic the natural enzyme which is prevalent in carbohydrate metabolism.

(vi) Corrosion inhibition property: protects the damage of mild steel which is an essential constructing element in various industries.

With the above scenario the primary objective of the research work reported in this thesis is:-

- To explore the structure-activity relationship between several kinds of biological, chemical as well as material properties and various complex structures tuned by flexibility as well as flexibility controlled nuclearity.

However, to achieve this primary objective, this work has been subdivided into certain tasks as follows :-

- To design and synthesize Schiff bases incorporating flexible organic moiety.

- To tune the flexibility by coordinating the ligand with different type of metal ions and using different metal ion precursor.
- To take advantage of the co-ligands to generate polynuclear metal complexes and to control the nuclearity.

On the basis of the above objectives the contents of each chapter included in the thesis are discussed briefly as follows:

Chapter 1: General Introduction and Background

A brief overview of the basic concepts and recent scientific developments towards the generation of Schiff base metal complexes and the importance of introducing the flexibility towards potential applications in various biological, chemical and material applications are discussed in this chapter. Finally, a brief summary of the research reported in this thesis and the relevance in the prospects of recent developments have been put forward.

Chapter 2: Nickel(II) complexes with a flexible piperazinyl moiety: studies on DNA and protein binding and catecholase like properties

In this chapter, four new mononuclear Ni(II) complexes $[Ni(L^1)]ClO_4$ **(1)**, $[Ni(L^2)]ClO_4$ **(2)**, $[Ni(SCN)_3(CH_3OH)$(aminoethyl-piperazineH)] **(3)**, and $[Ni(DMSO)_4$(aminoethylpiperazineH)$](ClO_4)_3$ **(4)** have been synthesized from two Schiff base ligands [**HL^1** = 1-phenyl-3-((2-(piperidin-4-yl)ethyl)imino)but-1-en-1-ol and **HL^2** = 4-((2-(pipera-zin-1-yl)ethyl)imino)pent-2-en-2-ol] by exploiting the flexibility of the piperazinyl moiety. Structural analysis reveals that **1** and **2** are square planar complexes with piperazine rings in boat conformation whereas hydrolysis of Schiff bases (**HL^1** and **HL^2**) occurs during formation of octahedral complexes (**3** and **4**) with piperazine rings in chair conformation. Screening tests were conducted to quantify the binding ability of complexes towards DNA, BSA and HSA and it was found that square planar complexes (**1** and **2**) showed more effective binding properties over octahedral complexes as hydrolysis of Schiff bases during complexation restricts the delocalization of electrons to make these two complexes (**3** and **4**) inactive towards all kind of activity. Furthermore, enzyme kinetic studies reflect that

square planar complexes (**1** and **2**) are also effective in mimicking catecholase like activities over octahedral complexes. Among all the complexes, **1** was found to be the most promising molecule among the series due to its large binding affinity towards different biomacromolecules and higher turnover frequency in the catechol oxidation reaction.

Chapter 3: Copper complexes with flexible piperazinyl arm: nuclearity driven catecholase activity and interactions with biomolecules

In chapter 2 efforts were made to synthesize Schiff Base complex with chair conformation however in all such cases the Schiff Base ligand gets hydrolyzed to precursor amine. In this chapter it was aimed to check the flexibility of the ligand upon reaction with other metal center. Exploration of the reactivity with copper ion produced three new Cu(II) complexes *viz*., $[Cu(HL^1)(Pyridine)(H_2O)](ClO_4)_2.2MeOH$ **(5)**, $[Cu_2(HL^1)_2(NO_3)_2](NO_3)_2.3H_2O$ **(6)** and $[Cu(HL_2)(NO_3)_2].MeCN$ **(7)** have been synthesized from those two Schiff base ligands where the flexible piperazinyl moiety takes up chair conformation. Structural analysis reveals that **5** and **7** are monomeric Cu(II) complex consisting of penta- and hexacoordinated Cu(II) centers, respectively, whereas **6** is a dinuclear Cu(II) complex with two different geometrical Cu(II) centers, one is square planar and the other is distorted octahedral. Screening tests were conducted to quantify the binding ability of complexes (**5, 6** and **7**) towards DNA and BSA as well as the DNA cleavage activity have been explored of these complexes using gel electrophoresis technique. Furthermore, enzyme kinetic studies are also performed for those three complexes towards effectiveness in mimicking of catecholase like activities. Antibacterial activities of these complexes are also scrutinized towards Methicillin-Resistant *Staphylococcus aureus* (MRSA) bacteria. Finally, the nuclearity driven activity of complex **6** towards DNA binding and catechol oxidations are further explained by DFT.

Chapter 4: Nickel(II) and copper(II) complexes constructed with flexible Schiff base ligand: Synthesis, X-ray crystal structure, enzyme catalysis and biological applications

The flexibility of Schiff base ligands (**HL^1** and **HL^2**) upon variation of different metal ions was explored in above two chapters but with changing reaction conditions or with variation of auxiliary anion with same metal has not produced any pair of complexes where the ligand is in two different conformation. For this reason a modified Schiff base ligand **HL^3** [2-(phenyl((2-(piperazin-1-yl)ethyl)imino)methyl)phenol] has been introduced. Structural features and different applications of four newly synthesized metal complexes formed by the reaction of this ligand **HL^3** with Cu(II) and Ni(II) salts are discussed in two parts.

4A - Investigation on chemical protease, nuclease and catecholase activity of copper(II) complexes with flexidentate Schiff base ligands

This part mainly deals with two Cu(II) complexes $[Cu(HL^3)(MeOH)(Py)](ClO_4)_2$ **(8)** and $[Cu(HL^3)(DMF)](NO_3)_2$ **(9)**. Crystallographic study reveals that like last chapter, here also the piperazinyl arm remains in chair form making the ligand effectively tridentate in nature leaving enough coordination position available for binding of the substrate. Affinity of the synthesized complexes towards BSA protein and DNA were carried out through binding and cleaving experiment which have been followed by cell cytotoxicity measurement. Possible catecholase like activity was also investigated. Interestingly both the complexes have shown interesting protease, nuclease and catecholase activity.

4B - Counter anion directed flexibility of Ni(II) Schiff base complexes: Lysozyme binding and glycosidase activity

In this part of the thesis ligand **HL^3** was reacted with two different Ni(II) salts and finally structurally two different complexes $[Ni(L^3)(MeOH)]\ (ClO_4)_2$ **(10)** and $[Ni_2(HL^3)_2(H_2O)_2(MeOH)_2]Cl_3.3MeOH$ **(11)** were synthesized. Among these two, the piperazinyl arm is in boat conformation in Ni(II) complex **10** and in chair conformation in Ni(II) complex **11** which is a chloro-bridged dimeric

molecule. Probable reason behind this structural diversity by coordination mode of chloride ion is described here. Apart from a structural point of view, the lysozyme binding activities and glycosidase activities of these two complexes were also determined. The results confirm that nuclearity can play an important role in above mentioned activity.

Chapter 5: A novel approach of pseudohalide promoted enhanced corrosion inhibition by antimicrobial zinc(II) Schiff base complexes

This chapter describes the structure-activity relationship of corrosion inhibition property of Zn(II) Schiff base complexes which were prepared in a stepwise well planned synthetic approach. In this regard, two complexes ($[Zn(L^4)_2](ClO_4)_2$ **(12)** and $[Zn(\mu\text{-fumarate})(L^4)]_n$ **(13)** derived from two ligands $\mathbf{L^4}$ [N^1,N^1-dimethyl-N^2-(1-(pyridin-2-yl)ethylidene)ethane-1,2-diamine] and $\mathbf{L^5}$ [N^1,N^1-diethyl-N^2-(1-(pyridin-2-yl)ethylidene)ethane-1,2-diamine] were synthesized and their detail electrochemical analyses reveal that the compounds are inert towards any anti-corrosion property like their parent organic ligand. Thus enhancement of hetero-atom availability *via* incorporation of azide as a co-ligand for greater adsorption of the molecules on the mild steel was planned and successful implementation of this idea produces four new Zn(II) complexes $[ZnL^4(N_3)_2]$ **(14)**, $[ZnL^5(N_3)_2]$ **(15)**, $[ZnL^6(N_3)_2]$ **(16)** and $[ZnL^7(N_3)_2]$ **(17))** where, ligands $\mathbf{L^6}$ [2-morpholino-N-(1-(pyridin-2-yl)ethylidene)ethanamine] and $\mathbf{L^7}$ [(2-(piperidin-1-yl)-N-(1-(pyridin-2-yl)ethylidene)ethanamine)] contained flexible morpholinyl and piperadinyl moieties in their chair conformation. Electrochemical polarization and impedance studies indicate that all these four Zn(II) azido Schiff base complexes have significant corrosion inhibition property in 15% HCl medium on mild steel. FE-SEM (Field emission scanning electron microscopy) and AFM (Atomic force microscopy) images depicted that metal surface is protected by these four Zn(II) complexes. Apart from these, the antimicrobial activities of these complexes have been scrutinized. Considering all above facts, it can be concluded that this kind of pseudo halide promoted enhanced corrosion inhibition approach is one of the

fruitful strategies to develop corrosion resistance metal complexes which are worth for further investigation.

Chapter 6: Targeted synthesis of cadmium(II) Schiff base complexes towards corrosion inhibition on mild steel

Being inspired by the results of the last chapter, this chapter is focused on the enhancement of the corrosion inhibion efficiency *via* incorporation of some robust metal ion such as cadmium as it is widely used as an electroplating element in aircraft for corrosion protection of airframe components. Thus, the reaction of cadmium salts with three ligands $\mathbf{L^4}$, $\mathbf{L^6}$ and $\mathbf{L^7}$ gave five Cd(II) Schiff base complexes $[Cd(L^4)_2](ClO_4)_2$ **(18),** $[Cd(L^4)(cyanoacetate)(OAc)]$ **(19),** $[Cd_2(L^4)_2(N_3)_4]$ **(20),** $[Cd(L^6)(N_3)_2]_n$ **(21),** $[Cd_2(L^7)_2(N_3)_4]_n$ **(22).** The corrosion inhibition property of these complexes on mild steel upon treatment with 15% HCl has been examined where azide complexes have shown significant corrosion inhibition property as revealed by electrochemical impedance spectroscopy and potentiodynamic polarization. FE-SEM images show that the mild steel surface was protected by cadmium complexes. Among azido complexes, polymeric complexes have higher inhibition activity (up to 94%) due to the more availability of hetero atoms which was further explained using density functional theory. Thus finally, it can be concluded that increasing adsorbing sites by increasing nuclearity could be one of the key factors to develop corrosion resistance polymeric metal complexes which are worth for further investigation.

Chapter 7: General conclusions and future scope

This chapter summarizes the salient features of the work and its future prospects.

LIST OF PUBLICATIONS

[1]. **Das, M.**, Nasani, R., Saha, M.,Mobin, S. M., Mukhopadhyay, S. (2015), Nickel(II) complexes with a flexible piperazinyl moiety: studies on DNA and protein binding and catecholase like properties, Dalton Transactions, 44, 2299-2310.(DOI: 10.1039/C4DT02675F)

[2]. **Das, M.**, Mandal, P., Malviya, N., Choudhuri, I., Charmier, M. A. J., Morgado, S., Mobin, S. M., Pathak, B., Mukhopadhyay, S. (2016), Copper complexes with a flexible piperazinyl arm: nuclearity driven catecholase activity and interactions with biomolecules, Journal of Coordination Chemistry, 69, 3619-3637.(DOI: 10.1080/00958972.2016.1236193)

[3]. **Das, M.**, Biswas, A., Kundu, K. B., Mobin, S. M.**,** Udayabhanu, G., Mukhopadhyay, S. (2017), Targeted synthesis of cadmium(II) Schiff base complexes towards corrosion inhibition on mild steel, RSc Advances, 7, 48569-48585. (DOI: 10.1039/C7RA08633D)

[4]. **Das, M.**, Kundu, K. B., Tiwari, R., Mandal, P.*,* Nayek, D., Ganguly, R., Mukhopadhyay, S. (2018), Investigation on chemical protease, nuclease and catecholase activity of two copper complexes with flexidentate Schiff base ligands, Inorganica Chimica Acta, 469, 111-122.(DOI: 10.2016/j.ica.2017.09.013)

[5]. **Das, M.**, Biswas, A., Charmier, M. A. J., Ganguly, R., Udayabhanu, G., Mukhopadhyay, S. - A novel approach of pseudo-halide promoted enhanced corrosion inhibition by antimicrobial zinc(II) Schiff base complexes (Manuscript under preparation)

[6]. Saha, M., **Das, M.**, Nasani, R., Choudhuri, I., Yousufuddin, M., Nayek, H. P., Shaikh, M. M., Pathak, B., Mukhopadhyay, S. (2015), Targeted water soluble copper-tetrazolate complexes: interactions with biomolecules and catecholase like activities, Dalton Transactions, 44, 20154-20167.(DOI: 10.1039/C5DT01471A)

[7]. Saha, M., Nasani, R., **Das, M.**, Mahata, A., Pathak, B., Mobin, S. M., Carrella, L. M.,Rentschler, E., Mukhopadhyay, S. (2014), Limiting nuclearity in formation of polynuclear metal complexes through [2 + 3] cycloaddition:

synthesis and magnetic properties of tri- and pentanuclear metal complexes, Dalton Transactions, 43, 8083-8093.(DOI: 10.1039/C4DT00378K)

[8]. Saha, M., Nasani, R., **Das, M.**, Mobin, S. M., Pathak, B., Mukhopadhyay, S. (2014), The effect of remote substitution on the formation of preferential isomers of cobalt(III)-tetrazolate complexes by microwave assisted cycloaddition, Inorganic Chemistry Frontiers, 1, 599-610.(DOI: 10.1039/C4QI00089G)

[9]. Saha, M., Malviya, N., **Das, M.**, Choudhuri, I., Mobin, S. M., Pathak, B., Mukhopadhyay, S. (2017), Effect on catecholase activity and interaction with biomolecules of metal complexes containing differently tuned 5-substituted ancillary tetrazolato ligands, Polyhedron, 121, 155-171.(DOI: 10.1016/j.poly.2016.09.035)

[10]. Malviya, N., Mandal, P., **Das, M.**, Ganguly, R., Mukhopadhyay, S. (2017), Nickel tetrazolato complexes synthesized by microwave irradiation: Catecholase like activity and interaction with biomolecules, Journal of Coordination Chemistry, 70, 261-278.(DOI: 10.1080/00958972.2016.1260121)

[11]. Malviya, N., **Das, M.**, Mandal, P., Mukhopadhyay, S. (2017), A smart organic gel template as metal cation and inorganic anion sensor, Soft Matter, 13, 6243-6249.(DOI: 10.1039/C7SM01199G)

(*N. B. Publications 6-11 are not included in the thesis work*)

LIST OF CONFERENCES

1. Laboratory Health & Safety Workshop (Organized by IIT Indore in collaboration with RSC) on 4th April,2014
2. Frontier Lecture Series in Chemistry (FLSC-2014) (Organized by IIT Indore in collaboration with JNCASR) on 30th and 31st Jan,2014
3. Workshop on "Intellectual Property Rights" (Organized by B.M. College of Technology, Indore) on 22nd Sep, 2015
4. Symposium on "Advances in Chemistry with Biological and Industrial Relevance" (Organized by B.M. College of Technology, Indore) on Feb,2016

5. National Conference on Advances in Chemistry and their Biological and Industrial Relevance (ACBIR-2014) (Organized by NIT Rourkela, Odisha.) on 10th and 11th Jan,2014 (Poster Presented)
6. Sixth International Conference on Metals in Genetics, Chemical Biology and Therapeutics (ICMG 2016) (Organized by IISc, Bangalore) on 17-20 Feb, 2016**.** (Poster Presented)

TABLE OF CONTENTS

List of Nomenclature

α	Alpha
β	Beta
γ	Gama
T	Fluorescence Lifetime
Å	Angstrom
X	Chi
Λ	Wavelength
M	Micro
Π	Pi
nm	Nanometer
ns	Nanosecond
mM	Milli Molar
μM	Micro Molar
Ksv	Stern Volmer Quenching Constant
ε	Molar Extinction coefficient
cm	Centimeter
°	Degree
Knt	Kelvin
mL	Milliliter
μL	Microliter
a. u.	Arbitrary Unit
Λex	Excitation Wavelength
λem	Emission Wavelength
pH	The negative logarithm of hydronium-ion concentration
H	Eta (Efficiency)
K_a	Binding Constant

List of Acronyms

AFM	Atomic force microscopy
3,5-DTBC	3,5-di-tert-butylcatechol
3,5-DTBQ	3,5-di-tert-butylbenzoquinone
BSA	Bovine Serum Albumin
CAPS	N-cyclohexyl-3-aminopropanesulfonic acid
CCDC	Cambridge Crystallographic Data Centre
CD	Circular Dichroism
$CDCl_3$	Chloroform - *d*
CLSI	Clinical & Laboratory Standards Institute
CPE	Constant Phase Element
DAPI	4′,6-Diamidine-2′-phenylindole dihydrochloride
DFT	Density Functional Theory
DMEM	Dulbecco's Modified Eagle's Medium
DMF	Dimethylformamide
DMPC	1,2-dimyristoyl-sn-glycero-3-phosphocholine
DMSO-d_6	Dimethyl sulfoxide – d_6
DNA	Deoxyribonucleic acid
EB	Ethidium Bromide
EDX	Energy-dispersive X-ray
EIS	Electrochemical Impedence Spectroscopy
ESI-MS	Electron Spin Ionization Mass Spectroscopy
FE-SEM	Field-emission Scanning Electron Microscope
GOF	Goodness of Factor
HEWL	Hen Egg White Lysozyme
HOMO	Highest Occupied Molecular Orbital

HSA	Human Serum Albumin
IR	Infrared
LUMO	Lowest Unoccupied Molecular Orbital
Val	Valine
MBC	Minimum Bactericidal Concentration
MeOH	Methanol
MHB	Mueller-Hinton broth
MIC	Minimum Inhibitory Concentration
MRSA	Methicillin-Resistant *Staphylococcus aureus*
MHA	Mueller-Hinton agar
MTT	3-(4,5-dimethylthiazol-2-yl)-2,5-diphenyltetrazolium bromide
NMR	Nuclear Magnetic Resonance
OCP	Open Circuit Potential
PBS	Phosphate-buffered saline
PDB	Protein Data Bank
PI	Propidium Iodide
SCXRD	Single Crystal X-Ray Diffraction
SDD	Spin Density Difference
SDS-PAGE	Sodium dodecyl sulfate polyacrylamide gel electrophoresis
SOMO	Singly Occupied Molecular Orbital
TOF	Turn Over Frequency
TON	Turn Over Number
TRIS	Tris(Hydroxymethyl)aminomethane
UV	Ultra Violet

List of Figures

Chapter 1

Chapter 2

Chapter 3

Chapter 4

Chapter 4A

Chapter 4B

Chapter 5

Chapter 6

List of Schemes

Chapter 1

Chapter 2

Chapter 3

Chapter 4A

Chapter 4B

Chapter 5

Chapter 6

List of Tables

Chapter 2

Chapter 3

Chapter 4A

Chapter 4B

Chapter 5

Chapter 6

Chapter 1

General Introduction and Background

Chapter 1

General introduction and background

1.1 Introduction

In the development of coordination chemistry Schiff bases have an essential impact over the years. Schiff base metal complexes have been contemplated broadly due to their ability to stabilize metal complexes with their attractive chemical and physical properties and their extensive variety of utilizations in various scientific areas. These types of complexes have been overwhelmingly investigated in recent years, and such studies have been subject of many papers and reviews. Apart from other several factors, flexibility within the Schiff base entity sometimes provides the driving force towards various kind of interactions which provides an essential understanding tool to envisage the structure-activity relationship in catalytic as well as bio-macromolecular interaction pathway. It is hard to cover in this chapter the discussion on Schiff base metal complexes, which grasps wide and differentiated subjects, containing immense territories of coordination chemistry and different parts of bioinorganic and material science. Therefore, the introduction part is limited to a brief discussion on the Schiff bases along with their flexible nature, their metal complexes and general applications of Schiff base complexes with an emphasis on enzyme catalysis, bio-macromolecular interaction studies, antimicrobial activities, anti-proliferative properties and finally very few application related to the material chemistry.

1.2 Schiff base ligands

Hugo Schiff first reported Schiff base in 1864.[1] Schiff bases are an important class of ligands because of their synthetic flexibility, their selectivity, and sensitivity towards the central metal atom and structural similarities with natural biological substances. The preparations of these compounds are simple and smart. They are prepared by condensing a carbonyl compound with an amine,

generally in refluxing alcohol. Schiff base ligands are deliberated as 'privileged ligands'[2] containing azomethine group (-HC=N-). The azomethine group is particularly suited for binding to metal ions *via* nitrogen atom lone pair. When Schiff bases contain one or more donor atoms in addition to –C=N- group they act as polydentate chelating ligands or macrocycles. In fact, Schiff bases can balance out a wide range of metals in different oxidation states. Thus it can control the utilization of metal complexes in a large variety of useful catalytic reactions and different types of interactions. Several studies [3-5] showed that the presence of a lone pair of electrons in a sp^2 hybridized orbital of the nitrogen atom of the azomethine group is of considerable chemical and biological importance. The chelating ability of the Schiff bases combined with the ease of preparation and flexibility in varying the chemical environment about the C=N group makes it an interesting class of ligand in coordination chemistry. Examples of few compounds are shown in Scheme 1.1.

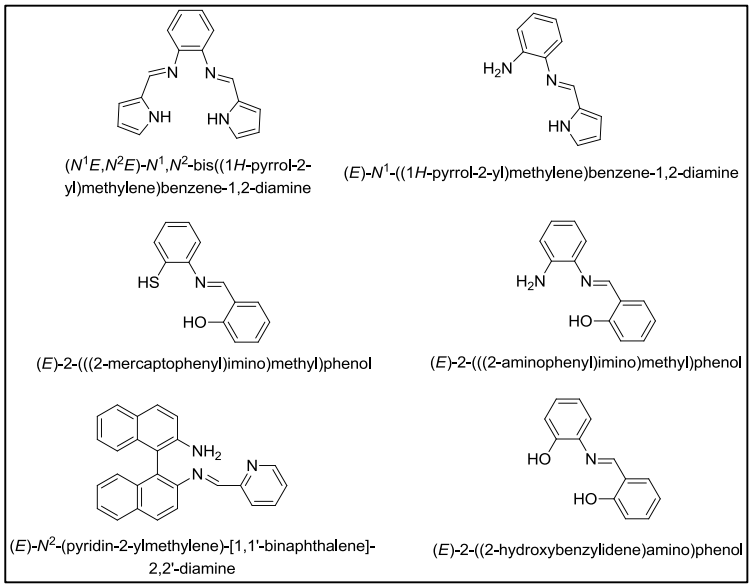

Scheme 1. 1. *Some examples of Schiff bases.*

Among the large variety of Schiff base moieties, salen type Schiff bases are very famous due to the easy synthetic route and higher stability. Although the term salen was formerly used only to define the tetradentate Schiff bases derived from salicylaldehyde and ethylenediamine, the term salen-type is presently utilized as a part of the writing to portray the class of (O, N, N, O) tetradentate bis-Schiff

ligands (Scheme. 1.2).[2] Stereogenic centers or other elements of chirality (planes, axes) can be introduced in the synthetic design of salen-type Schiff bases (Scheme. 1.2).[6, 7]

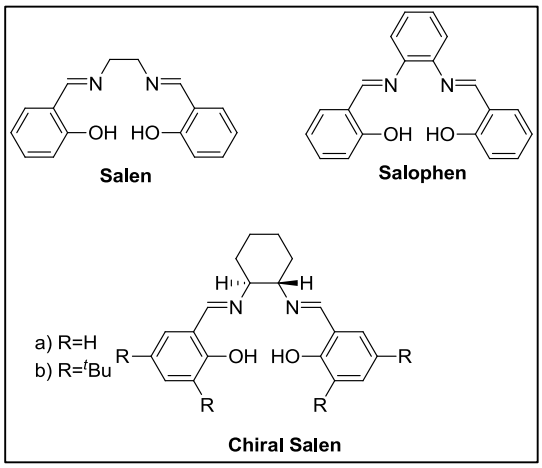

Scheme 1. 2. *Some examples of achiral and chiral Schiff bases.*

In addition to these, Schiff base macrocycles (Scheme 1.3) have been prepared by well- known self-condensation reaction of appropriate formyl- or keto- and primary amine precursors and find wide applications in macrocyclic and supramolecular chemistry.[8]

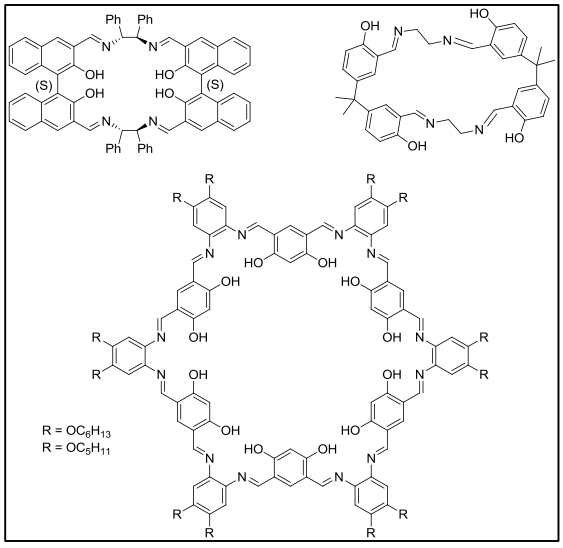

Scheme 1. 3. *Some examples of macrocyclic Schiff bases.*

1.2.1 Denticity, basicity and flexibiliy of Schiff bases

Schiff base ligands are classified according to the number of donor atoms contained and are known as uni-, di-, tri-, or quadridentate ligands. When two

or more donor sites of a ligand coordinate with the same central metal ion, a complex possessing a closed ring is formed. This special type of ring formation is known as chelation and the particular terminology "Chilate" was first introduced by Morgan and Drew in 1920. Schiff bases mainly possess nitrogen donor atoms, though many can act as bi-, tri-, tetra- or polydentate with mixed donor capabilities as shown in Scheme. 1.4.

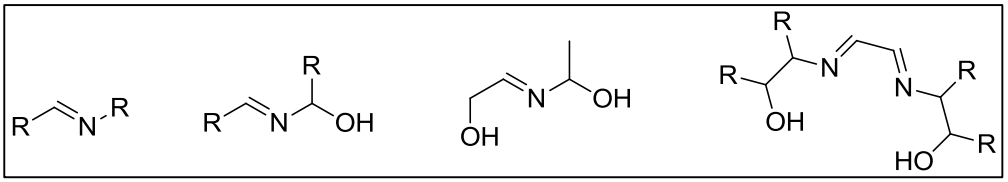

Scheme 1. 4. *Schiff bases of variying denticity.*

The basicity of the Schiff bases likewise assumes a key part in the development and stabilization of the complexes. Mainly the two donor atoms, N and O, of the chelated Schiff base possess two opposite electronic effects: phenolate oxygen is a hard donor which stabilizes the higher oxidation state of the metal ion, whereas the imine nitrogen is a boarderline donor and stabilizes the lower oxidation state of the metal ion.[9] Apart from this, sulfur donor ligands, being soft bases, want to consolidate with late transition element and with metal ions in lower oxidation state, the ONS donor Schiff bases can demonstrate beneficial interaction.[10] The presence of soft sulfur atoms softens the hardness of the oxygen atom, and this empowers such ligands to frame an expansive number of complexes with structural differences. The presence of –OH or –SH groups in the Schiff bases induce tautomerism in the compound, which leads to the formation of diverse complexes with different structural features. Also the deprotonation of thiolic, alcoholic and phenolic groups are favored due to the stabilization of various oxidation states of the central metal ion.

Ligand flexibility is one of the key factor to tune various structural beauty inside the metal-ligand framework. Specially, in case of Schiff bases, the flexibility is mainly characterized on the basis of few phenomena -

- Flexibility in denticity – Some Schiff bases possess different types of denticity *i.e.*, coordination behavior depends on few external conditions like pH, temperature, solvent effect etc.
- Flexibility in charge – Depending on above mentioned external effects few Schiff bases exerts different type of charges over the entire Schiff base moiety and this flexible phenomenon helps the entire moiety to coordinate with differently charged metal ions.
- Flexibility in geometry – On the basis of different types of coordination mode the geometry of Schiff bases get changed which indicates the ligand flexibility towards its geometry.

Although both the moieties (aldehyde/ketone or amine) can have interesting role to tune this type of flexibility in the Schiff base moiety but mainly the amine part plays crucial part in the design of such kind of flexible Schiff bases.[11] In this matter piperazine derived Schiff bases got a great attention in recent literature (Figure. 1.1 and Figure. 1.2.).[12] The structure of the metal complexes where the ligands bear the piperazine core, is primarily governed through the conformation adopted by the central piperazine ring.[13] Piperazine can adopt, along with the two extreme chair and boat conformations, the twisted-boat and the half-boat forms.[14] Past reports propose that the conformation adopted by the piperazine ring is influenced by metal ion size and presence of different co-ligands.[15-17] Different kinds of Schiff bases derived from morpholine, piperidine and other flexible amine moieties are also classified as a flexible Schiff base in the literature for their structural diversity.[18]

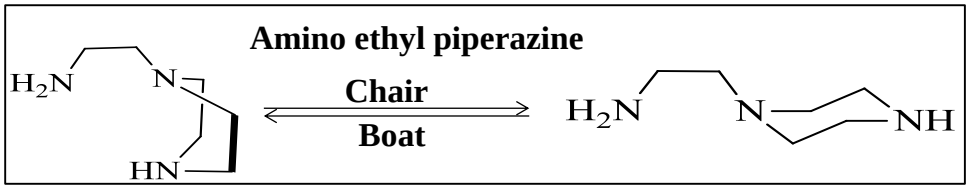

Figure 1. 1. *Chair-boat conformations of amino ethyl piperazine moiety.*

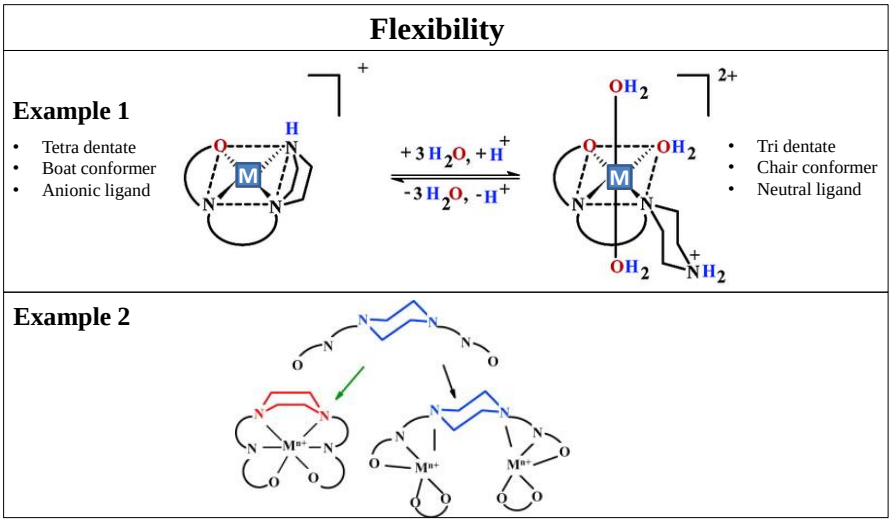

Figure 1. 2. *Pictorial representations of flexibility.*

1.3 Formation of Schiff base transition metal complexes

Reaction of metal salts with Schiff base ligands under suitable experimental conditions is the general procedure to prepare metal Schiff base complexes. Cozzi in his review has outlined five synthetic routes that are commonly employed for the preparation of Schiff base metal complexes and these are depicted in Scheme 1.5.[2]

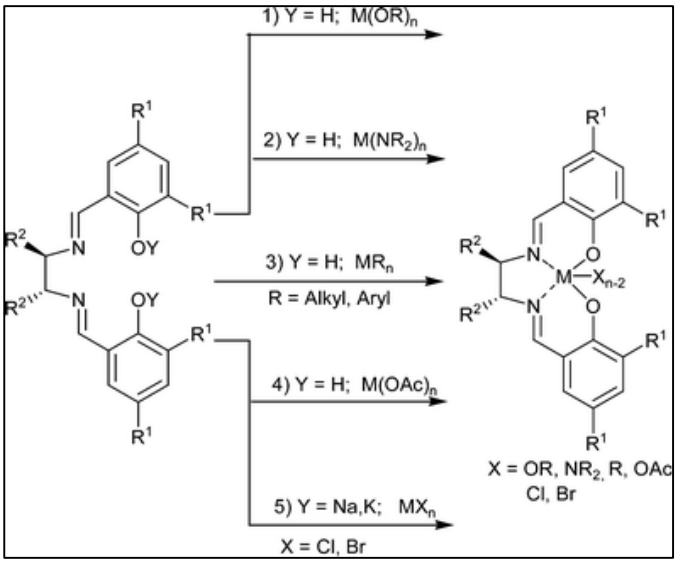

Scheme 1. 5. *Synthetic routes of metal Schiff base complexes*

The use of metal alkoxides ($M(OR)_n$) are involved in the synthetic Route 1. Alkoxides of early transition metals (M = Ti, Zr), are commercially available

and easy to handle whereas the other alkoxide derivatives specially the moisture sensitive derivatives of lanthanides are difficult to use. The reaction of a Schiff base with a metal alkoxide is an equilibrium reaction and the identity of the species generated is sometimes difficult to predict. Different complexes can be present in different concentrations, as a function of the equilibrium constant.

Metal amides $M(NMe_2)_4$ (M = Ti, Zr) are also used as precursors for the preparation of Schiff base metal complexes of early transition metals (Route 2). The reaction proceeds *via* the elimination of the acidic phenolic proton of the Schiff bases through the formation of volatile $NHMe_2$. The reaction of $Ti(NMe_2)_4$ or $Zr(NMe_2)_4$ with salen gives a Schiff base metal complex bearing two bisamido groups that can be reacted further.

The clean and effective way of using metal alkyl complexes as precursors (Route 3) is one of the key route for the formation of Schiff base metal complexes. Various metal alkyls in the main group of metals ($AlMe_3$, $GaMe_3$, $InMe_3$) are commercially available and can be used in the preparation of Schiff bases by a direct exchange reaction.

As indicated in route 4, many Schiff base metal complexes can be obtained through the treatment of the Schiff base with the corresponding metal acetate, normally by heating the Schiff base in the presence of the metal salt under reflux conditions. Copper, cobalt and nickel Schiff bases are prepared using the corresponding acetate $M(OAc)_2$ (M = Ni, Cu, Co).

The synthetic scheme presented in route 5 which is quite effective in obtaining salen-type metal complexes consists of a two-step reaction involving the deprotonation of the Schiff bases followed by reaction with metal halides.

A detailed discussion on synthesis and characterization of Schiff base metal complexes is not endeavored here, as there are various literature reviews on these viewpoints are already available.[19-21]

1.3.1 Transition metal complexes of flexible Schiff bases

Flexible ligands provide more potential for the formation of unique frameworks because of their freedom of conformation. The high flexibility and coordinating

properties make tridentate Schiff-base ligands very interesting and resourceful in terms of efficiency to modern coordination chemists.[22, 23] Although coordination chemistry of metal-Schiff base complexes is very old but the transition metal complexes of flexible Schiff base ligands with various coordination modes are relatively less studied.[24, 25] Among the library of transition metal complexes of flexible Schiff base ligands, there are relatively less examples on the topics of such flexible Schiff base metal complexes where the flexibility is tuned on the basis of stereochemistry of six membered ring.[11, 12, 17, 18, 26-29]

1.4 Applications of metal-Schiff base complexes

Versatility of Schiff base ligands and the biological, analytical and industrial applications of their complexes make further investigations in this area highly desirable. Among large varieties of applicable field for metal-Schiff base complexes, only a very few is in the main focus of interest in this thesis. Those particular applications along with other allied applications are categorized in the flow chart (Figure. 1.3.) followed by detailed explanation.

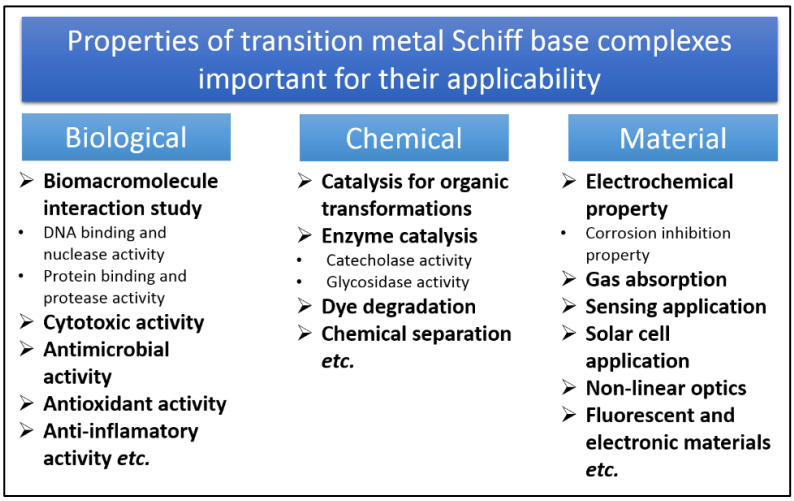

Figure 1. 3. *Applications of transition metal Schiff base complexes*

1.4.1 Biological properties

The improvement in the field of bioinorganic chemistry has expanded the enthusiasm for Schiff base complexes since it has been perceived that a significant number of these complexes may fill in as models for naturally

essential species. Although there are lots of biological significance of the transition metal Schiff base complexes, here only a few are discussed below which are relevant to this thesis work.

1.4.1.1 Biomacromolecular interaction study

Among library of biomacromolecules, only DNA and proteins are the basic focused target for this kind of interaction study.

1.4.1.1.1 Interactions with DNA

DNA is an important drug target and it regulates many biochemical processes that occur in the cellular system. There is a great interest in the literature for designing novel transition metal complexes capable of binding and cleaving duplex DNA with high sequence and structure selectivity.[30-34] Additionally, the metal ion type and different functional groups of ligands, which are responsible for the geometry of complexes can also affect the affinity of metal complexes to DNA. Moreover small Schiff base complexes of transition metals are of great interest for such kind of activities because of their assorted biological and pharmaceutical activities. The importance of certain compounds in medical diagnosis and genomic research is based on the ability of such compounds to bind and cleave double stranded DNA under physiological conditions. Studies on the interactions of DNA with transition metal complexes are very important for rational drug design and for the development of sensitive chemical probes for DNA.[35] These interactions would be either covalent or non-covalent. The labile part of the complexes get replaced by the nitrogen base of DNA in covalent interaction. On the other hand, the non-covalent DNA interactions include intercalative, electrostatic and groove binding of metal complexes along periphery of the DNA helix, the major and minor groove (Figure 1.4).

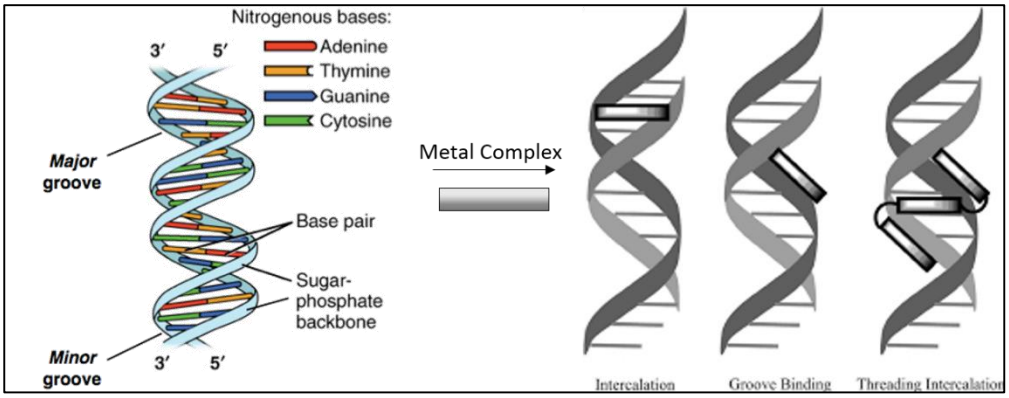

Figure 1. 4. *Various DNA binding modes of metal complexes*

The binding capacity of DNA is the primary source for making the comparison in cleavage effectiveness of the complexes to that of the control. DNA cleavage reactions involve mainly hydrolytic and oxidative cleavage pathways.[36] The formation of fragments may be deliberated to take place through enzymatic processes which occurs due to hydrolysis of phosphodiester. The oxidative cleavage of DNA is brought about by various methodologies and the methodology which involves irradiation with visible light of longer wavelength, has achieved significant importance for the major use in photodynamic therapy (PDT) of cancer.[37] The record of DNA cleavage by hydroxyl radicals abstraction of a hydrogen atom from sugar units and proposed general mechanism that anticipates the release of particular residues which emerge from change of sugars, which additionally relies on upon the position of hydrogen atom removal. Free radical scavengers inhibit the DNA cleavage reactions controlled by hydroxyl radical and peroxy derivative.[38, 39] Many small molecules exert their anti-cancer activities by binding with DNA, thereby altering DNA replication and inhibiting the growth of tumor cells.

Although there is a series transition metal Schiff base complexes showing promising DNA binding and cleavage property are reported in the literature [32, 40-42] but the comparison of this kind of activity on the basis of flexibility and nuclearity has not been explored so far. Thus this thesis is mainly focused on the flexible behavior of metal Schiff base complexes towards DNA binding and nuclease activity.

1.4.1.1.2 Interactions with proteins

Proteins are the most abundant and important component of every cell in the body from a functional point of view. From the hormones and enzymes that control digestion, the structure framing collagen in bones, the contractile proteins in muscles, to the hemoglobin and albumin in the circulatory system and immunoglobulins fighting infections, practically every life process depends on this class of molecules.

Albumin is the most abundant protein in the vertebrates' organisms (up to 40 mg/mL) and the most prominent plasma protein (about 60% of the total protein content of plasma). It is one of the first discovered and most intensely studied proteins.[43]

Another very important protein is lysozyme. Lysozyme is abundant in secretions including tears, saliva, human milk, and mucus. It is also present in cytoplasmic granules of the macrophages and the polymorph nuclear neutrophils (PMNs). Large amounts of lysozyme can be found in egg white.

The investigation of the binding amplitude and mechanism of interaction of small molecules with proteins is crucial for the understanding of drug pharmacodynamics and pharmacokinetics, as the nature and strength of that interaction have a great influence on drug absorption, distribution, metabolism, and excretion.[44] Apart from this, the cleavage of protein or protease mimic is important as the catalytic function of this enzyme hydrolyze proteins and liberate the amino acids needed by the body. Not only in digestion their use in medicine is also notable based on several clinical studies indicating their benefits in oncology, inflammatory conditions, blood rheology control, and immune regulation.

When approaching the evaluation of small molecules affinity for proteins, serum albumin (BSA and HSA) and lysozyme is usually selected as a relevant model due to its low cost and wide application.

Two main largely used serum albumins are human serum albumin and bovine serum albumin. Human serum albumin (HSA) is a major circulatory protein of well-known structure. Crystal structure analyses have revealed that

the drug binding sites are located in subdomains IIA and IIIA. A large hydrophobic cavity is present in the IIA subdomain. The geometry of the pocket in IIA is quite different from that found for IIIA. HSA has one tryptophan (Trp 214) in subdomain IIA, whereas BSA has two tryptophan moieties (Trp 135 and Trp 214), located in subdomains IA and IIA, respectively (figure 1.5).[45]

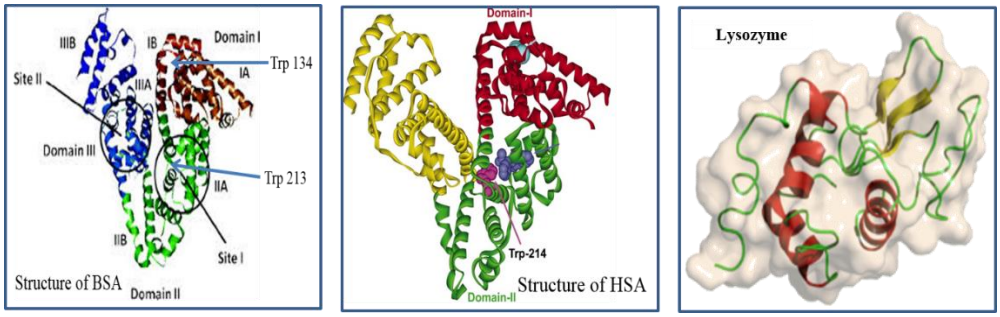

Figure 1. 5. *Structure of BSA, HSA and Lysozyme (left to right)*

The serum albumin interaction and binding ability of a large variety of mononuclear and polynuclear transition metal Schiff base complexes had been investigated.[46-49]

On the other hand, hen egg white lysozyme (HEWL), a glycoside hydrolase that breaks down the sugar linkages in the bacterial cell wall through its enzyme active cavity formed by Asp 52 and Glu 35 residues (Figure 1.8) [50] is a significant protein, which also has an affinity in binding towards small molecules including metal coordination complexes. For a few important metallodrugs, like NAMI-A, KP1019 *etc.*, which are in clinical trials, the HEWL had been used as a model system to investigate the drug–protein interactions as the scaffold of this protein is particularly suitable to probe the fundamental interactions of proteins with metal complexes. There are also few examples of transition metal complexes which have effective tendency to bind with lysozyme. [51-54]

In all the above cases, the interaction between protein and metal complexes often leads to a perturbation of the secondary structure of the protein, by disrupting the disulfide bonds and leading to a partial loss of α-helix conformation with the subsequent unfolding of the proteins, [55] or a change in the polarity of the environment to which the tryptophan residues are exposed [56], as a result of molecular interactions, such as excited-state reactions,

molecular rearrangements, energy transfer, ground-state complex formation or collision quenching.[57]

As ligand flexibility can tune the geometry as well as charge of the molecules thus evaluation of interaction study on the basis of flexibility is a prime interest of this thesis.

1.4.1.2 Anticancer activity

It has been reported that chelation is the cause and cure of many diseases including cancer. Cancer or malignant neoplasm is a class of diseases in which a group of cells display uncontrolled growth, invasion and even sometimes metastasis.[58] At present, the treatment for cancer basically includes surgery and chemotherapy, yet the impacts of the current chemotherapeutic medications are not good enough and they have abundant symptoms. The advancement of more successful medications for treating patients with tumor has been a primary endeavor over the past 50 years. In recent years, various Schiff bases derivatives have been found to be associated with anticancer properties.

Recent progress in the field of cell biology provide new targets for anticancer agent which act by the formation of DNA adducts with cancer cell and results in the inhibition of DNA replication.[59] The following figure 1.6 has shown the basic functions of cytotoxic metal complexes inside the cancer cells.

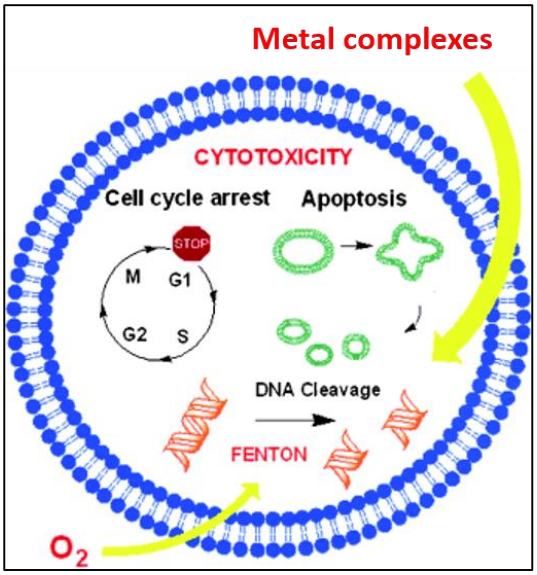

Figure 1. 6. *Mechanism of cytotoxic effects of metal complexes*

Sometimes metal complexes have shown cell selectivity thus it is a useful technique to arrest specific cancer cell. Although literature survey reveals that several Schiff base complexes of various metal ions have shown significant cytotoxic effects as promising anticancer drug [60-62] but still there are a large scope to tune this kind of activities by employing the flexibility. Thus this thesis mainly focused on cytotoxic effects of transition metal complexes derived from flexible Schiff bases.

1.4.1.3 Antimicrobial activity

An antimicrobial is an agent that kills microorganisms or inhibits their growth. Antimicrobial medicines can be grouped according to the microorganisms they act primarily against. For example, antibacterial agents are used against bacteria and antifungals agents are used against fungi. Early time, the serious irresistible infections caused by gram positive and gram negative pathogenic bacteria have expanded to danger level around the world. Anti-bacterial activity is the main part of investigation of this thesis work. The chemistry of biological science has produced a number of compounds that are now employed as antibacterial agents. Among them there are a plenty of transition metal Schiff base complexes which have potential antibacterial activity against different kind of bacteria like

Escherichia coli, *Staphylococcus aureus*, *Bacillus aureus* and *Aspergillus niger etc.*[63-66] Thus considering the all these facts, how the flexibility and nulearity tune this kind of activities is the prime interest of this thesis.

1.4.2 Chemical properties

Transition metal Schiff base complexes have several chemical properties which are useful for different applications. Frequently they have used in several organic transformation reactions as a catalyst.[67] They often used in dye degradation, chemical separation and sensing of toxic chemicals.

Enzyme catalysis is also one important useful application of transition metal Schiff base complexes.

1.4.2.1 Enzyme catalysis

An important goal in transition metal chemistry is the synthesis of molecules that exhibit catalytic activity analogous to the activity of enzymes. The driving force to demonstrate the enzyme active sites originates from their capability to give understanding to the mechanistic pathways of the native enzymes. It set up the part of that specific metal in the active site to configure better catalysts inspired by nature. In this regard, this thesis mainly concentrated on two enzyme catalysis applications - catecholase activity and glycosidase activity.

1.4.2.1.1 Catecholase activity

Nature uses several metalloenzymes to catalyze the controlled and selective oxidation of organic compounds. Among them an important enzyme is catecholase. Catecholase activity is the oxidation of a broad range of catechols to quinones through the four-electron reduction of molecular oxygen to water undertaken by catechol oxidase. Catechol is present in the vacuoles of cells of most of the plant tissues. Catechol oxidase is present in the cell cytoplasm. If the plant tissues are damaged, the catechol is released and the enzyme converts the catechol to ortho-quinone, which is a natural antiseptic.[68] Catecholase is a

dinuclear Cu^{II} containing enzyme with a type-3 active site which is responsible for catechol oxidation in higher plant which oxidises catechol to *o*-quinone. The crystal structure of the met form of the enzyme was determined in 1998. This revealed that the active site consists of a hydroxo bridged dicopper(II) centre in which each copper(II) centre is coordinated by three histidine nitrogen atoms and adopts an almost trigonal pyramidal environment with one nitrogen at the apical site.(Figure 1.7)[69]

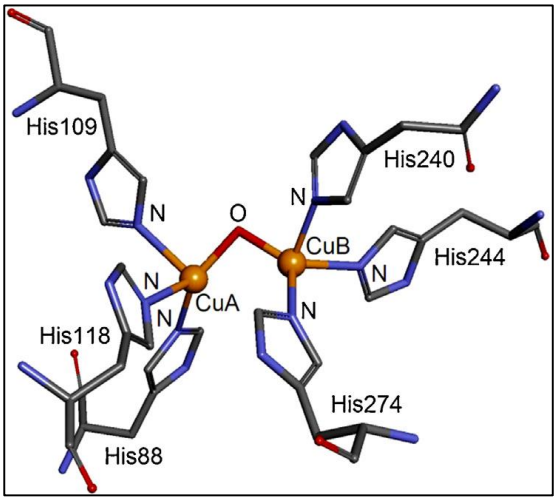

Figure 1. 7. *Coordination sphere of the dinuclear copper(II) centre of catechol oxidasefrom sweet potato in the met state (PDB ID: 1BT3).*

In general mainly two mechanistic pathways are established for catechol oxidation. Among them, the one which produces two molecules of o-quinone and water is followed by the enzyme catechol oxidase (Scheme 1.6 (mechanism B and C) and Scheme 1.7).

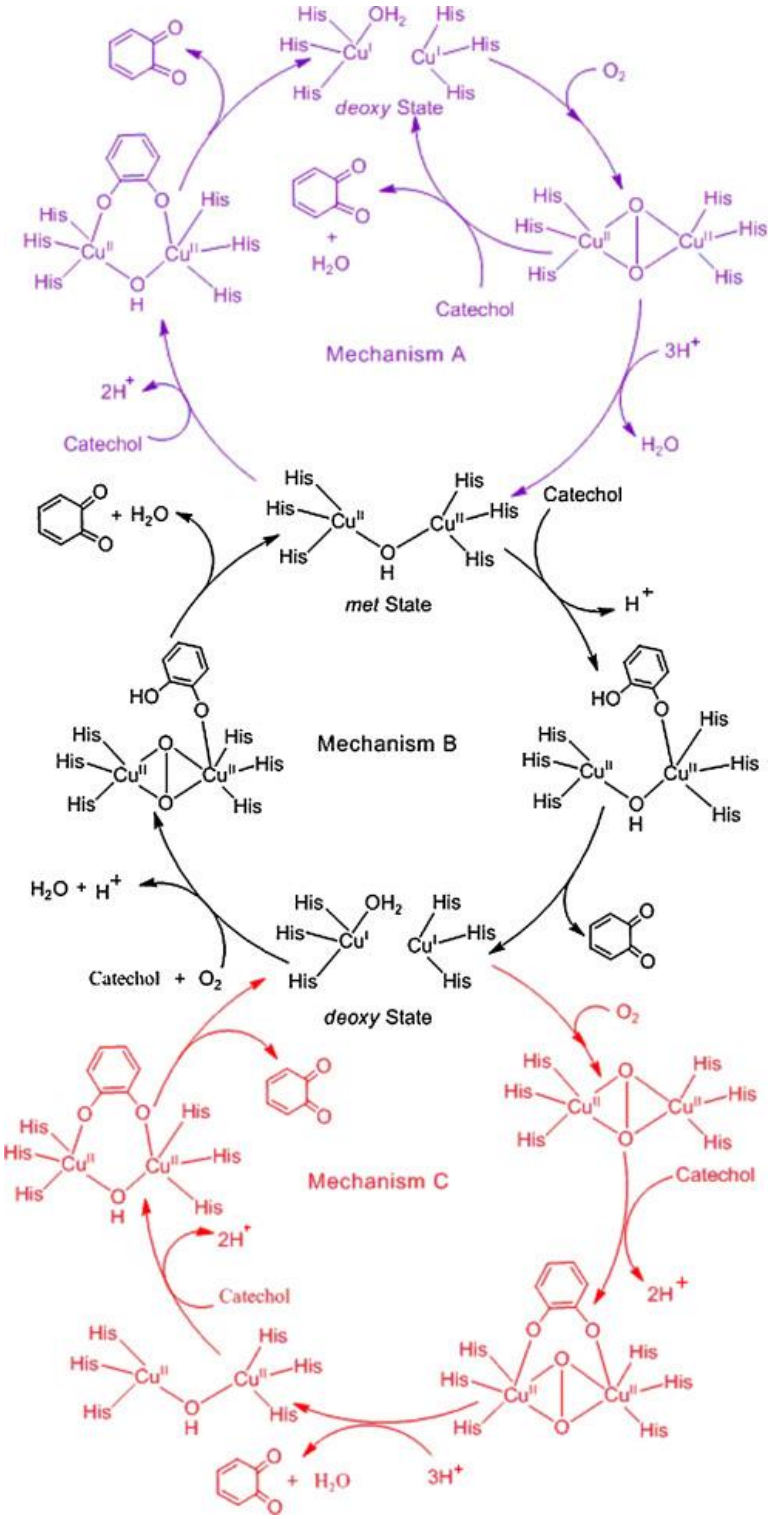

Scheme 1. 6. *Mechanistic pathways of catechol oxidase enzyme.[70]*

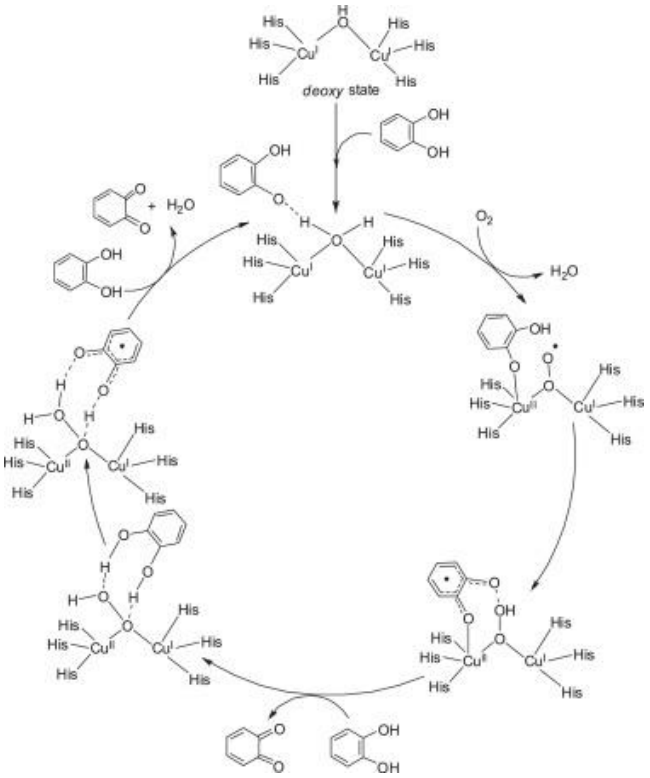

Scheme 1. 7. *Catalytic cycle of catechol oxidase as proposed by Siegbahn based on DFT calculation.[71]*

Henceforth the structure–activity relationship still gives scope for more up to date outlines to build structural and functional model systems with better activity near the enzyme for potential in industry. In literature four approaches have been used in the mechanistic studies on the model compounds for studying catecholase activity.

- Substrate-binding studies
- Structure-activity relationship
- Kinetic studies on catalytic reactions
- Stoichiometric oxidation of catechol substrates by the peroxo- and oxodicopper complexes

There are several copper, nickel, cobalt, zinc, manganese based Schiff base metal complexes which are already reported in literature and their mode of action towards enzyme catalysis is also mentioned. [72-79] Literature survey reveals that generally copper based model systems follow metal centered

pathway whereas Ni-Schiff base complexes follow ligand centered mechanism. Thus there is a scope of tuning the activity on the basis of flexibility. So this thesis mainly focused on the comparison of catecholase activity on the basis of flexibility among different transition metal complexes of flexible Schiff base ligands.

1.4.2.1.2 Glycosidase activity

Glycosidase or glycoside hydrolases are found in basically all domains of life. In prokaryotes, they are found both as intracellular and extracellular enzymes that are largely involved in nutrient acquisition. In higher organisms glycoside hydrolases are found within the endoplasmic reticulum and Golgi apparatus where they are involved in processing of N-linked glycoproteins, and in the lysosome. The structural and mechanistic details for these enzyme systems are available in the literature.[80, 81] Several artificial enzymes mimic the glycoside hydrolase to demonstrate the glycosyl transfer reactions observed in nature. Hence, these reactions are significantly important in the biological systems.[82] In these regard substantial research has been done to produce improved metal complexes as mimic of glycoside hydrolase.[83] Dinuclear metal complexes have been recognized at the active sites of many metalloenzymes [84] even in case of glycosidase also. Literature survey has reflected that there are an active part of both metal center in this hydrolysis mechanism (Scheme 1.8).[85]

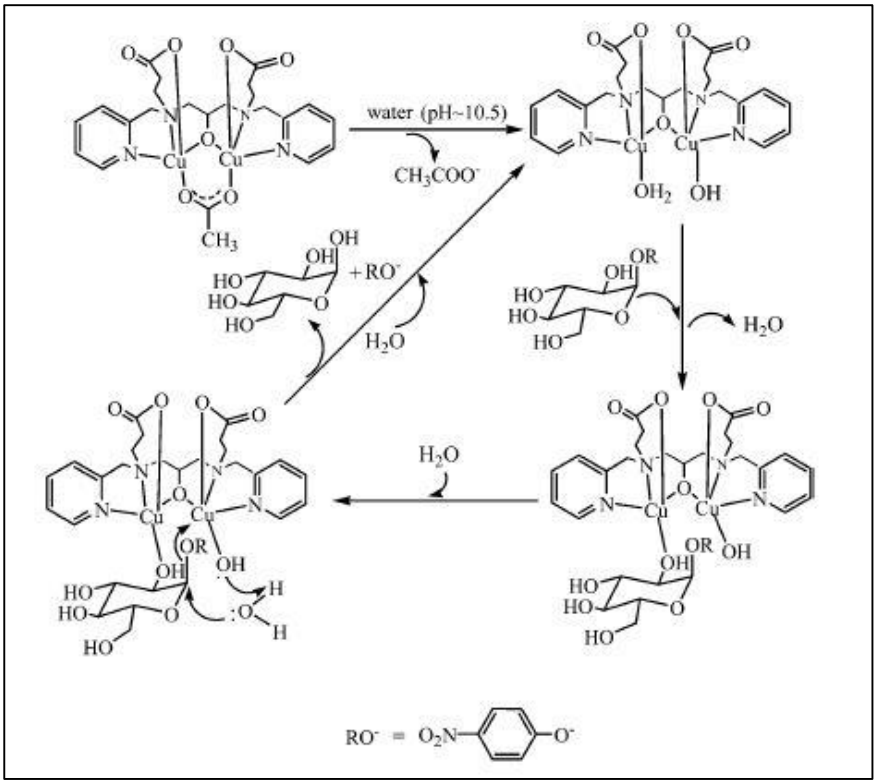

Scheme 1. 8. *Proposed mechanism for glycosidase activity of synthesized dinuclear copper complex.[85]*

As flexibile nature of Schiff base can tune the nuclearity also; thus the behavior of transition metal complexes of flexible Schiff base ligands is one of the prime interest of this thesis.

1.4.3 Material properties

Transition metal Schiff base complexes possess several materialistic properties like sensing of chemicals [86], gas absorption [87], non-linear optical property [88], photo-physical property [89], electrochemical property [90] and so on. These all properties are very useful in different industrial purpose. Among various kind properties this thesis is mainly focused on electrochemical behavior of transition metal Schiff base complexes for the application in the field of corrosion inhibition of mild steel.

1.4.3.1 Corrosion inhibition property

Corrosion can be defined as an irreversible chemical or electrochemical reaction of a material with the environment, which usually (but not always) results in a deterioration of the material and its properties. Mild steel is extensively used in many industries because of economically cost-effective and easy fabrication, but it is susceptible to undergo corrosion in aggressive environmental conditions. The damage due to corrosion is serious engineering problem and the national economies have suffered great losses due to corrosion.

Although corrosion is a complicated process but it can be easily comprehended as an electrochemical reaction involving the following three steps (Figure 1.8).[91]

1) Loss occurs from that part of the metal called the cathodic area because of the lower potential at this site. In this case iron is lost to the aggressive medium (oxidized from Fe^0 to Fe^{2+} state) and becomes oxidized to Fe^{2+} ion.
2) As a result of the formation of Fe^{2+}, two electrons are released to flow through the steel to the cathodic area.
3) Proton from acidic solution or oxygen in aquous solution moves to the cathode and completes the electric circuit by using the elctrons that flow to the cathode to form hydrogen gas or OH^- respectively at the surface of metal.

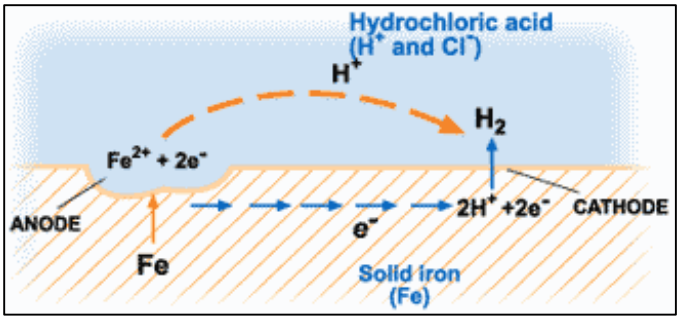

Figure 1. 8. *Reaction occurring during the corrosion of steel.*

Although sometime corrosion may happen even in inert atmosphere due to the presence of some bacteria. The overall processes in case of bacterial corrosion is depicted in Figure 1.9.

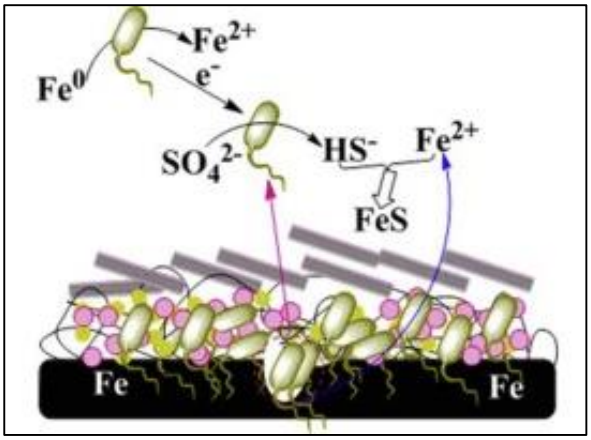

Figure 1. 9. *Corrosion in presence of bacteria*

Thus with this point of view control of corrosion is very important in in many technological processes. There are many ways for corrosion protection. Chemists usually gave more attention in corrosion inhibitor.

An inhibitor is a chemical substance or combination of substances which when added in very low concentrations in a corrosive environment effectively prevents or reduces corrosion without significant reaction with the components of the environment. Organic and inorganic both type of inhibitors are available in the literature. Role of inorganic inhibitors is mainly discussed in this thesis. In this scenario, Schiff bases are studied extensively due to the presence of >C=N– groups which allow the corresponding Schiff bases to get adsorbed on the surface of mild steel and to form a monolayer on the surface spontaneously. Therefore, it can act as an effective corrosion inhibitor [92, 93] for mild steel,[94-97] stainless steel,[98, 99] iron, nickel,[100] copper,[101] aluminum,[102] and alloy,[103] in various aggressive solutions. The Schiff base ligands form stable complexes closely packed in the coordination sphere of metal ion to generate another class of compounds for corrosion inhibition.[104-106] The inhibitors work on the metal surface through the adsorption mechanism. The interaction of inhibitor molecules with the metal surface is influenced by several factors, such as electron charge density, molecular size, geometry and number of hetero atoms, such as N, O, S present in the molecule.[107] With this point of view researchers have been focusing on metal coordination complexes to quantify their corrosion inhibition property.[90, 94,

108]. Thus corrosion inhibition effect of newly developed trasition metal Schiff base complexes as well as comparison of efficiencies on the basis of flexibility and nuclearity is a prime interest of this thesis.

1.5 Purpose and span of present investigation

The purpose of present work is to explore the structure-activity relationship between several kinds of above mentioned biological, chemical as well as material properties and various complex structures tuned by flexibility as well as flexibility controlled nuclearity.

In this regard the following flexible Schiff base ligands were slected in this study,

a) 1-phenyl-3-((2-(piperidin-4-yl)ethyl)imino)but-1-en-1-ol (**HL^1**)
b) 4-((2-(pipera-zin-1-yl)ethyl)imino)pent-2-en-2-ol (**HL^2**)
c) 2-(phenyl((2-(piperazin-1-yl)ethyl)imino)methyl)phenol (**HL^3**)
d) N^1,N^1-dimethyl-N^2-(1-(pyridin-2-yl)ethylidene)ethane-1,2-diamine (**L^4**)
e) N^1,N^1-diethyl-N^2-(1-(pyridin-2-yl)ethylidene)ethane-1,2-diamine (**L^5**)
f) 2-morpholino-N-(1-(pyridin-2-yl)ethylidene)ethanamine (**L^6**)
g) 2-(piperidin-1-yl)-N-(1-(pyridin-2-yl)ethylidene)ethanamine) (**L^7**)

Using these ligands total **twenty two** metal complexes of four metal ions (Ni^{2+}, Cu^{2+}, Zn^{2+}, and Cd^{2+}) were synthesized and characterized thoroughly using several analytical technique along with single crystal XRD.

Flexibility and nuclearity driven Biomacromolecular interaction study, cytotoxic activity and enzyme mimic activities of nickel and copper complexes (**1-11**) derived from different ligands (**HL^1/ HL^2/ HL^3**) are mainly discussed in **chapter 2** to **chapter 4**.

Use of pseudohalide (azide) as a coligand along with other ligands (**L^4/ L^5/ L^6/ L^7**) were explored to produce several zinc and cadmium complexes (**11-22**) as well as the flexibility and nuclearity controlled corrosion inhibition activity is discussed in **chapter 5** to **chapter 6**.

1.6 References

[1]. Schiff, H. (1864), Mittheilungen aus dem Universitätslaboratorium in Pisa: Eine neue Reihe organischer Basen, Justus Liebigs Annalen der Chemie, 131, 118-119.(DOI: 10.1002/jlac.18641310113)

[2]. Cozzi, P. G. (2004), Metal-Salen Schiff base complexes in catalysis: practical aspects, Chemical Society Reviews, 33, 410-421.(DOI: 10.1039/B307853C)

[3]. Patai, S., (1970), The Chemistry of Carbon Nitrogen Double Bond.Interscience Publishers Inc., New York.

[4]. De Clercq, B.,Verpoort, F. (2002), A new class of ruthenium complexes containing Schiff base ligands as promising catalysts for atom transfer radical polymerization and ring opening metathesis polymerization, Journal of Molecular Catalysis A: Chemical, 180, 67-76.(DOI: 10.1016/S1381-1169(01)00451-4)

[5]. Yamada, S. (1966), Recent aspects of the stereochemistry of schiff-base-metal complexes, Coordination Chemistry Reviews, 1, 415-437.(DOI: 10.1016/S0010-8545(00)80184-8)

[6]. Lopez, J.,Liang, S.,Bu, X. R. (1998), Unsymmetric chiral salen Schiff bases: A new chiral ligand pool from bis-schiff bases containing two different salicylaldehyde units, Tetrahedron Letters, 39, 4199-4202.(DOI: 10.1016/S0040-4039(98)00784-9)

[7]. Che, C.-M.,Huang, J.-S. (2003), Metal complexes of chiral binaphthyl Schiff-base ligands and their application in stereoselective organic transformations, Coordination Chemistry Reviews, 242, 97-113.(DOI: 10.1016/S0010-8545(03)00065-1)

[8]. Nelson, S. M. (1980), Developments in the synthesis and coordination chemistry of macrocyclic Schiff base ligands, Pure and Applied Chemistry, Vol. 52, p 2461.

[9]. Garnovskii, A. D.,Kharissov, B. I., (2003), Synthetic coordination and organometallic chemistry.CRC Press.

[10]. Ali, M. A. (1980), Magnetic and spectroscopic studies on nickel(II) and copper(II) complexes of some neutral tridentate ONS ligands, Canadian Journal of Chemistry, 58, 727-732.(DOI: 10.1139/v80-112)

[11]. Mukhopadhyay, S.,Mandal, D.,Ghosh, D.,Goldberg, I.,Chaudhury, M. (2003), Equilibrium Studies in Solution Involving Nickel(II) Complexes of Flexidentate Schiff Base Ligands: Isolation and Structural Characterization of the Planar Red and Octahedral Green Species Involved in the Equilibrium, Inorganic Chemistry, 42, 8439-8445.(DOI: 10.1021/ic0346174)

[12]. Keypour, H.,Rezaeivala, M.,Valencia, L.,Pérez-Lourido, P.,Khavasi, H. R. (2009), Synthesis and characterization of some new Co(II) and Cd(II) macroacyclic Schiff-base complexes containing piperazine moiety, Polyhedron, 28, 3755-3758.(DOI: 10.1016/j.poly.2009.08.021)

[13]. Costişor, O.,Pantenburg, I.,Tudose, R.,Meyer, G. (2004), New Copper(II) and Cobalt(II) Complexes with the N,N′-Bis(antipyryl-4-methyl)-piperazine (BAMP) Ligand: $Co_2(BAMP)Cl_4$ and $[Cu(BAMP)(H_2O)](ClO_4)_2$, Zeitschrift für anorganische und allgemeine Chemie, 630, 1645-1649.(DOI: 10.1002/zaac.200400239)

[14]. Boiocchi, M.,Bonizzoni, M.,Fabbrizzi, L.,Foti, F.,Licchelli, M.,Taglietti, A.,Zema, M. (2004), The influence of the boat-to-chair conversion on the demetallation of the nickel(II) complex of an open-chain tetramine containing a piperazine fragment, Dalton Transactions, 653-658.(DOI: 10.1039/B312980B)

[15]. Kubono, K.,Hirayama, N.,Kokusen, H.,Yokoi, K. (2003), Crystal Structure of {1,4-Bis[1-(3,5-dichlorophenolato-2-ylmethyl)-ylpropylamino-κ^2N,O]piperazine κ^2N,N'}cobalt(II), Analytical Sciences, 19, 645-646.(DOI: 10.2116/analsci.19.645)

[16]. Paital, A. R.,Mandal, D.,Huang, X.,Li, J.,Aromi, G.,Ray, D. (2009), Structure and dimensionality of coordination complexes correlated to piperazine conformation: from discrete $[Cu^{II}_2]$ and $[Cu^{II}_4]$ complexes to a $[\tau]1,3\text{-}N_3$-bridged $[Cu^{II}_2]_n$ chain, Dalton Transactions, 1352-1362.(DOI: 10.1039/B814681K)

[17]. Cretu, C.,Tudose, R.,Cseh, L.,Linert, W.,Halevas, E.,Hatzidimitriou, A.,Costisor, O.,Salifoglou, A. (2015), Schiff base coordination flexibility toward binary cobalt and ternary zinc complex assemblies. The case of the hexadentate ligand N,N′-bis[(2-hydroxybenzilideneamino)-propyl]-piperazine, Polyhedron, 85, 48-59.(DOI: 10.1016/j.poly.2014.08.035)

[18]. Laskar, I. R.,Maji, T. K.,Das, D.,Lu, T.-H.,Wong, W.-T.,Okamoto, K.-i.,Ray Chaudhuri, N. (2001), Syntheses, characterisation and solid state thermal studies of 1-(2-aminoethyl)piperidine (L), 1-(2-aminoethyl)pyrrolidine (L′) and 4-(2-aminoethyl)morpholine (L″) complexes of nickel(II): X-ray single crystal structure analyses of trans-$[NiL_2(CH_3CN)_2](ClO_4)_2$, trans-$[NiL_2(NCS)_2]$ and trans-$[NiL''_2(NCS)_2]$, Polyhedron, 20, 2073-2082.(DOI: 10.1016/S0277-5387(01)00803-8)

[19]. Kojima, M.,Taguchi, H.,Tsuchimoto, M.,Nakajima, K. (2003), Tetradentate Schiff base–oxovanadium(IV) complexes: structures and reactivities in the solid state, Coordination Chemistry Reviews, 237, 183-196.(DOI: 10.1016/S0010-8545(02)00227-8)

[20]. Costamagna, J.,Vargas, J.,Latorre, R.,Alvarado, A.,Mena, G. (1992), Coordination compounds of copper, nickel and iron with Schiff bases derived from hydroxynaphthaldehydes and salicylaldehydes, Coordination Chemistry Reviews, 119, 67-88.(DOI: 10.1016/0010-8545(92)80030-U)

[21]. Syamal, A.,Maurya, M. R. (1989), Coordination chemistry of schiff base complexes of molybdenum, Coordination Chemistry Reviews, 95, 183-238.(DOI: 10.1016/0010-8545(89)80026-8)

[22]. Hung, W.-C.,Lin, C.-C. (2009), Preparation, Characterization, and Catalytic Studies of Magnesium Complexes Supported by NNO-Tridentate Schiff-Base Ligands, Inorganic Chemistry, 48, 728-734.(DOI: 10.1021/ic801397t)

[23]. Fang, H.-C.,Yi, X.-Y.,Gu, Z.-G.,Zhao, G.,Wen, Q.-Y.,Zhu, J.-Q.,Xu, A.-W.,Cai, Y.-P. (2009), Construction of Low-Dimensional Cadmium Compounds with N_2O/N_2S Donor Tridentate Schiff Base Ligands, Crystal Growth & Design, 9, 3776-3788.(DOI: 10.1021/cg900515j)

[24]. Yang, X.,Lam, D.,Chan, C.,Stanley, J. M.,Jones, R. A.,Holliday, B. J.,Wong, W.-K. (2011), Construction of 1-D 4f and 3d-4f coordination polymers with flexible Schiff base ligands, Dalton Transactions, 40, 9795-9801.(DOI: 10.1039/C1DT11036E)

[25]. Sanmartín, J.,García-Deibe, Ana M.,Bermejo, Manuel R.,Novio, F.,Navarro, D.,Fondo, M. (2003), Mono- and Dinuclear Complexes of a Flexible Schiff Base Ligand − Crystal Structures of a Bishelicate and Two Acentric Monohelicates, European Journal of Inorganic Chemistry, 2003, 3905-3913.(DOI: 10.1002/ejic.200300248)

[26]. Karthick, C.,Gurumoorthy, P.,Musthafa, M. A. I.,Lakra, R.,Korrapati, P. S.,Rahiman, A. K. (2014), Dinuclear phenoxo-bridged "end-off" complexes containing a piperazine that shows chemical nuclease and cytotoxic activities, Journal of Coordination Chemistry, 67, 1794-1808.(DOI: 10.1080/00958972.2014.920501)

[27]. Kilic, A.,Tegin, I.,Tas, E.,Ziyadanogullan, R. (2011), Synthesis and characterization of an unsymmetric salicylaldimine ligand derived from 1-(2-Aminoethyl) piperazine and investigation of its analytical properties for the extraction and preconcentratoion of some divalent cations, Journal of the Iranian Chemical Society, 8, 68-77.(DOI: 10.1007/bf03246203)

[28]. Chakraborty, P.,Majumder, I.,Banu, K. S.,Ghosh, B.,Kara, H.,Zangrando, E.,Das, D. (2016), Mn(ii) complexes of different nuclearity: synthesis, characterization and catecholase-like activity, Dalton Transactions, 45, 742-752.(DOI: 10.1039/C5DT03659C)

[29]. Purkait, S.,Aullon, G.,Zangrando, E.,Chakraborty, P. (2017), Group 12 metal complexes of (2-piperazine-1-yl-ethyl)-pyridin-2-yl-methylene-amine: rare participation of terminal piperazine N in coordination leads to structural diversity, Dalton Transactions, 46, 2184-2195.(DOI: 10.1039/C6DT04578B)

[30]. Barone, G.,Terenzi, A.,Lauria, A.,Almerico, A. M.,Leal, J. M.,Busto, N.,García, B. (2013), DNA-binding of nickel(II), copper(II) and zinc(II) complexes: Structure–affinity relationships, Coordination Chemistry Reviews, 257, 2848-2862.(DOI: 10.1016/j.ccr.2013.02.023)

[31]. Krishnamoorthy, P.,Sathyadevi, P.,Cowley, A. H.,Butorac, R. R.,Dharmaraj, N. (2011), Evaluation of DNA binding, DNA cleavage, protein binding and in vitro cytotoxic activities of bivalent transition metal hydrazone complexes, European Journal of Medicinal Chemistry, 46, 3376-3387.(DOI: 10.1016/j.ejmech.2011.05.001)

[32]. Boerner, L. J. K.,Zaleski, J. M. (2005), Metal complex–DNA interactions: from transcription inhibition to photoactivated cleavage, Current Opinion in Chemical Biology, 9, 135-144.(DOI: 10.1016/j.cbpa.2005.02.010)

[33]. Alagesan, M.,Bhuvanesh, N. S. P.,Dharmaraj, N. (2013), Potentially cytotoxic new copper(ii) hydrazone complexes: synthesis, crystal structure and biological properties, Dalton transactions Cambridge England 2003, 42, 7210-23.(DOI: 10.1039/c3dt50371b)

[34]. Gupta, R. K.,Sharma, G.,Pandey, R.,Kumar, A.,Koch, B.,Li, P.-Z.,Xu, Q.,Pandey, D. S. (2013), DNA/protein binding, molecular docking, and in vitro anticancer activity of some thioether-dipyrrinato complexes, Inorganic chemistry, 52, 13984-96.(DOI: 10.1021/ic401662d)

[35]. Sigman, D. S.,Mazumder, A.,Perrin, D. M. (1993), Chemical nucleases, Chemical Reviews, 93, 2295-2316.(DOI: 10.1021/cr00022a011)

[36]. Liu, C.,Wang, M.,Zhang, T.,Sun, H. (2004), DNA hydrolysis promoted by di- and multi-nuclear metal complexes, Coordination Chemistry Reviews, 248, 147-168.(DOI: 10.1016/j.cct.2003.11.002)

[37]. Hussain, A.,Gadadhar, S.,Goswami, T. K.,Karande, A. a.,Chakravarty, A. R. (2012), Photo-induced DNA cleavage activity and remarkable photocytotoxicity of lanthanide(III) complexes of a polypyridyl ligand, Dalton transactions (Cambridge, England : 2003), 41, 885-95.(DOI: 10.1039/c1dt11400j)

[38]. Desbouis, D.,Troitsky, I. P.,Belousoff, M. J.,Spiccia, L.,Graham, B. (2012), Copper(II), zinc(II) and nickel(II) complexes as nuclease mimetics, Coordination Chemistry Reviews, 256, 897-937.(DOI: 10.1016/j.ccr.2011.12.005)

[39]. Li, X.-W.,Tao, L.,Li, Y.-T.,Wu, Z.-Y.,Yan, C.-W. (2012), Bimetallic complexes constructed from asymmetrical N,N′-bis(substituted)-oxamide: Cytotoxicities, and reactivities towards DNA and protein, European Journal of Medicinal Chemistry, 54, 697-708.(DOI: 10.1016/j.ejmech.2012.06.022)

[40]. Rajendiran, V.,Karthik, R.,Palaniandavar, M.,Stoeckli-Evans, H.,Periasamy, V. S.,Akbarsha, M. A.,Srinag, B. S.,Krishnamurthy, H. (2007), Mixed-ligand copper(II)-phenolate complexes: effect of coligand on enhanced DNA and protein binding, DNA cleavage, and anticancer activity, Inorganic chemistry, 46, 8208-21.(DOI: 10.1021/ic700755p)

[41]. Prasad, P.,Sasmal, P. K.,Khan, I.,Kondaiah, P.,Chakravarty, A. R. (2011), Schiff base oxovanadium(IV) complexes of phenanthroline bases showing DNA photocleavage activity at near-IR light and photocytotoxicity, Inorganica Chimica Acta, 372, 79-87.(DOI: 10.1016/j.ica.2011.01.086)

[42]. Shahabadi, N.,Kashanian, S.,Darabi, F. (2010), DNA binding and DNA cleavage studies of a water soluble cobalt(II) complex containing dinitrogen Schiff base ligand: The effect of metal on the mode of binding, European Journal of Medicinal Chemistry, 45, 4239-4245.(DOI: 10.1016/j.ejmech.2010.06.020)

[43]. Peters Jr, T., (1995), All about albumin: biochemistry, genetics, and medical applications.Academic press.

[44]. Liu, H.,Shi, X.,Xu, M.,Li, Z.,Huang, L.,Bai, D.,Zeng, Z. (2011), Transition metal complexes of 2, 6-di ((phenazonyl-4-imino) methyl)-4-methylphenol: Structure and biological evaluation, European Journal of Medicinal Chemistry, 46, 1638-1647.(DOI: 10.1016/j.ejmech.2011.02.012)

[45]. Sułkowska, A. (2002), Interaction of drugs with bovine and human serum albumin, Journal of Molecular Structure, 614, 227-232.(DOI: 10.1016/S0022-2860(02)00256-9)

[46]. Gharagozlou, M.,Boghaei, D. M. (2008), Interaction of water-soluble amino acid Schiff base complexes with bovine serum albumin: Fluorescence and circular dichroism studies, Spectrochimica Acta Part A: Molecular and Biomolecular Spectroscopy, 71, 1617-1622.(DOI: 10.1016/j.saa.2008.06.027)

[47]. Ray, A.,Koley Seth, B.,Pal, U.,Basu, S. (2012), Nickel(II)-Schiff base complex recognizing domain II of bovine and human serum albumin: Spectroscopic and docking studies, Spectrochimica Acta Part A: Molecular and Biomolecular Spectroscopy, 92, 164-174.(DOI: 10.1016/j.saa.2012.02.060)

[48]. Raja, D. S.,Bhuvanesh, N. S. P.,Natarajan, K. (2012), A novel water soluble ligand bridged cobalt(II) coordination polymer of 2-oxo-1,2-dihydroquinoline-3-carbaldehyde (isonicotinic) hydrazone: evaluation of the DNA binding, protein interaction, radical scavenging and anticancer activity, Dalton Transactions, 41, 4365-4377.(DOI: 10.1039/C2DT12274J)

[49]. Liu, H.,Li, L.,Guo, Q.,Dong, J.,Li, J. (2013), Synthesis, crystal structure, DNA- and albumin-binding properties of a chromium(III) complex with 1,10-phenanthroline and a Schiff base derived from glycine, Transition Metal Chemistry, 38, 441-448.(DOI: 10.1007/s11243-013-9709-5)

[50]. Procko, E.,Hedman, R.,Hamilton, K.,Seetharaman, J.,Fleishman, S. J.,Su, M.,Aramini, J.,Kornhaber, G.,Hunt, J. F.,Tong, L.,Montelione, G. T.,Baker, D. (2013), Computational Design of a Protein-Based Enzyme Inhibitor, Journal of Molecular Biology, 425, 3563-3575.(DOI: 10.1016/j.jmb.2013.06.035)

[51]. Razavet, M.,Artero, V.,Cavazza, C.,Oudart, Y.,Lebrun, C.,Fontecilla-Camps, J. C.,Fontecave, M. (2007), Tricarbonylmanganese(I)-lysozyme complex: a structurally characterized organometallic protein, Chemical Communications, 2805-2807.(DOI: 10.1039/B703887A)

[52]. Binkley, S. L.,Ziegler, C. J.,Herrick, R. S.,Rowlett, R. S. (2010), Specific derivatization of lysozyme in aqueous solution with $Re(CO)_3(H_2O)^{3+}$, Chemical Communications, 46, 1203-1205.(DOI: 10.1039/B923688K)

[53]. Casini, A.,Mastrobuoni, G.,Temperini, C.,Gabbiani, C.,Francese, S.,Moneti, G.,Supuran, C. T.,Scozzafava, A.,Messori, L. (2007), ESI mass spectrometry and X-ray diffraction studies of adducts between anticancer platinum drugs and hen egg white lysozyme, Chemical Communications, 156-158.(DOI: 10.1039/B611122J)

[54]. Santos-Silva, T.,Mukhopadhyay, A.,Seixas, J. D.,Bernardes, G. J. L.,Romão, C. C.,Romão, M. J. (2011), CORM-3 Reactivity toward Proteins:

The Crystal Structure of a Ru(II) Dicarbonyl−Lysozyme Complex, Journal of the American Chemical Society, 133, 1192-1195.(DOI: 10.1021/ja108820s)

[55]. Samari, F.,Hemmateenejad, B.,Shamsipur, M.,Rashidi, M.,Samouei, H. (2012), Affinity of Two Novel Five-Coordinated Anticancer Pt(II) Complexes to Human and Bovine Serum Albumins: A Spectroscopic Approach, Inorganic Chemistry, 51, 3454-3464.(DOI: 10.1021/ic202141g)

[56]. Ehteshami, M.,Rasoulzadeh, F.,Mahboob, S.,Rashidi, M.-R. (2013), Characterization of 6-mercaptopurine binding to bovine serum albumin and its displacement from the binding sites by quercetin and rutin, Journal of Luminescence, 135, 164-169.(DOI: 10.1016/j.jlumin.2012.10.044)

[57]. Lakowicz, J. R. (2000), On Spectral Relaxation in Proteins, Photochemistry and Photobiology, 72, 421-437.

[58]. Pizzo, P. A.,Poplack, D. G., (2015), Principles and practice of pediatric oncology.Lippincott Williams & Wilkins.

[59]. Jamieson, E. R.,Lippard, S. J. (1999), Structure, Recognition, and Processing of Cisplatin−DNA Adducts, Chemical Reviews, 99, 2467-2498.(DOI: 10.1021/cr980421n)

[60]. Abu-Dief, A. M.,Mohamed, I. M. A. (2015), A review on versatile applications of transition metal complexes incorporating Schiff bases, Beni-Suef University Journal of Basic and Applied Sciences, 4, 119-133.(DOI: 10.1016/j.bjbas.2015.05.004)

[61]. Bagihalli, G. B.,Avaji, P. G.,Patil, S. A.,Badami, P. S. (2008), Synthesis, spectral characterization, in vitro antibacterial, antifungal and cytotoxic activities of Co(II), Ni(II) and Cu(II) complexes with 1,2,4-triazole Schiff bases, European Journal of Medicinal Chemistry, 43, 2639-2649.(DOI: 10.1016/j.ejmech.2008.02.013)

[62]. Zhong, X.,Yi, J.,Sun, J.,Wei, H. L.,Liu, W. S.,Yu, K. B. (2006), Synthesis and crystal structure of some transition metal complexes with a novel bis-Schiff base ligand and their antitumor activities, European Journal of Medicinal Chemistry, 41, 1090-1092.(DOI: 10.1016/j.ejmech.2006.05.009)

[63]. Raman, N.,Kulandaisamy, A.,Thangaraja, C.,Jeyasubramanian, K. (2003), Redox and antimicrobial studies of transition metal(II) tetradentate Schiff base complexes, Transition Metal Chemistry, 28, 29-36.(DOI: 10.1023/a:1022544126607)

[64]. Chohan, Z. H.,Munawar, A.,Supuran, C. T. (2001), Transition Metal Ion Complexes of Schiff-bases. Synthesis, Characterization and Antibacterial Properties, Metal-Based Drugs, 8, 137-143.(DOI: 10.1155/mbd.2001.137)

[65]. Tümer, M.,Köksal, H.,Sener, M. K.,Serin, S. (1999), Antimicrobial activity studies of the binuclear metal complexes derived from tridentate Schiff base ligands, Transition Metal Chemistry, 24, 414-420.(DOI: 10.1023/a:1006973823926)

[66]. Jeewoth, T.,Li Kam Wah, H.,Bhowon, M. G.,Ghoorohoo, D.,Babooram, K. (2000), Synthesis and Anti-Bacterial/Catalytic Properties of Schiff Bases and Schiff Base Metal Complexes Derived from 2,3-Diaminopyridine, Synthesis and Reactivity in Inorganic and Metal-Organic Chemistry, 30, 1023-1038.(DOI: 10.1080/00945710009351817)

[67]. Gupta, K. C.,Sutar, A. K. (2008), Catalytic activities of Schiff base transition metal complexes, Coordination Chemistry Reviews, 252, 1420-1450.(DOI: 10.1016/j.ccr.2007.09.005)

[68]. Marbach, I.,Mayer, A. M. (1975), Changes in Catechol Oxidase and Permeability to Water in Seed Coats of *Pisum elatius*during Seed Development and Maturation, Plant Physiology, 56, 93-96.

[69]. Klabunde, T.,Eicken, C.,Sacchettini, J. C.,Krebs, B. (1998), Crystal structure of a plant catechol oxidase containing a dicopper center, Nat Struct Mol Biol, 5, 1084-1090.(DOI: 10.1038/4193)

[70]. Solomon, E. I.,Sundaram, U. M.,Machonkin, T. E. (1996), Multicopper Oxidases and Oxygenases, Chemical Reviews, 96, 2563-2606.(DOI: 10.1021/cr950046o)

[71]. Siegbahn, P. E. M. (2004), The catalytic cycle of catechol oxidase, Journal of Biological Inorganic Chemistry, 9, 577-590.(DOI: 10.1007/s00775-004-0551-2)

[72]. Comba, P.,Martin, B.,Muruganantham, A.,Straub, J. (2012), Structure, bonding, and catecholase mechanism of copper bispidine complexes, Inorganic Chemistry, 51, 9214-9225.(DOI: 10.1021/ic3004917)

[73]. Gupta, M.,Mathur, P.,Butcher, R. J. (2001), Synthesis, crystal structure, spectral studies, and catechol oxidase activity of trigonal bipyramidal Cu(II) complexes derived from a tetradentate diamide bisbenzimidazole ligand, Inorganic Chemistry, 40, 878-885.(DOI: 10.1021/ic000313v)

[74]. Majumder, S.,Sarkar, S.,Sasmal, S.,Sañudo, E. C.,Mohanta, S. (2011), Heterobridged dinuclear, tetranuclear, dinuclear-based 1-D, and heptanuclear-based 1-D complexes of copper(II) derived from a dinucleating ligand: Syntheses, structures, magnetochemistry, spectroscopy, and catecholase activity, Inorganic Chemistry, 50, 7540-7554.(DOI: 10.1021/ic200409d)

[75]. Mandal, S.,Mukherjee, J.,Lloret, F.,Mukherjee, R. (2012), Modeling tyrosinase and catecholase activity using new m-xylyl-based ligands with bidentate alkylamine terminal coordination, Inorganic Chemistry, 51, 13148-13161.(DOI: 10.1021/ic3013848)

[76]. Martínez, A.,Membrillo, I.,Ugalde-Saldívar, V. M.,Gasque, L. (2012), Dinuclear Copper Complexes with Imidazole Derivative Ligands: A Theoretical Study Related to Catechol Oxidase Activity, The Journal of Physical Chemistry B, 116, 8038-8044.(DOI: 10.1021/jp300444m)

[77]. Patra, A.,Giri, G. C.,Sen, T. K.,Carrella, L.,Mandal, S. K.,Bera, M. (2014), Bis(μ-alkoxo) bridged dinuclear CuII2 and ZnII2 complexes of an isoindol functionality based new ligand: Synthesis, structure, spectral characterization, magnetic properties and catechol oxidase activity, Polyhedron, 67, 495-504.(DOI: 10.1016/j.poly.2013.09.034)

[78]. Guha, A.,Banu, K. S.,Banerjee, A.,Ghosh, T.,Bhattacharya, S.,Zangrando, E.,Das, D. (2011), Bio-relevant manganese(II) compartmental ligand complexes: Syntheses, crystal structures and studies of catalytic activities, Journal of Molecular Catalysis A: Chemical, 338, 51-57.(DOI: 10.1016/j.molcata.2011.01.025)

[79]. Guha, A.,Banu, K. S.,Das, S.,Chattopadhyay, T.,Sanyal, R.,Zangrando, E.,Das, D. (2013), A series of mononuclear nickel(II) complexes of Schiff-base ligands having N,N,O- and N,N,N-donor sites: Syntheses, crystal structures, solid state thermal property and catecholase-like activity, Polyhedron, 52, 669-678.(DOI: 10.1016/j.poly.2012.07.088)

[80]. Henrissat, B.,Bairoch, A. (1996), Updating the sequence-based classification of glycosyl hydrolases, Biochemical Journal, 316, 695-696.(DOI:

[81]. Henrissat, B.,Davies, G. (1997), Structural and sequence-based classification of glycoside hydrolases, Current Opinion in Structural Biology, 7, 637-644.(DOI: 10.1016/S0959-440X(97)80072-3)

[82]. Bjerre, J.,Hauch Fenger, T.,Marinescu, L. G.,Bols, M. (2007), Synthesis of Some Trifluoromethylated Cyclodextrin Derivatives and Analysis of Their Properties as Artificial Glycosidases and Oxidases, European Journal of Organic Chemistry, 2007, 704-710.(DOI: 10.1002/ejoc.200600762)

[83]. Baty, J.,Sinnott, M. L. (2004), Efficient electrophilic catalysis of 1,5-anhydrocellobiitol hydrolysis by AlIII; implications for the conservation of "rosin-alum" sized paper, Chemical Communications, 866-867.(DOI: 10.1039/B316417A)

[84]. Lippard, S. J. (1993), Bioinorganic chemistry: a maturing frontier, Science, 261, 699-701.(DOI: 10.1126/science.8342037)

[85]. Haldar, S.,Patra, A.,Bera, M. (2014), Exploring the catalytic activity of new water soluble dinuclear copper(ii) complexes towards the glycoside hydrolysis, RSC Advances, 4, 62851-62861.(DOI: 10.1039/C4RA09800E)

[86]. Singh, L. P.,Bhatnagar, J. M. (2004), Copper(II) selective electrochemical sensor based on Schiff Base complexes, Talanta, 64, 313-319.(DOI: 10.1016/j.talanta.2004.02.020)

[87]. Park, S.,Mathur, V. K.,Planalp, R. P. (1998), Syntheses, solubilities and oxygen absorption properties of new cobalt(II) Schiff-base complexes, Polyhedron, 17, 325-330.(DOI: 10.1016/S0277-5387(97)00308-2)

[88]. Di Bella, S. (2001), Second-order nonlinear optical properties of transition metal complexes, Chemical Society Reviews, 30, 355-366.(DOI: 10.1039/B100820J)

[89]. Che, C.-M.,Kwok, C.-C.,Lai, S.-W.,Rausch, A. F.,Finkenzeller, W. J.,Zhu, N.,Yersin, H. (2010), Photophysical Properties and OLED Applications of Phosphorescent Platinum(II) Schiff Base Complexes, Chemistry – A European Journal, 16, 233-247.(DOI: 10.1002/chem.200902183)

[90]. Mahdavian, M.,Attar, M. M. (2009), Electrochemical behaviour of some transition metal acetylacetonate complexes as corrosion inhibitors for mild steel, Corrosion Science, 51, 409-414.(DOI: 10.1016/j.corsci.2008.11.010)

[91]. Dwivedi, D.,Lepkova, K.,Becker, T. (2017), Carbon steel corrosion: a review of key surface properties and characterization methods, RSC Advances, 7, 4580-4610.(DOI: 10.1039/C6RA25094G)

[92]. Gupta, N. K.,Quraishi, M. A.,Verma, C.,Mukherjee, A. K. (2016), Green Schiff's bases as corrosion inhibitors for mild steel in 1 M HCl solution: experimental and theoretical approach, RSC Advances, 6, 102076-102087.(DOI: 10.1039/C6RA22116E)

[93]. Ansari, K. R.,Quraishi, M. A.,Singh, A. (2014), Schiff's base of pyridyl substituted triazoles as new and effective corrosion inhibitors for mild steel in hydrochloric acid solution, Corrosion Science, 79, 5-15.(DOI: 10.1016/j.corsci.2013.10.009)

[94]. Keleş, H.,Emir, D. M.,Keleş, M. (2015), A comparative study of the corrosion inhibition of low carbon steel in HCl solution by an imine compound and its cobalt complex, Corrosion Science, 101, 19-31.(DOI: 10.1016/j.corsci.2015.07.013)

[95]. Singh, P.,Singh, D. P.,Tiwari, K.,Mishra, M.,Singh, A. K.,Singh, V. P. (2015), Synthesis, structural investigations and corrosion inhibition studies on Mn(II), Co(II), Ni(II), Cu(II) and Zn(II) complexes with 2-amino-benzoic acid (phenyl-pyridin-2-yl-methylene)-hydrazide, RSC Adv., 5, 45217-45230.(DOI: 10.1039/c4ra11929k)

[96]. Ashassi-Sorkhabi, H.,Shaabani, B.,Seifzadeh, D. (2005), Corrosion inhibition of mild steel by some schiff base compounds in hydrochloric acid, Applied Surface Science, 239, 154-164.(DOI: 10.1016/j.apsusc.2004.05.143)

[97]. Singh, P.,Singh, A. K.,Singh, V. P. (2013), Synthesis, structural and corrosion inhibition properties of some transition metal(II) complexes with o-hydroxyacetophenone-2-thiophenoyl hydrazone, Polyhedron, 65, 73-81.(DOI: 10.1016/j.poly.2013.08.008)

[98]. Hosseini, S. M. A.,Azimi, A.,Sheikhshoaei, I.,Salari, M. (2010), Corrosion Inhibition of 302 Stainless Steel with Schiff Base Compounds, J. Iran. Chem. Soc., 7, 799-806.(DOI: 10.1007/BF03246071)

[99]. Shabani-Nooshabadi, M.,Ghandchi, M. S. (2015), Santolina chamaecyparissus extract as a natural source inhibitor for 304 stainless steel corrosion in 3.5% NaCl, Journal of Industrial and Engineering Chemistry, 31, 231-237.(DOI: 10.1016/j.jiec.2015.06.028)

[100]. BİlgİÇ, S.,Çaliskan, N. (2001), An investigation of some Schiff bases as corrosion inhibitors for austenitic chromium–nickel steel in H_2SO_4, Journal of Applied Electrochemistry, 31, 79-83.(DOI: 10.1023/a:1004182329826)

[101]. Ehteshamzade, M.,Shahrabi, T.,Hosseini, M. G. (2006), Inhibition of copper corrosion by self-assembled films of new Schiff bases and their modification with alkanethiols in aqueous medium, Applied Surface Science, 252, 2949-2959.(DOI: 10.1016/j.apsusc.2005.05.003)

[102]. Şafak, S.,Duran, B.,Yurt, A.,Türkoğlu, G. (2012), Schiff bases as corrosion inhibitor for aluminium in HCl solution, Corrosion Science, 54, 251-259.(DOI: 10.1016/j.corsci.2011.09.026)

[103]. Thirugnanaselvi, S.,Kuttirani, S.,Emelda, A. R. (2014), Effect of Schiff base as corrosion inhibitor on AZ31 magnesium alloy in hydrochloric acid solution, Transactions of Nonferrous Metals Society of China, 24, 1969-1977.(DOI: 10.1016/S1003-6326(14)63278-7)

[104]. Mishra, M.,Tiwari, K.,Singh, A. K.,Singh, V. P. (2015), Versatile coordination behaviour of a multi-dentate Schiff base with manganese(II),

copper(II) and zinc(II) ions and their corrosion inhibition study, Inorganica Chimica Acta, 425, 36-45.(DOI: 10.1016/j.ica.2014.10.026)

[105]. Soliman, S. A.,Metwally, M. S.,Selim, S. R.,Bedair, M. A.,Abbas, M. A. (2014), Corrosion inhibition and adsorption behavior of new Schiff base surfactant on steel in acidic environment: Experimental and theoretical studies, Journal of Industrial and Engineering Chemistry, 20, 4311-4320.(DOI: 10.1016/j.jiec.2014.01.038)

[106]. Ansari, K. R.,Quraishi, M. A. (2014), Bis-Schiff bases of isatin as new and environmentally benign corrosion inhibitor for mild steel, Journal of Industrial and Engineering Chemistry, 20, 2819-2829.(DOI: 10.1016/j.jiec.2013.11.014)

[107]. Aytaç, A.,Özmen, Ü.,Kabasakaloğlu, M. (2005), Investigation of some Schiff bases as acidic corrosion of alloy AA3102, Materials Chemistry and Physics, 89, 176-181.(DOI: 10.1016/j.matchemphys.2004.09.003)

[108]. Mahdavian, M.,Naderi, R. (2011), Corrosion inhibition of mild steel in sodium chloride solution by some zinc complexes, Corrosion Science, 53, 1194-1200.(DOI: 10.1016/j.corsci.2010.12.013)

Chapter 2

Nickel(II) complexes with flexible piperazinyl moiety : studies on DNA and protein binding and catecholase like properties

Chapter 2

Nickel(II) complexes with flexible piperazinyl moiety : studies on DNA and protein binding and catecholase like properties

2.1 Introduction

Use of transition metals by nature in different biological processes drive the quest of the scientists to understand the underlying principles of its functionality which eventually helps to develop different structural and more importantly functional model systems.[1-6] Apart from studying different biological processes induced by metal ions many new molecules have been also developed over the years showing interesting properties like antibacterial, antifungal, antimicrobial and anticancer/antiproliferative activity where the transition metal ion performs a pivotal role in terms of structural organization and overall functionality. Furthermore, interactions of small metal complexes with DNA and proteins are the key research areas of current years as there are enough potentials of development of new therapeutic agent particularly showing antitumor properties and possibility of the transportation of these molecules throughout the physiological system *via* protein binding.[7-10] Among the various transition metal ions nickel has already shown promising activities in many of the above mentioned areas. Though many transition metal complexes so far have been tried and screened as a potential pharmaceutics, nickel complexes in medicinal biochemistry is comparatively rare. However, there are few reports where nickel complexes have been screened for DNA binding along with DNA adduct formation, oxidative damage of DNA and DNA-DNA crosslink formation revealing the antitumor activity.[11-15] The amazing binding properties of serum albumin towards different endogenous and exogenous compounds provide the vital ability for this group of plasma protein

to take an active role for possible drug delivery. Study of interaction of small molecules with different types of serum albumin is also crucial for the understanding of metallopharmaceutical pharmacokinetics and structure-activity relationship. However, the nature of interaction between proteins and different nickel complexes which have been studied so far is limited in nature and requires more studies for generalization. [16-19]

On the other hand di-nuclear nickel (II) centers have been also studied for the possible catechol oxidase like properties.[20-23] Most of the researchers have focused on di-nuclear nickel systems so far to match the original enzyme structurally where a dimeric copper active center exists. The use of flexible ligands in metal complexes has a great benefit to tune the overall charge, coordination mode and geometry as per expectation. More over the flexibility of the ligands imparts adaptability in the metal complex to tune it as per desired properties. So it was planned to investigate several application of nickel complexes on the basis of flexibility although there are only few reports where mononuclear nickel complexes have been studied for possible catecholase like activities.[24, 25] Furthermore investigation on the effect of overall charge I the metal complex could be found interesting as there are certain reports where extra positive charge on ligand can induce higher activity towards catechol oxidation.[24, 25]

Herein, the synthesis and characterization of four new mononuclear nickel complexes$[Ni(L^1)]ClO_4$ **(1)** [**HL^1** = 1-Phenyl-3-(2-piperazin-1-yl-ethylimino)-but-1-en-1-ol], $[Ni(L^2)]ClO_4$ **(2)** [**HL^2** = 4-((2-(piperazin-1-yl)ethyl)imino)pent-2-en-2-ol] $[Ni(SCN)_3(CH_3OH)(aminoethylpiperazineH)]$ **(3)** and $[Ni(DMSO)_4(aminoethylpiperazineH)](ClO_4)_3$ **(4)** are reported. The interaction of complexes **1** and **2** with DNA, BSA and HSA have been also studied which show promising results with very high affinity towards DNA and albumin proteins. Moreover, **1** and **2** were also investigated for possible catechol like activity and particularly **1** has shown very high activity towards the catalytic oxidation of 3,5-di-tert-butylcatechol (3,5-DTBC).

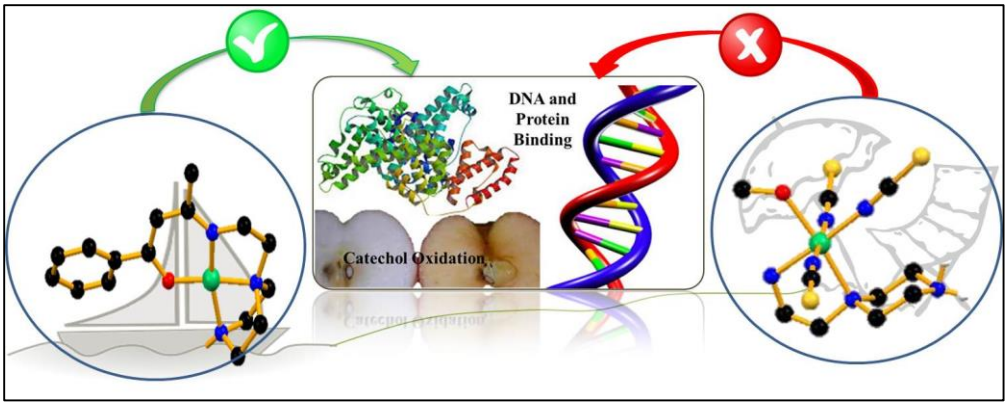

Figure 2. 1*. Pictorial representation to show potential activity of boat conformer complexes than two chair conformer complexes.*

2.2 Experimental

2.2.1 Materials and methods

All the chemical reagents required were purchased from sigma and used without further purification. Infrared spectra (4000–500cm^{-1}) were recorded with a BRUKER TENSOR 27 instrument in KBr pellets. NMR spectra were recorded in AVANCE III 400 Ascend Bruker BioSpin machine at ambient temperature. Mass spectrometric analyses had done on Bruker-Daltonics, microTOF-Q II mass spectrometer and elemental analyses were carried out with a ThermoFlash 2000 elemental analyzer. Spectrophotometric measurements were performed on a Varian UV-Vis spectrophotometer (Model: Cary 100) (for absorption) and Fluoromax-4p Spectrofluorometer from Horiba JobinYvon (Model: FM-100) (for emission) using a quartz cuvette with path length of 1 cm. Circular dichroism spectra were recorded by using a Jasco J-815 spectrometer (Jasco, Tokyo, Japan). Far-ultraviolet (UV) (190–260 nm) spectra were recorded in 0.1 cm path length cell (Hellma, Muellheim/Baden, Germany) using a step size of 0.5 nm, bandwidth of 1 nm and scan rate of 20 nm min^{-1}.

Caution! *Perchlorate compounds are potentially explosive. Only a small amount of material should be prepared and handled with care*

2.2.2 X-ray crystallography

Single crystal X-ray structural studies of **1**, **2, 3** and **4** were performed on a CCD Agilent Technologies (Oxford Diffraction) SUPER NOVA diffractometer. Data for all the complexes were collected at 150(2) K using graphite-monochromoated MoKα radiation (λ_α = 0.71073 Å).The strategy for the data collection was evaluated by using the CrysAlisPro CCD software. The data were collected by the standard 'phi-omega scan techniques and were scaled and reduced using CrysAlisPro RED software. The structures were solved by direct methods using SHELXS-97 and refined by full matrix least- squares with SHELXL-97, refining on F^2. [26] The positions of all the atoms were obtained by direct methods. All non-hydrogen atoms were refined anisotropically. The remaining hydrogen atoms were placed in geometrically constrained positions and refined with isotropic temperature factors, generally 1.2 U_{eq} of their parent atoms. The crystal and refinement data are summarized in Table 2.1. For complex **2,** the C8 and C9 has been modelled for disorder.

Table 2. 1. *Crystallographic data and structure refinement parameters for* ***1****,* ***2****,* ***3*** *and* ***4****.*

Complex	**1**	**2**	**3**	**4**
Empirical Formula	$C_{16}H_{21}ClN_3NiO_5$	$C_{11}H_{20}ClN_3NiO_5$	$C_{10}H_{19}N_6NiOS_3$	$C_{14}H_{39}Cl_3N_3NiO_{16}S_4$
Formula weight	429.52	368.46	394.19	798.78
Crystal system	Orthorhombic	Orthorhombic	Orthorhombic	Monoclinic
Space group	P b c a	P 21 21 21	P c a 21	P 21
a (Å)	10.1342(2)	7.6658(3)	15.8598(3)	10.2345(2)
b (Å)	17.1147(3)	10.5251(6)	9.9515(2)	11.2429(2)
c (Å)	21.5781(4)	18.7540(6)	10.9722(2)	14.6064(2)
α (°)	90	90	90	90
β (°)	90	90	90	94.1040(10)
γ (°)	90	90	90	90
V ($Å^3$)	3742.59(12)	1513.13(12)	1731.73(6)	1676.38(5)
λ (Å)	1.5418	0.71073	0.71073	0.71073
ρ_{calcd} (mg m^{-3})	1.525	1.617	1.512	1.582
Z	8	4	4	2

T (K)	150(2)	150(2)	150(2)	150(2)
μ (mm^{-1})	3.098	1.483	1.488	1.133
F(0 0 0)	1784	768	820	830
Crystal size (mm^3)	0.33 × 0.26 × 0.21	0.33 × 0.26 × 0.21	0.33 × 0.26 × 0.21	0.23 × 0.17 × 0.14
θ ranges (°)	4.10 - 72.18	3.29 - 25.00	3.05 - 24.99	2.97 - 25.00
h/k/l	-9,12/-20,21/-25,26	-9,7/-11,12/-20,22	-18,18/-11,11/-13,13	-12,11/-13,12/-17,17
Reflections collected	26518	10881	12554	13277
Independent reflections	3684	2656	3023	4893
T_{max} and T_{min}	0.5624 and 0.4280	0.7460 and 0.6404	0.7452 and 0.6394	0.8575 and 0.7806
Data/restraints/parameters	3684 / 0 / 273	2656 / 0 / 194	3023 / 1 / 203	4893 / 1 / 390
GOF	1.063	1.087	1.051	1.051
Final R indices [I > 2σ(I)]	R1 = 0.0469,	R1 = 0.0302,	R1 = 0.0292,	R1 = 0.0363,
	wR2 = 0.1400	wR2 = 0.0784	wR2 = 0.0749	wR2 = 0.0975
R indices (all data)	R1 = 0.0546,	R1 = 0.0338,	R1 = 0.0302,	R1 = 0.0383,
	wR2 = 0.1490	wR2 = 0.0815	wR2 = 0.0761	wR2 = 0.0998
Largest peak and hole(e $Å^{-3}$)	0.477 and 0.365	0.385 and -0.218	0.428 and 0.454	0.484 and -0.299

2.2.3 Synthesis of 1-phenyl-3-((2-(piperidin-4-yl)ethyl)imino)but-1-en-1-ol (HL^1)

1.62 g (10 mmol) of phenyl acetyl acetone dissolved in 10 mL of chloroform was added into a solution of 1.29 g of amino ethyl piperazine (10 mmol) in 5 mL of chloroform. The mixture was stirred for 2 hours at room temperature. After evaporating the volatile solvent a yellow oily compound (HL^1) is formed. Yield: 72%. ^{1}H NMR (400.13 MHz, 298 K, $CDCl_3$): δ 11.37 (s, 1H,-OH), 7.34-7.88 (m, 5H,aromatic H), 5.67 (s, 1H,vinyl H), 3.44 (q, 2H, cyclohexene $–CH_2$), 2.94 (t,4H, cyclohexene $–CH_2$), 2.61 (t, 2H, cyclohexene $–CH_2$), 2.51 (br t, 4H, aliphatic $–CH_2$), 1.88 (s, 4H,-CH_3 merged with -NH) ^{13}C NMR (100.61 MHz,

293 K, DMSO): δ 187.8, 164.5, 140.5, 130.3, 128.1, 126.8, 92.3, 58.2, 54.4, 45.9, 40.5, 19.6.$C_{16}H_{23}N_3O$(m/z) calculated - 273.18 (M); obtained - 274.18 $(M+H)^+$

2.2.4 Synthesis of 4-((2-(piperazin-1-yl)ethyl)imino)pent-2-en-2-ol (HL^2)

1.00 g (10 mmol) of acetyl acetone dissolved in 10 mL of chloroform was added into a solution of 1.29 g of amino ethyl piperazine (10 mmol) in 5 mL of chloroform. The mixture was stirred for 2 hours at room temperature. After evaporating the volatile solvent a yellow oily compound (HL^2) is formed. Yield: 72%. ^{1}H NMR (400.13 MHz, 298 K, $CDCl_3$): δ 10.78 (s, 1H, -OH), 4.94 (s, 1H, vinyl H), 3.33 (q, 2H, cyclohexene –CH_2), 2.89 (t, 4H, aliphatic –CH_2), 2.51 (t, 2H, cyclohexene –CH_2), 2.44 (br t, 4H, cyclohexene –CH_2), 1.97 (s, 4H, -CH_3 merged with -NH) 1.90 (s, 3H, -CH_3) ^{13}C NMR (100.61 MHz, 293 K, $CDCl_3$): δ 194.3, 162.1, 94.8, 57.5, 53.9, 45.5, 39.7, 28.3, 18.6. $C_{11}H_{21}N_3O$ (m/z) calculated - 211.16 (M); obtained – 212.17 $(M+H)^+$.

2.2.5 Synthesis of $[Ni(L^1)]ClO_4$ (1)

15 mL of methanolic solution containing HL^1 (0.13 g, 0.5mmol) and $Ni(ClO_4)_2.6H_2O$ (0.182g, 0.5mmol) was stirred at room temperature for 1hr and resulting red coloured solution was concentrated by evaporating the solvent. Finally after 2 or 3 days red needle shaped crystals were obtained from the reaction mixture after layering the mother liquor with diethyl ether. Yield: 85%. Anal.Calcd. (%): $C_{16}H_{21}ClN_3NiO_5$ C, 44.74; H, 4.93; N, 9.78. Found (%): C, 42.88; H, 5.13; N, 9.87. $[C_{16}H_{21}N_3NiO]^+$ (m/z) calculated – 330.05 $(M)^+$; obtained – 330.10 $(M)^+$. Selected IR on KBr (ν/cm^{-1}): 1597 (–C=N), 1097(ClO_4^-)

2.2.6 Synthesis of $[Ni(L^2)]ClO_4$ (2)

5 mL of methanolic solution containing HL^2 (0.11 g, 0.5 mmol) was added drop wise to a 10 mL solution of $Ni(ClO_4)_2.6H_2O$ (0.18 g, 0.5 mmol) and the resultant

mixture was stirred at room temp for 1 h and resulting red coloured solution was concentrated by evaporating the solvent. Layering of the reaction mixture with diethyl ether furnished red coloured needle shaped crystal after few days. Yield: 85%. Anal.Calcd. (%): $C_{11}H_{19}ClN_3NiO_5$ C, 35.96; H, 5.21; N, 11.44. Found (%): C, 35.65; H, 5.43; N, 10.95. $[C_{11}H_{19}N_3NiO]^+$ (m/z) calculated – 267.98 $(M)^+$; obtained – 268.19 $(M)^+$. Selected IR on KBr (ν/cm^{-1}): 1605 (–C=N), 1105 (ClO_4^-).

2.2.7 Synthesis of $[Ni(SCN)_3(CH_3OH)(aminoethylpiperazineH)]$ (3)

At first 15 mL of methanolic solution containing HL^1 (0.14 g, 0.5 mmol) and $Ni(ClO_4)_2.6H_2O$ (0.182 g, 0.5mmol) was stirred at room temp for 30 min. When the reaction mixture became red in colour, a 10 mL methanolic solution of NH_4SCN (0.08 g, 1mmol) was added to it. The solution became green in colour and it was then concentrated by evaporating the solvent. Finally after 6 or 7 days green block shaped crystals of **3** was obtained from the reaction mixture after layering with diethyl ether. Yield: 55%. Anal. Calcd. (%) : $C_{10}H_{18}N_6NiOS_3$ C, 30.55; H, 4.61; N, 21.37. Found (%): C, 29.02; H, 4.85; N, 20.33. $[C_7H_{15}N_4NiS]^+$ (m/z) calculated – 245.03 $[M]^+$; obtained – 245.05 $[M]^+$. Selected IR on KBr (ν/cm^{-1}): 2092 (nitrogen bonded SCN).

2.2.8 Synthesis of $[Ni(DMSO)_4(aminoethylpiperazineH)](ClO_4)_3$ (4)

10 mL aqueous solution containing HL^2 (0.11 g, 0.5 mmol) and $Ni(ClO_4)_2.6H_2O$ (0.18 g, 0.5 mmol) was stirred at room temperature for 1 hr and the resultant green solution was kept in the air for few days until the solvent evaporates to furnish a green powder. Thedried green compound was dissolved in DMSO and layered by methanol for crystallisation. Green block shaped crystals of **4** was obtained after one week time. Yield: 52%. Anal. Calcd. (%) : $C_{14}H_{39}Cl_3N_3NiO_{16}S_4$ C, 21.05; H, 4.92; N, 5.26. Found (%): C, 19.99; H, 5.07;

N, 5.52. $[C_8H_{21}N_3NiOS]^{3+}$ (m/z) calculated – 265.07 $(M)^+$; obtained – 282.27 $(M+H_2O)$.

2.2.9 DNA binding Study

All the experiments concerning the interaction of the complexes with calf thymus (CT) DNA were performed in Tris–HCl buffer (50 mMTris–HCl, pH 7.4). A buffer solution of CT DNA gave a ratio of UV absorbance at 260 and 280 nm of about 1.8:1, specifying the CT DNA sufficiently free from protein. The DNA concentration was measured by its extinction coefficient at 260 nm (6600 M^{-1} cm^{-1}) after 1:100 dilutions. Stock solutions were stored at 4 °C and used not more than 4 days. Absorption titration was done by keeping fixed metal complex concentration at 10 μM while changing the CT-DNA concentration from 0 to 200μM. During titration equal quantity of CT-DNA was added to both complex solution and reference solution to eliminate the absorbance of CT-DNA itself. Furthermore DNA binding for complexes (**1** and **2**) is measured by a special fluorescence spectral technique; ETBr displacement assay from ETBr bound CT-DNA in Tris-HCl buffer at biological pH 7.4. The changes in fluorescence intensities at 605 nm (520 nm excitation) of EB (20μM) bound to DNA were measured with respect to concentration of the complex (0-100μM). EB was non-emissive in Tris-HCl buffer solution (pH 7.4) due to fluorescence quenching of the free EB by the solvent molecules.

2.2.10 Protein binding study

The binding interactions experiments of complexes **1** and **2** with BSA and HSA protein were carried out using standard Trp fluorescence with excitation at 295 nm and the corresponding emission at 340 nm, using a Fluoromax-4p Spectrofluorometer [from Horiba JobinYvon (Model: FM-100)] with a rectangular quartz cuvette of 1 cm path length. A stock solution of BSA and HSA protein were prepared in TRIS-HCl buffer (pH ~7.4). Concentrated stock solutions of complexes **1** and **2** were prepared by dissolving them separately in TRIS-HCl buffer and diluted suitably with TRIS-HCl buffer to get the required

concentrations. An aqueous solution (2 mL) of BSA or HSA protein (10μM) was titrated by successive additions of the respective complexes (0-100μM). Interaction with proteins is also monitored by measuring increment of absorption band at 278nm in UV-Vis spectroscopy through successive addition of 0-100 μM of **1** and **2** in 10 μM protein solutions.

2.2.11 Circular dichroism measurements

Four successive scans recorded at a scan speed of 50 nm^{-1} were averaged out to obtain the CD spectra of serum albumins. Appropriate blank (tris buffer) was subtracted to attain the final result. Monitoring the far UV-CD spectra (200-250 nm) provides important information to get insight about the change in secondary structure of serum albumin proteins. At first the spectra of free BSA (10μM) and HSA (10μM) was recorded and then changes in CD spectra were obtained by monitoring the binding of metal complexes upon addition of 20μM of metal complexes successively.

2.2.12 Catecholase activity study

100 equivalent of 3,5-di-tertbutylcatechol (3,5-DTBC) in methanol were added to 10^{-4} M solutions of **1**, **2**, and **3** in methanol under aerobic condition. Absorbance of the resultant reaction mixture was plotted with respect to wavelength at a regular interval of 10 min in a spectrophotometer in the range of 300-500 nm. The dependence of the rate on various concentration and different kinetic parameters were obtained by treatment of a 10^{-4} M solution of different complexes with 20 to 500 equivalents of substrate and monitoring the upsurge in absorbance at 402 nm (the peak corresponding to the quinone band maxima) as a function of time.

Note: *Due poor solubility of **4** in MeOH and Aqueous. Buffer, the catecholase study and protein binding study were not performed.*

2.2.13 Detection of Hydrogen Peroxide in the Catalytic Reactions

Modification of iodometric method is employed to detect H_2O_2 quantitatively during the catalytic reaction. Reaction mixtures were prepared as in the kinetic

experiments. After 1 h of reaction an equal volume of water was added to extract the formed quinone using dichloromethane. The aqueous layer was acidified with H_2SO_4 to pH≈2 to stop further oxidation, and 1 mL of a 10% solution of KI and three drops of 3% solution of ammonium molybdate were added. In the presence of hydrogen peroxide I^- is oxidized to I_2, $H_2O_2 + 2I^- + 2H^+ \rightarrow 2H_2O + I_2$, and with an excess of iodide ions, the tri-iodide ion is formed according to the reaction $I_2(aq) + I^- \rightarrow I_3^-$. The reaction rate is slow but increases with increasing concentrations of acid, and the addition of an ammonium molybdate solution condenses the reaction almost immediate. The formation of I_3^- could be monitored by UV-vis spectroscopy due to the development of the characteristic I_3^- band (λ = 353 nm, ε = 26 000 M^{-1} cm^{-1}).

2.2.14 Detection of d-d transition band in the Catalytic Reactions

Time dependent UV-Vis spectra was recorded in the range 500-1100 nm after mixing of complex with 3,5 DTBC. Formation of new band (d-d transition band) near 700-800nm indicates that coordination number of Ni(II) changes from four to five or six during formation of complex-substrate aggregate.

2.2.15 Supplementary materials

CCDC 995060,995058, 995061 and 995059 contain the supplementary crystallographic data for **1**, **2, 3** and **4**, respectively. These data can be obtained free of charge via http://www.ccdc.cam.ac.uk/conts/retrieving.html, or from the Cambridge Crystallographic Data Centre, 12 Union Road, Cambridge CB2 1EZ, UK; fax: (+44) 1223-336-033; or e-mail: deposit@ccdc.cam.ac.uk.

2.3 Results and discussions

2.3.1 Syntheses of the complexes

The reaction of 1-Phenyl-1,3-butanedione/ acetyl acetone with amino ethyl piperazine in 1:1 molar ratio in chloroform led to the formation of Schiff base ligand $\mathbf{HL^1}$ and $\mathbf{HL^2}$ respectively (Scheme 2.1). However, synthesis of the

ligand **HL²** was reported previously [27] . Upon reaction of **HL¹** and **HL²** with nickel perchlorate in methanol a red coloured solution was obtained which upon further concentration and layering with diethyl ether furnished red needle shaped compounds $[Ni(L^1)]ClO_4$ **(1)** and $[Ni(L^2)]ClO_4$ **(2),** respectively (Scheme 2.1). However, a similar procedure like synthesis of **1** and further addition of ammonium thiocyanate in the reaction mixture induces hydrolysis of the Schiff-base and furnished $[Ni(SCN)_3(CH_3OH)(aminoethylpiperazineH)]$ (**3)** (Scheme 2.1). Occurrence of such type of hydrolysis are also reported previously.[28] In case of compound **4**, a similar method which has been followed for **3** (water is used as solvent instead of methanol) furnished a green coloured solution (possibly formation of an octahedral nickel complex) [29] and it was almost evaporated to dryness to obtain a green coloured powder. Upon dissolution of this green compound in DMSO (only solvent in which the green compound gets dissolved) and subsequent layering with methanol produced green coloured crystals of $[Ni(DMSO)_4(aminoethylpiperazineH)](ClO_4)_3$ (**4**) (Scheme 2.1).

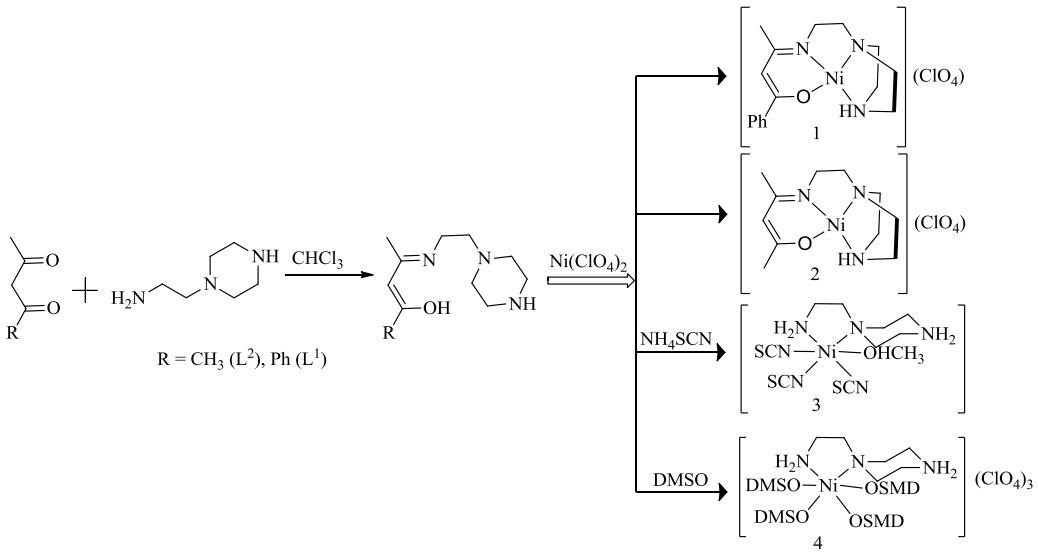

Scheme 2. 1*. Formation of metal complexes* ***1-4****.*

In this case also similar hydrolysis of the Schiff-base moiety has been observed. Both the ligands **HL¹** and **HL²** have been characterized by ^1H and ^{13}C NMR and ESI-MS spectroscopy. The new ligand **HL¹** has shown all the characteristic peaks in ^1H NMR and ^{13}C NMR (Figure 2.2).

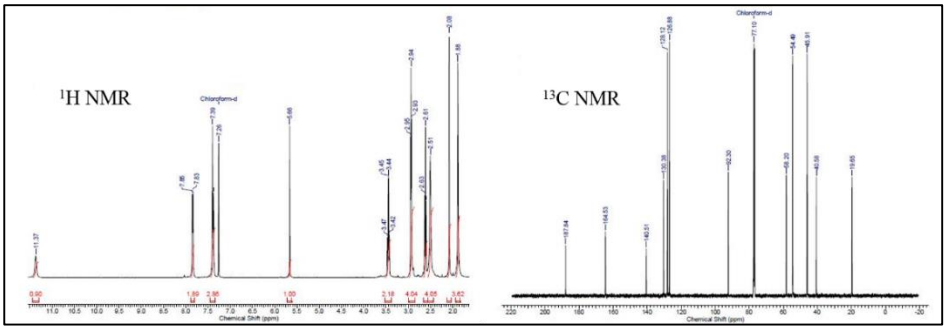

Figure 2. 2*. ^{1}H and ^{13}C NMR of* ***HL^{1}****.*

The molecular peak was observed at 274.18 in ESI-MS spectrum (Figure 2.3). All the complexes have been characterized by ESI-MS spectroscopy (except **4** because of poor solubility), elemental analyses and singly crystal X-ray crystallography. IR spectra of complexes **1** and **2** have a prominent band around 1600 cm^{-1} assignable to ν(C=N) stretching mode.[30]

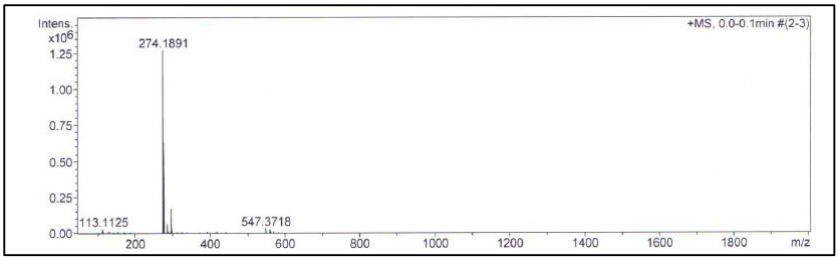

Figure 2. 3*. ESI- Mass spectrum of* ***HL^{1}****.*

Moreover complexes **1**, **2** and **3** show medium intensity band in the range of 3240-3305 cm^{-1} due to ν(N-H) stretching.[30] However, for compound **4** ν(N-H) stretching band is not visible because of the presence of relatively broad and stronger band centred around 3443 cm^{-1} of DMSO molecule in the complex.[31] In addition compound **1**, **2** and **4** show very strong band around 1100 cm^{-1} characteristics of presence of perchlorate counterion. [30] For compound **3** two well resolved bands for thiocyanate have been observed at 2118 and 2092 cm^{-1}, respectively. [30] The ESI-Mass spectra of compound **1** and **2** show the molecular ion peak at 330 and 268, respectively (Figure 2.4). In case of **3** the peak corresponding to $[Ni(SCN)(2\text{-Piperazin-1-yl-ethylamine})]^{+}$ was observed at 245 (Figure 2.4). Complex **4** cannot be characterized by ESI-Mass spectroscopy because of low solubility of the compound.

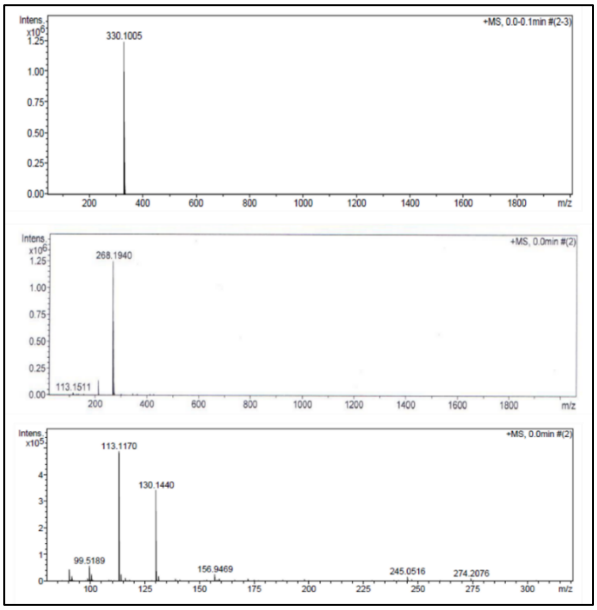

Figure 2. 4*. ESI- Mass spectrum of* ***1****,* ***2*** *and* ***3****. (top to bottom)*

2.3.2 Structure description of the complexes (1) and (2)

These two structures are monomeric in nature and with square planner environment surrounding the nickel ions. The ligands are acting in tetradentate fashion with three N and one O atom completing the square base (Figure 2.5).

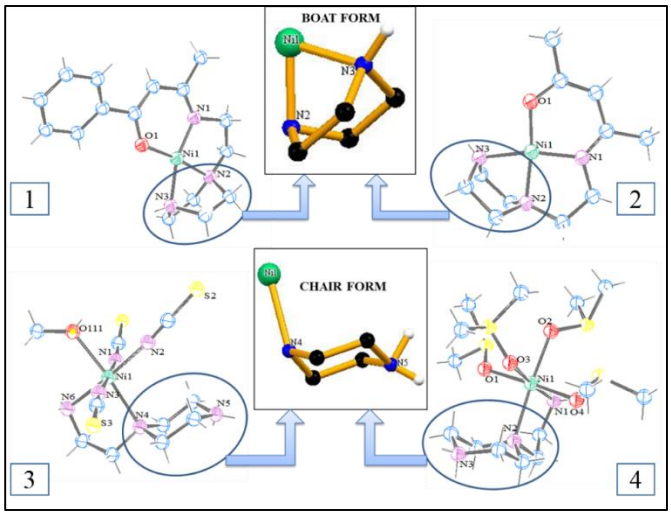

Figure 2. 5*. Different coordination environment of complexes (****1****,* ***2****,* ***3*** *and* ***4****) Boat and Chair conformation of piperazine moiety (Inset).*

In both the complexes the bond lengths between Ni atom and N/O-donor centers are within the range of 1.8112(17) – 1.934(2) Å (Table 2.2), quite similar to those which have been reported earlier. [29]

Table 2. 2*. Selected bond lengths (Å) and bond angles (°) for* ***1*** *and* ***2****.*

Complex	**1**	**2**
Ni(1)-O(1)	1.8112(17)	1.814(2)
Ni(1)-N(1)	1.830(2)	1.832(3)
Ni(1)-N(2)	1.883(2)	1.883(3)
Ni(1)-N(3)	1.934(2)	1.928(3)
O(1)-Ni(1)-N(1)	98.07(9)	98.14(12
N(1)-Ni(1)-N(2)	88.56(11)	89.20(12)
O(1)-Ni(1)-N(3)	96.92(9)	96.95(12)
N(2)-Ni(1)-N(3)	76.58(10)	76.01(12)

The average co-ordination bond angle around Ni center of square planner geometry is around 90° whereas least bond angle was observed for N(2)-Ni(1)-N(3) (~76°) (Table 2.2) due to the formation of chelated five membered ring piperazinyl moiety in boat conformation. In compound **1** perchlorate ion was found to be disordered in nature. Furthermore, the independent molecules get connected with each other through hydrogen bonding *viz*. C8-H8A...O1 and C7-H7B...C16 to form a 1D chain (Figure 2.6).

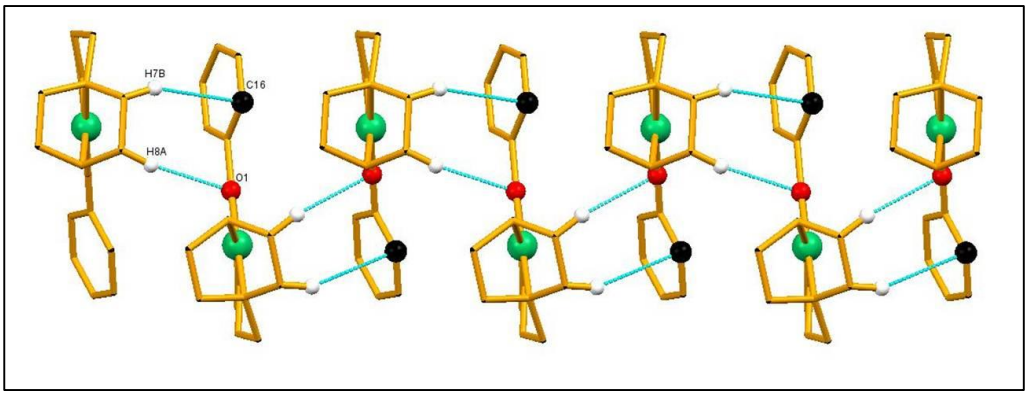

Figure 2. 6*. 1D Chain like network of complex* ***1****.*

Two such adjacent molecules are further joined by hydrogen bonding through perchlorate ion *viz*. C9-H9A...O111, C5-H5A...O111 and C16-H16...O333. Two such strands are additionally joined by the same interconnecting perchlorate ion *via* C6-H6B...O111 and C5-H5B...O222 (Figure 2.7).

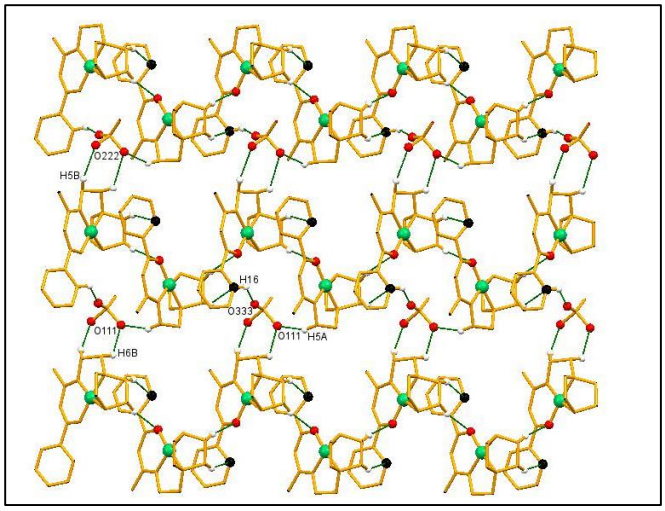

Figure 2. 7*. 2D hydrogen bonded sheet of complex* ***1***

This hydrogen bonded sheet structure in *bc*-plane is further extended along *a*-axis through C13-H13...O222 bonding to provide a 3D structure (Figure 2.8).

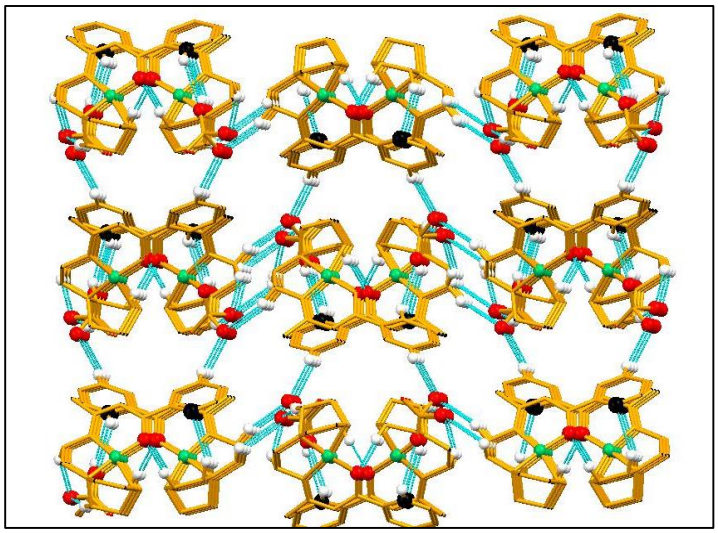

Figure 2. 8*. 3D Non-Covalent polymeric network of complex* ***1****.*

On the other hand in compound **2** each counter perchlorate ion connects six different molecules through the following hydrogen bonding *viz*. C5-H5C...O333, N3-H3N...O333, C7-H7B...O333, C8-H8A...O333, C6-H6B...O111, C10-H10B...O444, C8-H8A...O222 and C7-H7A...O222 (Figure 2.9), which ultimately leads to formation of a 3D network.

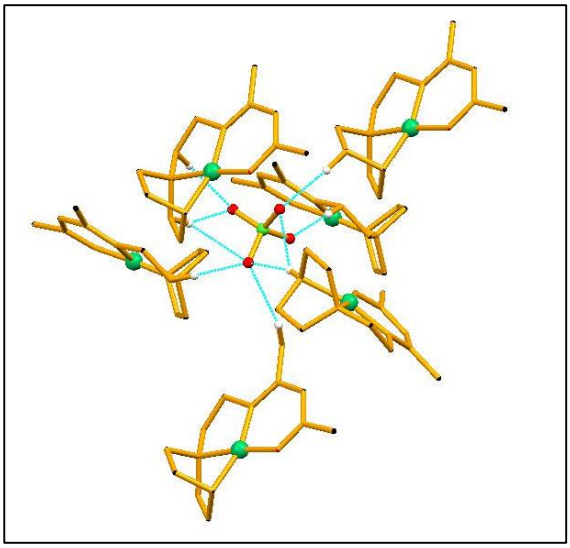

Figure 2. 9*. Figure of complex* ***2*** *with supramolecular network.*

2.3.3 Structure description of the complexes (3) and (4)

These two complexes are monomeric octahedral crystals of nickel ions which are crystallized in orthorhombic and monoclinic crystal systems, respectively. The two N donor atoms of amino ethyl piperazine fulfill the two coordination sites of octahedral geometry (Figure 2.5). The piperzinyl ring takes the chair conformation where secondary nitrogen atom coordinates one extra proton and stays away from the coordination. The octahedral geometry surrounding the metal center is completed by three coordinating thiocyanate ions getting attached to the nickel center via nitrogen atom and one methanol molecule which is coordinating in *trans* fashion with respective to tertiary nitrogen atom of amino ethyl piperazine. The protonated piperzinyl ring induced a hydrogen bonded 1D chain through N5-H5...S1 (Figure 2.10) which is propagated along *a*-axis. Two such adjacent parallel chains are further joined by N5-H5...S3 and C5-H5B...S3 to form 2D hydrogen bonded network in *ab*-plane (Figure 2.10). These 2D networks are further connected along the *c*-axis through O111-H101...S3 and N6-H2N...S2 to complete a 3D hydrogen bonded network (Figure 2.10). The molecules are further joined by each other through hydrogen bonding to form a 3D hydrogen bonded network.

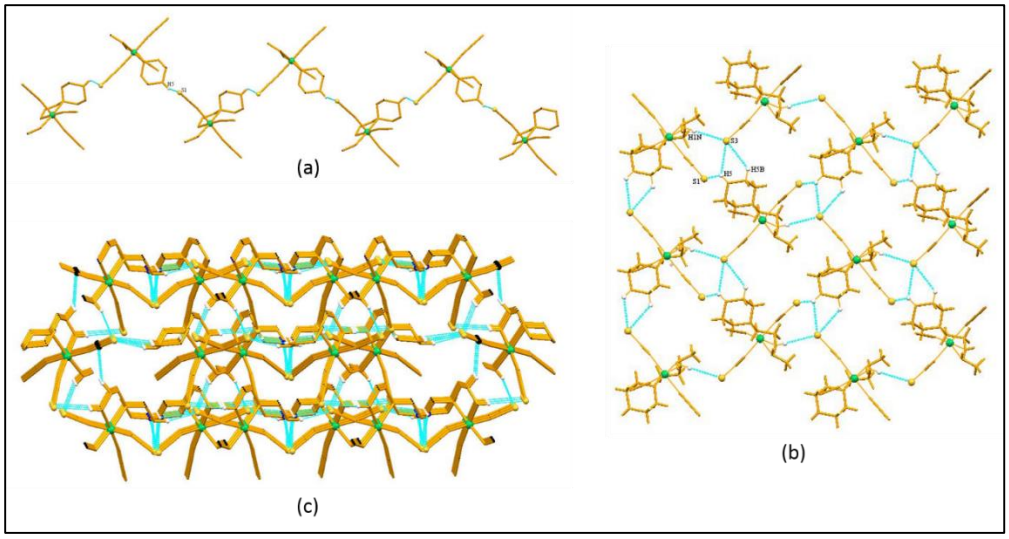

Figure 2. 10*. (a) 1D chain like structure complex* ***3****. (b) 2D hydrogen bonded sheet like network of complex* ***3****. (c) 3D hydrogen bonding network of complex* ***3****.*

In compound **4** also the piperzinyl ring takes the chair conformation and act as bi-dentate ligand whereas the rest of the coordination positions are fulfilled by DMSO molecules (Figure 2.5). Three perchlorate counter ions are present in each molecule. The separated molecules are arranged in a linear fashion along *b*-axis directly through a distant hydrogen bonding viz. C5-H5B...C9. However there are eleven perchlorate ions observed surrounding a single molecule and connected through different hydrogen bonding; among them at least three perchlorate ions help to connect the adjacent molecules through hydrogen bonded network to maintain 1D chain. [C6-H6A...O555; N3-H...O666; C14-H14C...O222; C9-H9B...O222; C10-H10B...O444; N1-H2N...O777; C14-H14C...O222; C9-H9B...O444 and C10-H10B...O444] (Figure 2.11).

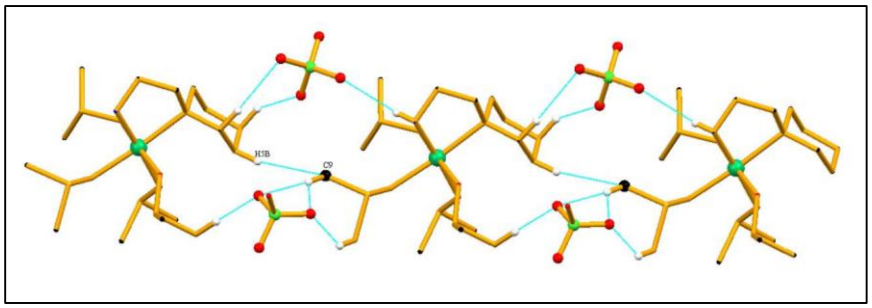

Figure 2. 11*. 1D chain like structure of complex* ***4.***

However, considering all the hydrogen bonding surrounding one particular molecule the structure is quite complex and it provides a 3D-

polymeric hydrogen bonded network. In both the complexes the bond lengths between Ni atom and N/O-donor centers are within the range of 2.040(3) – 2.255(3) Å (Table 2.3), quite similar to those octahedral complexes which have been reported earlier.[29] All the hydrogen bonding parameters of all the complexes are compiled together in Table 2.4.

Table 2. 3*. Selected bond lengths (Å) and bond angles (°) for* ***3*** *and* ***4****.*

3		**4**	
Ni(1)-N(2)	2.042(2)	Ni(1)-O(4)	2.045(3)
Ni(1)-N(3)	2.059(2)	Ni(1)-O(1)	2.052(3)
Ni(1)-N(6)	2.061(2)	Ni(1)-N(1)	2.084(4)
Ni(1)-N(1)	2.070(3)	Ni(1)-O(3)	2.093(3)
Ni(1)-O(111)	2.165(2)	Ni(1)-O(2)	2.110(3)
Ni(1)-N(4)	2.257(2)	Ni(1)-N(2)	2.238(3)
N(2)-Ni(1)-N(3)	90.22(10)	O(4)-Ni(1)-N(1)	89.35(14)
N(3)-Ni(1)-N(6)	90.12(11)	O(1)-Ni(1)-N(1)	94.33(14)
N(2)-Ni(1)-N(1)	89.12(10)	O(4)-Ni(1)-O(3)	87.92(11)
N(6)-Ni(1)-N(1)	90.38(11)	O(1)-Ni(1)-O(3)	88.53(12)
N(2)-Ni(1)-O(111)	85.40(10)	O(4)-Ni(1)-O(2)	93.70(12)
N(3)-Ni(1)-O(111)	90.98(9)	O(1)-Ni(1)-O(2)	89.41(12)
N(6)-Ni(1)-O(111)	91.01(9)	N(1)-Ni(1)-O(2)	91.51(14)
N(1)-Ni(1)-O(111)	86.35(10)	O(3)-Ni(1)-O(2)	86.17(12)
N(2)-Ni(1)-N(4)	101.00(9)	O(4)-Ni(1)-N(2)	85.09(13)
N(3)-Ni(1)-N(4)	90.33(10)	O(1)-Ni(1)-N(2)	92.20(13)
N(6)-Ni(1)-N(4)	82.59(10)	N(1)-Ni(1)-N(2)	82.61(15)
N(1)-Ni(1)-N(4)	92.38(10)	O(3)-Ni(1)-N(2)	99.64(12)

Table 2. 4. *Hydrogen bonding interactions of all complexes.*

D–H···A	*d*(D–H) (Å)	*d*(H···A) (Å)	*d*(D···A) (Å)	*d*(D–H···A) (°)
1				
C8–H8A···O1	0.99	2.457	3.434	168.62
C7–H7B···C16	0.991	2.826	3.151	155.81
C9–H9A···O111	0.99	2.646	3.343	170.5
C5–H5A···O111	0.99	2.491	3.403	153.08

C16–H16···O333	0.949	2.61	3.304	130.24
C6–H6B···O111	0.99	2.646	3.343	128.55
C5–H5B···O222	0.989	2.51	3.446	157.92
C13–H13···O222	0.95	2.484	3.313	145.74
2				
C5–H5C···O333	0.979	2.59	3.484	151.75
C8–H8A···O333	0.991	2.688	3.567	148.01
C8–H8A···O222	0.991	2.643	3.584	158.47
C7–H7A···O222	0.99	2.552	3.51	162.81
N3–H3N···O444	0.766	2.635	3.279	142.8
N3–H3N···O333	0.766	2.388	3.133	164.23
C7–H7B···O333	0.98	2.671	3.641	166.62
C6–H6B···O111	0.99	2.604	3.591	174.88
C10–H10B···O444	0.99	2.562	3.375	139.41
3				
N5–H5···S1	0.879	2.942	3.283	105.14
N6–H1N···S3	0.794	2.838	3.626	171.66
N5–H5···S3	0.879	2.914	3.523	127.77
C5–H5B···S3	0.99	2.99	3.702	129.71
O111–H101···S3	0.797	2.504	3.261	159.03
N6–H2N···S2	0.817	2.782	3.576	164.28
4				
C6–H6A···O555	0.99	2.563	3.545	171.53
N1–H1N···O555	1.041	2.342	3.186	137.29
N3–H3N···O101	0.903	2.427	2.998	121.32
C12–H12B···O101	0.98	2.682	3.563	149.82
N3–H3N···O333	0.903	2.172	2.987	149.74
C10–H10B···O444	0.98	2.6	3.405	139.47
C5–H5B···C9	0.99	2.888	2.852	164.7
C14–H14C···O222	0.981	2.463	3.413	162.94
C9–H9B···O222	0.98	2.552	3.528	173.98
N1–N2H···O777	0.823	2.487	3.275	160.8
C9–H9B···O444	0.98	2.709	3.485	136.47

2.3.4 DNA binding studies between complexes and CT-DNA

As nickel complexes have a tendency to interact with DNA and proteins therefore various spectroscopic studies of nickel complexes have been performed (**1**, **2** and **3**) with CT-DNA, BSA and HSA to understand the interaction of synthesized complexes on them. In complex **1** two bands were observed in the high energy region at 340 and 250 nm, respectively. These bands are assigned as intra-ligand charge transfer band due to n → π* and π → π* transition. Any interaction with DNA is expected to perturb the intra-ligand centered spectral transitions. With the increase amount of CT-DNA it has been observed that for complex **1** the π → π* transition is showing hyperchromism along with a slight red shift (Figure 2.12). This strong hyperchromic effect indicates considerable interaction of complex **1** with CT-DNA. The DNA binding affinities of the complexes were compared by calculating the intrinsic binding constant K_b by following equation:[18]

$$\frac{[\mathrm{DNA}]}{(\varepsilon_a - \varepsilon_f)} = \frac{[\mathrm{DNA}]}{(\varepsilon_b - \varepsilon_f)} + \frac{1}{K_b(\varepsilon_b - \varepsilon_f)}$$

where [DNA] is the concentration of DNA in base-pairs, ε_a is the apparent extinction coefficient calculated using absorbance/ [complex], ε_f is the extinction coefficient of the complex in its free form, and ε_b is the extinction coefficient of the complex in the bound form. In both the cases when data was fitted in the above equation it gave a straight line with a slope of $1/(\varepsilon_b - \varepsilon_f)$ and an intercept of $1/K_b(\varepsilon_b - \varepsilon_f)$. The value of K_b was determined from the ratio of slope to intercept (Figure 2.12)

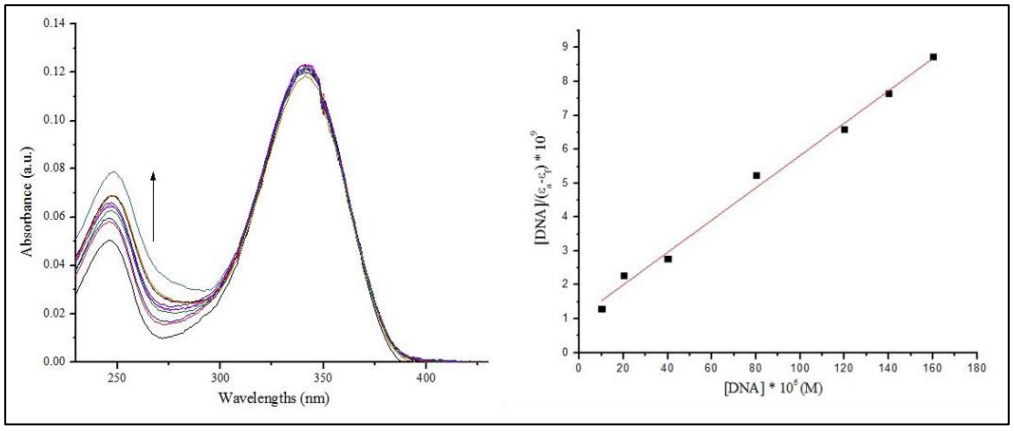

Figure 2. 12. *(Left) Absorption titration spectra of fixed concentration (10 μM) of complexe 1 with increasing concentrations (0–200 μM) of CT-DNA. (Right) Binding isotherms of complex **1**.*

which was found to be 4.5×10^4 M^{-1} which is on higher side as per different nickel complexes are reported so far.[15] However, for compound **2** and **3** no suitable CT band was observed in the above mentioned region which can be monitored and therefore any UV-vis study for these two compounds for DNA interaction was not performed.

To understand the interaction between complexes with CT DNA more clearly steady state competitive binding experiments using complexes **1** and **2** (complex **3** did not respond in this study) as quenchers were undertaken where ethidium bromide (EB) was used as a fluorescent probe. EB is a planar cationic dye which emits intense strong fluorescent light in presence of DNA due to its strong intercalation between the adjacent DNA base pair. When complexes intercalate in DNA the probable binding sites for EB in DNA get decreased hence the fluorescent intensity of EB gets quenched. As the concentration of the nickel complexes increases, the reduction in the fluorescence intensity clearly indicates that the EB molecules are displaced from their DNA binding sites and are replaced by the metal complexes under investigation. The fluorescence quenching spectra of DNA bound EB by complexes **1** and **2** are shown in (Figure 2.13)**.**

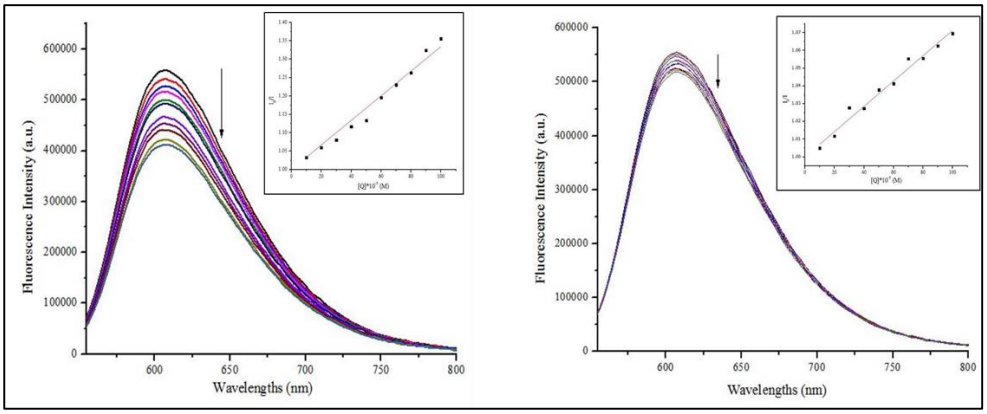

Figure 2. 13. *ETBr displacement assay of complex **1**(left) and complex **2** (right). Corresponding stern-volmer plot is in inset.*

Both the spectra are indicative of displacement of EB from CT-DNA as there is appreciable reduction in fluorescent intensity. However, this displacement is more prominent in **1** than **2**. Furthermore, K_q values for complexes **1** and **2** have been found to be 3.3 x 10^4 and 7.1 x 10^2 M^{-1}, respectively which was obtained from classical Stern-Volmer equation.[9] The binding constant (K_b) values obtained from the plot of log[(F_0-F)/F] vs log[Q] (from Scatchard equation) [14] (Figure 2.14) were found to be 5.6 ×10^3 and 2.3 × 10^3 M^{-1} for complex **1** and **2**, respectively, reflecting more binding of complex **1** with DNA to leach out more number of EB molecules originally bound to DNA than that of for complex **2**.

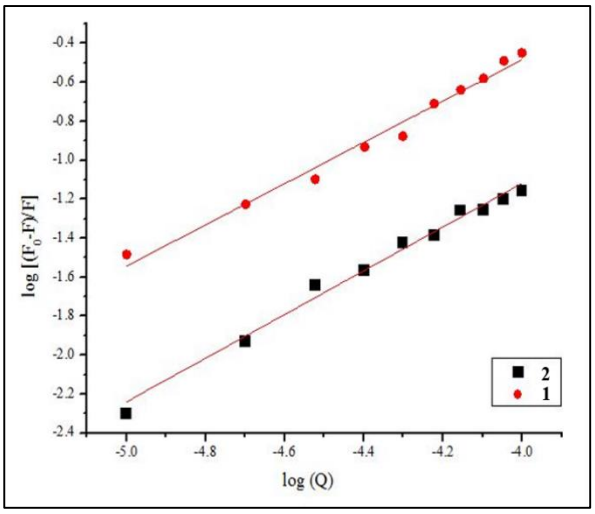

Figure 2. 14*. Scatchard plot for determination of K_b for CT-DNA of **1** and **2**.*

2.3.5 Interaction of complexes with serum albumins by fluorescence quenching study

Interaction of transition metal complexes with proteins are generally monitored by intrinsic fluorescence intensity. Binding of prospective molecules particularly to blood plasma protein are in center of attraction as the transport of drugs through the bloodstream is affected *via* the interaction of drugs with them.[32] To study the interaction of synthesized complexes with different proteins fluorescence quenching studies with BSA and HSA were carried out. The florescence property in BSA is mainly attributed due to the presence of three amino acids *viz*. tryptophan, tyrosine and phenyl alanine residues.[32] However, fluorescence quenching may happen because of several reasons like excited state reactions, ground state complex formation, energy transfer, molecular rearrangement and collision quenching. The fluorescence spectrum of **1** with BSA indicates that there is a progressive decrease in the fluorescence intensity along with a significant red shift. The intensity of the fluorescent band observed at 340 nm was quenched to the extent of 15% of its initial intensity (Figure 2.15). The shifting of the emission maxima towards lower energy indicates the probable energy transfer from the indole unit of the tryptophan to the protein bound compound. The fluorescence quenching data was further analyzed by the Stern−Volmer relation which again can be expressed in terms of bimolecular quenching rate constant and average life time of the fluorophore as shown in following equation [33]

$$\frac{F_0}{F} = 1 + k_q \tau_0 [Q] = 1 + K_{SV}[Q]$$

where F_0 and F are the fluorescence intensities in the absence and the presence of a quencher, k_q is the bimolecular quenching rate constant, τ_0 is the average life time of fluorophore in the absence of a quencher and [Q] is the concentration of a quencher (metal complexes). K_{SV} is the Stern–Volmer quenching constant in M^{-1}. However, in this case a plot with upward curvature concave towards y-axis was obtained. This positive deviation indicates a probable two way quenching by collision and as well as by complex formation with the same

quencher. Moreover the value of k_q which shows normally the value in the range 10^{10} $M^{-1}s^{-1}$ for dynamic quenching was found to be 7.7 x 10^{12} $M^{-1}s^{-1}$ indicating the role of static quenching in the present case.[34] The value obtained for K_{SV} was 4.8 x 10^4 is also on higher side indicating a strong binding between BSA and **1**. The effect of addition of complex **1** in HSA has a more dramatic effect on fluorescence quenching. The intensity of the fluorescent band decreased up to 5% of its initial intensity (Figure 2.15). In Stern-Volmer plot at lower concentration of quencher **1** it shows linearity however at higher concentration it shows quite high positive deviation from linearity. It indicates the formation of more than one ground state complex HSA-**1** system, so it can be predicted that at lower concentration of **1** the quenching could be started by a stable ground-state complex formation (1:1 type) however at higher concentration an upward bending in the direction of the F_0/F axis specifies the formation of the second (1:2 type) **1**–HSA complex.

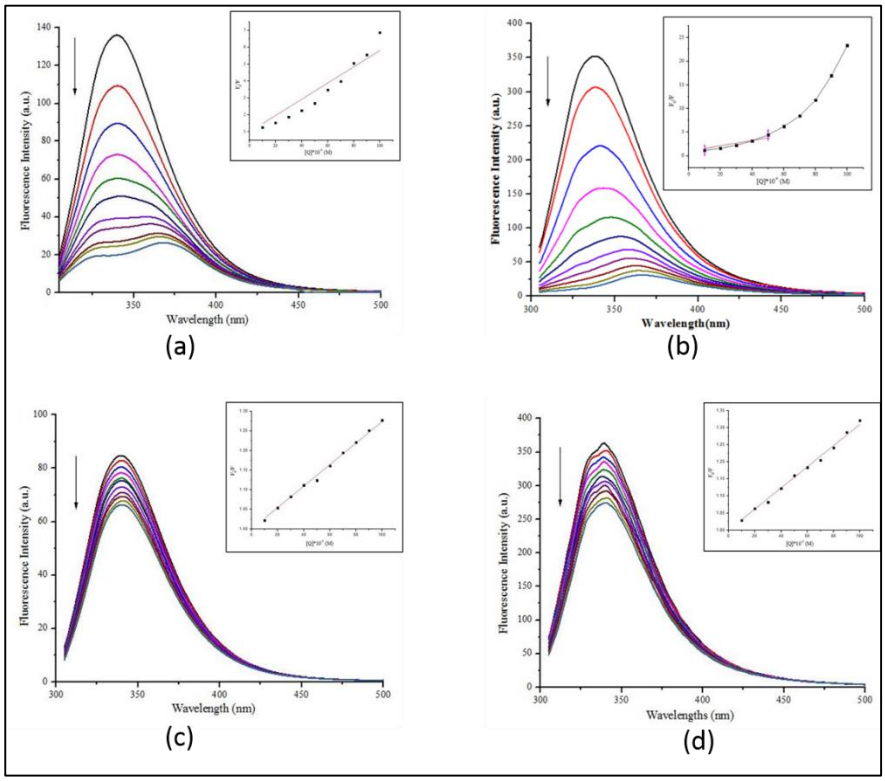

Figure 2. 15. *(a) & (b) Fluorescence quenching of BSA and HSA by* ***1*** *(c) & (d) Fluorescence quenching of BSA and HSA by* ***2***

Such 1:2 type complex formation for **1**–HSA system may have stimulated due to the more flexible environment of HSA (than that of BSA) that have preferred to form some loose binding interaction of **1** with HSA.[35]

To determine the binding constant and number of binding site Scatchard equation was employed which is given by $\log\left[\frac{F_0-F}{F}\right] = \log K_a + n \log[Q]$

Where K_a and n are the binding constant and number of binding sites respectively, and F_0 and F are the fluorescence intensities in the absence and presence of the quencher respectively. Thus, a plot of $\log(F_0 - F)/F$ versus log[Q] (Figure 2.16) can be used to determine the value of binding constant (from intercept) and number of binding sites (from slope).

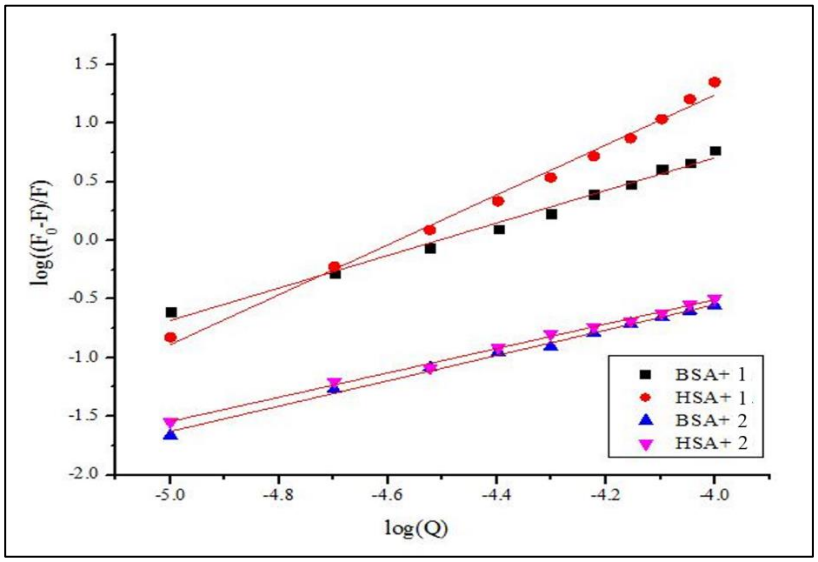

Figure 2. 16*. (a) Fluorescence quenching of BSA by **1**. (b) Fluorescence quenching of HSA by **1**. (c) Fluorescence quenching of BSA by **2**. (d) Fluorescence quenching of HSA by **2**.*

Calculation shows that the binding constant for **1**-HSA is quite high 5.6 × 10^9 M^{-1} and the n value obtained was 2.12. The Ka and n value obtained for 2-BSA pair are 1.7 × 10^6 and 1.34 respectively which are also relatively on higher side with respect to other nickel complexes reported so far. All the relative data are compiled in Table 2.5.

Table 2. 5*. Table for Stern-Volmer quenching const., binding const., binding site.*

System	K_{SV} (M^{-1})	K_q ($M^{-1}S^{-1}$)	K_a (M^{-1})	N
1-BSA	4.8×10^{4}	7.7×10^{12}	1.7×10^{6}	1.34
2-BSA	2.7×10^{3}	4.3×10^{11}	4.9×10^{3}	1.07
1-HSA	1.4×10^{5}	2.2×10^{13}	5.6×10^{9}	2.12
2-HSA	3.1×10^{3}	5.0×10^{11}	5.1×10^{3}	1.03

The interaction of complex **2** with BSA and HSA in terms of florescence quenching is depicted in Figure 2.14c and Figure 2.14d. The quenching of fluorescent band at 340 nm went up to 79% and 76% of their initial intensity for BSA and HSA, respectively. The K_a and n values obtained for these cases are found to be 4.9×10^3, 5.1×10^3, 1.07 and 1.03, respectively. It clearly indicates that the affinities of interaction of complex **2** with different proteins are respectively weaker than complex **1**. A probable reason for that can be envisaged as ligand **HL^1** will be less electron donating than **HL^2** because of the presence of electron withdrawing phenyl group the relatively higher positive charge on metal-ion may induce more interaction with the donating site of the proteins in case of compound **1** with respect to **2**.

To get further insight regarding the type of quenching (static or dynamic) which is prevailing UV-vis absorption measurement of the protein with increasing concentration of the nickel complexes was performed. Dynamic quenching generally only affects the excited state of the fluorophores and there are no changes observed in absorption spectra. However, formation of complex in ground state generally induces perturbation in the protein structure resulting a change in absorption spectrum of the fluorophore.[17] In present case there is a considerable increase in the intensity of absorption for BSA and HSA respectively in the same wave length when they have been treated with complex **1** separately with the gradual increase in the concentration of the nickel complex (Figure 2.17). This result indicates clearly that there is a formation of protein-**1** complex in the ground state which is causing a change in the conformation of the protein and static quenching is contributing a major part in the total

quenching of the fluorescence in the above mentioned study. [17] A similar experiment with BSA and HSA when both of them have been treated with increasing concentration of complex **2** revealed similar results (Figure 2.17). However the rate of decrease in absorption intensity is comparatively less and which reconfirms a weaker interaction of complex **2** with the proteins with respect to complex **1**.

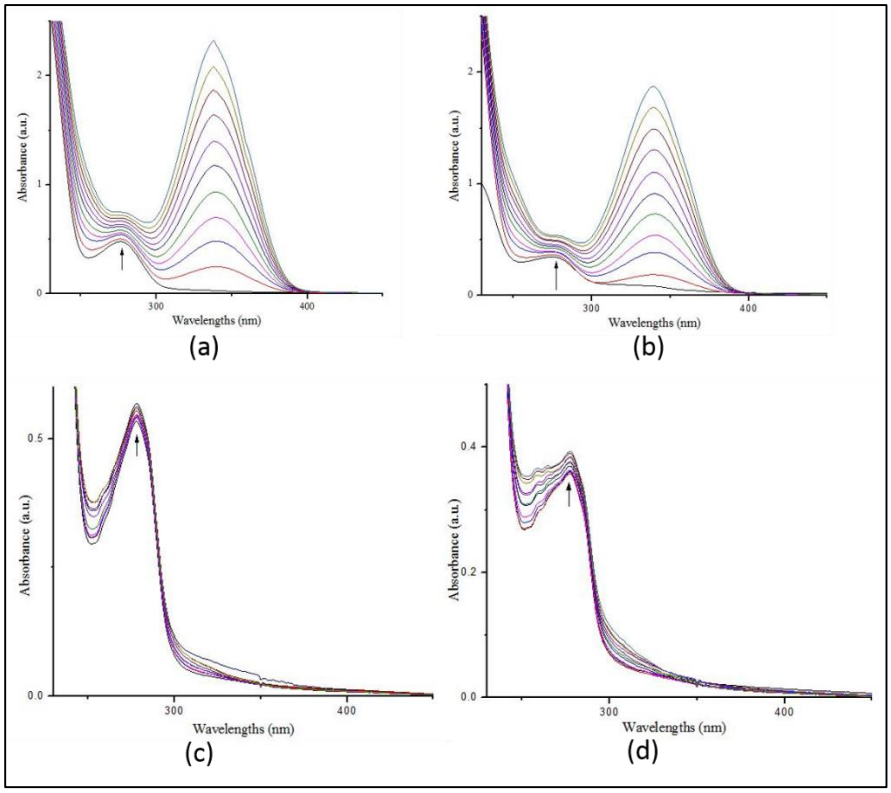

Figure 2. 17*. UV-VIS Absorption titration of BSA (10μM) and HSA (10μM) by successive addition of complex **1**.[Graph-(a) & (b)] and complex **2** [Graph-(c) & (d)]*

2.3.6 Circular dichroism studies

To have a better understanding in nickel complex - protein binding mechanism and secondary structure changes of protein, CD measurement was performed. (Figure 2.18) A negative CD band was observed with two characteristic bands at 208 and 222 nm which is indicative of negative cotton effect as a consequence $n \rightarrow \pi^*$ transition in the peptide bond of α-helical structure.[36] It was observed

when treated with complex there is reduction in both of these bands without much shift of the peaks when treated with nickel complexes.

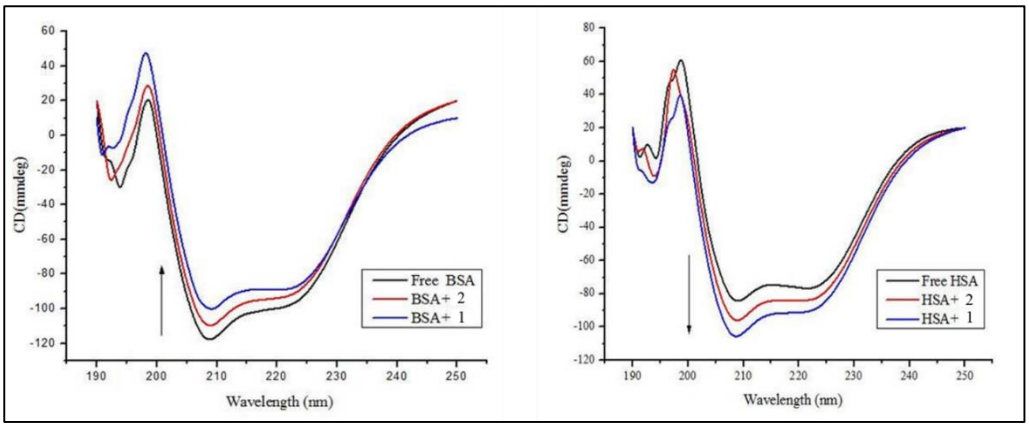

***Figure 2. 18**. Changes of CD spectra of BSA (left) and HSA (right) by **1** and **2**.*

The reduction is more in the case complex **1** then **2** indicating a stronger influence on the disruption of helical structure of the protein for **1**. However, when the complexes **1** and **2** were treated with HSA in 1:1 ratio, the trend observed was something different. An increase in the percentage of α-helix formation was observed in both the cases with an increase in the intensity of negative band at 209 nm (Figure 2.18). Though this phenomenon is relatively rare however there are some examples where some metal complexes or other molecules when treated with proteins can increase the helicity of the α-helix with increase in its concentration.[37] It has been envisaged that metal center may interact with carboxylate group present in the protein *via* coordinative interaction and simultaneously the ligand present in it can also exhibit hydrophobic interaction with the hydrophobic moieties in the protein chain. These two way interaction may have a cumulative effect of increase in percentage of α-helix component of HSA. These results indicated that the interaction between metal complexes with BSA and HSA may be not of similar nature however in the both cases the interaction causes a disruption in protein chain leading to the decrease of fluorescence intensities of the protein. The secondary structure composition of the peptide was estimated from CD spectra using K2D3 program.[38] All the results are tabulated and presented in Table 2.6.

Table 2. 6. *Table for CD measurement analysis.*

System	α-Helix %	β-Sheet %
Free BSA	68.87	9.59
BSA-**1**	68.33	9.72
BSA-**2**	68.55	9.64
Free HSA	67.88	9.85
HSA-**1**	68.38	9.79
HSA-**2**	68.34	9.81

2.3.7 Catecholase activity study

To study the catecholase like activity of the synthesized metal complexes 3,5-di-tert-butylcatechol (3,5-DTBC) was taken as the substrate in the presence of two bulky *t*-butyl substituent in the ring which shows a low quinone-catechol reduction potential.[39] The reactions were carried out at 25°C in aerobic condition and it was monitored by UV-Vis spectroscopic technique. The oxidation product 3,5-di-*tert*-butylquinone (3,5-DTBQ) is highly stable and shows a maximum absorption at about 400 nm in methanol. To monitor the reaction a 10^{-4} M methanolic solution of different complexes (**1** and **2**) were treated with 100 equivalent of 3,5-BTDC in which upon addition of catechol as substrate a new band starts to gradually appear at about 402 nm with time due to the formation of the oxidized product 3,5-DTBQ (Figure 2.19).

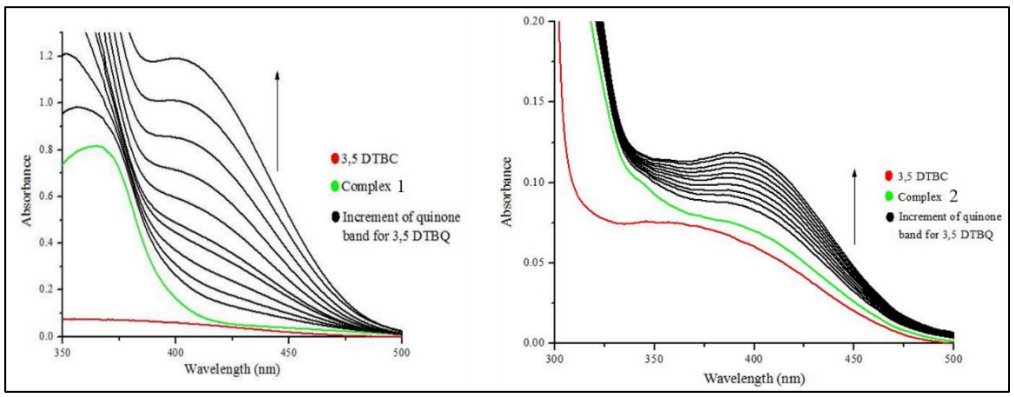

Figure 2. 19. *Catecholase activity with time dependent spectral pattern of complex **1** (left) and **2** (right) after addition of 3,5 DTBC.*

To understand the kinetic aspect of catalysis for **1** and **2**, the rate constant for a catalyst complex was determined by traditional initial rate method (detail description in experimental section). The observed rate versus substrate concentration data were then analyzed on the basis of the Michaelis–Menten approach of enzymatic kinetics. The Michaelis−Menten constant (K_M) and maximum initial rate (V_{max}) were determined by linearization using Lineweaver−Burk plots (Figure 2.20). [40]

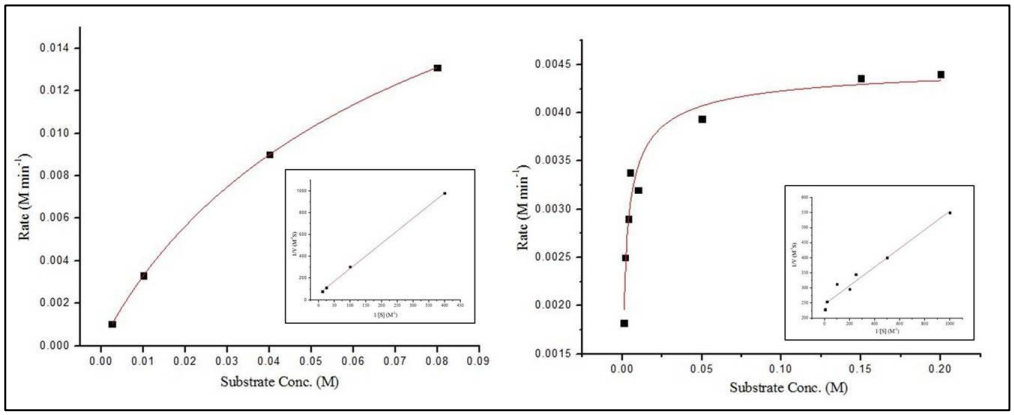

Figure 2. 20. *Michael-menten plot for **1** (left) and **2** (right). Inset- lineweaver burk plot.*

The turnover number values (k_{cat}) were obtained by dividing the V_{max} values by the concentration of the corresponding complexes. All the data unambiguously demonstrate that both the complexes **1** and **2** are very much active. Complex **3** did not respond to any kind of catalytic activity towards catechol oxidation as well. The unusual high activity of the mononuclear complex **1** and **2** may be attributed to the fact that the positive charge on the piperazinyl moiety may help the facilitation of catalyst-substrate interaction by forming a positive channel which might be a prerequisite for showing better catalytic activities. A similar mechanism has been proposed to explain the activity of copper/zinc superoxide dismutase where positively charged arginine and lysine residue play a role to attract the anion and guiding them towards the catalytic center.[20]

To draw probable mechanism (Scheme 2.2) of catecholase activity of **1** (comparatively higher K_{cat} value), the investigation for the probable complex-substrate intermediate through ESI-MS, change in d-d transition band of Ni(II)

upon interaction with 3,5 DTBC through UV-Vis spectroscopy, and qualitative as well as quantitative detection of I^{3-} band (~353nm.) by UV-Vis spectroscopy for indication of formation of H_2O_2 during catalytic oxidation procedure were carried out. ESI-MS positive spectrum of a 1:100 proportionate mixture of the complex **1** and 3,5 DTBC was recorded. After 5 minute of mixing the spectrum exhibit two major peaks at *m/z* = 243 and 463, respectively, along with one small peak at 573.4 (Figure 2.21). The former two peaks correspond respectively to the quinone-sodium aggregates $[(3,5\ DTBQ)Na]^+$ and $[(3,5\ DTBQ)_2Na]^+$.[41]

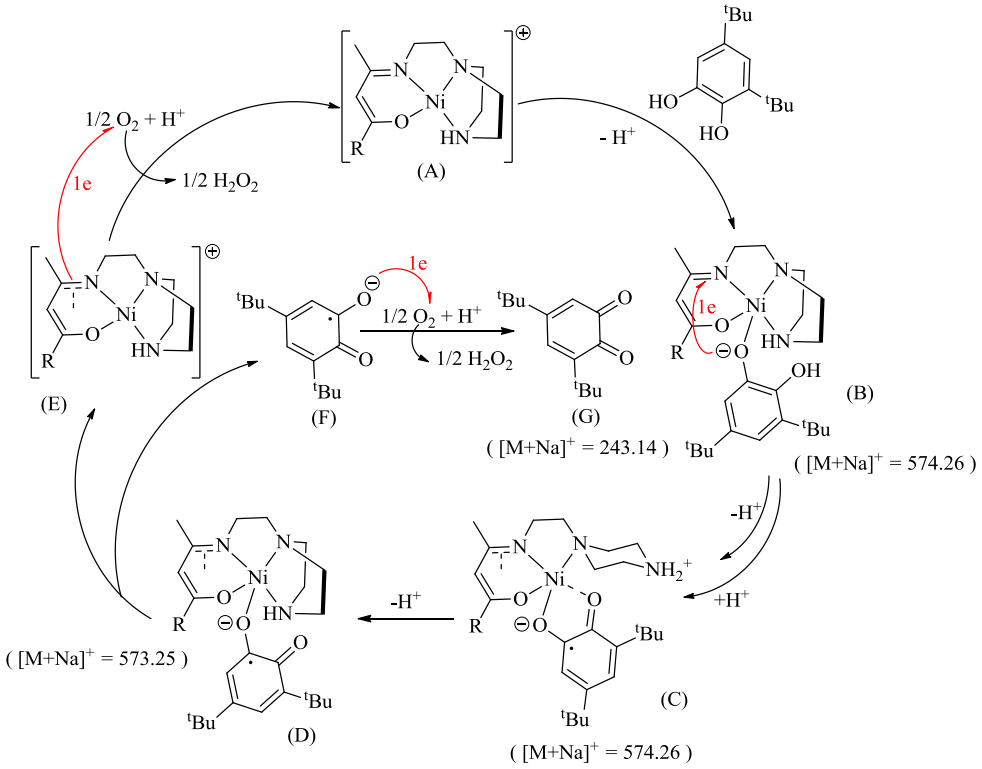

Scheme 2. 2. *Probable catalytic cycle of oxidation of 3,5 DTBC by Ni(II) square planar complexes. (Calculated mass is given when R=Ph)*

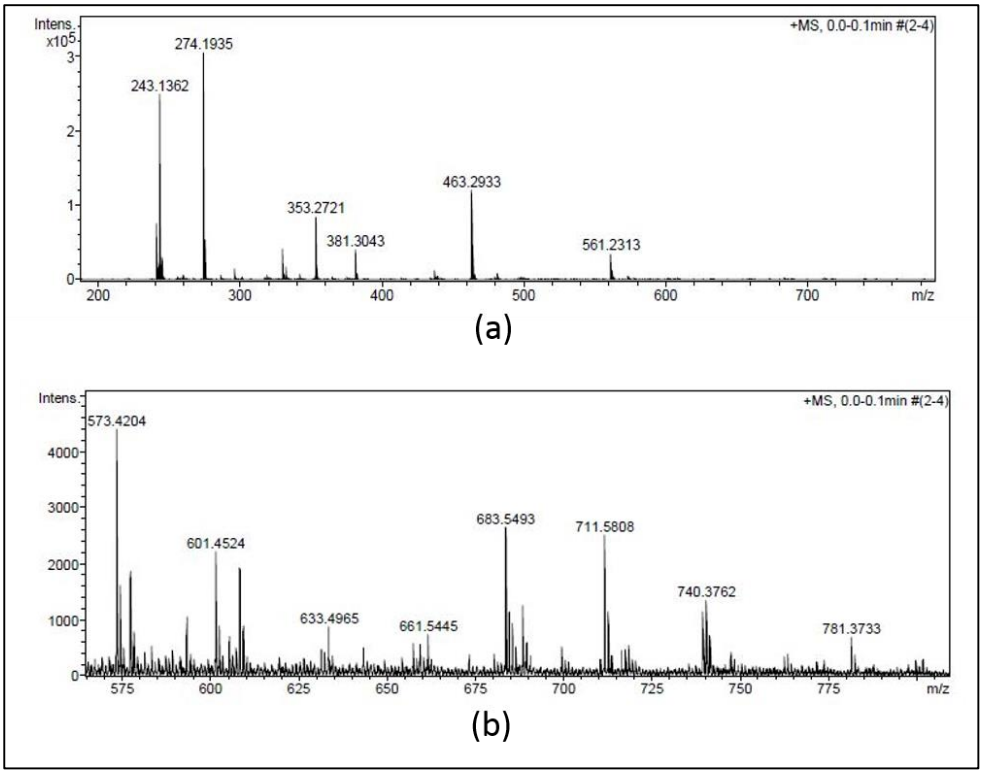

Figure 2. 21. *(a) Electrospray mass spectrum (ESI-MS positive) of a 1:100 1/3,5-DTBC mixture in methanol, recorded within 10 min of mixing. (b) Corresponding Zoomed spectra.*

The later smaller peak at 573.4 could be due to the formation of complex-substrate aggregate ("C" / "D" in Scheme 2.2) with a little deviation which is similar with earlier report.[42] Thus it is difficult to propose the exact structure of intermediate with the help of ESI-MS. Monitoring the catalytic reaction by UV-Vis spectroscopy reveals gradual formation of a very broad d-d transition bands (possibly combination of many bands) in the region of 650-900 nm (Figure 2.22). This result indicates the change of coordination environment of Ni(II) center from tetra-coordinated to penta- or hexacordinated.[43] It is also important to note that, the dioxygen of atmosphere is reduced to H_2O_2 during the oxidation process. Oxidation of I^- to I_2 followed by the generation of I_3^-, qualitatively detected by UV-Vis spectral study of solution (Figure 2.23), obtained after proper work up of the mixture of catechol, complex and KI, specifically indicates that dioxygen is reduced to H_2O_2, as reported by earlier investigators.[21] Quantitative analysis of H_2O_2 indicates that 0.8 mol (≈1) of

H_2O_2 was shown to be produced per mol of 3,5 DTBC along with formation of 1 mol of 3,5 DTBQ, which strongly supports the mechanism of reaction involving a two electron reduction process of aerial oxygen, as indicated in previous reports.[44]

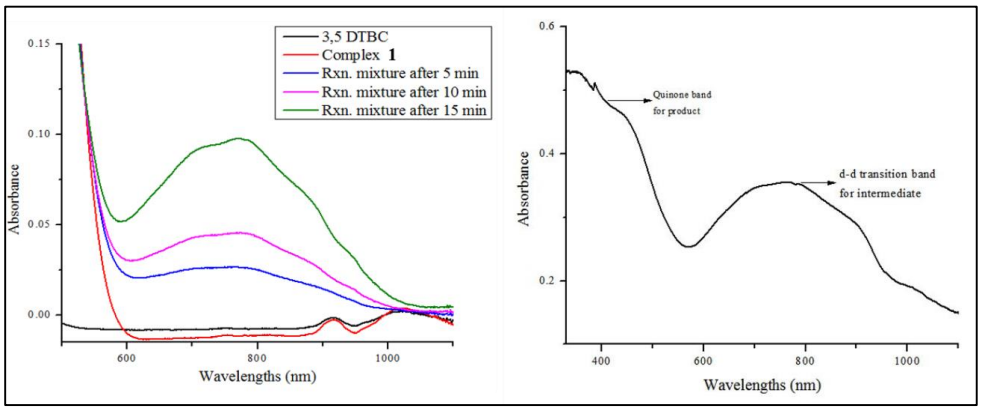

Figure 2. 22. *(Left) Change in d-d transition band of Ni(II) with time upon reaction with 3,5 DTBC. (Right) After 35min of reaction showing both species (1. Quinone band ≈ 400 nm for product and 2. d-d transition band for complex-substrate aggregate) in solutions.*

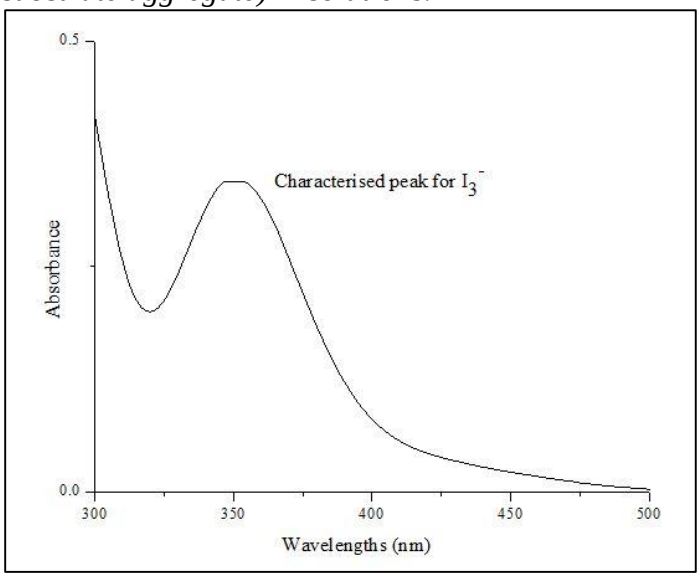

Figure 2. 23. *Characterized peak for I^{3-} for qualitative detection of H_2O_2 during catalytic oxidation process.*

With the help of the all above experiments hereby it is proposed that the oxidation process is occurring in a radical pathway and possibly through a pentacordinated intermediate as represented in Scheme 2.2. According to the reported generalized catecholase reaction mechanism [24] electron transfer is mainly facilitated by metal center and then further delocalized via C=N bond of

metal Schiff-base complex to the adjacent conjugate system. In the present case complex **1** shows better catecholase activity than **2** may due to the more delocalization of electrons along the conjugated aromatic ring via C=N in **1**. All the obtained kinetic parameters are presented in Table 2.7.

Table 2. 7. *Table for various kinetic parameter of catecholase activity.*

Complex	**Catalyst Conc. (M)**	**V_{max} (M min^{-1})**	**Std. Error**	**K_M(M)**	**Std. Error**	**K_{cat} / T.O.N (h^{-1})**
1	0.0002	0.02671	3.4×10^{-4}	0.08335	0.00283	8.0×10^{3}
2	0.0001	0.00455	2.8×10^{-4}	0.00158	3.7×10^{-4}	2.7×10^{3}

2.4 Conclusions

In conclusion two new square planar nickel complexes $[Ni(L^1)]ClO_4$ **(1)** and $[Ni(L^2)]ClO_4$ **(2)** with Schiff base ligands **HL^1** and **HL^2** have been synthesized and characterized. Two more octahedral complexes were generated with combination of thiocyanate ion and **HL^1** and DMSO and **HL^2**, respectively where the Schiff-base ligand gets hydrolyzed and the resultant precursor amines takes up a chair conformation to act as bidentate ligand to furnish $[Ni(SCN)_3(CH_3OH)(aminoethylpiperazineH)]$ **(3)** and $[Ni(DMSO)_4(aminoethylpiperazineH)](ClO_4)_3$ **(4)** where the secondary nitrogen atom in piperazinyl ring remains protonated and staying away from coordination. All the complexes though primarily mononuclear in nature have shown complex hydrogen bonded network in three dimensions Complex **1** showed strong interaction with DNA in both UV-visible absorption studies and competitive binding experiment in presence of ethidium bromide. The Scatchard plot gives a binding constant of 5.675 X 10^3 M^{-1} for compound **1** and 2.340 X10^3 M^{-1} for compound **2**. The interaction of compound **1** with albumin protein show intense interaction between metal complex and protein with very high fluorescence quenching. The Stern–Volmer quenching constant value obtained was to the tune of 10^{13} M^{-1} indicates that both static and dynamic quenching occurring simultaneously. The binding constant value obtained particularly for **1**-HSA complex is exceptionally high and the number of binding site obtained

was found to be almost equals to two. Moderate interaction is also detected between the complex **2** and BSA and HSA with reasonable values of different kinetic parameters. This interaction gains further support from the data obtained from CD spectra of albumin proteins in presence of metal complexes **1** and **2**. Apart from the above mentioned interaction with biomolecules both the complexes **1** and **2** exhibited promising catecholase like activity with TON value to the order of $10^3\ h^{-1}$.

2.5 References

[1]. Tietze, D.,Tischler, M.,Voigt, S.,Imhof, D.,Ohlenschläger, O.,Görlach, M.,Buntkowsky, G. (2010), Development of a Functional cis-Prolyl Bond Biomimetic and Mechanistic Implications for Nickel Superoxide Dismutase, Chemistry – A European Journal, 16, 7572-7578.(DOI: 10.1002/chem.200903306)

[2]. Barnett, S. M.,Goldberg, K. I.,Mayer, J. M. (2012), A soluble copper–bipyridine water-oxidation electrocatalyst, Nat Chem, 4, 498-502.(DOI: 10.1038/nchem.1350)

[3]. Shaik, S. (2010), Biomimetic chemistry: Iron opens up to high activity, Nat Chem, 2, 347-349.(DOI: 10.1038/nchem.638)

[4]. Mukherjee, A., (2010), Biomimetics Learning from Nature.InTech.

[5]. Wigington, B. N.,Drummond, M. L.,Cundari, T. R.,Thorn, D. L.,Hanson, S. K.,Scott, S. L. (2012), A Biomimetic Pathway for Vanadium-Catalyzed Aerobic Oxidation of Alcohols: Evidence for a Base-Assisted Dehydrogenation Mechanism, Chemistry – A European Journal, 18, 14981-14988.(DOI: 10.1002/chem.201202499)

[6]. Meunier, B., (2000), Biomimetic oxidations catalyzed by transition metal complexes.Imperial college press, London.

[7]. Boerner, L. J. K.,Zaleski, J. M. (2005), Metal complex–DNA interactions: from transcription inhibition to photoactivated cleavage, Current Opinion in Chemical Biology, 9, 135-144.(DOI: 10.1016/j.cbpa.2005.02.010)

[8]. Silveira, V. C.,Abbott, M. P.,Cavicchioli, M.,Goncalves, M. B.,Petrilli, H. M.,de Rezende, L.,Amaral, A. T.,Fonseca, D. E. P.,Caramori, G. F.,da Costa Ferreira, A. M. (2013), Peculiar reactivity of a di-imine copper(II) complex regarding its binding to albumin protein, Dalton Transactions, 42, 6386-6396.(DOI: 10.1039/C3DT00108C)

[9]. Patra, A.,Sen, T. K.,Ghorai, A.,Musie, G. T.,Mandal, S. K.,Ghosh, U.,Bera, M. (2013), Synthesis, Structure, Spectroscopic Characterization, and Protein Binding Affinity of New Water-Soluble Hetero- and Homometallic Tetranuclear $[Cu^{II}_2Zn^{II}_2]$ and $[Cu^{II}_4]$ Clusters, Inorganic Chemistry, 52, 2880-2890.(DOI: 10.1021/ic302099y)

[10]. Li, X.-W.,Tao, L.,Li, Y.-T.,Wu, Z.-Y.,Yan, C.-W. (2012), Bimetallic complexes constructed from asymmetrical N,N′-bis(substituted)-oxamide: Cytotoxicities, and reactivities towards DNA and protein, European Journal of Medicinal Chemistry, 54, 697-708.(DOI: 10.1016/j.ejmech.2012.06.022)

[11]. Kalaivani, P.,Saranya, S.,Poornima, P.,Prabhakaran, R.,Dallemer, F.,Vijaya Padma, V.,Natarajan, K. (2014), Biological evaluation of new nickel(II) metallates: Synthesis, DNA/protein binding and mitochondrial mediated apoptosis in human lung cancer cells (A549) via ROS hypergeneration and depletion of cellular antioxidant pool, European Journal of Medicinal Chemistry, 82, 584-599.(DOI: 10.1016/j.ejmech.2014.05.075)

[12]. Lauria, A.,Bonsignore, R.,Terenzi, A.,Spinello, A.,Giannici, F.,Longo, A.,Almerico, A. M.,Barone, G. (2014), Nickel(II), copper(II) and zinc(II) metallo-intercalators: structural details of the DNA-binding by a combined experimental and computational investigation, Dalton Transactions, 43, 6108-6119.(DOI: 10.1039/C3DT53066C)

[13]. Bal, W.,Lukszo, J.,Kasprzak, K. S. (1997), Mediation of Oxidative DNA Damage by Nickel(II) and Copper(II) Complexes with the N-Terminal Sequence of Human Protamine HP2, Chemical Research in Toxicology, 10, 915-921.(DOI: 10.1021/tx970029p)

[14]. li, P.,Niu, M.,Hong, M.,Cheng, S.,Dou, J. (2014), Effect of structure and composition of nickel(II) complexes with salicylidene Schiff base ligands on

their DNA/protein interaction and cytotoxicity, Journal of Inorganic Biochemistry, 137, 101-108.(DOI: 10.1016/j.jinorgbio.2014.04.005)

[15]. Le, F.,Sun, D.,Liu, D.,Zheng, C.,Liu, Y.,Liu, J. (2013), Stabilization of G-quadruplex DNA and antitumor activity by different structures of nickel (II) complexes, Inorganic Chemistry Communications, 38, 20-27.(DOI: 10.1016/j.inoche.2013.09.060)

[16]. Krishnamoorthy, P.,Sathyadevi, P.,Butorac, R. R.,Cowley, A. H.,Bhuvanesh, N. S. P.,Dharmaraj, N. (2012), Variation in the biomolecular interactions of nickel(II) hydrazone complexes upon tuning the hydrazide fragment, Dalton Transactions, 41, 6842-6854.(DOI: 10.1039/C2DT30121K)

[17]. Ramachandran, E.,Raja, D. S.,Mike, J. L.,Wagner, T. R.,Zeller, M.,Natarajan, K. (2012), Evaluation on the role of terminal N-substitution in 6-methoxy-2-oxo-1,2-dihydroquinoline-3-carbaldehyde thiosemicarbazones on the biological properties of new water-soluble nickel(II) complexes, RSC Advances, 2, 8515-8525.(doi: 10.1039/C2RA21199H)

[18]. Krishnamoorthy, P.,Sathyadevi, P.,Butorac, R. R.,Cowley, A. H.,Bhuvanesh, N. S. P.,Dharmaraj, N. (2012), Copper(I) and nickel(II) complexes with 1 : 1 vs. 1 : 2 coordination of ferrocenyl hydrazone ligands: Do the geometry and composition of complexes affect DNA binding/cleavage, protein binding, antioxidant and cytotoxic activities?, Dalton Transactions, 41, 4423-4436.(doi: 10.1039/C2DT11938B)

[19]. Basu, A.,Thiyagarajan, D.,Kar, C.,Ramesh, A.,Das, G. (2013), Synthesis, crystal structure and bio-macromolecular interaction studies of pyridine-based thiosemicarbazone and its Ni(II) and Cu(II) complexes, RSC Advances, 3, 14088-14098.(doi: 10.1039/C3RA40904J)

[20]. Chattopadhyay, T.,Mukherjee, M.,Mondal, A.,Maiti, P.,Banerjee, A.,Banu, K. S.,Bhattacharya, S.,Roy, B.,Chattopadhyay, D. J.,Mondal, T. K.,Nethaji, M.,Zangrando, E.,Das, D. (2010), A Unique Nickel System having Versatile Catalytic Activity of Biological Significance, Inorganic Chemistry, 49, 3121-3129.(doi: 10.1021/ic901546t)

[21]. Biswas, A.,Das, L. K.,Drew, M. G. B.,Aromí, G.,Gamez, P.,Ghosh, A. (2012), Synthesis, Crystal Structures, Magnetic Properties and Catecholase Activity of Double Phenoxido-Bridged Penta-Coordinated Dinuclear Nickel(II) Complexes Derived from Reduced Schiff-Base Ligands: Mechanistic Inference of Catecholase Activity, Inorganic Chemistry, 51, 7993-8001.(doi: 10.1021/ic202748m)

[22]. Das, L. K.,Biswas, A.,Kinyon, J. S.,Dalal, N. S.,Zhou, H.,Ghosh, A. (2013), Di-, Tri-, and Tetranuclear Nickel(II) Complexes with Oximato Bridges: Magnetism and Catecholase-like Activity of Two Tetranuclear Complexes Possessing Rhombic Topology, Inorganic Chemistry, 52, 11744-11757.(doi: 10.1021/ic401020m)

[23]. Ghosh, T.,Adhikary, J.,Chakraborty, P.,Sukul, P. K.,Jana, M. S.,Mondal, T. K.,Zangrando, E.,Das, D. (2014), A radical pathway in catecholase activity with nickel(ii) complexes of phenol based "end-off" compartmental ligands, Dalton Transactions, 43, 841-852.(doi: 10.1039/C3DT51419F)

[24]. Adhikary, J.,Chakraborty, P.,Das, S.,Chattopadhyay, T.,Bauzá, A.,Chattopadhyay, S. K.,Ghosh, B.,Mautner, F. A.,Frontera, A.,Das, D. (2013), A Combined Experimental and Theoretical Investigation on the Role of Halide Ligands on the Catecholase-like Activity of Mononuclear Nickel(II) Complexes with a Phenol-Based Tridentate Ligand, Inorganic Chemistry, 52, 13442-13452.(doi: 10.1021/ic401819t)

[25]. Guha, A.,Banu, K. S.,Das, S.,Chattopadhyay, T.,Sanyal, R.,Zangrando, E.,Das, D. (2013), A series of mononuclear nickel(II) complexes of Schiff-base ligands having N,N,O- and N,N,N-donor sites: Syntheses, crystal structures, solid state thermal property and catecholase-like activity, Polyhedron, 52, 669-678.(doi: 10.1016/j.poly.2012.07.088)

[26]. Sheldrick, G. (2008), A short history of SHELX, Acta Crystallographica Section A, 64, 112-122.(doi: doi:10.1107/S0108767307043930)

[27]. Faulkner, W. R.,Rostek, J. C. (1990), Eur. Pat. Appl, EP 399986 A1 19901128.

[28]. Naiya, S.,Sarkar, B.,Song, Y.,Ianelli, S.,Drew, M. G. B.,Ghosh, A. (2010), Carbonyl compound dependent hydrolysis of mono-condensed Schiff bases: A trinuclear Schiff base complex and a mononuclear mixed-ligand ternary complex of copper(II), Inorganica Chimica Acta, 363, 2488-2495.(doi: 10.1016/j.ica.2010.04.010)

[29]. Mukhopadhyay, S.,Mandal, D.,Ghosh, D.,Goldberg, I.,Chaudhury, M. (2003), Equilibrium Studies in Solution Involving Nickel(II) Complexes of Flexidentate Schiff Base Ligands: Isolation and Structural Characterization of the Planar Red and Octahedral Green Species Involved in the Equilibrium, Inorganic Chemistry, 42, 8439-8445.(doi: 10.1021/ic0346174)

[30]. Nakamoto, K., (2009), Infrared and Raman Spectra of Inorganic and Coordination Compounds, Theory and Applications in Inorganic Chemistry.6th ed. John Wiley & Sons, Inc.: Hoboken, New Jersey.

[31]. Garwood, G.,Condrate, R. (1978), The IR spectra of dimethyl sulphoxide adsorbed on several cation-substituted montmorillonites, Clays Clay Miner., 26, 273.

[32]. Krishnamoorthy, P.,Sathyadevi, P.,Cowley, A. H.,Butorac, R. R.,Dharmaraj, N. (2011), Evaluation of DNA binding, DNA cleavage, protein binding and in vitro cytotoxic activities of bivalent transition metal hydrazone complexes, European Journal of Medicinal Chemistry, 46, 3376-3387.(doi: 10.1016/j.ejmech.2011.05.001)

[33]. Lin, S.,Wrobleski, S. T.,Hynes Jr, J.,Pitt, S.,Zhang, R.,Fan, Y.,Doweyko, A. M.,Kish, K. F.,Sack, J. S.,Malley, M. F.,Kiefer, S. E.,Newitt, J. A.,McKinnon, M.,Trzaskos, J.,Barrish, J. C.,Dodd, J. H.,Schieven, G. L.,Leftheris, K. (2010), Utilization of a nitrogen–sulfur nonbonding interaction in the design of new 2-aminothiazol-5-yl-pyrimidines as p38α MAP kinase inhibitors, Bioorganic & Medicinal Chemistry Letters, 20, 5864-5868.(doi: 10.1016/j.bmcl.2010.07.102)

[34]. Li, X.-W.,Li, X.-J.,Li, Y.-T.,Wu, Z.-Y.,Yan, C.-W. (2013), Syntheses and structures of new trimetallic complexes bridged by N-(5-chloro-2-hydroxyphenyl)-N′-[3-(dimethylamino)propyl]oxamide: Cytotoxic activities,

and reactivities towards DNA and protein, Journal of Photochemistry and Photobiology B: Biology, 118, 22-32.(doi: 10.1016/j.jphotobiol.2012.10.009)

[35]. Ray, A.,Koley Seth, B.,Pal, U.,Basu, S. (2012), Nickel(II)-Schiff base complex recognizing domain II of bovine and human serum albumin: Spectroscopic and docking studies, Spectrochimica Acta Part A: Molecular and Biomolecular Spectroscopy, 92, 164-174.(doi: 10.1016/j.saa.2012.02.060)

[36]. Li, D.,Zhu, M.,Xu, C.,Ji, B. (2011), Characterization of the baicalein–bovine serum albumin complex without or with Cu2+or Fe3+ by spectroscopic approaches, European Journal of Medicinal Chemistry, 46, 588-599.(doi: 10.1016/j.ejmech.2010.11.038)

[37]. Chatterjee, T.,Pal, A.,Dey, S.,Chatterjee, B. K.,Chakrabarti, P. (2012), Interaction of Virstatin with Human Serum Albumin: Spectroscopic Analysis and Molecular Modeling, PLOS ONE, 7, e37468.(doi: 10.1371/journal.pone.0037468)

[38]. Louis-Jeune, C.,Andrade-Navarro, M. A.,Perez-Iratxeta, C. (2012), Prediction of protein secondary structure from circular dichroism using theoretically derived spectra, Proteins: Structure, Function, and Bioinformatics, 80, 374-381.(doi: 10.1002/prot.23188)

[39]. Dey, S. K.,Mukherjee, A. (2013), Zero-Order Catechol Oxidase Activity by a Mononuclear Manganese(III) Complex Showing High Turnover Comparable to Catechol Oxidase Enzyme, ChemCatChem, 5, 3533-3537.(doi: 10.1002/cctc.201300596)

[40]. Jana, A.,Aliaga-Alcalde, N.,Ruiz, E.,Mohanta, S. (2013), Structures, Magnetochemistry, Spectroscopy, Theoretical Study, and Catechol Oxidase Activity of Dinuclear and Dimer-of-Dinuclear Mixed-Valence $Mn^{III}Mn^{II}$ Complexes Derived from a Macrocyclic Ligand, Inorganic Chemistry, 52, 7732-7746.(doi: 10.1021/ic400916h)

[41]. Sarkar, S.,Majumder, S.,Sasmal, S.,Carrella, L.,Rentschler, E.,Mohanta, S. (2013), Triple bridged μ-phenoxo-bis(μ-carboxylate) and double bridged μ-phenoxo-μ1,1-azide/μ-methoxide dicopper(II) complexes: Syntheses,

structures, magnetochemistry, spectroscopy and catecholase activity, Polyhedron, 50, 270-282.(doi: 10.1016/j.poly.2012.10.050)

[42]. Banu, K. S.,Chattopadhyay, T.,Banerjee, A.,Bhattacharya, S.,Suresh, E.,Nethaji, M.,Zangrando, E.,Das, D. (2008), Catechol Oxidase Activity of a Series of New Dinuclear Copper(II) Complexes with 3,5-DTBC and TCC as Substrates: Syntheses, X-ray Crystal Structures, Spectroscopic Characterization of the Adducts and Kinetic Studies, Inorganic Chemistry, 47, 7083-7093.(doi: 10.1021/ic701332w)

[43]. Gatteschi, D.,Scozzafava, A. (1977), Single crystal polarized electronic spectra of a five-coordinate macrocyclic complex of nickel(II), Inorganica Chimica Acta, 21, 223-227.(doi: 10.1016/S0020-1693(00)86265-9)

[44]. Marion, R.,Muthusamy, G.,Geneste, F. (2012), Continuous flow catalysis with a biomimetic copper(II) complex covalently immobilized on graphite felt, Journal of Catalysis, 286, 266-272.(doi: 10.1016/j.jcat.2011.11.011)

Chapter 3

Copper complexes with flexible piperazinyl arm: nuclearity driven catecholase activity and interactions with biomolecules

Chapter 3

Copper complexes with flexible piperazinyl arm: nuclearity driven catecholase activity and interactions with biomolecules

3.1 Introduction

Copper has been reported as a bio-essential element for a long time [1] but its biological importance is only getting explored in the past few decades during the development of bioinorganic chemistry and successful studies of interaction of model complexes with various bio-macromolecules.[2-5] Copper based enzymes which are capable of possessing molecular oxygen at ambient condition have received a considerable attention to the scientists to develop such biologically active model systems which are able to oxidize catechol moiety to its corresponding diquinones following an enzyme catalysis pathway [6]. These oxidation reactions are also having great role in medicinal aspect for the determination of the hormonally active catecholamines: adrenaline, noradrenaline and l-dopa.[7, 8] Apart from studying different biological processes induced by copper, many new molecules have been also developed over the years showing interesting properties like antibacterial, antifungal, antimicrobial and anticancer/antiproliferative activity where the copper center performs a pivotal role in terms of structural organization and overall functionality.[9-12] Furthermore, interactions of copper complexes with DNA and proteins are current key research areas as it has enough potential for the development of new therapeutic agents particularly showing anti-tumor properties and the possibility of transporting these molecules throughout the physiological system *via* protein binding.[13-15] As copper complexes are capable of binding and cleaving DNA selectively under physiological conditions without using any external reagent thus metal based pseudonucleases generate a new era in the field of nucleic acid chemistry for their versatile use in foot

printing, sequence-specific binding to nucleic acids, and as new structural probes and therapeutic agents.[16, 17]

In the previous chapter synthesis of two new Schiff base ligands **HL^1** and **HL^2** [**HL^1** = 1-phenyl-3-((2-(piperazin-4-yl)ethyl)imino)but-1-en-1-ol and **HL^2** = 4-((2-(piperazin-1-yl)ethyl)imino)pent-2-en-2-ol] with a flexible piperazinyl ring which can take either chair or boat form during complexation has been discussed.[18] It has been also observed that during complexation with nickel ion both the ligands prefer boat form of flexible piperazinyl moiety to act as tetradentate ligand to fulfill the square planar geometry surrounding nickel center. Moreover, the complexes have shown interesting DNA and protein binding activities and quite high catalytic activities towards catechol oxidation. However, after several attempts it was observed that to synthesize any nickel complex of the same ligands where the piperazinyl ring has taken chair form is quite impossible in such system. In an endeavor to explore the probable influence of the ligand on similar properties when the piperazinyl ring is adopting preferentially chair conformation (where extra positive ligand in the ligand backbone can have profound influence on catecholase like activity) [19] those Schiff base ligands have been reacted with copper salts to obtain two mononuclear and one dinuclear copper complexes namely $[Cu(HL^1)(pyridine)(H_2O)](ClO_4)_2.2MeOH$ **(5)**, $[Cu_2(HL^1)_2(NO_3)_2](NO_3)_2.3H_2O$ **(6)** and $[Cu(HL^2)(NO_3)_2].MeCN$ **(7)**.
Interaction of complexes with DNA applying both binding and cleavage experiment are carried out. Affinity of complexes towards BSA protein is also determined. Moreover, complexes were also investigated for possible catecholase like activity. Furthermore, the Schiff bases and copper (II) complexes were screened for their antibacterial activity against Methicillin-Resistant nosocomial Gram-positive bacteria *Staphylococcus aureus* (MRSA). Interestingly all the experimental results indicate that dinuclear copper complex **6** is more active than other two mononuclear complexes towards DNA binding and cleavage, BSA binding and catechol oxidation. Furthermore, compound **6** has also shown considerable activity towards *Staphylococcus aureus* as a new

promising compound, exhibiting high antimicrobial activity as per other reported copper complexes in literature.[20, 21] Computational studies for DNA bindings and catechol oxidations are performed which also reflects the similar trend of activity order among the Cu(II) complexes as observed in experimental condition.

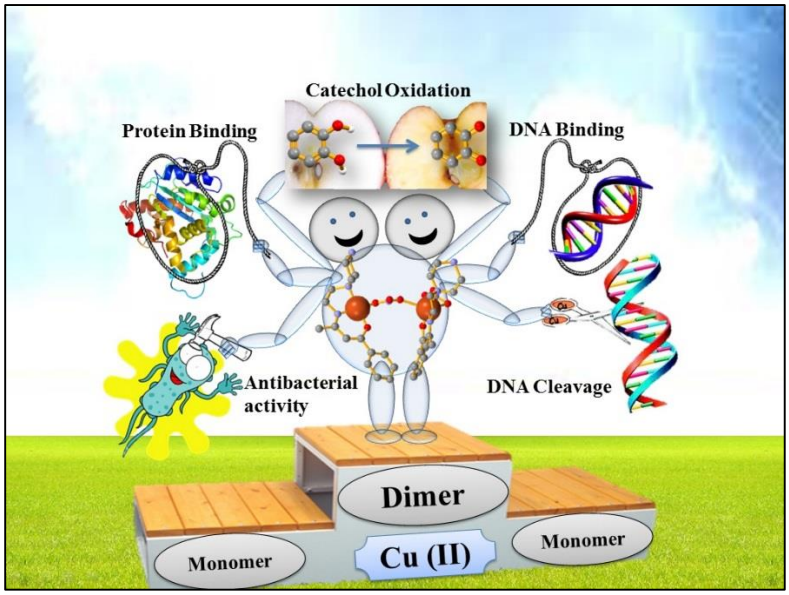

Figure 3. 1*. Pictorial representation to show higher activity of dinuclear complex than two monomer complexes.*

3.2 Experimental section

3.2.1 Materials and methods

All the chemical reagents required were purchased from sigma and used without further purification. The specifications of all the instruments used for analysis purpose were same as described in the section 2.2.1 of the previous chapter 2. Ligands **HL^1** and **HL^2** were prepared following reported methods [18].

3.2.2 X-ray crystallography

Single crystal X-ray structural studies of **5, 6** and **7** were performed following the similar protocol as mentioned in the section 2.2.2 of previous chapter 2. The structures were solved by direct methods using SHELXS-97 and refined by full

matrix least- squares with SHELXL-97, refining on F^2.[22] The crystal and refinement data are summarized in Table 3.1

Table 3. 1. *Crystallographic data and structure refinement parameters for* ***5****,* ***6****, and* ***7****.*

Complex	**5**	**6**	**7**
Empirical Formula	$C_{23}H_{29}Cl_2CuN_4O_{12}$	$C_{32}H_{44}Cu_2N_{10}O_{16}$	$C_{13}H_{23}CuN_6O_7$
Formula weight	687.94	951.85	438.91
Crystal system	Monoclinic	Monoclinic	Monoclinic
Space group	P 21/c	I 2/a	P 21/n
a (Å)	12.8829(4)	9.9050(2)	10.5658(2)
b (Å)	9.4603(2)	16.6715(3)	14.6046(2)
c (Å)	25.0205(5)	52.6457(10)	12.5972(2)
α (°)	90	90	90
β (°)	99.087(3)	94.498(2)	94.980(2)
γ (°)	90	90	90
V ($Å^3$)	3011.13(13)	8666.7(3)	1936.53(5)
λ (Å)	0.71073	1.5418	0.71073
ρ_{calcd} (mg m^{-3})	1.518	1.459	1.505
Z	4	8	4
T (K)	150(2)	150(2)	150(2)
μ (mm^{-1})	0.968	1.887	1.175
F(0 0 0)	1416	3936	912
Crystal size (mm^3)	0.23 × 0.16 × 0.13	0.23 × 0.18 × 0.13	0.33 × 0.26 × 0.21
θ ranges (°)	3.01 - 25.00	3.37 - 50.00	2.98 - 25.00
h/k/l	-15,15/-10,11/-29,29	-9,8/-16,16/-52,52	-12,12/-17,17/-14,14
Reflections collected	23960	19630	15337
Independent reflections	5289	4457	3406
T_{max} and T_{min}	0.8845 and 0.8080	0.7915 and 0.6708	0.7904 and 0.6978
Data/restraints/parameters	5289 / 2 / 388	4457 / 0 / 556	3406 / 0 / 251
Goodness-of-fit	1.088	1.056	1.038
Final R indices [I > 2σ(I)]	R1 = 0.0537, wR2 = 0.1441	R1 = 0.0782, wR2 = 0.2254	R1 = 0.0633, wR2= 0.1751
R indices (all data)	R1 = 0.0628, wR2 = 0.1517	R1 = 0.0831, wR2 = 0.2329	R1 = 0.0685, wR2= 0.1805
Largest peak and hole (e $Å^{-3}$)	0.714 and -0.517	1.601 and -0.599	2.870 and -1.378

3.2.3 Synthesis of $[Cu(HL^1)(Pyridine)(H_2O)](ClO_4)_2.2MeOH$ (5)

15 mL of methanolic solution containing **HL^1** (0.14 g, 0.5 mmol) and $Cu(ClO_4)_2.6H_2O$ (0.18 g, 0.5 mmol) was stirred at room temp for 1 h after adding 1 drop of pyridine into that reaction mixture and resulting sky blue coloured solution was concentrated by evaporating the solvent. Finally after 2 or 3 days red needle shaped crystals were obtained from the reaction mixture after layering the mother liquor with diethyl ether. Yield: 78%. Anal. Calcd. (%) : $C_{23}H_{38}Cl_2CuN_4O_{12}$ C, 39.69; H, 5.50; N, 8.05. Found (%): C, 39.71; H, 5.11; N, 8.32. $[C_{16}H_{22}CuN_3O]^+$ (m/z) calculated – 335.11 $(M)^+$; obtained – 335.11 $(M)^+$. Selected IR on KBr (ν/cm^{-1}): 1597 (–C=N), 1097(ClO_4^-).

3.2.4 Synthesis of $[Cu_2(HL^1)_2(NO_3)_2](NO_3)_2.3H_2O$ (6)

5 mL of methanolic solution containing **HL^1** (0.14 g, 0.5 mmol) was added drop wise to a 10 mL solution of $Cu(NO_3)_2.3H_2O$ (0.12 g, 0.5 mmol) and the resultant mixture was stirred at room temp for 1hr and then the solution was concentrated by evaporating the solvent. Layering of the reaction mixture with diethyl ether furnished suitable crystal after few days. Yield: 82%. Anal. Calcd. (%) : $C_{32}H_{46}Cu_2N_{10}O_{14}$ C, 41.69; H, 5.03; N, 15.19. Found (%): C, 41.71; H, 5.12; N, 15.15. $[C_{32}H_{44}Cu_2N_7O_5]^+$ (m/z) calculated – 732.20 $(M)^+$; obtained – 732.17 $(M)^+$. Selected IR on KBr (ν/cm^{-1}): 1605 (–C=N), 1342 (NO_3^-).

3.2.5 Synthesis of $[Cu(HL^2)(NO_3)_2]$.MeCN (7)

At first 15 mL of methanolic solution containing **HL^2** (0.11 g, 0.5 mmol) and $Cu(NO_3)_2.3H_2O$ (0.12 g, 0.5 mmol) was stirred at room temp for 1h. Then after evaporating the solvent, the sticky compound obtained was dissolved in MeCN. Finally after 6 or 7 days green block shaped crystal of **7** was obtained from this solution after layering with diethyl ether. Yield: 55%. Anal. Calcd. (%) : $C_{13}H_{24}CuN_6O_7$ C, 35.49; H, 5.50; N, 19.10. Found (%): C, 35.12; H, 5.59; N, 18.91. $[C_{11}H_{20}CuN_3O]^+$ (m/z) calculated – 273.09 $(M)^+$; obtained – 273.08 $(M)^+$. Selected IR on KBr (ν/cm^{-1}): 1605 (–C=N), 1342 (NO_3^-).

3.2.6 DNA binding study

ETBr displacement assay for DNA binding study of complexes (**5, 6** and **7**) is measured following the protocol as mentioned in the section 2.2.9 of previous chapter 2.

3.2.7 DNA cleavage experiments

In each experiment, the extent of DNA cleavage was monitored by agarose gel electrophoresis. A solution of 25 µL containing pBR322 DNA (0.25 µg/µL), the metal complexes (50-400 µM), and H_2O_2 (60 µM) was incubated for 1h at 40°C. Subsequently, 2 µL of 6X DNA loading buffer containing 0.25% bromophenol blue, 0.25% xylene cyanol and 60% glycerol was added to the reaction mixture and loaded onto a 1% agarose gel containing 1.0 mg/mL of ethidium bromide. The electrophoresis was performed at 65V for 1.5 h in a TAE buffer. The bands were visualized under UV light and photographed. The cleavage efficiencies were measured by determination of the ability of each complex to convert the supercoiled DNA (SC) to the nicked circular form (NC). After electrophoresis, the proportion of DNA in each fraction was estimated quantitatively on the basis of the band intensities using the BIORAD Gel Documentation System. The intensity of each band relative to that of the plasmid supercoiled form was multiplied by 1.43 to take account of the reduced affinity for ethidium bromide.[23]

3.2.8 Protein binding study

The binding interactions experiments of complexes **5, 6** and **7** with BSA protein were carried out following the protocols as mentioned in the section 2.2.10 of previous chapter 2.

3.2.9 Catecholase activity study

Catecholase like activities of complexes **5**, **6**, and **7** were also studied following the similar procedure as described in the section 2.2.12 of previous chapter 2.

3.2.10 Detection of hydrogen peroxide in the catalytic reactions

Modification of iodometric method as described in the section 2.2.13 of chapter 2, is employed to detect H_2O_2 during the catalytic reaction.

3.2.11 Antimicrobial study

The reference strain MRSA Methicillin-Resistant *Staphylococcus aureus* ATCC® 43300™ was used in this study. The bacterial isolates were streaked from -80ºC stocks into Mueller-Hinton agar (MHA) (Oxoid Ltd., Basingstoke, UK) plates and incubated overnight at 37ºC. From this streaking, one isolated colony was inoculated into 5 mL of Mueller-Hinton broth (MHB) and incubated for a further 18 hours at 37ºC with shaking (approx. 220 rpm). Ligands and complexes were incorporated in the wells and incubated at 37ºC for 18h. After the incubation period being complete, the diameter of the inhibition zone generated by each compound using an antibiogram zone measuring scale was measured (Figure 3.2). From the results obtained **HL^1** and complex **6** were then selected for further experiments.

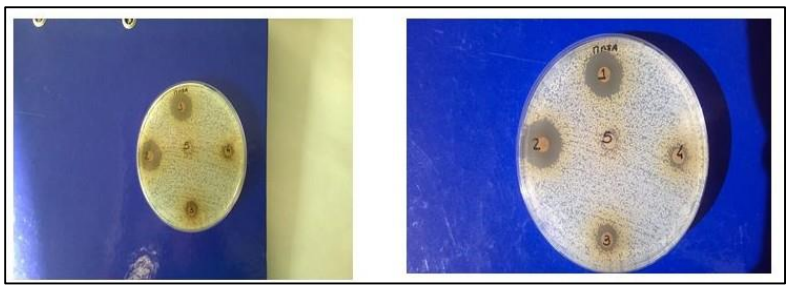

***Figure 3. 2**. Results obtained using ligands **HL^1** (spot 1), **HL^2** (spot 4), Complex **5** (spot 3), Complex **6** (spot 2) and Complex **7** (spot 5) against Staphylococcus aureus (MRSA).*

3.2.12 Antibacterial activity

The antibacterial activity was evaluated by determining the Minimum Inhibitory Concentration (MIC) of the compounds. This was accomplished using the broth microdilution method by following the CLSI guidelines. [24] The MIC, calculated by the dilution factor of the starting concentration, was considered at that concentration of compound where no visible growth was observable. The wells having no growth were plated (5 µl) into MHA-plates and incubated overnight at 37ºC. On the following day, the results were recorded and the

minimum concentration of compound with no growth obtained was considered as the Minimum Bactericidal Concentration (MBC). All experiments were carried out in triplicate in three separate occasions.

3.2.13 Supplementary materials

CCDC 1016329, 1016328, and 1016327 contain the supplementary crystallographic data for **5**, **6** and **7**, respectively. These data can be obtained free of charge via http://www.ccdc.cam.ac.uk/conts/retrieving.html, or from the Cambridge Crystallographic Data Centre, 12 Union Road, Cambridge CB2 1EZ, UK; fax: (+44) 1223-336-033; or e-mail: deposit@ccdc.cam.ac.uk.

3.3 Results and discussions

3.3.1 Syntheses of the complexes

The ligands **HL^1** and **HL^2** are obtained by simple condensation reaction using previously reported methodology describer in earlier chapter [18] with sufficient purity and yield for use without further purification in the synthesis of two mono- and one di- nuclear copper(II) complexes. Complexes **5**, **6** and **7** were synthesized according to Scheme 3.1.

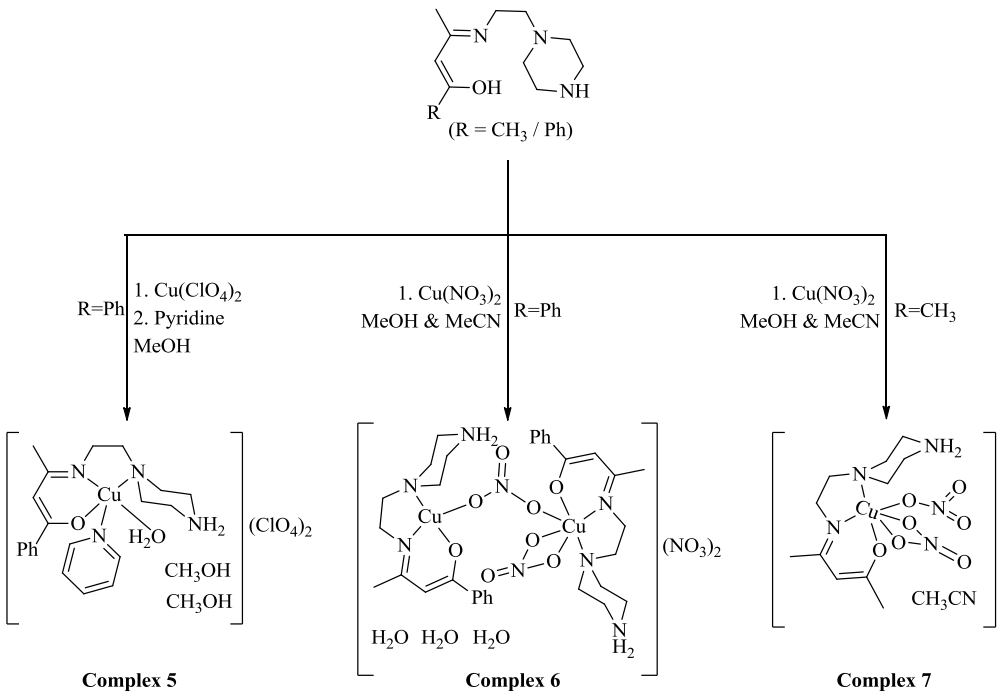

Scheme 3. 1. *Formation of mononuclear and dinuclear metal complexes (**5-7**).*

All the complexes have been characterized by IR and ESI-MS spectroscopy, elemental analysis and single crystal X-ray crystallography. The characteristics band around 1600 cm^{-1} in the IR spectra of all three complexes are assigned for ν(C=N) stretching mode. [25] A strong band around 1100 cm^{-1} in complex **5** indicates the presence of perchlorate counter anion.[25]

Nitrate stretching frequency is observed at the region of 1350-1385 cm^{-1} in IR spectra of both the complexes **6** and **7** respectively. ESI-MS spectra of complex **5** and **6** show molecular ion peak at 335 for $[Cu(L^1)]^+$ and 732 for $[Cu_2(L^1)_2(NO_3)]^+$ respectively (Figure 3.3). Thus a solution state ESI-MS spectrum of complex **6** clearly indicates presence of dimeric species in solution phase. Similarly complex **7** shows molecular ion peak at 273 corresponding to $[Cu(L^2)]^+$ (Figure 3.3). In all of the three cases mono positive molecular ion is getting generated during ESI-MS experiment due to formation of mono anionic Schiff base ligands.

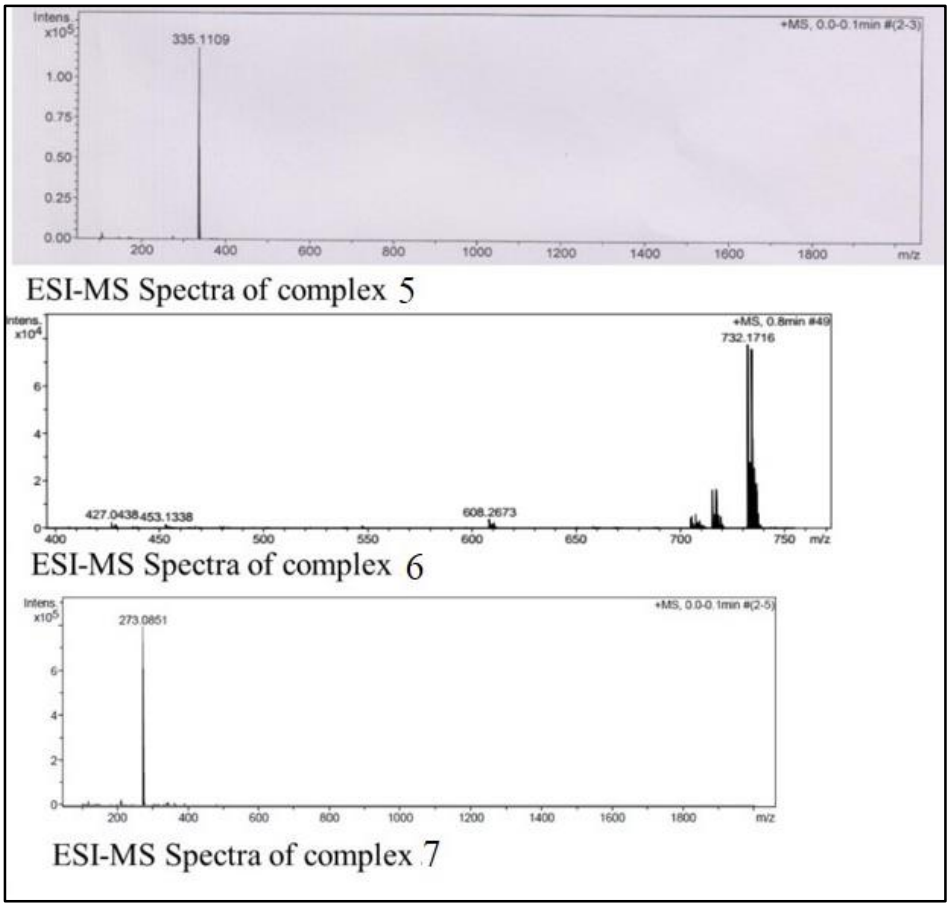

Figure 3. 3. *ESI-MS Spectra of three complexes (**5-7**).*

The electronic spectra of **5-7** (Figure 3.4) have been studied in the solution state using CH_3OH as solvent. The solutions of **5-7** in methanol exhibit absorption in 250-682 nm ranges [**5**: 256, 682 nm; **6**: 250, 291, 336, 617 nm; **7**: 250, 298, 633 nm]. The transition around 600-700 nm corresponds to a d-d transition of copper (II) moiety and band around 300 nm for intramolecular LMCT transition.[26] In case of **5** and **7**, d-d transitions are observed at about 680 and 630 nm respectively which indicate pentacoordinated and hexacoordinated structures around central atom [27, 28] but in case of **6**, it was observed that there was a broad band in the range 530-720nm which may be due to the two different types of Cu(II) centers (tetracoordinated and hexacoordinated) present in solution phase of dimeric complex **6**.[29]

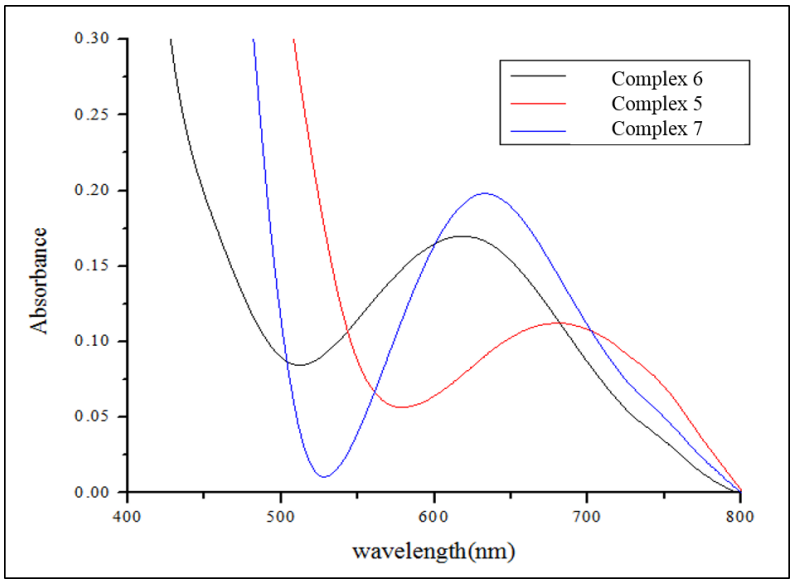

***Figure 3. 4**. UV-Vis Spectra of complexes (**5-7**).*

3.3.2 Crystal structure of complex 5, 6 and 7

Crystal structures of these three complexes portray a wide combination of Cu (II) centered coordination geometry where four (Complex **6)**, five (Complex **5)** and six (Complex **6** and **7**) coordinated copper complexes are formed *via* almost similar type of reaction. In all the complexes, the major coordination bond lengths between Cu atom and N/O-donor centers are within the range of 1.900(5) to 2.423(3) Å (Table 3.2), matches perfectly to earlier report.[30] However, few exceptions are found in the form of Cu(1)-O(8) and Cu(1)-O(4) in complex **6** and Cu(1)-O(3) in complex **7**, which are mainly caused by Jahn-Teller distortion as mentioned in previous report.[31-33]

Table 3. 2.** Selected bond lengths (Å) and bond angles (°) for **5**, **6** and **7

Complex	**5**	**6**	**7**
Cu(1)-O(1)	1.934(2)	1.900(5)	1.921(3)
Cu(1)-N(1)	1.940(3)	2.061(6)	2.075(4)
Cu(1)-N(2)	1.883(2)	1.921(5)	1.921(4)
Cu(1)-O(2)	.....	1.985(4)	2.021(3)
Cu(1)-O(8)	.....	2.586	2.671
Cu(1)-O(4)	.....	2.75	.....
Cu(1)-O(5)	.....	.....	2.423(3)

Cu(2)-O(5)	.....	1.887(5)	.....
Cu(2)-N(5)	.....	1.915(5)	.....
Cu(2)-O(7)	.....	1.975(4)	.....
Cu(2)-N(4)	.....	2.052(5)	.....
Cu(1)-N(4)	2.024(3)	.....	.....
Cu(1)-O(101)	2.265(3)	.....	.....
O(1)-Cu(1)-N(1)	93.50(12)	172.6(2)	178.93(15)
O(1)-Cu(1)-N(4)	85.49(11)	.....	.....
N(1)-Cu(1)-N(2)	83.86(12)	85.2(2)	85.37(15)
N(4)-Cu(1)-N(2)	95.23(12)	.....	.....
O(1)-Cu(1)-O(101)	95.35(11)	.....	.....
N(1)-Cu(1)-O(101)	98.91(13)	.....	.....
N(4)-Cu(1)-O(101)	95.17(12)	.....	.....
N(2)-Cu(1)-O(101)	92.52(12)	.....	.....
N(1)-Cu(1)-N(4)	165.92(13)	.....	.....
O(1)-Cu(1)-N(2)	172.01(12)	94.6(2)	94.46(15)
O(1)-Cu(1)-O(2)	.....	87.44(19)	86.13(13)
N(2)-Cu(1)-O(2)	.....	174.2(2)	173.58(15)
O(2)-Cu(1)-N(1)	.....	93.5(2)	94.16(14)
N(2)-Cu(1)-O(5)	.....	.....	102.15(15)
O(1)-Cu(1)-O(5)	.....	.....	90.32(15)
O(2)-Cu(1)-O(5)	.....	.....	84.23(13)
N(1)-Cu(1)-O(5)	.....	.....	88.68(14)
O(3)-Cu(1)-O(2)	.....	.....	52.83
O(5)-Cu(2)-N(5)	.....	95.1(2)	.....
O(5)-Cu(2)-O(7)	.....	89.77(19)	.....
N(5)-Cu(2)-O(7)	.....	166.0(2)	.....
O(5)-Cu(2)-N(4)	.....	167.1(2)	.....
N(5)-Cu(2)-N(4)	.....	84.4(2)	.....
O(7)-Cu(2)-N(4)	.....	93.80(19)	.....
N(7)-O(2)-Cu(1)	.....	112.7(4)	.....
N(8)-O(7)-Cu(2)	.....	119.0(4)	.....
O(4)-Cu(1)-O(8)	.....	129.27	.....
O(8)-Cu(1)-N(2)	.....	96.01	.....

The mononuclearcomplex **5** crystalizes in the space group $P2_{1/C}$. The central metal atom is coordinated to the tridentate Schiff base ligand **HL^1** and one pyridine and one water molecule to give penta-coordinated square pyramidal geometry (Figure 3.5). N, N, O donor sites of Schiff base **HL^1** and N donor site of pyridine are on the equatorial face of square pyramidal geometry while O donor site from water molecule lies on the axial position of square pyramid. The piperazinyl ring takes the chair conformation where secondary nitrogen atom coordinates one extra proton and stays away from the coordination. The distortion of the coordination geometry of penta-coordinated system can be calculated by the τ_5 value, a reference to describe the degree of distortion for square-pyramid and trigonal-bipyramid [square pyramid, $\tau_5 = 0$; trigonal-bipyramid, $\tau_5 = 1$; $\tau = (\beta - \alpha)/60°$, α and β are the two largest angles around the central atom] [34]. The τ_5 value for complex **5** is 0.101, indicating a distorted square-pyramidal geometry adopted by copper center.

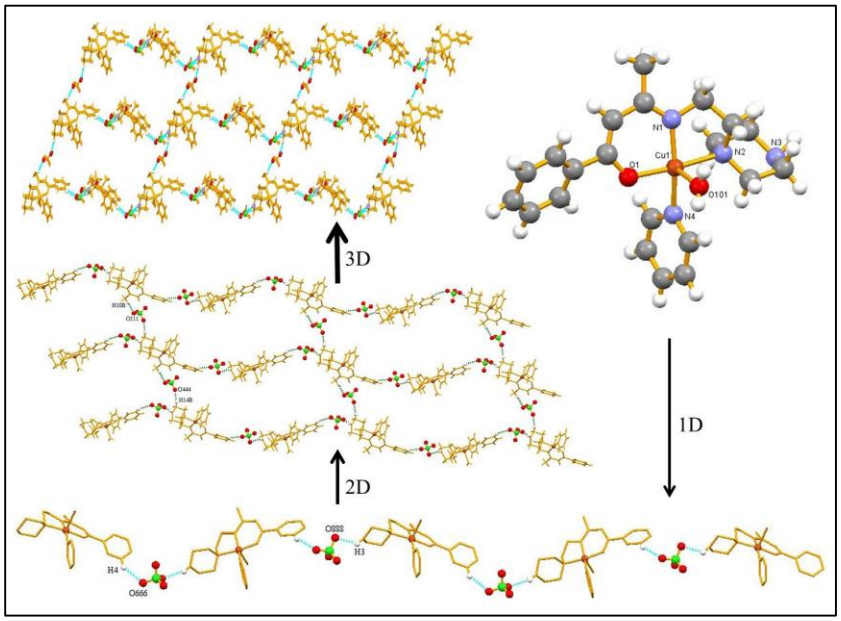

Figure 3. 5. *Monomer unit of complex* ***5*** *and its supra-molecular networks.*

In complex **5**, the average co-ordination bond angle around the Cu center of square pyramidal geometry is around 92° whereas the least bond angle was observed for N(1)–Cu(1)–N(2) (~83°) (Table 3.2) due to the formation of a chelated five membered ring. Furthermore, the independent molecules get connected to each other for making 1D supra-molecular chain like structure

(Figure 3.5) *via* formation of hydrogen bonding (*viz*. C4–H4···O666 and N3–H3···O888) with intermediate perchlorate anion. Each 1D chain is further connected *via* C10–H10B···O111 and C14–H14B···O444 hydrogen bonding network to build a 2D sheet like structure (Figure 3.5). These parallel 2D sheets are also interconnected through C10–H10B···O111 and C14–H14B···O444 to build a three dimensional structure (Figure 3.5).

Complex **6** is binuclear copper complex with space group *I*2/a. Here both the copper centers have different coordination number and geometry. Cu(1) is in six coordinated distorted octahedral geometry while Cu(2) is a four coordinated metal center with square planar geometry (Figure 3.6). This geometry of Cu(2) metal center is further proved by τ_4 index which defines the distortion between a perfect tetrahedron (τ_4 = 1) and a perfect square planar geometry (τ_4 = 0) using the formula: $\tau_4 = [360° - (\alpha + \beta)]/141°$, with α and β (in °) being the two largest angles around the central metal in the complex [35]. The τ_4 value for Cu(1) is 0.190, satisfying a somewhat distorted square planar geometry for this metal center. Though this is relatively an unusual example of metal complex where two different geometrical Cu (II) centers are existing together, but similar reports are available in the literature [31]. The average co-ordination bond angle around Cu(1) center of distorted octahedral geometry is around 93°. Two *trans* angles O(4)–Cu(1)–O(8) (129.27°) and O(4)–Cu(1)–N(2) (134.57°) at Cu(1) deviate extensively from the linearity of a perfect octahedron. As a consequence, Cu(1) reveals a considerably distorted octahedral geometry, which can be attributed to the chelating influence of nitrate ligand [36]. Furthermore, for complex **6**, each individual molecule gets attached with nearby molecules by several hydrogen bonding (*viz*. C6–H6B···O4, C1–H1B···O4, C21–H21B···O3, C19–H19A···O2, C22–H22A···O2, C22–H22A···O8, C20–H20B···O8, C20–H20B···O7, C17–H17B···O6 and C18–H18A···O6) to build a 1D chain (Figure 3.6). Each 1D chain is further connected to other chain by more hydrogen bonding (*viz*. N6–H6···O222, C17–H17A···O111, C19–H19B···O111, C4–H4A···O333, C3–H3B···O333 and N3–H3···O333) with non-coordinated nitrate ion to build a railway track like 2D

supra-molecular network (Figure 3.6). Now 2D network is further expanded through C6–H6A···O3 hydrogen bonding to build a 3D supra-molecular system (Figure 3.6).

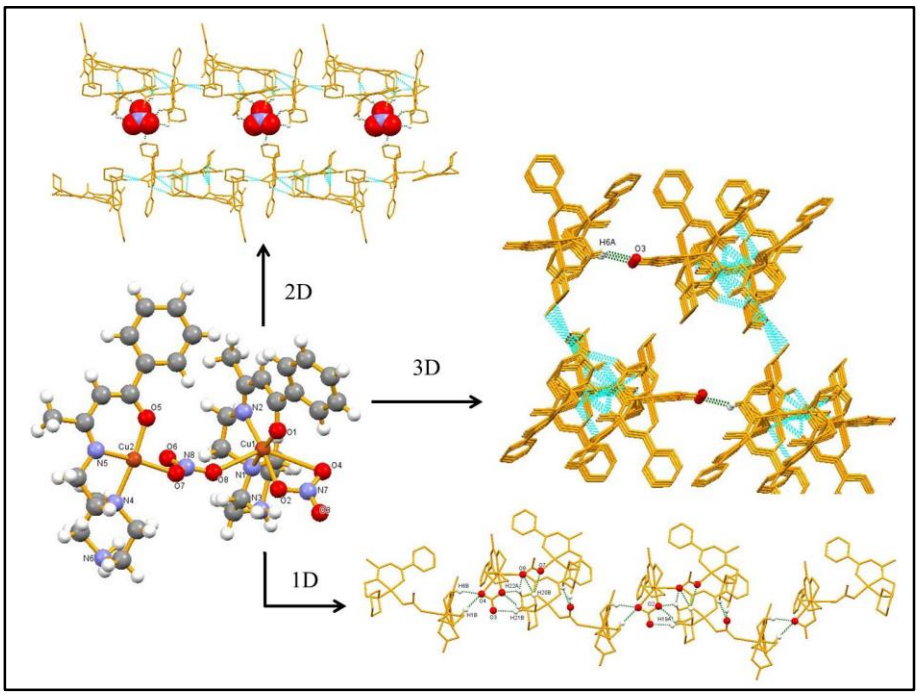

Figure 3. 6. *Dinuclear unit of Complex* ***6*** *and its 1D, 2D and 3D supra-molecular polymeric networks.*

The structure determination of complex **7** which is crystalized in space group *P*21/n, reveals that it consists mononuclear six coordinated copper center with distorted octahedral geometry. The average coordination bond angles around metal center are quite similar as in Cu(1) center of complex **6.** Similarly one *trans* angle O(3)–Cu(1)–O(5) (137.06°) at metal center deviate extensively from the linearity to generate distorted octahedral geometry (Figure 3.7). Hydrogen bonding networks like, N3–N1H···O1, N3– N1H ···O7, C2–H2A···O4 and C3–H3B···O2 play an important role to create a 1D zig-zag supra-molecular network (Figure 3.7). These nearby 1D chains are joined with each other via C6–H6A···O4 and C7– H7A ···O3 hydrogen bonding to generate 2D sheet like structure (Figure 3.7).

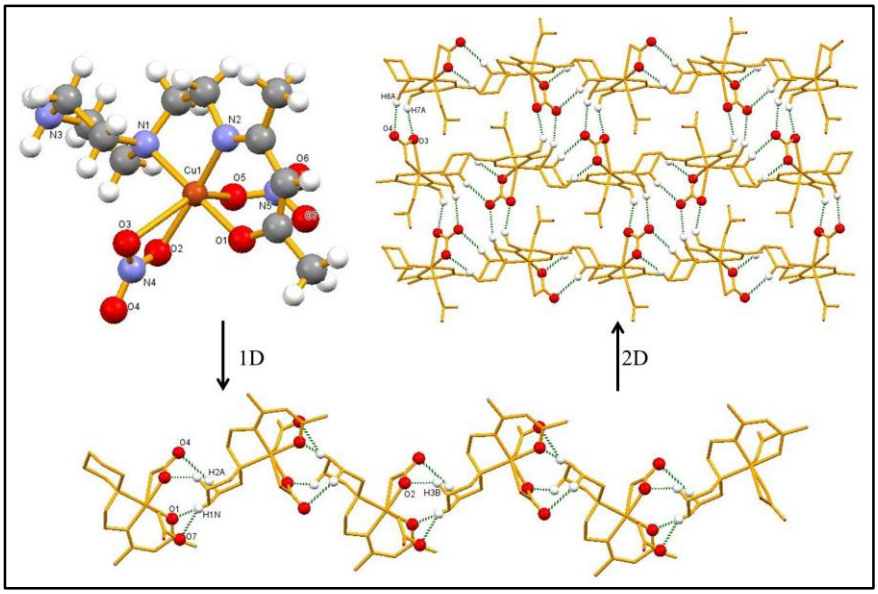

Figure 3. 7*. Monomer unit of complex **7** and its supra-molecular networks.*

3.3.3 Complex-DNA interaction studies

Copper-Schiff base complexes are well known for their interaction with DNA [37-40]. The fluorescence quenching spectra of DNA bound ETBr by complexes **5, 6** and **7** are shown in Figure 3.8. Reduction in fluorescence intensity at 607 nm in all the spectra clearly indicates that ETBr molecules get displaced from DNA by the addition of copper complexes successively. Though these displacement is not so significant but it lies in the range of earlier report.[41] Furthermore, K_{SV} values for complexes **5, 6** and **7** have been found to be 6.2 × 10^2, 1.1 × 10^3 and 7.7 × 10^2 M^{-1}, respectively, which were obtained from the classical Stern–Volmer equation [14].

$$\frac{F_0}{F} = 1 + K_{SV}[Q]$$

Where, F_0 and F are the fluorescence intensity of the ETBr – CT DNA adducts before and after the addition of complexes, K_{SV} is the Stern–Volmer constant, and [Q] is the concentration of the desired complex added. The binding constant (K_a) values obtained from the plot of log[(F_0 − F)/F] vs. log[Q] (from Scatchard equation) [42] (Figure 3.8) were found to be 1.2 × 10^3, 5.5 × 10^4 and 8.5 × 10^2 M^{-1} for complex **5, 6** and **7**, respectively which signifies moderate to weak

binding affinity but comparable with respect to other mono- and dinuclear Schiff base copper systems.[43-48]

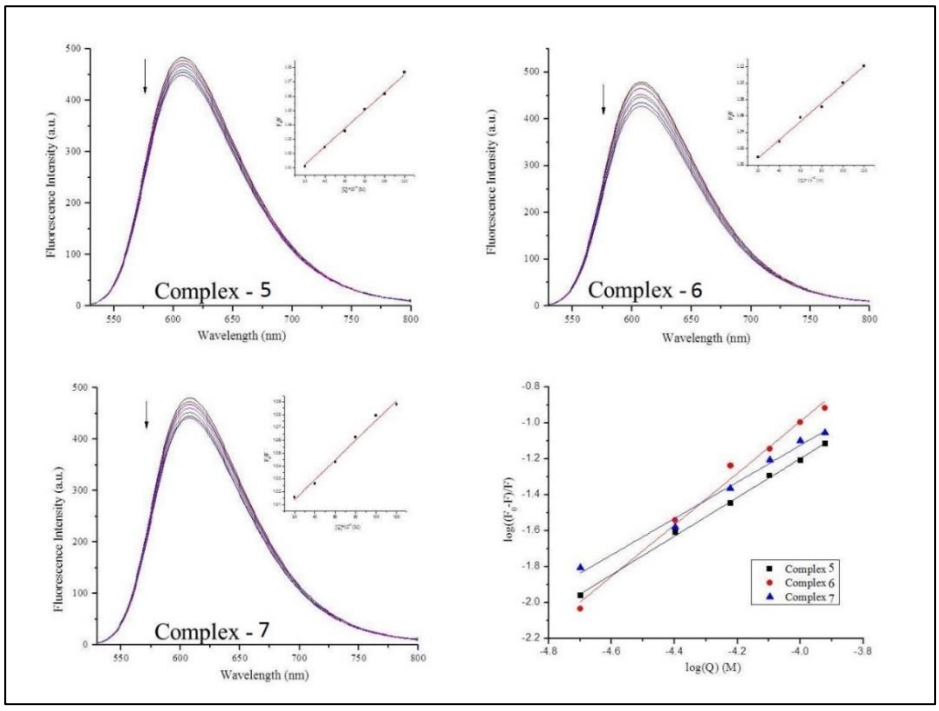

Figure 3. 8. *ETBr displacement assay of complex* ***5-7****. Stern-volmer plot is in inset. Scatchard plot for complex* ***5-7*** *(bottom right).*

This binding constant values indicate that the order of binding affinity of complexes towards DNA (or, ETBr displacement ability) is **6** > **5** > **7**. Probable reason for this phenomenon is may be the charge density. Being neutral in nature and for less conjugative Schiff base moiety in **5,** complex **7** become less active towards DNA while positively charged binuclear copper complex **6** interacts more with DNA. The control assay experiment was also performed using only the Schiff base $\mathbf{HL^1}$ but there was no such observable kind of activity. Furthermore the repeated experiment was performed in case of complex **6** taking 0.5eqv of complex **6** compared to complex **5** and **7** (with same number of copper ions for all the complexes). Still it was observed that nuclearity is playing the crucial role to show higher activity in case of complex **6**.

3.3.4 DNA cleavage studies

The efficiencies by which the metal complexes sensitize DNA cleavage are determined by the interaction of plasmid pBR322 DNA with complexes **5**, **6** and **7.** Gel electrophoresis technique of the plasmid is employed to monitor the transition from the naturally occurring, covalently closed circular form (Form I) to the nicked circular relaxed form (Form II). The cleavage of supercoiled (SC) DNA (Form I) to the nicked circular (NC) DNA (Form II) with the variation of the concentrations (50-400 μM) of these complexes in presence or absence of external oxidizing agent are represented in Figure 3.9 and Figure 3.10.which is comparable with previous report.[49]

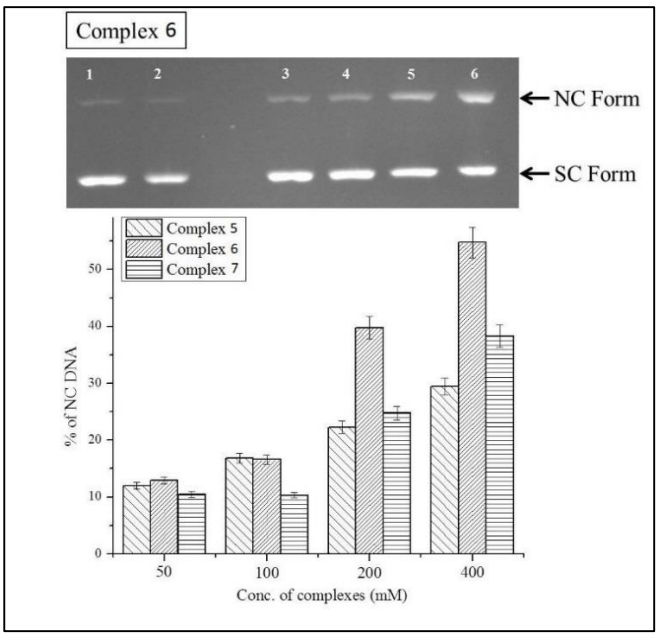

Figure 3. 9*. Gel electrophoresis diagram showing pBR322 DNA cleavage by complex* ***6****.*

*Above- Lane 1 – DNA Control; Lane 2 – DNA+H_2O_2; Lane 3 – DNA+ H_2O_2+**6**(50μM); Lane 4 – DNA+ H_2O_2+**6**(100μM); Lane 5 – DNA+ H_2O_2+**6**(200μM); Lane 6 – DNA+ H_2O_2+**6**(400μM). Below – Histogram of DNA cleavage activity (in terms of % of NC DNA) of three complexes with respect to concentrations.*

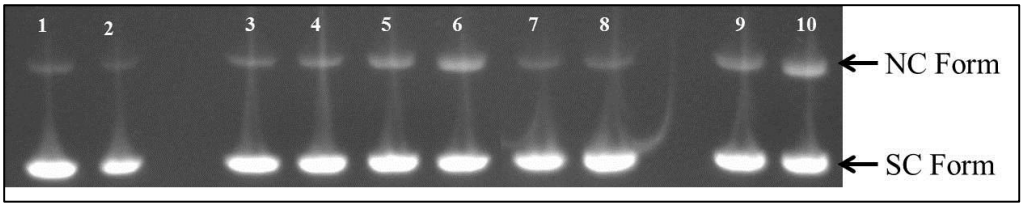

Figure 3. 10. *Gel electrophoresis diagram showing pBR322 DNA cleavage by complex **5** and **7**.*

*Lane 1 – DNA Control; Lane 2 – DNA+H_2O_2; Lane 3 – DNA+ H_2O_2+**5**(50µM); Lane 4 – DNA+ H_2O_2+**5**(100µM); Lane 5 – DNA+ H_2O_2+**5**(200µM); Lane 6 – DNA+ H_2O_2+**5**(400µM); Lane 7 – DNA+ H_2O_2+**7**(50µM); Lane 8 – DNA+ H_2O_2+**7**(100µM); Lane 9 – DNA+ H_2O2+**7**(200µM); Lane 10 – DNA+ H_2O_2+**7**(400µM).*

Analysis of these results revealed that there is no significant cleavage in the control while the increment of the metal complexes concentrations the enhancement of DNA cleavage has been observed. This cleavage is due to the enhanced reaction of copper ions with H_2O_2 thereby producing diffusible hydroxyl radicals or molecular oxygen, both of which are capable of damaging DNA by Fenton type chemistry.[50] To elucidate the mechanism involved in the DNA cleavage by especially complex **6**, experiments are carried out in presence of hydroxyl radical scavengers (DMSO and EtOH), singlet oxygen quencher (NaN_3) and superoxide radical scavenger (SOD). Though it is difficult to propose exact reason but the result (Figure 3.11) shows that NaN_3 inhibits more than other three scavengers to cleave DNA from SC form to NC form.

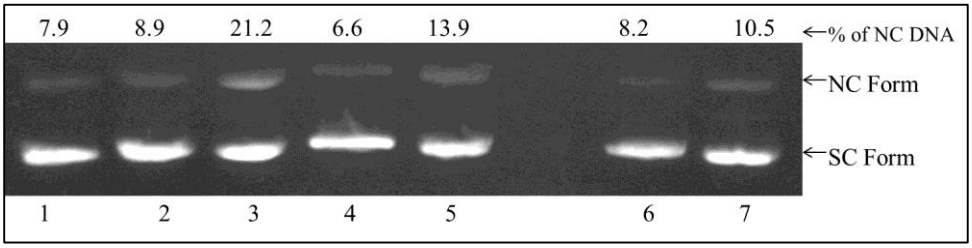

Figure 3. 11. *Gel electrophoresis image for detection of mechanism of cleavage Lane 1 – DNA+ 6; Lane 2 – DNA +6+DMSO; Lane 3 – DNA +6+EtOH; Lane 4 – DNA +6+NaN_3; Lane 5– DNA +6+SOD; Lane 6 – DNA +6+DAPI; Lane 7 – DNA +6+Methyl Green*

This phenomenon indicates that Cu(II) complexes cleave SC form of pBR322 DNA by producing singlet molecular oxygen. The groove binding preferences of the complex **6** was verified using the minor groove binder DAPI and the major groove binder methyl green.[51] Figure 3.11 indicates that minor groove binders produced a slight inhibition of the DNA damage mediated by the complex (Lane 6), suggesting that the complex **6** preferentially interacts through minor groove of DNA helix. The control experiment was performed using only copper nitrate (various concentrations) and H_2O_2. It was observed that at 400µM concentration of copper nitrate it show 28.5% of NC DNA formation whereas at similar concentration with respect to copper ion *i.e.* 200µM of complex **6** produces above 40% of NC DNA.

3.3.5 Protein binding studies

Interaction of transition metal complexes with BSA protein are generally monitored by the intrinsic fluorescence intensity. Generally tryptophan, tyrosine, and phenylalanine residues are the main intrinsic component for showing fluorescence intensity of a protein [52]. Fluorescence quenching refers to any process, which decreases the fluorescence intensity of a fluorophore due to variety of molecular interactions including excited-state reactions, molecular rearrangements, energy transfer, ground-state complex formation, and collision quenching. The fluorescence spectrum of three complexes (Figure 3.12 and Figure 3.13) with BSA indicates that there is a progressive decrease in the fluorescence intensity along with a significant red shift in case of complex **6**.

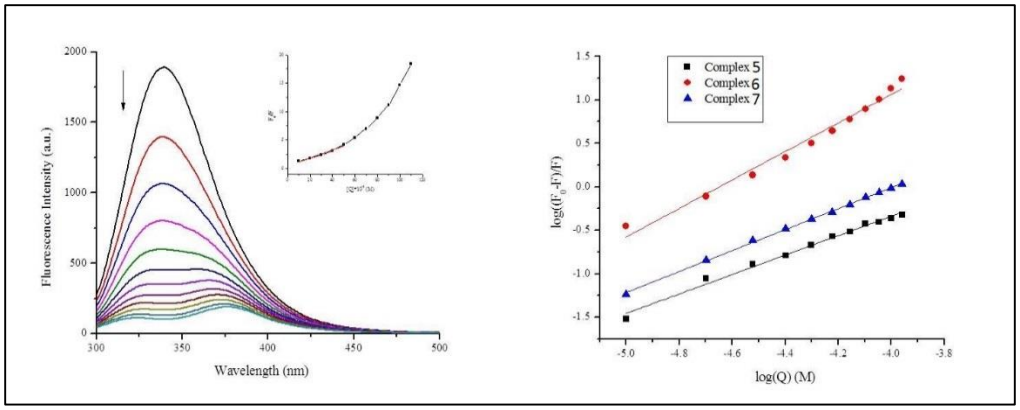

Figure 3. 12. *Left-Fluorescence quenching of BSA by* ***6****. Stern-Volmer plot is in Inset. Right-Scatchard plot for various systems of fluorescence quenching.*

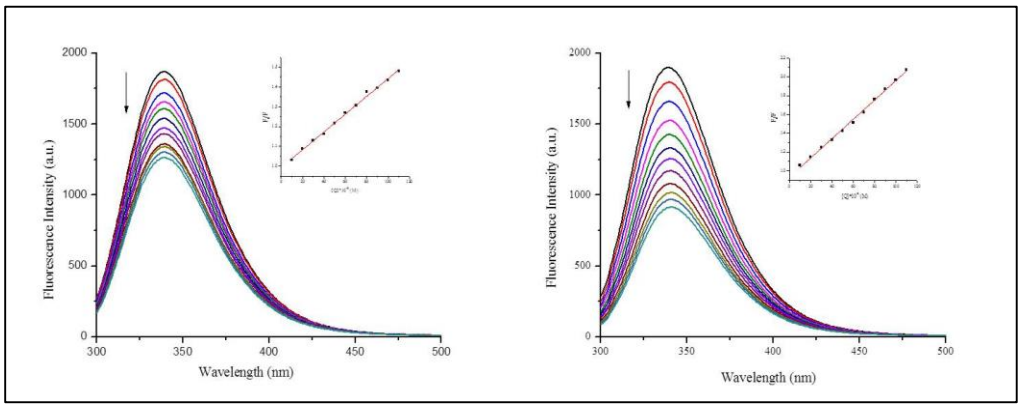

Figure 3. 13. *Fluorescence quenching of BSA by* ***5****(left) and* ***7*** *(right). Stern-Volmer plot is in Inset.*

This shifting of the emission maxima towards lower energy indicates the probable energy transfer from the indole unit of the tryptophan to the protein bound compound.[18] The fluorescence quenching data was further analyzed by the Stern−Volmer relation which again can be expressed in terms of bimolecular quenching rate constant and average life time of the fluorophore as shown in following equation [18].

$$\frac{F_0}{F} = 1 + k_q \tau_0 [Q] = 1 + K_{SV}[Q]$$

where F_0 and F are the fluorescence intensities in the absence and the presence of a quencher, k_q is the bimolecular quenching rate constant, τ_0 is the average life time of fluorophore in the absence of a quencher and [Q] is the concentration of a quencher (Metal complexes). K_{SV} is the Stern–Volmer quenching constant

in M^{-1}. However, in case of complex **6,** a plot with upward curvature concave in the direction of the *y*-axis was found. By this positive deviation it is clearly indicated that there must be probable two ways quenching by collision as well as by complex formation with the same quencher. In a Stern-Volmer plot, at lower concentration of quencher **6** shows linearity, however at higher concentrations it shows a high positive deviation from linearity. This indicates the formation of more than one ground state complex BSA-**6** system, so it can be predicted that at lower concentration of **6** the quenching could be started by a stable ground-state complex formation (1:1 type), however at higher concentration an upward bending in the direction of the F_0/F axis specifies the formation of the second (1:2 type) BSA-**6** complex. To determine the binding constant and number of binding site Scatchard equation was employed which is given by

$$\log\left[\frac{F_0 - F}{F}\right] = \log K_a + n \log[Q]$$

Where K_a and n are the binding constant and number of binding sites respectively, and F_0 and F are the fluorescence intensities in the absence and presence of the quencher respectively. Thus, a plot of $\log(F_0 - F)/F$ versus log[Q] (Figure 3.12) can be used to determine the value of binding constant (from intercept) and number of binding sites (from slope). All the data from Stern-Volmer plot and Scatchard plot is tabulated in Table 3.3. These results indicate that complex **6** has more binding affinity towards BSA than other two. More over protein binding capacity of all these three complexes are more than reported nickel complexes with same Schiff base ligand [18]. The repeated experiment was performed in case of complex **6** taking 0.5 eqv of complex **6** compared to complex **5** and **7** (with same number of copper ions for all the complexes). Moreover in this case also it was observed that complex **6** is more active with respect to complex **5** or **7** indicating a possible role of nuclearity.

Table 3. 3. *Various parameters obtained from bio-macromolecular interaction study.*

System	**DNA Interaction With**			**BSA Interaction With**		
Complex	**5**	**6**	**7**	**5**	**6**	**7**
K_{SV} (M^{-1})	6.2×10^2	1.1×10^3	7.7×10^2	4.5×10^3	7.0×10^4	1.0×10^4
K_q ($M^{-1}S^{-1}$)	…….	…….	…….	7.2×10^{11}	1.1×10^{13}	1.6×10^{12}
K_a (M^{-1})	1.2×10^3	5.5×10^4	8.5×10^2	1.3×10^4	4.0×10^7	6.4×10^4
n	1.06	1.43	1.01	1.11	1.63	1.2

3.3.6 Catecholase activity study

Catecholase like activity of the synthesized metal complexes was studied taking 3,5-di-*tert*-butylcatechol (3,5-DTBC) as the substrate in the presence of two bulky *t*-butyl substituent in the ring for showing a low quinone-catechol reduction potential.[6, 53] The reactions were carried out at 25°C in aerobic condition and it was monitored by UV-Vis spectroscopic technique. The oxidation product 3,5-di-*tert*-butylquinone (3,5-DTBQ) is highly stable and shows a maximum absorption at about 400 nm in methanol. To monitor the reaction a 10^{-4} M methanolic solution of these three complexes were treated with 100 equivalent of 3,5-BTDC in which upon addition of catecholic substrate a new band starts to gradually appear at about 402 nm with time due to the formation of the oxidized product 3,5-DTBQ (Figure 3.14).

To understand the kinetic aspect of catalysis for complex **5, 6** and **7**, the rate constant for a catalyst complex was determined by traditional initial rate method (detail description in experimental section). The observed rate versus substrate concentration data were then analyzed on the basis of the Michaelis–Menten approach of enzymatic kinetics to determine the Michaelis−Menten constant (K_M) and maximum initial rate (V_{max}) using Michaelis−Menten plots and Lineweaver-Burk plots [54]. The turnover frequency values (k_{cat}) were obtained by dividing the V_{max} values by the concentration of the corresponding complexes. All the data (Table 3.4) unambiguously demonstrate that all the three complexes are very much active.

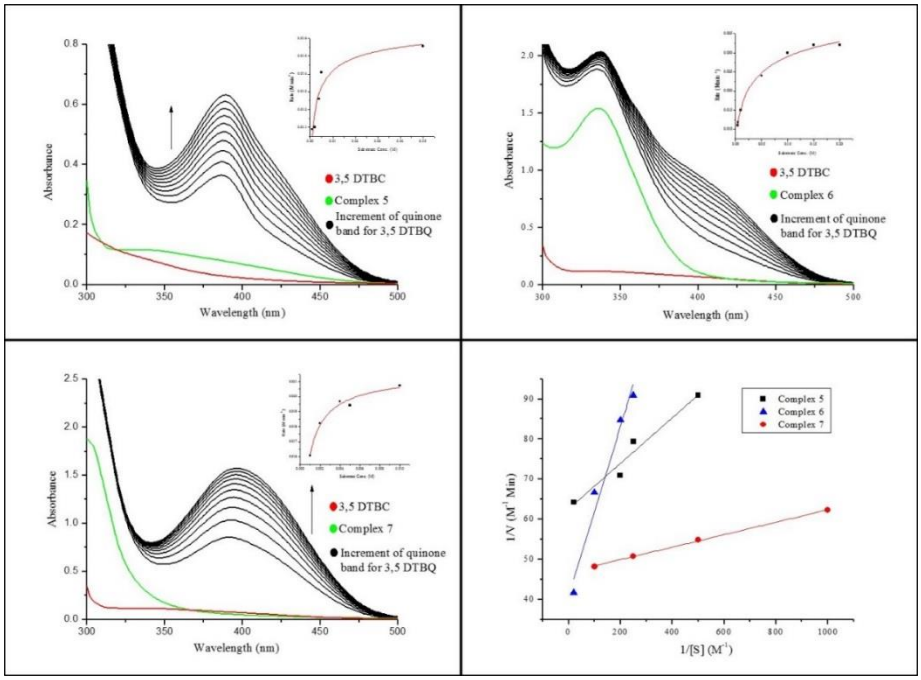

Figure 3. 14*. Time dependent spectral patterns for catecholase activity of complexes* ***5-7****. Lineweaver Burk plot (Bottom right).*

Table 3. 4*. Table for various kinetic parameters of catecholase activity.*

Complex	**Complex Conc. (M)**	**V_{max} (M min^{-1})**	**Std. Error**	**K_M (M)**	**Std. Error**	**k_{cat} / T.O.N (h^{-1})**
5	0.0001	0.01724	0.00365	3.9×10^{-4}	2.5×10^{-4}	10.3×10^{3}
6	0.0001	0.04763	0.0092	0.04271	0.03571	28.5×10^{3}
7	0.0001	0.02175	0.00135	2.6×10^{-4}	8.9×10^{-5}	13.0×10^{3}

This activity may be due to the fact that the positive charge on the piperazinyl moiety may help the facilitation of catalyst-substrate interaction by forming a positive channel which might be a prerequisite for showing better catalytic activities. A similar mechanism has been proposed to explain the activity of copper/zinc superoxide dismutase where positively charged arginine and lysine residue play a role to attract the anion and guiding them towards the catalytic center [55]. The turnover frequency (k_{cat}) 28.5×10^3 h^{-1} obtained for compound **6** has been quite high with respect to other dimeric copper complexes reported so far [56-58].

The investigation regarding the probable complex-substrate aggregate (Figure 3.15) was done through ESI-MS spectroscopy (Figure 3.16). The molecular ion peaks (m/z value) are observed at 362.13 for $[Cu(HL^1)(Py)–DTBC–(Py)(HL^1)Cu + K]^{3+}$ (Structure A in Scheme 3.2) in case of complex **5**; at 1043.51 for $[Cu_2(HL^1)_2(NO_3)_2–DTBC + Na]^+$ (Structure B in Scheme 3.3) in case of complex **6** and at 384.13 for $[Cu(HL^2)–DTBC–(HL^2)Cu]^{2+}$ (Structure C in Scheme 3.2) in case of complex **7** with little bit of deviation which is in the range of earlier report [59].

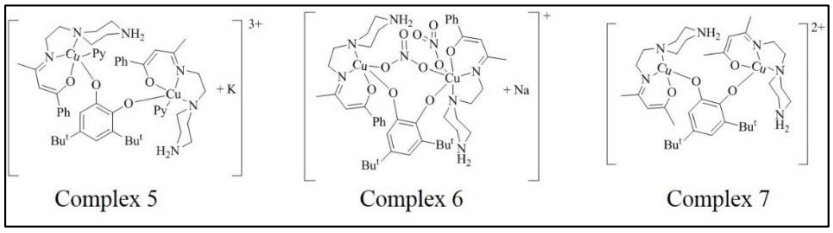

Figure 3. 15. *Probable complex-substrate aggregate of complexes* ***5-7****.*

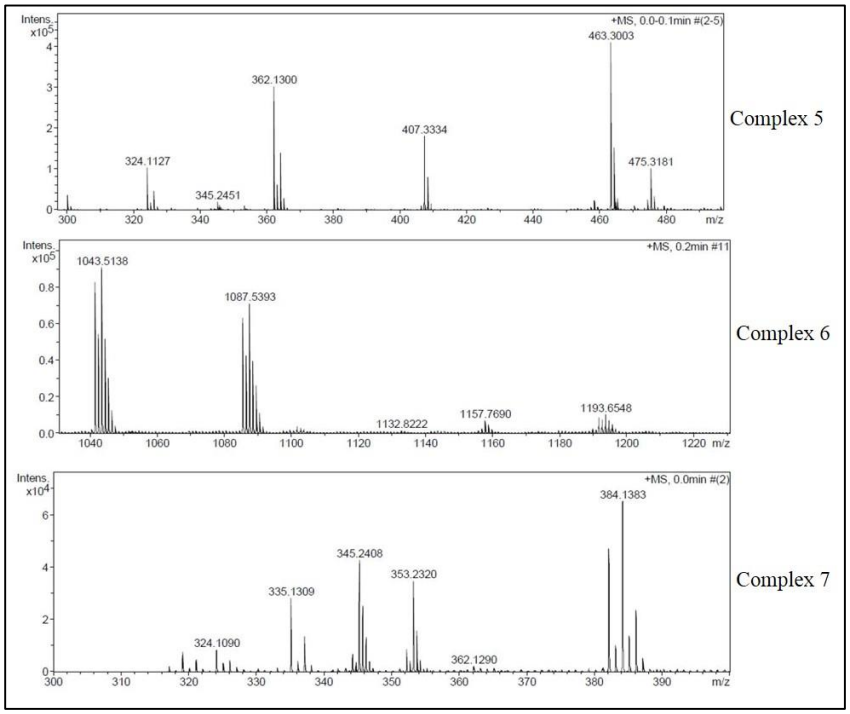

Figure 3. 16. *ESI-MS spectrum of a 1:100 Complexes (***5***,* ***6*** *and* ***7****) / 3,5-DTBC mixture in methanol, recorded within 10 min of mixing.*

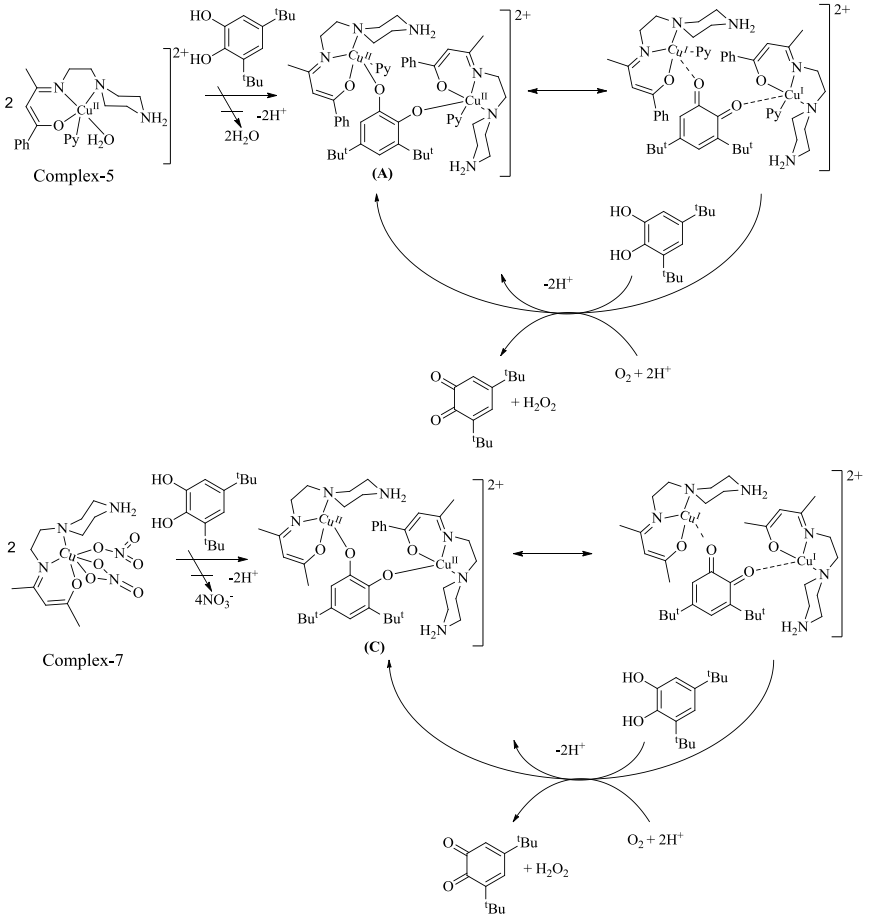

Scheme 3. 2. *Probable catechol oxidation mechanism by complex* ***5*** *and* ***7****.*

This result suggest that for mononuclear copper complexes two mononuclear units are involved to catalyze the catechol oxidation reaction for one substrate (*i.e*. one 3,5 DTBC) where as in case of binuclear copper complex **6**, one dimer is attached with one 3,5 DTBC to form a complex-substrate aggregate. The probable reaction mechanism for mononuclear complexes **5** and **7** are represented in Scheme 3.2 and for dinuclear complex **6** is represented in Scheme 3.3. Similar kind of mechanisms are reported earlier [60]. As complex **6** has shown best suitable catalytic activities among these three, more attention was focused on the mechanism for compound **6** as a representative species. In this case one molecule of 3,5 DTBC gets attached with two metal centers in a bridging fashion by removal of one nitrate to form complex-substrate aggregate **B** (Scheme 3.3). After that simultaneous or step wise reduction of Cu centers takes place with subsequent removal of oxidized catechol moiety. After that a

second catechol moiety gets inserted into the copper centers to complete the cycle.

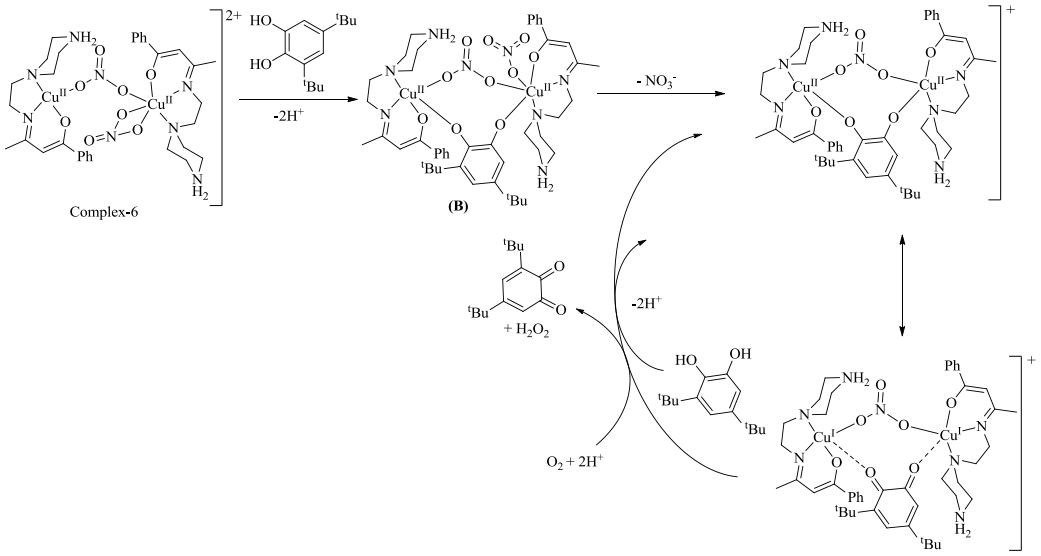

Scheme 3. 3*. Probable catechol oxidation mechanism by complex* ***6****.*

Formation of H_2O_2 during catalytic oxidation procedure gives some insight into the plausible mechanistic pathway for catechol oxidation. Taking complex **6** as a representative, a positive result was obtained for quantitative detection of I_3^- band (~353nm.) (Figure 3.17) by UV-Vis spectroscopy (applying reported methodology [61]) which is indicative for the formation of H_2O_2 during the process. According to previous report, either water or dihydrogen peroxide can be formed as a side product in the catalytic oxidation of catechol by copper(II) complexes [62]. Though there are few reports of formation of H_2O_2 in the reaction mixture [63-66] but it should be noted that the reports containing the studies aimed to definitely establish the mode of the dioxygen reduction to either water or dihydrogen peroxide are quite scarce. Curiously, in some cases the formation of dihydrogen peroxide is correlated with the detection of the semiquinone intermediate species in the catalytic reaction [67, 68]. It is indeed plausible that the dihydrogen peroxide may get formed as a product of the oxidation of the copper(I)-semiquinone intermediate, as proposed by Kodera *et al.*[67]. The mode of oxidation can be rationalized as follows. In case of

dicopper(II) complexes, the simultaneous reduction of two copper(II) centers to the copper(I) state results in the oxidation of one equivalent of catechol, leading to the release of one quinone molecule.

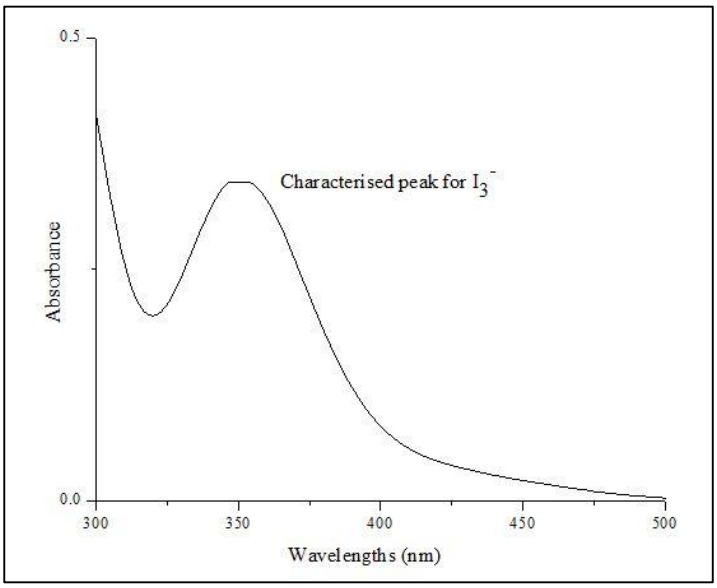

Figure 3. 17*. Characterized peak for I^{3-} for qualitative detection of H_2O_2 during catalytic oxidation process.*

In case of mononuclear copper(II) complexes (or dinuclear intermediate species, formed by self-assembly of two mononuclear units via DTBC bridge), only one electron transfer may occur, resulting in the formation of copper(I)-semiquinonate intermediate species. The reaction of such species with dioxygen may result in the two-electrons reduction of the latter, leading to the reoxidation of the copper(I) ion, a release of the quinone molecule and dihydrogen peroxide formation.

All the above experiments were performed keeping the number of metal centers constant for all the three complexes to compare their activities. The results indicate that the dinuclear complex shows higher activity towards DNA binding ($K_a = 3.1\times10^4\ M^{-1}$), BSA binding ($K_a = 2.5\times10^7\ M^{-1}$) and catecholase like activity ($K_{cat} = 17.3\times10^3\ h^{-1}$) implying that the nuclearity of the metal complex is playing a part towards greater activity.

3.3.7 Antibacterial activity

Nosocomial infections or more commonly hospital-acquired infections are defined as an infection in a patient or health care professional not evident prior to accessing a hospital or health care facility [69]. These infections cause problems for both patient health and have a health-economic impact (1.4 million patients admitted to a hospital will experience nosocomial derived difficulties at any given time) [70]. The most frequent nosocomial infections reported are caused by bacteria as the Gram-positive Methicillin-Resistant *Staphylococcus aureus* (MRSA). This bacteria, a non-motile, non-spore-forming coccus and a significant human pathogenic bacterium, is one that is currently causing the majority of nosocomial infections [69, 71]. For these reasons, in this study the antibacterial activity of Schiff base ligands and copper complexes were evaluated. The free Schiff bases did not show significant antibacterial activity. Complex **6** was found to exhibit moderate activity against S. aureus (MRSA) with a Minimum Inhibitory Concentration (MIC) value of 10.7 mg/L (10 μg/mL) compared to commercially available antibiotics including vancomycin (MIC of 1 μg/mL) and linezolid (MIC ranged from 2-4 μg/mL) [72]. Complex **6** reported in this paper proved to be effective against *S. aureus* (MRSA) and is a promising compound showing potent activity against multidrug resistant (Table 3.5). These results highlight the antibacterial activity of copper complex **6** which opens up the possibility to further explore this compound against clinical multidrug resistant strains.

Table 3. 5*. Minimum Concentration inhibitory (MIC) and (MBC) MRSA results for the selected compounds against MRSA strain.*

Compounds	**MW g/mol**	**Solvent**	**Concentration (M)**	**MRSA MIC mg/L**	**MRSA MBC mg/L**
HL[1]	273.18	Methanol	0.461	491.7	491.7
Complex **6**	335.11	Methanol	0.010	10.7	103.8

3.3.8 Computational study

The density functional theory (DFT) calculations were performed to understand the DNA binding and the catechol oxidation catalyzed by Cu(II) complexes (**5**, **6** and **7**). Here the DNA structure as a deoxyguanosine monophosphate (dGMP) [73] unit was modelled where one of the phosphate oxygen is methylated to satisfy the valency. So, the dGMP unit is negatively charged. All the calculations are carried out using UB3LYP level of theory as implemented in the Gaussians 09 package [74]. The 6-311++G** basis set is used for the main group elements (C, N, O, P, and H) and LANL2DZ ECP basis set is used for Cu [75, 76]. These complexes in two different solvents using the polarizable continuum model [77] were optimized as the experiments are performed in two different solvents (water for DNA cleavage and methanol for catechol oxidation). The vibrational frequency calculations are performed for all the structures to confirm their nature of the stationary points.

3.3.9 Theoretical comparison of DNA binding Study

The optimized structures of the Cu(II) complexes and dGMP are presented in Figure 3.18 (a-d). The frontier orbitals of the dGMP and the Cu(II) complexes (**5-7**) are investigated to understand their role towards the DNA binding. In Figure 3.19 it was shown that HOMO (higher occupied molecular orbital) energy of the dGMP structure with respect to the LUMO (lowest unoccupied molecular orbital) energies of the Cu(II) complexes (**5-7**) to understand the binding of DNA to the Cu-complexes [78, 79]. The HOMO energy of the dGMP fragment is -3.66 eV and the LUMO energies of the **5**, **6** and **7** are -4.90 eV, -5.28 eV, and -3.42 eV, respectively. Therefore, the LUMO is highly stabilized for complex **6** (-5.28 eV) in comparison to complex **5** (-4.90 eV) and **7** (-3.42 eV). So, the electron transfer (Figure 3.19) will be highly favourable from HOMO of dGMP to complex **6**. On the other hand, the LUMO (-3.42 eV) of complex **7** is higher in energy than HOMO (-3.66 eV) of dGMP. So, the electron transfer will not be favourable from dGMP fragment to **7**. The dGMP bonded Cu(II) complexes (**5-7**) are modelled where the phosphate group of the dGMP

fragment binds to the Cu-centre of the metal complexes (Figure 3.20 a-c). All three dGMP-bonded complexes are fully relaxed and found to be minima in their potential energy surfaces.

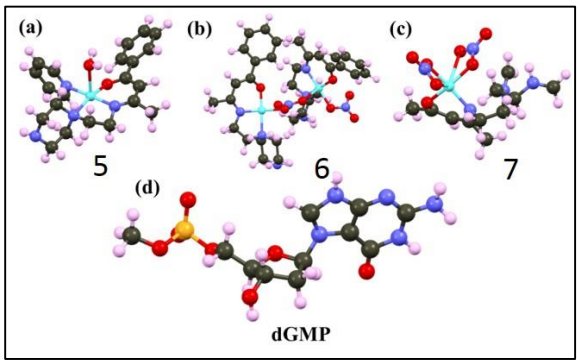

Figure 3. 18*. Optimized structure of Cu(II) complexes [(a)* ***5****, (b)* ***6****, (c)* ***7****] and (d) dGMP fragment. Here, black, sea-green, blue, red, orange and pink colour balls denote the carbon, copper, nitrogen, oxygen, phosphorous and hydrogen atoms respectively.*

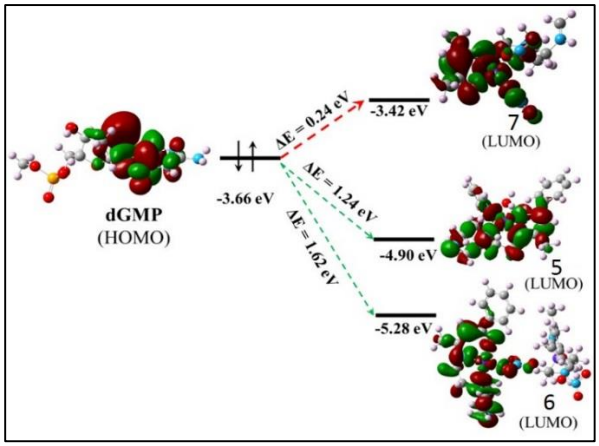

Figure 3. 19*. Qualitative energy diagram of the dGMP fragment (HOMO) and Cu-complexes* ***5****-****7****(LUMO). Isosurface value is 0.03 e.Å*$^{-3}$.

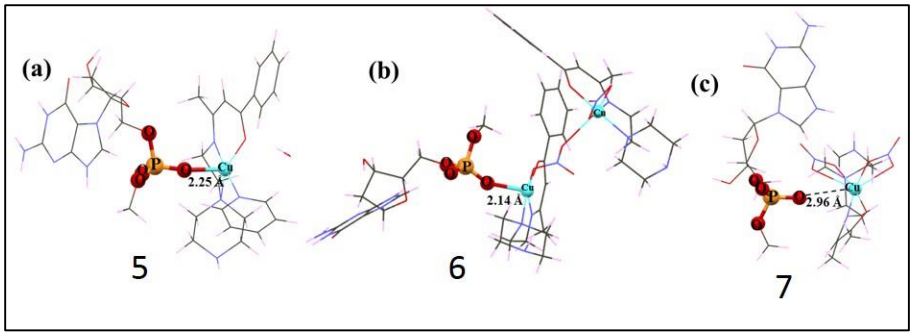

Figure 3. 20*. Optimized geometries of the Cu-dGMP complexes (****5****,* ***6*** *and* ***7****).*

The binding energy (E_B) of the dGMP fragment with the Cu(II) complex is calculated using the following equation:

$E_B = E_{Cu\text{-}dGMP} - (E_{dGMP} + E_{Cu\text{-}complex})$

Where $E_{Cu\text{-}dGMP}$ is the total energy of the Cu-dGMP complex. $E_{Cu\text{-}complex}$ and E_{dGMP} are the single point energies of the Cu-complex and dGMP fragment within the geometry of the Cu-dGMP complex. The calculated dGMP binding energies are –6.60 kcal/mol, –10.66 kcal/mol and –3.14 kcal/mol for the complexes **5**, **6** and **7**, respectively. Therefore, this is very much in consistent with the experimental DNA binding constant of **5-7**.

3.3.10 Theoretical comparison of catechol oxidation study

The ground state structures of all the three Cu(II) complexes are presented in Figure 3.18 (a-c). Mono-nuclear Cu(II) complexes (**5** and **7)** have open-shell doublet (S=1/2) configuration whereas bi-nuclear Cu(II) complex (**6)** has open-shell triplet (S=1) configuration. During the oxidation reaction, catechol molecule first binds to the metal centre.[19, 80] In case of bi-nuclear Cu(II) complex (**6)**, one catechol molecule binds to one metal complex but for mono-nuclear Cu(II) complexes (**5** and **7**), two metal complexes bind to one catechol molecule. Thus, during the catechol oxidation reaction, the bi-nuclear metal complex will be reduced by two-electrons ($2e^-$) whereas mono-nuclear complexes will be reduced by one electron (e^-). So, during the catechol oxidation process, Cu(II) complexes are reduced to Cu(I). All the three reduced Cu(I) complexes (**5-7**) are calculated to be most stable with an open-shell singlet structure (S=0). The spin density difference (SDD) of the Cu(II) and Cu(I) complexes were plotted to understand their role towards the catechol oxidation reaction. It was also found that a drastic change in the spin multiplicity of all the three Cu(II) complexes which can be clearly seen from their spin density difference plots (Figure 3.21 a-c). It shows that initial spin density is mainly concentrated on the Cu centre of the Cu(II) complexes whereas the spin density vanishes after the reduction of the Cu-complexes.

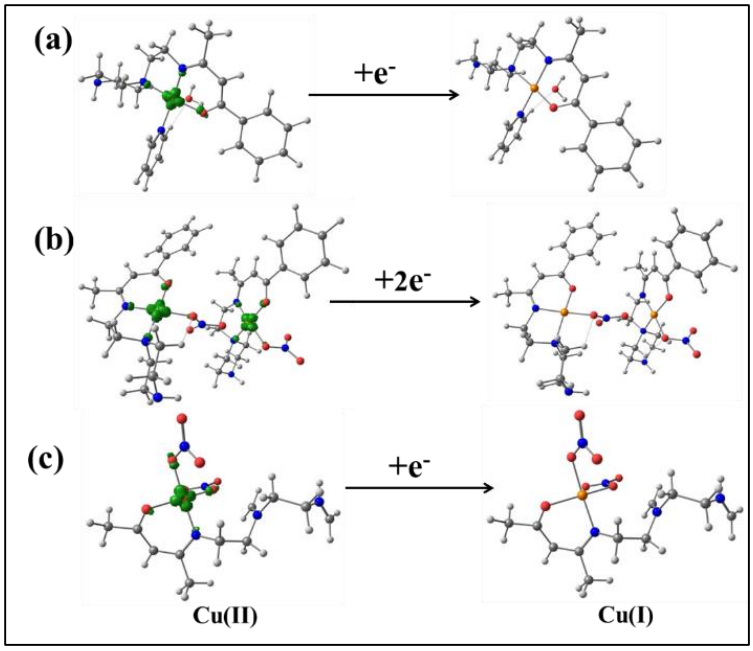

Figure 3. 21. *Spin density difference (SDD) plots of Cu(II) and Cu(I) complexes (**5-7**). Isosurface value is set to 0.03 e.Å^{-3}.*

The SOMO-LUMO gap of the Cu(II) (before reduction) and HOMO-LUMO gap of the Cu(I) complexes (after reduction) were also calculated and it shows that the HOMO-LUMO gap is higher in the Cu(I) systems compared to the SOMO-LUMO gap of the Cu(II) systems. This could be due to the change (from d^9 to a more stable d^{10} configuration) in their electronic configuration. The SOMO-LUMO gap of Cu(II) complexes (**5-7**) were also investigated to find out their reactivity towards the catechol oxidation. It was found that dinuclear complex **6** (1.36 eV) has lower SOMO-LUMO gap compared to complex **5** (4.08 eV) and complex **7** (2.44 eV) (Figure 3.22 and Table 3.6). It proves that complex **6** is more reactive towards the catechol oxidation compared to complex **5** and **7**. Thus, the bi-nuclear complex shows superior catalytic activity over others and this can be related with their SOMO energies. The calculated SOMO energies are -6.08, -7.19, and -5.88 eV for **5**, **6** and **7**, respectively. It shows, the SOMO is highly stabilized in the bi-nuclear complex and thus ready to accept an electron, which is turn triggers the catechol oxidation reaction. The catechol oxidation trend (**6**>**7**>**5**) is very much in agreement with the experimental findings.

Furthermore the catechol oxidation trend (**6**>**7**>**5**) can get influenced by an additional factor which is nothing but the geometry around the metal ion. It is reported that with more asymmetric nature of the geometry around metal ion the activity towards catechol oxidation increases [81]. Taking the crystallographic data for the complexes **5**-**7** and following the mentioned correlation, it has been found that the higher/lower distances of the Cu first coordination sphere are 2.265/1.934 = 1.17 for **5**; 2.75/1.985 = 1.385 for **6**; and 2.423/1.921 = 1.26 for **7**. That means the distortion of the symmetry follows the following trend **6**>**7**>**5**, which is manifested in terms of catalytic activity of the complexes.

Table 3. 6. *Table for SOMO-LUMO data in catechol oxidation by different complexes. (Solvent – Methanol)*

Systems	**SOMO (eV)**	**LOMO (eV)**	**Δ (eV)**
Complex-**5**	-6.08	-2.00	4.08
Complex-**6**	-7.19	-5.83	1.36
Complex-**7**	-5.88	-3.43	2.44

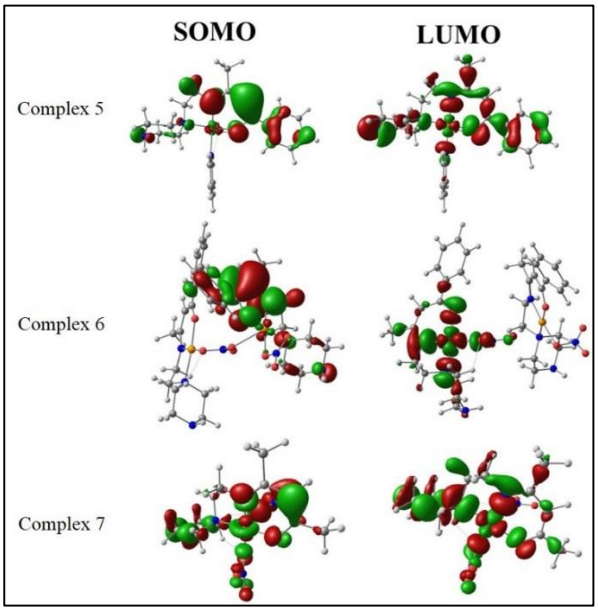

Figure 3. 22*. SOMO-LUMO diagram of complexes* ***5-7*** *in catechol oxidation process*

3.4 Conclusions

In conclusion three new Cu(II) complexes $[Cu(HL^1)(Pyridine)(H_2O)](ClO_4)_2.2MeOH$ **(5)**, $[Cu_2(HL^1)_2(NO_3)_2](NO_3)_2.3H_2O$ **(6)** and $[Cu(HL_2)(NO_3)_2].MeCN$ **(7)** have been synthesized and characterized. Various types of Cu(II) center's geometry like tetra, penta and hexacoordination are the main structural features of this scheme. Furthermore complex **6** was found to be relatively unusual kind of coordination where two Cu(II) centers are lying in different geometrical environment. ETBr displacement assay, gel electrophoresis experiment, and fluorescence quenching technique for BSA clearly indicate that all these three complexes have DNA binding and cleavage as well as protein binding activity. Apart from this, these complexes are quite active towards catechol oxidation and anti-bactecrial property. Finally relative studies from all the above data clearly reflect that dinuclear complex **6** is the most promising molecule towards all these activities. The nuclearity driven activity of complex **6** towards DNA binding and catechol oxidations are further explained by DFT.

3.5 References

[1]. Linder, M. C.,Goode, C. A., (1991), Biochemistry of Copper.Plenum: New York.

[2]. Kaim, W.,Rall, J. (1996), Copper—A "Modern" Bioelement, Angewandte Chemie International Edition in English, 35, 43-60.(DOI: 10.1002/anie.199600431)

[3]. Sorrell, T. N. (1989), Synthetic models for binuclear copper proteins, Tetrahedron, 45, 3-68.(DOI:10.1016/0040-4020(89)80033-X)

[4]. Kitajima, N.,Moro-oka, Y. (1994), Copper-Dioxygen Complexes. Inorganic and Bioinorganic Perspectives, Chemical Reviews, 94, 737-757.(DOI: 10.1021/cr00027a010)

[5]. Bhat, S. S.,Kumbhar, A. A.,Heptullah, H.,Khan, A. A.,Gobre, V. V.,Gejji, S. P.,Puranik, V. G. (2011), Synthesis, Electronic Structure, DNA and Protein Binding, DNA Cleavage, and Anticancer Activity of Fluorophore-Labeled

Copper(II) Complexes, Inorganic Chemistry, 50, 545-558.(DOI: 10.1021/ic101534n)

[6]. Dey, S. K.,Mukherjee, A. (2013), Zero-Order Catechol Oxidase Activity by a Mononuclear Manganese(III) Complex Showing High Turnover Comparable to Catechol Oxidase Enzyme, ChemCatChem, 5, 3533-3537.(DOI: 10.1002/cctc.201300596)

[7]. Fernandes, C.,Neves, A.,Bortoluzzi, A. J.,Mangrich, A. S.,Rentschler, E.,Szpoganicz, B.,Schwingel, E. (2001), A new dinuclear unsymmetric copper(II) complex as model for the active site of catechol oxidase, Inorganica Chimica Acta, 320, 12-21.(DOI: 10.1016/S0020-1693(01)00470-4)

[8]. Moura, E.,Afonso, J.,Hein, L.,Vieira-Coelho, M. A. (2006), α_2-Adrenoceptor subtypes involved in the regulation of catecholamine release from the adrenal medulla of mice, Br. J. Pharmacol., 149, 1049.(DOI: 10.1038/sj.bjp.0706950)

[9]. del Campo, R.,Criado, J. J.,García, E.,Hermosa, M. a. R.,Jiménez-Sánchez, A.,Manzano, J. L.,Monte, E.,Rodríguez-Fernández, E.,Sanz, F. (2002), Thiourea derivatives and their nickel(II) and platinum(II) complexes: antifungal activity, Journal of Inorganic Biochemistry, 89, 74-82.(DOI: 10.1016/S0162-0134(01)00408-1)

[10]. Kasuga, N. C.,Sekino, K.,Koumo, C.,Shimada, N.,Ishikawa, M.,Nomiya, K. (2001), Synthesis, structural characterization and antimicrobial activities of 4- and 6-coordinate nickel(II) complexes with three thiosemicarbazones and semicarbazone ligands, Journal of Inorganic Biochemistry, 84, 55-65.(DOI: 10.1016/S0162-0134(00)00221-X)

[11]. Vessieres, A.,Top, S.,Beck, W.,Hillard, E.,Jaouen, G. (2006), Metal complex SERMs (selective oestrogen receptor modulators). The influence of different metal units on breast cancer cell antiproliferative effects, Dalton Transactions, 529-541.(DOI: 10.1039/B509984F)

[12]. Bhat, I.-u.-H.,Tabassum, S. (2009), Synthesis of new piperazine derived Cu(II)/Zn(II) metal complexes, their DNA binding studies, electrochemistry and anti-microbial activity: Validation for specific recognition of Zn(II) complex to

DNA helix by interaction with thymine base, Spectrochimica Acta Part A: Molecular and Biomolecular Spectroscopy, 72, 1026-1033.(DOI: 10.1016/j.saa.2008.12.037)

[13]. Silveira, V. C.,Abbott, M. P.,Cavicchioli, M.,Goncalves, M. B.,Petrilli, H. M.,de Rezende, L.,Amaral, A. T.,Fonseca, D. E. P.,Caramori, G. F.,da Costa Ferreira, A. M. (2013), Peculiar reactivity of a di-imine copper(II) complex regarding its binding to albumin protein, Dalton Transactions, 42, 6386-6396.(DOI: 10.1039/C3DT00108C)

[14]. Patra, A.,Sen, T. K.,Ghorai, A.,Musie, G. T.,Mandal, S. K.,Ghosh, U.,Bera, M. (2013), Synthesis, Structure, Spectroscopic Characterization, and Protein Binding Affinity of New Water-Soluble Hetero- and Homometallic Tetranuclear [$Cu^{II}_2Zn^{II}_2$] and [Cu^{II}_4] Clusters, Inorganic Chemistry, 52, 2880-2890.(DOI: 10.1021/ic302099y)

[15]. Li, X.-W.,Tao, L.,Li, Y.-T.,Wu, Z.-Y.,Yan, C.-W. (2012), Bimetallic complexes constructed from asymmetrical N,N′-bis(substituted)-oxamide: Cytotoxicities, and reactivities towards DNA and protein, European Journal of Medicinal Chemistry, 54, 697-708.(DOI: 10.1016/j.ejmech.2012.06.022)

[16]. Pratviel, G.,Bernadou, J.,Meunier, B. (1995), Carbon—Hydrogen Bonds of DNA Sugar Units as Targets for Chemical Nucleases and Drugs, Angewandte Chemie International Edition in English, 34, 746-769.(DOI: 10.1002/anie.199507461)

[17]. Patra, A. K.,Bhowmick, T.,Roy, S.,Ramakumar, S.,Chakravarty, A. R. (2009), Copper(II) complexes of L-arginine as netropsin mimics showing DNA cleavage activity in red light, Inorganic chemistry, 48, 2932-43.(DOI: 10.1021/ic8017425)

[18]. Das, M.,Nasani, R.,Saha, M.,Mobin, S. M.,Mukhopadhyay, S. (2015), Nickel(II) complexes with a flexible piperazinyl moiety: studies on DNA and protein binding and catecholase like properties, Dalton Transactions, 44, 2299-2310.(DOI: 10.1039/C4DT02675F)

[19]. Adhikary, J.,Chakraborty, P.,Das, S.,Chattopadhyay, T.,Bauzá, A.,Chattopadhyay, S. K.,Ghosh, B.,Mautner, F. A.,Frontera, A.,Das, D. (2013),

A Combined Experimental and Theoretical Investigation on the Role of Halide Ligands on the Catecholase-like Activity of Mononuclear Nickel(II) Complexes with a Phenol-Based Tridentate Ligand, Inorganic Chemistry, 52, 13442-13452.(DOI: 10.1021/ic401819t)

[20]. Reddy, P. M.,Rohini, R.,Krishna, E. R.,Hu, A.,Ravinder, V. (2012), Synthesis, Spectral and Antibacterial Studies of Copper(II) Tetraaza Macrocyclic Complexes, International Journal of Molecular Sciences, 13, 4982-4992.(DOI: 10.3390/ijms13044982)

[21]. Islam, S. M.,Roy, A. S.,Mondal, P.,Mubarak, M.,Mondal, S.,Hossain, D.,Banerjee, S.,Santra, S. C. (2011), Synthesis, catalytic oxidation and antimicrobial activity of copper(II) Schiff base complex, Journal of Molecular Catalysis A: Chemical, 336, 106-114.(DOI: 10.1016/j.molcata.2011.01.006)

[22]. Sheldrick, G. (2008), A short history of SHELX, Acta Crystallographica Section A, 64, 112-122.(DOI: 10.1107/S0108767307043930)

[23]. Bernadou, J.,Pratviel, G.,Bennis, F.,Girardet, M.,Meunier, B. (1989), Potassium monopersulfate and a water-soluble manganese porphyrin complex, [Mn(TMPyP)](OAc)$_5$, as an efficient reagent for the oxidative cleavage of DNA, Biochemistry, 28, 7268-7275.(DOI: 10.1021/bi00444a019)

[24]. Wayne, P., (2011), Performance Standards for Antimicrobial Susceptibility Testing; Twenty-Second Informational Supplement.Clinical and Laboratory Standards Institute, pp. M100-S21

[25]. Nakamoto, K., (2009), Infrared and Raman Spectra of Inorganic and Coordination Compounds, Theory and Applications in Inorganic Chemistry.6th ed. John Wiley & Sons, Inc.: Hoboken, New Jersey.

[26]. Lever, A. B. P., (1984), Inorganic Electronic Spectroscopy.2nd ed. Elsevier Science, New York.

[27]. Tak, A. A.,Arjmand, F.,Tabassum, S. (2002), Synthesis of New Five Coordinated Copper(II) and Nickel(II) Complexes of L-Valine and Kinetic Study of Copper(II) with Calf Thymus DNA, Metal-Based Drugs, 9, 81-90.(DOI: 10.1155/mbd.2002.81)

[28]. Nandy, M.,Shit, S.,Garribba, E.,Gómez García, C. J.,Mitra, S. (2015), Double azido/cyanato bridged copper(II) dimers incorporating tridentate nitrogen donors Schiff base: Structure, EPR and magnetic studies, Polyhedron, 102, 137-146.(DOI: 10.1016/j.poly.2015.07.034)

[29]. Matović, Z.,Ristić, B.,Joksović, M.,Trifunović, S.,Pelosi, G.,Ianelli, S.,Ponticelli, G. (2000), Square-planar copper(II) complexes with a novel tetradentate amido-carboxylate ligand. Crystal structure of $[Co(H_2O)_6][Cu(mda)] \cdot 2H_2O$, Transition Metal Chemistry, 25, 720-726.(DOI: 10.1023/A:1007051908027)

[30]. Bullock, S. J.,Harding, L. P.,Moore, M. P.,Mills, A.,Piela, S. A. F.,Rice, C. R.,Towns-Andrews, L.,Whitehead, M. (2013), Synthesis of ligands containing N-oxide donor atoms and their assembly into metallosupramolecular structures, Dalton Transactions, 42, 5805-5811.(DOI: 10.1039/C3DT00090G)

[31]. Biswas, S.,Naiya, S.,Gómez-García, C. J.,Ghosh, A. (2012), Synthesis of the first heterometalic star-shaped oxido-bridged $MnCu_3$ complex and its conversion into trinuclear species modulated by pseudohalides (N_3^-, NCS^- and NCO^-): Structural analyses and magnetic properties, Dalton Transactions, 41, 462-462.(DOI: 10.1039/c1dt11333j)

[32]. Sajidu, S. M. I.,Persson, I.,Masamba, W. R. L.,Henry, E. M. T. (2008), Mechanisms of heavy metal sorption on alkaline clays from Tundulu in Malawi as determined by EXAFS, Journal of Hazardous Materials, 158, 401-409.(DOI: 10.1016/j.jhazmat.2008.01.087)

[33]. Köppel, H.,Yarkony, D. R.,Barentzen, H., (08-Dec-2009), The Jahn-Teller Effect: Fundamentals and Implications for Physics and Chemistry.Springer Science & Business Media, Springer Heidelburg Dordrecht London New York.

[34]. Addison, A. W.,Rao, T. N.,Reedijk, J.,van Rijn, J.,Verschoor, G. C. (1984), Synthesis, structure, and spectroscopic properties of copper(II) compounds containing nitrogen-sulphur donor ligands; the crystal and molecular structure of aqua[1,7-bis(N-methylbenzimidazol-2[prime or minute]-yl)-2,6-dithiaheptane]copper(II) perchlorate, Journal of the Chemical Society, Dalton Transactions, 1349-1356.(DOI: 10.1039/DT9840001349)

[35]. Yang, L.,Powell, D. R.,Houser, R. P. (2007), Structural variation in copper(I) complexes with pyridylmethylamide ligands: structural analysis with a new four-coordinate geometry index, τ_4, Dalton Transactions, 955-964.(DOI: 10.1039/B617136B)

[36]. Simmons, C. J.,Hathaway, B. J.,Amornjarusiri, K.,Santarsiero, B. D.,Clearfield, A. (1987), The first determination of the energy difference between solid-state conformers by x-ray diffraction. 1. The crystal structure of the pseudo-Jahn-Teller complex (nitrito)bis(2,2'-bipyridyl)copper(II) nitrate at 20, 100, 165 and 296 K and of its isostructural zinc(II) analog at 295 K. 2. The possibility of using x-ray diffraction to characterize adiabatic potential energy surfaces and relative ligand strengths, Journal of the American Chemical Society, 109, 1947-1958.(DOI: 10.1021/ja00241a009)

[37]. Gökçe, C.,Gup, R. (2013), Synthesis, characterization and DNA interaction of new copper(II) complexes of Schiff base-aroylhydrazones bearing naphthalene ring, Journal of Photochemistry and Photobiology B: Biology, 122, 15-23.(DOI: 10.1016/j.jphotobiol.2013.02.014)

[38]. Yang, X.-B.,Huang, Y.,Zhang, J.-S.,Yuan, S.-K.,Zeng, R.-Q. (2010), Synthesis, characterization and DNA interaction of copper (II) complexes with Schiff base ligands derived from 2-pyridinecarboxaldehyde and polyamines, Inorganic Chemistry Communications, 13, 1421-1424.(DOI: 10.1016/j.inoche.2010.08.006)

[39]. Duan, R.-R.,Wang, L.,Huo, W.-Q.,Chen, S.,Zhou, X.-H. (2014), Synthesis, characterization, and DNA binding of two copper(II) complexes as DNA fluorescent probes, Journal of Coordination Chemistry, 67, 2765-2782.(DOI: 10.1080/00958972.2014.946918)

[40]. Gao, C.,Ma, X.,Lu, J.,Wang, Z.,Tian, J.,Yan, S. (2011), Synthesis, structure, DNA binding, and cleavage activity of two copper(II) complexes, Journal of Coordination Chemistry, 64, 2157-2169.(DOI: 10.1080/00958972.2011.587514)

[41]. Mussardo, P.,Corda, E.,González-Ruiz, V.,Rajesh, J.,Girotti, S.,Martín, M. A.,Olives, A. (2011), Study of non-covalent interactions of luotonin A

derivatives and the DNA minor groove as a first step in the study of their analytical potential as DNA probes, Analytical and Bioanalytical Chemistry, 400, 321-327.(DOI: 10.1007/s00216-010-4640-5)

[42]. li, P.,Niu, M.,Hong, M.,Cheng, S.,Dou, J. (2014), Effect of structure and composition of nickel(II) complexes with salicylidene Schiff base ligands on their DNA/protein interaction and cytotoxicity, Journal of Inorganic Biochemistry, 137, 101-108.(DOI: 10.1016/j.jinorgbio.2014.04.005)

[43]. Barone, G.,Terenzi, A.,Lauria, A.,Almerico, A. M.,Leal, J. M.,Busto, N.,García, B. (2013), DNA-binding of nickel(II), copper(II) and zinc(II) complexes: Structure–affinity relationships, Coordination Chemistry Reviews, 257, 2848-2862.(DOI: 10.1016/j.ccr.2013.02.023)

[44]. Lakshmipraba, J.,Arunachalam, S.,Vijay Solomon, R.,Venuvanalingam, P. (2015), Synthesis, DNA binding and docking studies of copper(II) complexes containing modified phenanthroline ligands, Journal of Coordination Chemistry, 68, 1374-1386.(DOI: 10.1080/00958972.2015.1014349)

[45]. Ou, Z. B.,Lu, Y. H.,Lu, Y. M.,Chen, S.,Xiong, Y. H.,Zhou, X. H.,Mao, Z. W.,Le, X. Y. (2013), A copper(II) complex with 2-(2′-pyridyl)benzimidazole and l-arginine: synthesis, structure, antibacterial activities, and DNA interaction, Journal of Coordination Chemistry, 66, 2152-2165.(DOI: 10.1080/00958972.2013.800195)

[46]. Sun, J.,Deng, S.-Y.,Zhang, L.,He, J.,Jiang, L.,Mao, Z.-W.,Ji, L.-N. (2009), DNA affinity and cleavage by naphthalene-based mononuclear and dinuclear copper(II) complexes, Journal of Coordination Chemistry, 62, 3284-3295.(DOI: 10.1080/00958970903055875)

[47]. Raman, N.,Sakthivel, A.,Jeyamurugan, R. (2010), Synthesis, structural characterization, antimicrobial, DNA-binding, and photo-induced DNA cleavage activity of some bio-sensitive Schiff base copper(II) complexes, Journal of Coordination Chemistry, 63, 4380-4397.(DOI: 10.1080/00958972.2010.539212)

[48]. Sun, Y.-G.,Li, K.-L.,Xu, Z.-H.,Lv, T.-Y.,Wang, S.-J.,You, L.-X.,Ding, F. (2013), Synthesis, characterization, and interaction with DNA of Cu(II) and

Zn(II) complexes with 2,2′-bipyridyl-6,6′-dicarboxylic acid, Journal of Coordination Chemistry, 66, 2455-2464.(DOI: 10.1080/00958972.2013.806655)

[49]. Patra, A. K.,Roy, S.,Chakravarty, A. R. (2009), Synthesis, crystal structures, DNA binding and cleavage activity of l-glutamine copper(II) complexes of heterocyclic bases, Inorganica Chimica Acta, 362, 1591-1599.(DOI: 10.1016/j.ica.2008.08.003)

[50]. Louie, A. Y.,Meade, T. J. (1999), Metal Complexes as Enzyme Inhibitors, Chemical Reviews, 99, 2711-2734.(DOI: 10.1021/cr9804285)

[51]. Ahmad, M.,Afzal, M.,Tabassum, S.,Kalińska, B.,Mrozinski, J.,Bharadwaj, P. K. (2014), Synthesis and structure elucidation of a cobalt(II) complex as topoisomerase I inhibitor: In vitro DNA binding, nuclease and RBC hemolysis, European Journal of Medicinal Chemistry, 74, 683-693.(DOI: 10.1016/j.ejmech.2013.10.025)

[52]. Chatterjee, S.,Mukherjee, T. K. (2014), Spectroscopic investigation of interaction between bovine serum albumin and amine-functionalized silicon quantum dots, Physical Chemistry Chemical Physics, 16, 8400-8408.(DOI: 10.1039/C4CP00372A)

[53]. Merkel, M.,Möller, N.,Piacenza, M.,Grimme, S.,Rompel, A.,Krebs, B. (2005), Less Symmetrical Dicopper(II) Complexes as Catechol Oxidase Models—An Adjacent Thioether Group Increases Catecholase Activity, Chemistry – A European Journal, 11, 1201-1209.(DOI: 10.1002/chem.200400768)

[54]. Jana, A.,Ruiz, E.,Mohanta, S. (2013), Structures, Magnetochemistry, Spectroscopy, Theoretical Study, and Catechol Oxidase Activity of Dinuclear and Dimer-of-Dinuclear Mixed-Valence Mn, Inorganic Chemistry, 52, 7732-7746.(DOI: 10.1021/ic400916h)

[55]. Chattopadhyay, T.,Mukherjee, M.,Mondal, A.,Maiti, P.,Banerjee, A.,Nethaji, M.,Zangrando, E.,Das, D. (2010), A Unique Nickel System having Versatile Catalytic Activity of Biological Significance, Inorganic Chemistry, 49, 3121-3129.(DOI: 10.1021/ic901546t)

[56]. Banu, K. S.,Chattopadhyay, T.,Banerjee, A.,Bhattacharya, S.,Zangrando, E.,Das, D. (2009), Catechol oxidase activity of dinuclear copper(II) complexes of Robson type macrocyclic ligands: Syntheses, X-ray crystal structure, spectroscopic characterization of the adducts and kinetic studies, Journal of Molecular Catalysis A: Chemical, 310, 34-41.(DOI: 10.1016/j.molcata.2009.05.016)

[57]. Chakraborty, P.,Adhikary, J.,Ghosh, B.,Sanyal, R.,Chattopadhyay, S. K.,Bauzá, A.,Frontera, A.,Zangrando, E.,Das, D. (2014), Relation between the Catalytic Efficiency of the Synthetic Analogues of Catechol Oxidase with Their Electrochemical Property in the Free State and Substrate-Bound State, Inorganic chemistry, 53, 8257-8269.(DOI: 10.1021/ic5005177)

[58]. Majumder, S.,Sarkar, S.,Sasmal, S.,Sañudo, E. C.,Mohanta, S. (2011), Heterobridged dinuclear, tetranuclear, dinuclear-based 1-D, and heptanuclear-based 1-D complexes of copper(II) derived from a dinucleating ligand: Syntheses, structures, magnetochemistry, spectroscopy, and catecholase activity, Inorganic Chemistry, 50, 7540-7554.(DOI: 10.1021/ic200409d)

[59]. Banu, K. S.,Chattopadhyay, T.,Banerjee, A.,Bhattacharya, S.,Suresh, E.,Nethaji, M.,Zangrando, E.,Das, D. (2008), Catechol Oxidase Activity of a Series of New Dinuclear Copper (II) Complexes with 3 , 5-DTBC and TCC as Substrates : Syntheses , X-ray Crystal Structures , Spectroscopic Characterization of the Adducts and Kinetic Studies, Inorganic Chemistry, 47, 7083-7093.(DOI: 10.1021/ic701332w)

[60]. Shyamal, M.,Mandal, T. K.,Panja, A.,Saha, A. (2014), Influence of anionic co-ligands on the structural diversity and catecholase activity of copper(ii) complexes with 2-methoxy-6-(8-iminoquinolinylmethyl)phenol, RSC Advances, 4, 53520-53530.(DOI: 10.1039/C4RA08025D)

[61]. Biswas, A.,Das, L. K.,Drew, M. G. B.,Aromí, G.,Gamez, P.,Ghosh, A. (2012), Synthesis, Crystal Structures, Magnetic Properties and Catecholase Activity of Double Phenoxido-Bridged Penta-Coordinated Dinuclear Nickel(II) Complexes Derived from Reduced Schiff-Base Ligands: Mechanistic Inference

of Catecholase Activity, Inorganic Chemistry, 51, 7993-8001.(DOI: 10.1021/ic202748m)

[62]. Monzani, E.,Quinti, L.,Perotti, A.,Casella, L.,Gullotti, M.,Randaccio, L.,Geremia, S.,Nardin, G.,Faleschini, P.,Tabbì, G. (1998), Tyrosinase Models. Synthesis, Structure, Catechol Oxidase Activity, and Phenol Monooxygenase Activity of a Dinuclear Copper Complex Derived from a Triamino Pentabenzimidazole Ligand, Inorganic Chemistry, 37, 553-562.(DOI: 10.1021/ic970996n)

[63]. Chyn, J.-P.,Urbach, F. L. (1991), Autoxidation of 3,5-di-t-butylcatechol catalyzed by two pyrazolatebridged dicopper complexes with different structural features, Inorganica Chimica Acta, 189, 157-163.(DOI: 10.1016/S0020-1693(00)80184-X)

[64]. Balla, J.,Kiss, T.,Jameson, R. F. (1992), Copper(II)-catalyzed oxidation of catechol by molecular oxygen in aqueous solution, Inorganic Chemistry, 31, 58-62.(DOI: 10.1021/ic00027a012)

[65]. Selmeczi, K.,Réglier, M.,Giorgi, M.,Speier, G. (2003), Catechol oxidase activity of dicopper complexes with N-donor ligands, Coordination Chemistry Reviews, 245, 191-201.(DOI: 10.1016/j.cct.2003.08.002)

[66]. Ackermann, J.,Meyer, F.,Kaifer, E.,Pritzkow, H. (2002), Tuning the Activity of Catechol Oxidase Model Complexes by Geometric Changes of the Dicopper Core, Chemistry – A European Journal, 8, 247-258.(DOI: 10.1002/1521-3765(20020104)8:1<247::AID-CHEM247>3.0.CO;2-P)

[67]. Kodera, M.,Kawata, T.,Kano, K.,Tachi, Y.,Itoh, S.,Kojo, S. (2003), Mechanism for Aerobic Oxidation of 3,5-Di-tert-butylcatechol to 3,5-Di-tert-butyl-o-benzoquinone Catalyzed by Di-μ-hydroxo-dicopper(II) Complexes of Peralkylated Ethylelnediamine Ligands, Bulletin of the Chemical Society of Japan, 76, 1957-1964.(DOI: 10.1246/bcsj.76.1957)

[68]. Kaizer, J.,Pap, J.,Speier, G.,Párkányi, L.,Korecz, L.,Rockenbauer, A. (2002), Synthesis, structure and catecholase activity of dinuclear copper and zinc complexes with an N_3^- ligand, Journal of Inorganic Biochemistry, 91, 190-198.(DOI: 10.1016/S0162-0134(02)00459-2)

[69]. John V. Bennett,William Robert Jarvis,Brachman, P. S., (2007), Epidemiology of Healthcare-Assosiated Infections. In: Bennett & Brachman's Hospital Infections, 5th edn. Lippincott Williams & Wilkins, USA, pp. 5-7

[70]. Ducel, G.,Fabry, J.,Nicolle, L., (2002), Prevention of hospital-acquired infections.2nd ed. World Health Organization, pp. 9-15

[71]. Brusch, J. L., (2011), Overview of endocarditis. In: Endocarditis Essentials, Jones and Barlett Publishers, USA, pp. 7–10

[72]. Thangamani, S.,Mohammad, H.,Abushahba, M. F. N.,Sobreira, T. J. P.,Hedrick, V. E.,Paul, L. N.,Seleem, M. N. (2016), Antibacterial activity and mechanism of action of auranofin against multi-drug resistant bacterial pathogens, Scientific Reports, 6, 22571.(DOI: 10.1038/srep22571)

[73]. Miao, T.-F.,Li, J.,Li, S.,Wang, N.-L. (2014), Theoretical Studies on DNA-Photocleavage Efficiency and Mechanism of Functionalized Ru(II) Polypyridyl Complexes, The Journal of Physical Chemistry A, 118, 5692-5699.(DOI: 10.1021/jp502937b)

[74]. Becke, A. D. (1988), Density-functional exchange-energy approximation with correct asymptotic behavior, Physical Review A, 38, 3098-3100.(DOI: 10.1103/PhysRevA.38.3098)

[75]. Lee, C.,Yang, W.,Parr, R. G. (1988), Development of the Colle-Salvetti correlation-energy formula into a functional of the electron density, Physical Review B, 37, 785-789.(DOI: 10.1103/PhysRevB.37.785)

[76]. Frisch, M. J.,Trucks, G. W.,Schlegel, H. B.,Scuseria, G. E.,Robb, M. A.,Cheeseman, J. R.,Scalmani, G.,Barone, V.,Mennucci, B.,Petersson, G. A.,Nakatsuji, H.,Caricato, M.,Li, X.,Hratchian, H. P.,Izmaylov, A. F.,Bloino, J.,Zheng, G.,Sonnenberg, J. L.,Hada, M.,Ehara, M.,Toyota, K.,Fukuda, R.,Hasegawa, J.,Ishida, M.,Nakajima, T.,Honda, Y.,Kitao, O.,Nakai, H.,Vreven, T.,Montgomery Jr., J. A.,Peralta, J. E.,Ogliaro, F.,Bearpark, M. J.,Heyd, J.,Brothers, E. N.,Kudin, K. N.,Staroverov, V. N.,Kobayashi, R.,Normand, J.,Raghavachari, K.,Rendell, A. P.,Burant, J. C.,Iyengar, S. S.,Tomasi, J.,Cossi, M.,Rega, N.,Millam, N. J.,Klene, M.,Knox, J. E.,Cross, J. B.,Bakken, V.,Adamo, C.,Jaramillo, J.,Gomperts, R.,Stratmann, R. E.,Yazyev, O.,Austin,

A. J.,Cammi, R.,Pomelli, C.,Ochterski, J. W.,Martin, R. L.,Morokuma, K.,Zakrzewski, V. G.,Voth, G. A.,Salvador, P.,Dannenberg, J. J.,Dapprich, S.,Daniels, A. D.,Farkas, Ö.,Foresman, J. B.,Ortiz, J. V.,Cioslowski, J.,Fox, D. J. (2009), Gaussian 09, Gaussian, Inc.: Wallingford, CT, USA.

[77]. Tomasi, J.,Mennucci, B.,Cammi, R. (2005), Quantum Mechanical Continuum Solvation Models, Chemical Reviews, 105, 2999-3094.(DOI: 10.1021/cr9904009)

[78]. Liu, X. W.,Li, J.,Deng, H.,Zheng, K. C.,Mao, Z. W.,Ji, L. N. (2005), Experimental and DFT studies on the DNA-binding trend and spectral properties of complexes $[Ru(bpy)_2L]^{2+}$ (L = dmdpq, dpq, and dcdpq), Inorganica Chimica Acta, 358, 3311-3319.(DOI: 10.1016/j.ica.2005.05.006)

[79]. Mei, W. J.,Liu, J.,Zheng, K. C.,Lin, L. J.,Chao, H.,Li, A. X.,Yun, F. C.,Ji, L. N. (2003), Experimental and theoretical study on DNA-binding and photocleavage properties of chiral complexes Δ- and Λ- $[Ru(bpy)_2L]$ (L = *o*-hpip, *m*-hpip and *p*-hpip), Dalton Transactions, 7, 1352-1359.(DOI: 10.1039/B212443B)

[80]. Chakraborty, P.,Adhikary, J.,Ghosh, B.,Sanyal, R.,Chattopadhyay, S. K.,Bauzá, A.,Frontera, A.,Zangrando, E.,Das, D. (2014), Relation between the Catalytic Efficiency of the Synthetic Analogues of Catechol Oxidase with Their Electrochemical Property in the Free State and Substrate-Bound State, Inorganic Chemistry, 53, 8257-8269.(DOI: 10.1021/ic5005177)

[81]. Vázquez-Fernández, M. Á.,Bermejo, M. R.,Fernández-García, M. I.,González-Riopedre, G.,Rodríguez-Doutón, M. J.,Maneiro, M. (2011), Influence of the geometry around the manganese ion on the peroxidase and catalase activities of Mn(III)–Schiff base complexes, Journal of Inorganic Biochemistry, 105, 1538-1547.(DOI: 10.1016/j.jinorgbio.2011.09.002)

Chapter 4

Nickel(II) and copper(II) complexes constructed with flexible Schiff base ligand: Synthesis, X-ray crystal structure, enzyme catalysis and biological applications

Chapter 4

Nickel(II) and copper(II) complexes constructed with flexible Schiff base ligand: Synthesis, X-ray crystal structure, enzyme catalysis and biological applications

The flexibility of Schiff base ligands (**HL^1** and **HL^2**) upon variation of different metal ions was explored in previous two chapters but with changing reaction conditions or with variation of auxiliary anion with same metal has not produced any pair of complexes where the ligand is in two different conformation. For this reason a modified Schiff base ligand **HL^3** [2-(phenyl((2-(piperazin-1-yl)ethyl)imino)methyl)phenol] has been introduced. Structural features and different applications of four newly synthesized metal complexes formed by the reaction of this ligand **HL^3** with Cu(II) and Ni(II) salts are discussed in two parts.

4A - Investigation on chemical protease, nuclease and catecholase activity of copper(II) complexes with flexidentate Schiff base ligands

And

4B - Counter anion directed flexibility of Ni(II) Schiff base complexes: Lysozyme binding and glycosidase activity

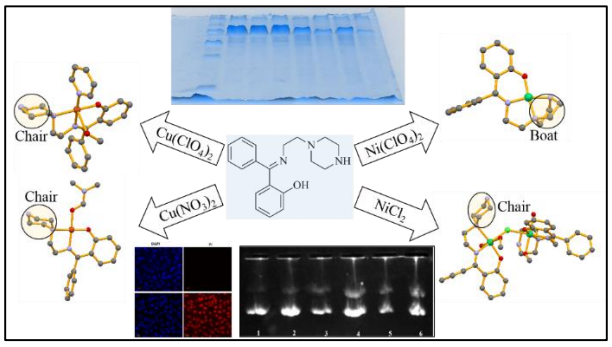

***Figure 4. 1**. Schematic representation of metal ion and counter anion dependent flexibility towards various applications.*

Chapter 4A

Investigation on chemical protease, nuclease and catecholase activity of copper(II) complexes with flexidentate Schiff base ligands

4A.1 Introduction

Bioinorganic chemistry is an embryonic area in chemical biology for diverse use of metal complexes in therapeutic applications.[1, 2] Transition metal complexes with their tunable coordination geometry, versatile redox and spectroscopic properties are suitable for designing metal-based therapeutic agents.[3] Currently, much of the information regarding the role of metals in natural systems has been obtained through comparative studies on metalloenzymes and model metal complexes.[4] Thus, use of transition metals by nature in different biological processes drives the quest of the scientist to understand the underlying principles of its functionality, which eventually helps to develop different structural and more importantly functional model systems.[5] Among the large variety of enzymatic systems, protease, nuclease, and catecholase get a great attention in recent years.[6-9] Inside big library of model mimicking metalloenzyme, copper is one of widely used metals as it has been reported as a bio-essential element for a long time[10] but its biological importance is only getting explored in the past few decades during the development of bioinorganic chemistry and successful studies of interaction of model complexes with various bio-macromolecules have been taken up as a consequence.[11-14]

Metal based synthetic proteases are one of the focus point to bioinorganic chemists due to its significance as artificial peptidases and anti-metastasis agents.[15] Thus there is a great interest in designing the artificial metalloproteases that can cleave proteins at a specific site.[16] Development of

peptide bond cleaving reagents (artificial peptidases) is thought-provoking as peptide bond is the most stable chemical bonds in nature ($t_{1/2}$, 7-600 years at ambient temperature; pH 7).[17] These cleaving agents will be valuable in investigating the arrangement of structures of proteins. Small metal complexes may assume the role of proteases and could be utilized to create responsive intermediates for peptide bond cleavage at chosen sites on proteins.[18, 19]

Apart from protease activity, DNA binding and nuclease activity of small metal complexes is one of the important phenomena in bioinorganic chemistry. As copper complexes are capable of binding and cleaving DNA selectively under physiological conditions without using any external reagent thus metal based pseudonucleases generate a new era in the field of nucleic acid chemistry for their versatile use in foot printing, sequence-specific binding to nucleic acids, and as new structural probes and therapeutic anti-proliferative agents.[20, 21]

Moreover, copper based enzymes which are capable of possessing molecular oxygen at ambient condition have received a considerable attention to the scientists to develop such biologically active model systems which are able to oxidize some catechol moiety to its corresponding diquinones following an enzyme catalysis pathway.[22] These oxidation reactions are also having great role in medicinal aspect for the determination of the hormonally active catecholamines: adrenaline, noradrenaline and l-dopa.[23, 24]

There were reports in literature where copper complexes have played active role in chemical nuclease as well as protease activity.[9, 25] Here in this chapter we have planned to make such copper based systems which can diversely show protease, nuclease as well as catecholase activity. In this scenario we have developed one new fliexidentate Schiff base ligand 2-(phenyl((2-(piperazin-1-yl)ethyl)imino)methyl)phenol (**HL^3**) to synthesize two copper complexes $[Cu(HL^3)(MeOH)(Py)](ClO_4)_2$ **(8)** and $[Cu(HL^3)(DMF)](NO_3)_2$ **(9)**. The idea of using the flexidentate ligand was to allow the copper complexes to bind the substrate more easily as the flexibility of the ligand can pave the way for increased metal-substrate interaction. In case of the chosen ligand the piperazinyl arm of the Schiff base can show flexible behavior by adopting either

chair or boat conformation.[5, 26] However, in this study the piperazinyl arm remains in chair form making the ligand effectively tridentate in nature leaving enough coordination position available for binding of the substrate. Affinity of the synthesized complexes towards BSA protein has been explored and further scrutiny towards protease activity is also carried out. Interaction of complexes with DNA, applying both binding and cleavage experiment are also experimented followed by cell cytotoxicity measurement. Moreover, complexes were also investigated for possible catecholase like activity. Interestingly both the complexes have shown interesting versatile activity towards protease, nuclease and catecholase activity.

4A.2 Experimental section

4A.2.1 Materials and methods

All the chemical reagents required were purchased from sigma and used without further purification. The specifications of all the instruments used for analysis purpose were same as described in the section 2.2.1 of the previous chapter 2.

4A.2.2 X-ray crystallography

The crystals were mounted onto quartz fibers and the X-ray diffraction intensity data were measured at 153 K with a Bruker APEX II diffractometer equipped with a CCD detector, employing Mo Kα radiation (λ = 0.71073 Å), with the SMART suite of programs.[27] All data were processed and corrected for Lorentz and polarization effects with SAINT and for absorption effects with SADABS.[28] Structure solution and refinement were carried out with the SHELXTL suite of programs.[29] Data were corrected for absorption effects using the multi-scan method (SADABS). The structures were solved by Patterson maps to locate the heavy atoms, followed by difference maps for the light, non-hydrogen atoms. All non-hydrogen atoms were refined with anisotropic thermal parameters. Crystal data and structural parameters are provided in Table 4A.1.

***Table 4A. 1**. Crystallographic data and structure refinement parameters for **8** and **9**.*

Complex	**8**	**9**
Empirical Formula	$C_{25}H_{32}Cl_2CuN_4O_{10}$	$C_{22}H_{30}CuN_6O_8$
Formula weight	682.98	570.06
Crystal system	Monoclinic	Triclinic
Space group	P 2_1/c	P -1
a (Å)	17.4916(7)	8.9789(3)
b (Å)	10.6731(4)	10.1049(3)
c (Å)	15.2492(7)	14.9074(4)
α (°)	90	108.7631(17)
β (°)	97.6228(19)	99.4028(18)
γ(°)	90	99.2970(19)
V (Å^3)	2821.71	1229.84(7)
λ (Å)	0.71073	0.71073
ρ_{calcd} (mg m^{-3})	1.608	1.539
Z	4	2
T (K)	153(2)	153(2)
μ (mm^{-1})	0.968	1.887
F(0 0 0)	1412	594
Crystal size (mm^3)	0.20 × 0.18 × 0.14	0.10 × 0.06 × 0.04
θ ranges (°)	2.53 – 22.09	2.36 – 22.77
h/k/l	-24,21/-14,14/-20,20	-12,12/-14,14/-21,21
Reflections collected	47762	41983
Independent reflections	7613	7330
T_{max} and T_{min}	0.73 and 0.87	0.90 and 0.96
Data/restraints/parameters	7613 / 2 / 427	7330 / 0 / 336
GOF	1.015	1.017
Final R indices [I > 2σ(I)]	R1 = 0.0523, wR2 = 0.1121	R1 = 0.0398, wR2 = 0.0866
R indices (all data)	R1 = 0.1195, wR2 = 0.1360	R1 = 0.0615,wR2 = 0.0962
Largest peak and hole (e Å^{-3})	0.445 and -0.487	0.624 and -0.447

4A.2.3 Synthesis of 2-(phenyl((2-(piperazin-1-yl)ethyl)imino)methyl)phenol (HL^3)

1.98 g (10 mmol) of 2-Hydroxybenzophenone dissolved in 10 mL of chloroform was added into a solution of 1.29 g of amino ethyl piperazine (10 mmol) in 5 mL of chloroform. The mixture was stirred for 2 hours at room temperature. After evaporation of the volatile solvent, a yellow oily compound (**HL^3**) is formed. Yield: 72%. ^{1}H NMR (400.13 MHz, 298 K, $CDCl_3$): δ 15.66 (s, 1H, phenolic OH), 6.57–7.52 (m, 9H, aromatic H), 3.39-3.48 (t, 2H, aliphatic –CH_2), 2.79-2.88 (m, 4H, cyclohexene –CH_2), 2.60-2.68 (t, 2H, aliphatic –CH_2), 2.34-2.43 (t, 4H, cyclohexene –CH_2) (Figure 4A.1); ^{13}C NMR (100.61 MHz, 293 K, DMSO): δ 174.6, 163.7, 133.9, 132.5, 131.5, 129.1, 128.8, 127.3, 119.7, 118.2, 117.2, 59.4, 54.6, 48.8, 46.0. (Figure 4A.2) $C_{19}H_{23}N_3O$ (m/z) calculated – 309.18 $(M)^+$; obtained – 310.5 $(M + H)^+$ (Figure 4A.3)

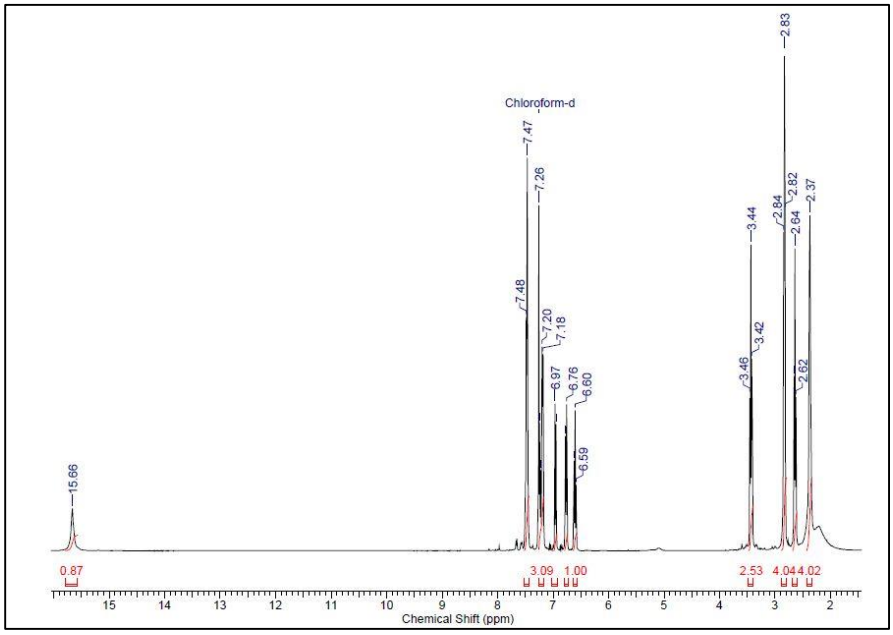

***Figure 4A. 1**. ^{1}H NMR for Ligand (**HL^3**)*

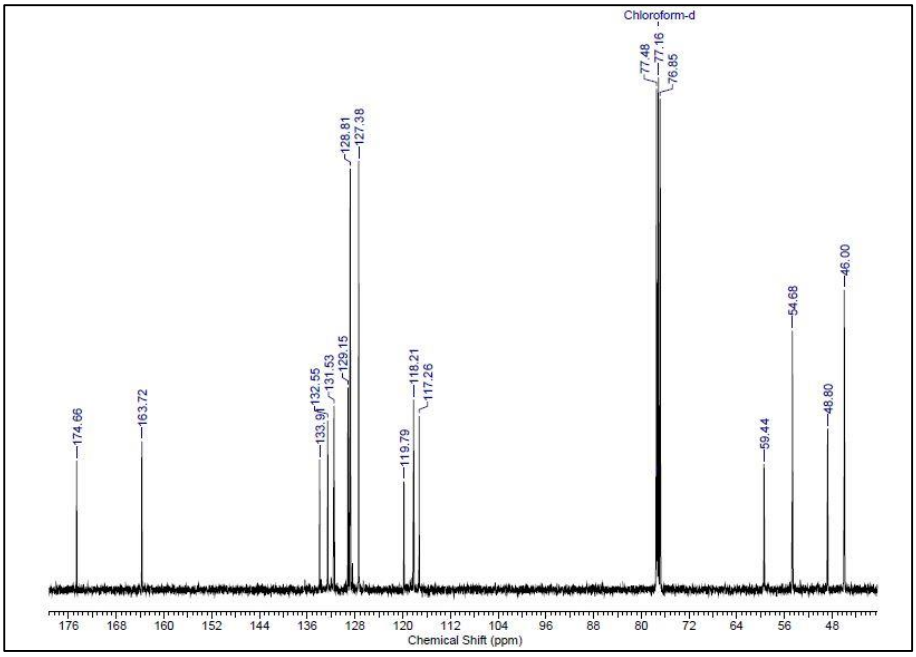

Figure 4A. 2*. ^{13}C NMR for Ligand (**HL³**)*

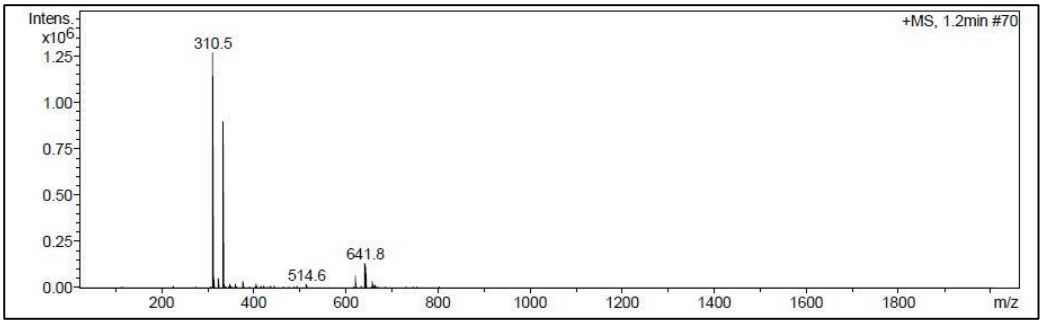

Figure 4A. 3. *ESI-MS Spectra of Ligand (**HL³**)*

4A.2.4 Synthesis of $[Cu(HL^3)(MeOH)(Py)](ClO_4)_2$ (8)

At first 15 mL of methanolic solution containing **HL³** (0.15 g, 0.5 mmol) and $Cu(ClO_4)_2.6H_2O$ (0.18 g, 0.5 mmol) was stirred at room temp for 1h. Then after evaporating the solvent, the concentrated solution was kept for few days. Finally after 6 or 7 days green block shaped crystals of **8** were obtained from the slow evaporation of reaction mixture. Yield: 82%. Anal. Calcd. (%) : $C_{24}H_{28}Cl_2CuN_4O_9$ C, 44.28; H, 4.34; N, 8.61. Found (%): C, 44.12; H, 4.88; N, 8.55. $[C_{24}H_{28}CuN_4O]^{2+}$ (m/z) calculated – 226.0 (m/z); obtained – 226.0 (m/z). (Figure 4A.4) Selected IR on KBr (ν/cm^{-1}): 1595 (–C=N), 1045 (ClO_4^-).

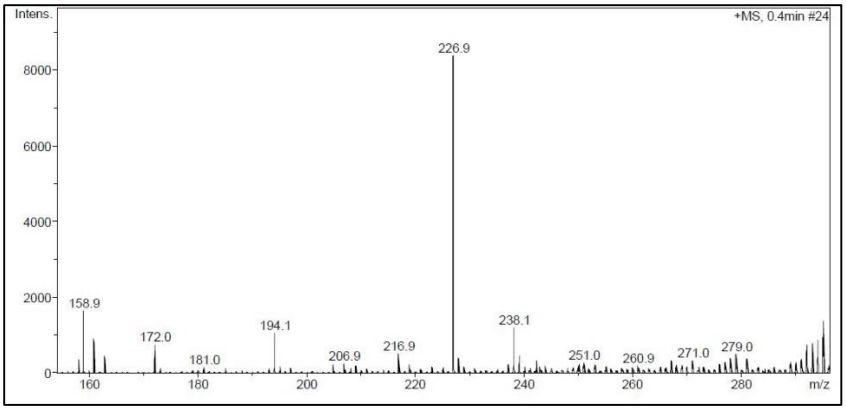

Figure 4A. 4*. ESI-MS Spectra of Complex* ***8***

4A.2.5 Synthesis of $[Cu(HL^3)(DMF])(NO_3)_2$ (9)

At first 15 mL of methanolic solution containing **HL^3** (0.15 g, 0.5 mmol) and $Cu(NO_3)_2.3H_2O$ (0.12 g, 0.5 mmol) was stirred at room temp for 1h. Then after evaporating the solvent, the sticky compound obtained was dissolved in DMF. Finally after 6 or 7 days green block shaped crystal of **9** was obtained from this solution after layering with diethyl ether. Yield: 76%. Anal. Calcd. (%) : $C_{22}H_{30}CuN_6O_8$ C, 46.34; H, 5.30; N, 14.74. Found (%): C, 46.22; H, 5.46; N, 14.92. $[C_{22}H_{28}CuN_4O_2]^{2+}$ (m/z) calculated – 221.0 (m/z); obtained – 221.0 (m/z). (Figure 4A.5) Selected IR on KBr (ν/cm^{-1}): 1605 (–C=N), 1342 (NO_3^-).

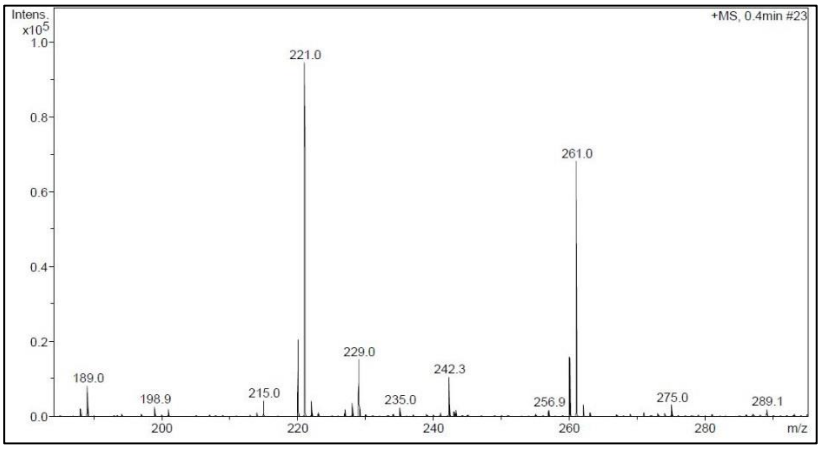

Figure 4A. 5*. ESI-MS Spectra of Complex* ***9***

4A.2.6 Protein binding study

The binding interactions experiments of complexes **8** and **9** with BSA protein were carried out following the protocols as mentioned in the section 2.2.10 of previous chapter 2.

4A.2.7 Circular dichroism measurements

The change in the secondary structure of BSA protein after interaction with complexes **8** and **9** were studied by the circular dichroism measurements following the similar protocols as mentioned in the section 2.2.11 of previous chapter 2.

4A.2.8 Protease activity study

Two different concentrations of **8** and **9** (250 and 500 μM) were incubated with 0.3 mg per mL BSA in 10 mM Tris-HCl (pH, 7.4) (in presence and absence of H_2O_2) and incubated overnight at 37 °C. The samples were mixed with Laemmli buffer and denatured in a boiling water bath for 5 minutes then desolved on 10% SDS-PAGE in 1x Trisglycine buffer. After electrophoresis gels were scanned and stained in a Coomassie brilliant blue staining solution (0.1% w/v Coomassie brilliant blue R250 in 45% v/v methanol and 10% v/v acetic acid), and destained in a destaining solution (45% v/v methanol, 45% v/v water and 10% v/v acetic acid). The destained gels were then scanned on a digital scanner (Canon) and photographs of the fractionated Coomassie stained protein bands were taken by using a gel documentation system (BioRad).

4A.2.9 Deconvoluted ESI-MS study for protease activity

ESI-MS spectra was recorded after incubation of BSA protein with H_2O_2 in presence and absence of complexes at the range of 1500-2500. And further the collected data was deconvoluted using machine software Bruker daltronics to get the exact mass of native protein.

4A.2.10 Cell culture

Hela cells (Human cervical carcinoma cell lines) were procured from National Centre For Cell Science (NCCS), Pune, India and grown in DMEM (GIBCO) supplemented with 5 % FBS (fetal bovine serum), and 100 IU mL^{-1} of penicillin, 100 mg mL^{-1} of streptomycin and 0.25 mg mL^{-1}. The cells were maintained at 37º C in a humidified CO_2 (5%) incubator. The adherent cultures were grown as a monolayer and were passaged once in every 3-4 days.

4A.2.11 MTT assay for the study of cell cytotoxicity

To investigate the cytotoxicity effect of copper Schiff base complex on HeLa cells, an *in vitro* colorimetric MTT (3-(4,5-dimethylthiazol-2-yl)-2,5-diphenyltetrazolium bromide) assay has been performed. This assay is based on the metabolic reduction of soluble MTT into an insoluble colored formazan product which is measured spectrophotometrically after dissolving in DMSO. The compounds were used at various concentrations ranging from 0 to 500 µM (50, 90, 100, 150, 200, 300, 500 µM) with quadruplet sets for each concentration. After 48, and 72 h of drug treatment, the cell viability was measured spectrophotometrically at 595 nm using a microplate reader (Biorad, USA). The IC_{50} value for each compound was calculated using Origin 8.1 (OriginLab, USA) software as the concentration of the compound tested which inhibited the growth of 50% of the cells relative to the untreated control cells.

4A.2.12 Confocal microscopy

HeLa cells were harvested at the exponential growth phase and were plated into 96 well flat bottom culture plates at a cell density of 10^4 per well in 2 mL of DMEM complete medium. The cells were incubated for an additional 24 h at 37º C for growth and adherence of the cells. After this incubation period, the medium was then aspirated and was replaced with 2 mL of fresh incomplete medium containing Cu(II) complexes at its IC_{50} concentration and incubated for 16 h. After the drug treatment, the medium was aspirated and cells incubated

with DAPI solution (100 ng mL^{-1}) for 15 min at 37º C. The cells were washed twice with PBS (pH 7.4) prior to treatment with propidium idodie (PI) staining solution (1 mg mL^{-1}) for 15 min at 37º C. The stained cells were then washed properly to remove the excess PI. Images were acquired on the confocal microscope (Olympus Ix 83) and analyzed using the FluoView software.

4A.2.13 Catecholase activity study

Catecholase like activities of complexes **8**, and **9** were also studied following the similar procedure as described in the section 2.2.12 of previous chapter 2.

4A.2.14 Detection of hydrogen peroxide in the catalytic reactions

Modification of iodometric method as described in the section 2.2.13 of chapter 2, is employed to detect H_2O_2 during the catalytic reaction.

4A.2.15 Supplementary Materials

CCDC 1421492, and 1421493 contain the supplementary crystallographic data for complex **8** and **9**, respectively. These data can be obtained free of charge via http://www.ccdc.cam.ac.uk/conts/retrieving.html, or from the Cambridge Crystallographic Data Centre, 12 Union Road, Cambridge CB2 1EZ, UK; fax: (+44) 1223-336-033; or e-mail: deposit@ccdc.cam.ac.uk.

4A.3 Results and discussion

4A.3.1 Synthesis and characterization

Synthesis of ligand (**HL^3**) and its four metal complexes are depicted in the scheme 4A.1.

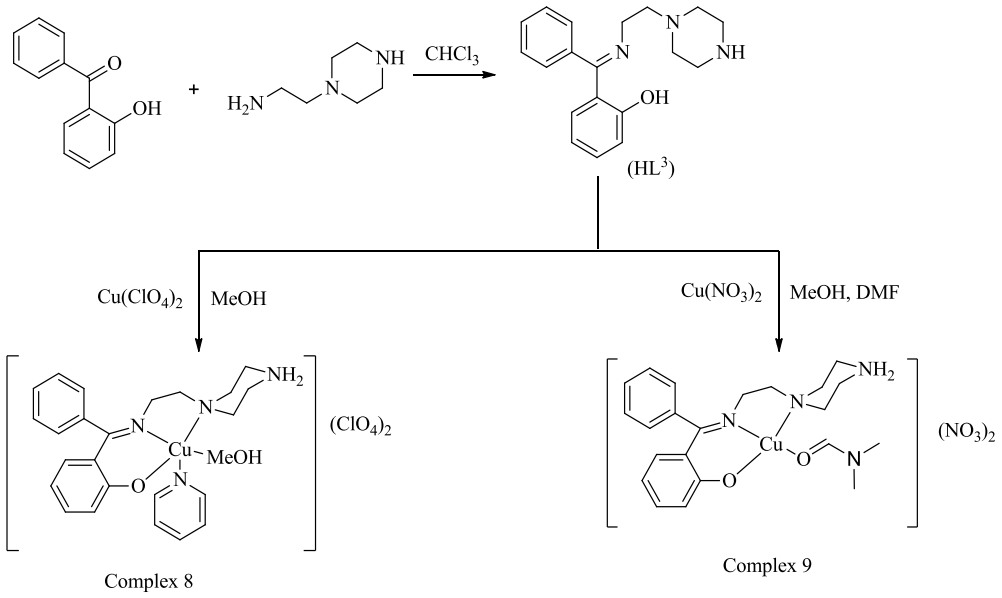

Scheme 4A. 1**. Formation of two Cu(II) Schiff base complexes **8** & **9

This ligand has been characterized by ^{1}H and ^{13}C NMR and ESI-MS spectroscopy. All the complexes have been characterized by IR and ESI-MS spectroscopy, elemental analysis and single crystal X-ray crystallography. From the integrated ^{1}H NMR spectroscopy of **HL^{3}**, peaks for aromatic protons have been observed in the region 6.5-.8.0 ppm. The phenolic –OH proton shows signal at 15.66 ppm. The aliphatic protons are detected within the usual range of 2.37 - 3.46 ppm. ^{13}C NMR spectra also confirmed the proposed structure for ligand (**HL^{3}**). The IR spectra of ligand and complexes have shown characteristic band for –C=N in the region 1590-1610 cm^{-1}.[30] FT-IR signals for non-coordinated ClO_4^- and NO_3^- were also observed at 1042 cm^{-1} and 1342 cm^{-1}, respectively.[30] The electronic spectra of complex **8** and **9** (Figure 4A.6) have been studied in the solution state using CH_3OH as solvent. The broad peaks in between 200-500 nm indicate the intramolecular LMCT transition.[31] The d-d transitions for copper (II) ions were observed centered around 620 nm.

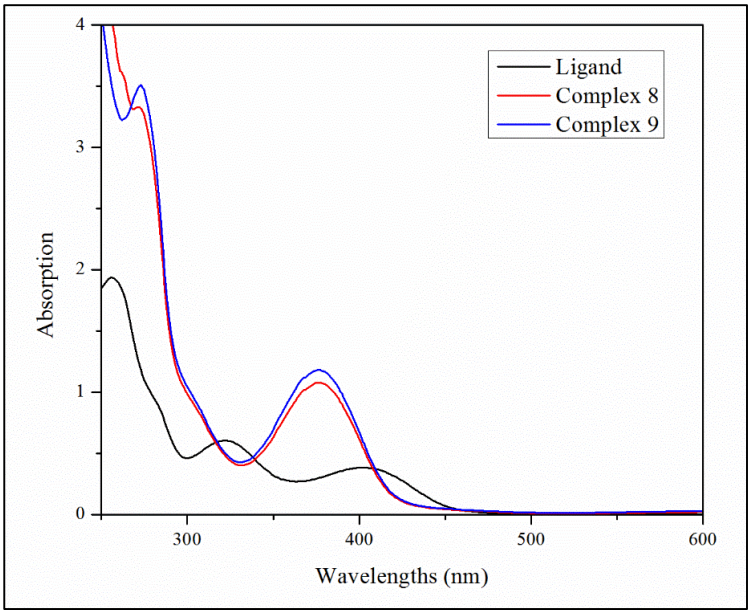

Figure 4A. 6. *Electronic spectra of two copper complexes **8** & **9**.*

4A.3.2 Crystal structure of complex 8 and 9

Crystal structures of these two complexes exhibit two different types of Cu (II) centered coordination geometry where complex **8** is penta-coordinated and complex **9** is tetra-coordinated.

The mono metallic complex **8** crystalizes in the space group $P2_{1/C}$. The central metal atom is coordinated to the tridentate Schiff base ligand (**HL^3**) and one pyridine and one methanol molecule to give penta-coordinated square pyramidal geometry (Figure 4A.7). N, N, O donor sites of Schiff base (**HL^3**) and N donor site of pyridine are on the equatorial face of square pyramidal geometry while O donor site from methanol molecule lies on the axial position of square pyramid.

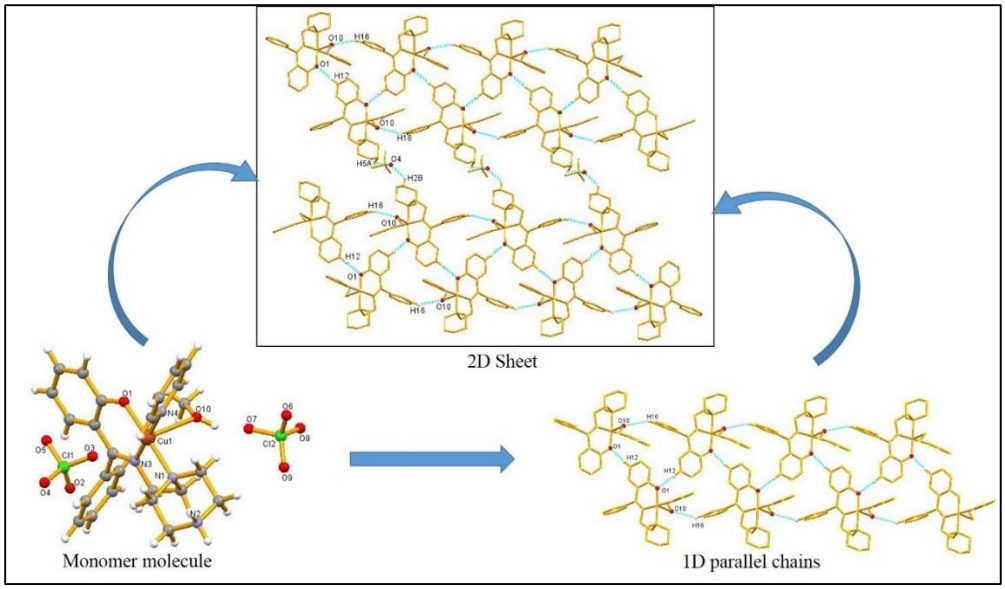

Figure 4A. 7*. Supramolecular interactions of complex* ***8***

The piperazinyl ring takes the chair conformation where secondary nitrogen atom coordinates one extra proton and stays away from the coordination. The distortion of the coordination geometry of penta-coordinated system can be calculated by the τ_5 value, a reference to describe the degree of distortion for square-pyramid and trigonal-bipyramid [square pyramid, $\tau_5 = 0$; trigonal-bipyramid, $\tau_5 = 1$; $\tau = (\beta - \alpha)/60°$, α and β are the two largest angles around the central atom].[32] The τ_5 value for complex **8** is 0.003, indicating a perfect square-pyramidal geometry adopted by copper center. In complex **8**, the average co-ordination bond angle around the Cu center of square pyramidal geometry is 89.25°, whereas the least bond angle was observed for N(3)–Cu(1)–N(1) (~85.91°) (Table 4A.2) due to the formation of a chelated five membered ring.

Table 4A. 2*. Selected bond lengths (Å) and bond angles (°) for* ***8*** *and* ***9***

Complex	**8**	**9**
Cu(1)-O(1)	1.876(2)	1.862(2)
Cu(1)-N(1)	2.081(2)	1.930(2)
Cu(1)-N(3)	1.935(3)	.....
Cu(1)-O(2)	.....	1.968(2)
Cu(1)-N(2)	.....	2.043(2)

Cu(1)-N(4)	2.002(3)	.....
Cu(1)-O(10)	2.699(3)	.....
O(1)-Cu(1)-N(1)	178.0(1)	.....
O(10)-Cu(1)-N(1)	89.95(9)	.....
N(1)-Cu(1)-N(3)	84.9(1)	.....
N(1)-Cu(1)-N(4)	96.1(1)	.....
N(3)-Cu(1)-O(1)	93.2(1)	.....
N(3)-Cu(1)-O(10)	85.6(1)	.....
N(1)-Cu(1)-N(2)	.....	87.25(7)
N(1)-Cu(1)-O(1)	.....	94.05(7)
N(1)-Cu(1)-O(2)	.....	175.14(2)
N(2)-Cu(1)-O(1)	.....	178.20(7)
N(2)-Cu(1)-O(2)	.....	89.25(6)
O(1)-Cu(1)-O(2)	.....	89.39(6)

Furthermore, the independent molecules get connected to each other for making 1D supra-molecular chain like structure (Figure 4A.7) *via* formation of C16–H16···O10 hydrogen bonding. Similar kind of 1D chain oriented in opposite direction connected to each other *via* C12–H12···O1 hydrogen bonding. Furthermore these kinds of two parallel chains are linked through C5–H5A···O4 and N2–H2B···O4 hydrogen bonding networks to build a 2D plane.

Complex **9** is crystalized in the space group *P-1* where the central metal lies in tetra-coordinated geometry. Three coordination sites of central metal atom are fulfilled by Schiff base ligand (**HL^3**) and one site is occupied by a DMF molecule. The square planar geometry of Cu(1) is further proved by τ_4 index which defines the distortion between a perfect tetrahedron ($\tau_4 = 1$) and a perfect square planar geometry ($\tau_4 = 0$) using the formula: $\tau_4 = [360° - (\alpha + \beta)]/141°$, with α and β (in °) being the two largest angles around the central metal in the complex.[33] The τ_4 value for Cu(1) is 0.04, satisfying somewhat a perfect square planar geometry for this metal center. Individual molecules get connected with each other through an intermediate nitrate anion forming hydrogen bonding like N3–H3A···O5, N3–H3A···O3, C16–H16B···O3, C21–H21A···O3, C9–H9···O4 and C15–H15B···O4 to make a 1D chain. Two such 1D chains are

further connected through C4–H4···O4 and C9–H9···O4 hydrogen bonding to make a 2D sheet (Figure 4A.8).

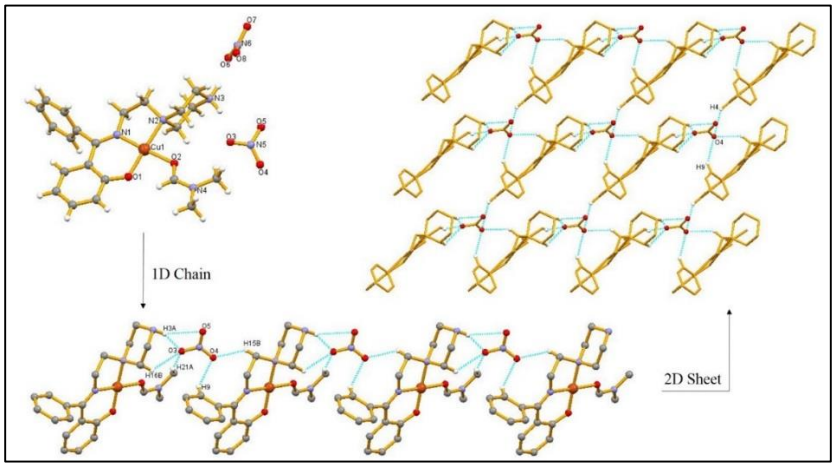

Figure 4A. 8*. Supramolecular interactions of complex* ***9****.*

4A.3.3 Protein binding studies

Qualitative analysis of the binding of chemical compounds to BSA is usually detected by inspecting the fluorescence spectra. Generally, the fluorescence of BSA is caused by two intrinsic moiety of the protein, namely tryptophan and tyrosine. Changes in the emission spectra of tryptophan are common in response to protein conformational transitions, subunit associations, substrate binding, or denaturation. Therefore, the intrinsic fluorescence of BSA can provide considerable information on their structure and dynamics and is often utilized in the study of protein folding and association reactions. The interaction of BSA with these compounds was studied by fluorescence measurement at room temperature.

The addition of above compounds to the solution of BSA resulted a significant decrease of the fluorescence intensity of BSA at near about 340 nm. The fluorescence quenching data was further analyzed by the Stern-Volmer relation which again can be expressed in terms of bimolecular quenching rate constant and average life time of the fluorophore as shown in following equation.[5]

$$\frac{F_0}{F} = 1 + k_q\tau_0[Q] = 1 + K_{SV}[Q]$$

where F_0 and F are the fluorescence intensities in the absence and the presence of a quencher, k_q is the bimolecular quenching rate constant, τ_0 is the average life time of fluorophore in the absence of a quencher and [Q] is the concentration of a quencher (Metal complexes). K_{SV} is the Stern-Volmer quenching constant in M^{-1}. To determine the binding constant and number of binding site Scatchard equation was employed which is given by

$$\log\left[\frac{F_0 - F}{F}\right] = \log K_a + n\log[Q]$$

Where K_a and n are the binding constant and number of binding sites respectively, and F_0 and F are the fluorescence intensities in the absence and presence of the quencher respectively. Thus, a plot of $\log(F_0 - F)/F$ versus log[Q] (Figure 4A.9) can be used to determine the value of binding constant (from intercept) and number of binding sites (from slope).

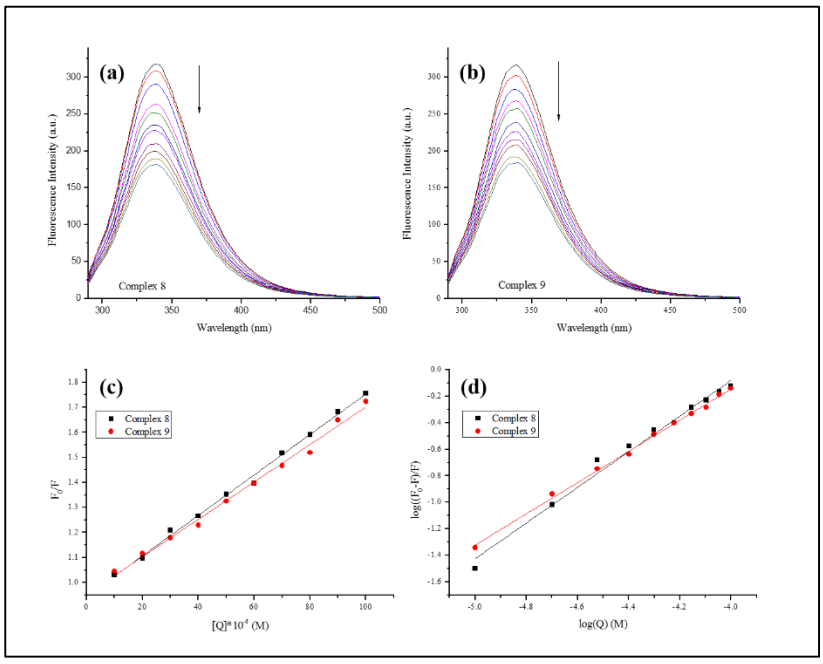

Figure 4A. 9. *(a) & (b) Fluorescence quenching of BSA by complex **8** & **9** (c) Stern-Volmer plot of both complexes (**8** and **9**); (d) Scatchard plot of both complexes (**8** and **9**).*

4A.3.4 Three-dimensional fluorescence spectroscopy

Three dimensional (3D) fluorescence spectroscopy is one of the useful technique in protein-ligand binding experiment. In this 3D representation, the fluorescence intensity, excitation and emission wavelengths are plotted in three different axes to explore a panorama mode presentation. Certain conformational features from the contour plot can be found after ligand (metal complex in this case) binding. The 3D spectra of BSA exhibited two peaks [peak 1 and peak 2 (Figure 4A.10)] which might be quenched after interaction with the Cu(II) complexes. Peak 1 is categorized for tryptophan and tyrosine residues of BSA and peak 2 is endorsed to the polypeptide backbone which occurs particularly for the presence of the π-π* transition.[34, 35] Figure 4A.10 signifies the 3D spectra BSA in the absence and presence of the Cu(II) complexes at pH 7.4. The consequences are summarized in Table 4A.3, which definitely suggest that the complex induces micro-environmental and conformational adjustments in BSA.[36] Although the result obtained from 3D fluorescence spectroscopy is almost same for both the complexes and quite comparable with the results of previous reports[36] but in both cases peak 1 and peak 2 are quenched in the presence of the Cu(II) complexes implying the involvement of specific interactions between the complex and BSA.

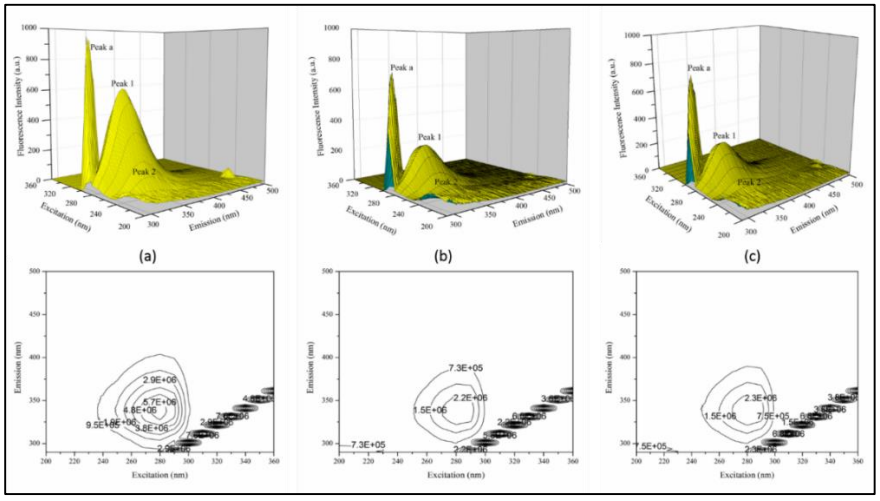

Figure 4A. 10*. 3D fluorescence spectra and contour plot of BSA (10 μM) in the (a) absence and (b) presence of the complex* ***8*** *(50 μM), (c) presence of the complex* ***9*** *(50 μM).*

Table 4A. 3*. 3D fluorescence spectral parameters for BSA in the absence and presence Cu(II) complexes.*

System	Peak 1 (nm)		Δλ (nm)	Intensity	Peak 2 (nm)		Δλ (nm)	Intensity
	λ_{ex}	λ_{em}			λ_{ex}	λ_{em}		
BSA	280	340	60	622.8	240	340	100	121.7
BSA+**8**	280	340	60	276.1	240	340	100	45.1
BSA+**9**	280	340	60	293.2	240	340	100	55.9

4A.3.5 Circular dichroism studies

CD measurement was performed to get enhanced understanding in copper complex - protein binding mechanism and secondary structure changes of protein. Figure 4A.11 shows the CD spectra of BSA along with BSA-**8** and BSA-**9** complex respectively.

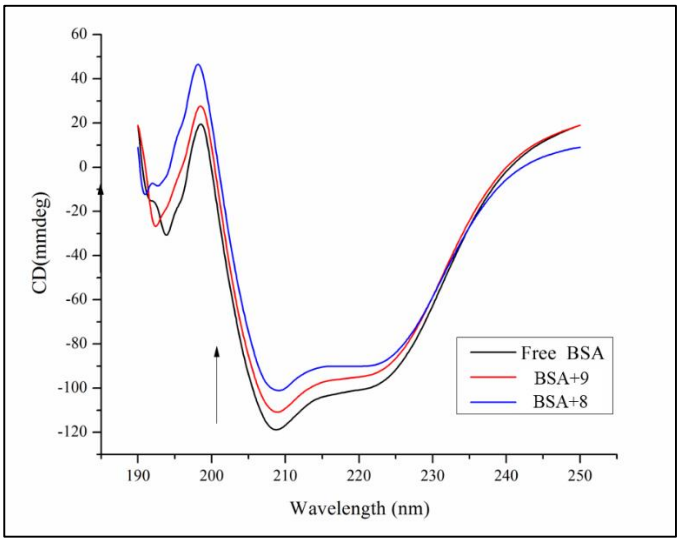

Figure 4A. 11*. CD plot for showing interaction of BSA with complexes **8** and **9**.*

A negative CD band was detected with two characteristic bands at 208 and 222 nm which is symbolic of negative cotton effect as a consequence of n → π* transition in the peptide bond of α-helical structure.[5] By treating with complex it was observed that there is reduction in both of these bands without much shift of the peaks. The reduction is more in the case of complex **8** than **9**, signifying a stronger impact on the interference of helical structure of the protein for **8**. All the calculated parameters are represented in Table 4A.4 are quite comparable with previous results.[5, 37]

Table 4A. 4*. Table for CD measurement analysis.*

System	α-Helix %	β-Sheet %
Free BSA	68.9	9.4
BSA-**8**	68.47	9.41
BSA-**9**	68.59	9.6

4A.3.6 Protease activity study

The scrutiny of protein peptide bond cleaving ability of synthesized molecule is one of the key primary analysis tool for probable application towards mimicking of protease enzymes which are very essential in digestion as they break the peptide bonds in the protein foods to liberate the amino acids needed by the body. BSA protein was chosen to analyze the ability of complex **8** and **9** to cleave protein peptide bonds. No significant protein cleavage is observed in the absence of an activator like hydrogen peroxide (Figure. 4A.12).

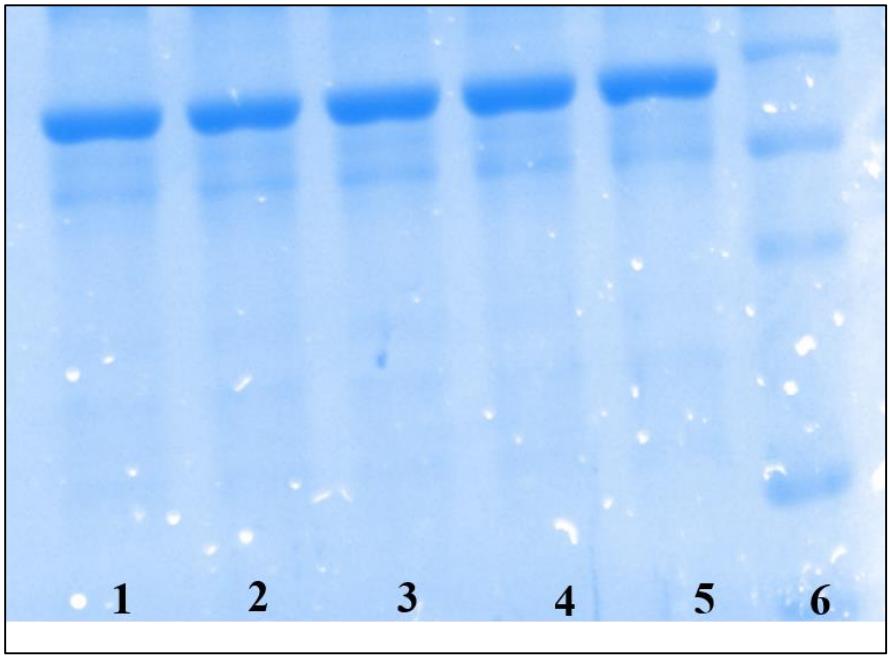

Figure 4A. 12. *SDS-PAGE diagram of cleavage of bovine serum albumin (BSA, 4 μM) using various concentrations of complex* ***8*** *and* ***9*** *in the absence of* H_2O_2*. Lane* ***1****, BSA; Lane 2, BSA+****8****(250 μM); Lane 3, BSA+****8****(500 μM); Lane 4, BSA+****9****(250 μM); Lane 5, BSA+****9****(500 μM); Lane 6, Molecular weight marker*

When the protein, BSA (4 Mm, M.Wt. 66.5 KD) was incubated at 50 °C with complex **8** and **9** (250 μM and 500 μM) in the presence of H_2O_2 (500 μM) at pH

7.4 and then subjected to SDS-PAGE,[16] both the complexes show protein cleavage compared with the untreated BSA control band and BSA molecular weight marker band. (Figure 4A.13)

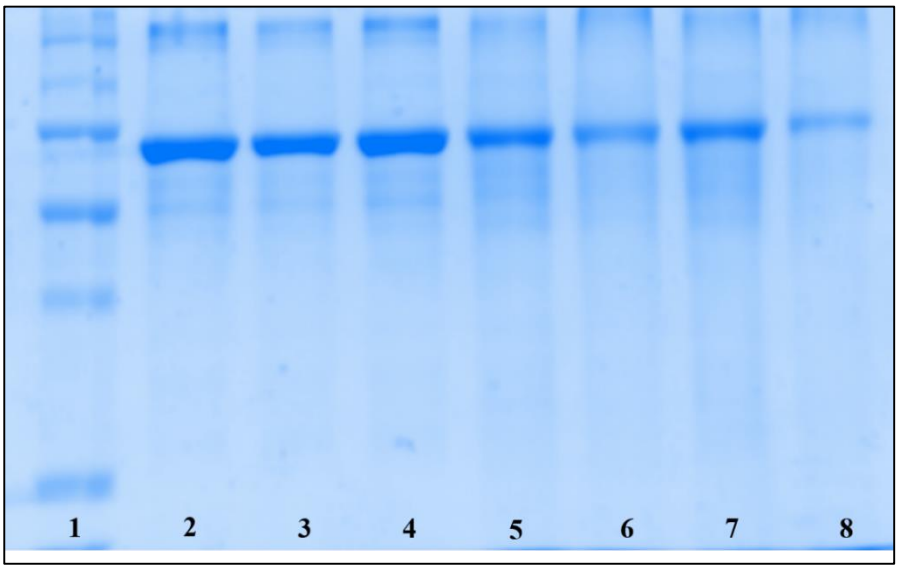

Figure 4A. 13*. SDS-PAGE diagram of cleavage of bovine serum albumin (BSA, 4 μM) using various concentrations of complex* ***8*** *and* ***9*** *in the presence of* H_2O_2*. Lane 1, Molecular weight marker; Lane 2, BSA; Lane 3, BSA+*H_2O_2 *(250 μM); Lane 4, BSA+* H_2O_2 *(500 μM); Lane 5, BSA+* H_2O_2 *(500 μM) +* ***8*** *(250 μM); Lane 6, BSA+* H_2O_2 *(500 μM) +* ***8*** *(500 μM); Lane 7, BSA+* H_2O_2 *(500 μM) +* ***9*** *(250 μM); Lane 8, BSA+* H_2O_2 *(500 μM) +* ***9*** *(500 μM).*

Both the complexes display spreading or dwindling of the BSA band signifying that the nonspecific binding of the complexes to BSA for cleaving of BSA into very small fragments.[9] To get further indication of protein cleavage the deconvoluted ESI-MS analysis of BSA (4 μM) was done in the absence and presence of complex **8** and **9** (100 μM) after incubation with H_2O_2 for 3 h. In the absence of copper complexes, a significantly intense peak was found for getting the deconvoluted mass spectra [38] with the m/z value (66588.7) corresponding to uncleaved BSA (Figure 4A.14).[9] When BSA was incubated with copper complexes no measurable peak intensity for deconvolution was observed in the mass spectrum (Figure 4A.14) revealing complete degradation of the protein by copper complexes.

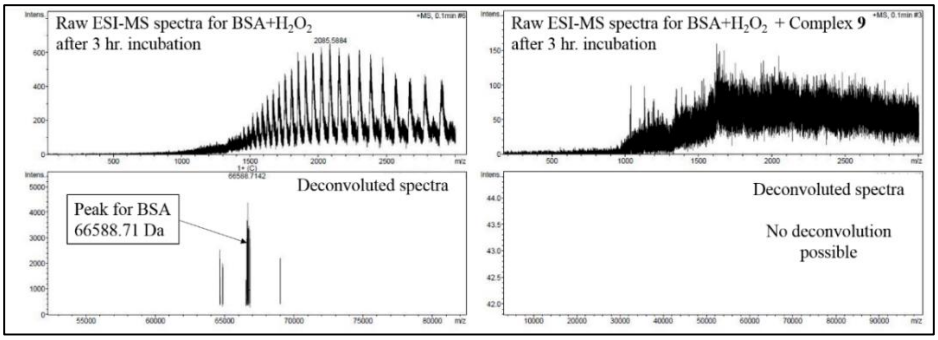

Figure 4A. 14. *(Left)- ESI-MS spectra of BSA after incubation with H_2O_2 and its corresponding deconvoluted spectra. (Right) - ESI-MS spectra of BSA after incubation with H_2O_2 and Complex* ***9*** *and its corresponding deconvoluted spectra.*

4A.3.7 DNA binding studies

Copper-Schiff base complexes are notable for their interaction with DNA.[39-42] Ethidium Bromide (EB) is one of the standout amongst the most sensitive fluorescent probes that binds to DNA through intercalation.[43] Modest binding of drugs to DNA with EB could provide significant data with respect to the DNA binding affinity. Figure 4A.15 demonstrates the emission spectra of the DNA-EB network with increasing amounts of test compounds. The displacement technique depends on the lessening of fluorescence intensity because of the uprooting of EB from a DNA arrangement by a quencher and the quenching is because of the diminishment of the quantity of binding sites on the DNA that is accessible to the EB. Further quantitative assessment of the magnitude of interaction was ascertained by the classical Stern-Volmer equation:

$$F_0/F = 1 + Ksv\,[Q]$$

Where F_0 and F are the emission intensities of EB bound CT-DNA in the absence and presence of the quencher (complexes) concentration [Q], respectively, which gave the Stern-Volmer quenching constant (Ksv). The Ksv value is obtained with a slope from the plot of F_0/F versus [Q] which is shown in Figure 4A.15. The quenching constant (Ksv) values were obtained from the slope, thus indicating the strong binding of the complexes towards DNA. The quenching constant (Ksv) values were obtained from the slope, which were listed in Table

4A.5. The binding constant (K_a) values obtained from the plot of log [(F_0 − F)/F] vs. log [Q] (from Scatchard equation). [44] All the binding parameters, listed in the Table 4A.5 are quite comparable with earlier reports.[8, 45-49] This observed phenomenon of binding affinity of copper complexes towards DNA is mainly due to the positively charged nature of these two metal complexes. This type of ionic metal complexes have a general tendency to bind with DNA more effectively as explained earlier.[26] Like protein binding capacity here also chair conformation of pipeazinyl arm induces positive charge density over the coordination sphere which helps to make an electrostatic interaction of metal complexes with DNA prior to binding.

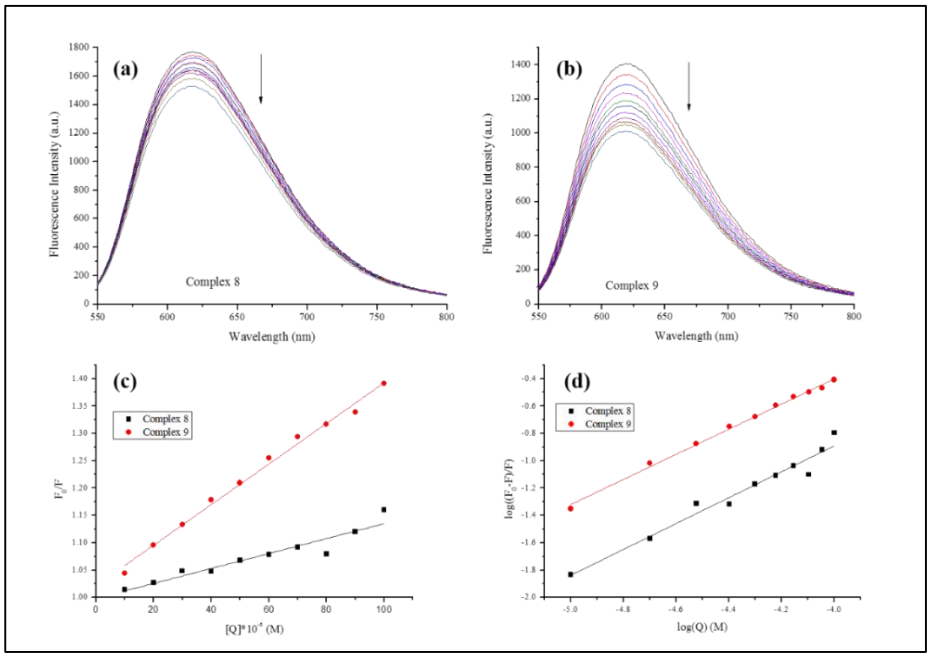

Figure 4A. 15*. (a) & (b) Fluorescence quenching of EB-DNA by complex **8** and **9**; (c) & (d) Stern-Volmer and Scatchard plot of both complexes.*

Table 4A. 5*. Various parameters obtained from bio-macromolecular interaction study.*

System	**DNA Interaction With**		**BSA Interaction With**	
Complex	**1**	**2**	**1**	**2**
K_{SV} (M^{-1})	1.3×10^3	3.8×10^3	8.0×10^3	7.4×10^3
K_q ($M^{-1}S^{-1}$)	…….	…….	1.2×10^{12}	1.1×10^{12}
K_a (M^{-1})	7.7×10^2	1.8×10^3	1.9×10^5	3.1×10^4
n	0.9	1.43	1.3	1.1

4A.3.8 DNA nuclease activity

Determination of the effectiveness of metal complexes towards DNA cleavage has been investigated by the interaction of plasmid pBR322 DNA with complexes **8** and **9.** Monitoring the transition of plasmid DNA from the naturally occurring, covalently closed circular form (Form I) to the nicked circular relaxed form (Form II) is investigated using agarose gel electrophoresis. Figure 4A.16 represents the cleavage of supercoiled (SC) DNA (Form I) to the nicked circular (NC) DNA (Form II) in different concentrations of two complexes in presence or absence of external oxidizing agent. The overall outcome is quite analogous with previous report.[50]

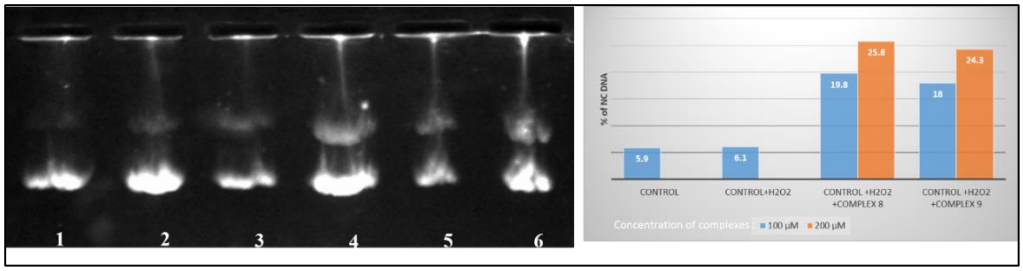

Figure 4A. 16*. Gel electrophoresis diagram showing pBR322 DNA cleavage by complex **8** and **9**.*

*Lane 1 – DNA Control; Lane 2 – DNA+H_2O_2; Lane 3 – DNA+ H_2O_2+**8**(100µM); Lane 4 – DNA+ H_2O_2+**8**(200µM); Lane 5 – DNA+ H_2O_2+**9**(100µM); Lane 6 – DNA+ H_2O_2+**9**(200µM). Right – Histogram of DNA cleavage activity (in terms of % of NC DNA) of two complexes with respect to concentrations.*

After careful investigation of these results it is quite clear that there is no significant cleavage in the control while the presence of metal complexes effective enhancement of DNA cleavage is observed. This cleavage is due to the reaction of copper ions with H_2O_2 and thereby production of diffusible hydroxyl radicals or molecular oxygen, both of which are capable of damaging DNA by Fenton type chemistry.[51] To clarify the mechanism for the DNA cleavage by the complexes, experiments are carried out taking only complex **8** (representative purpose) in presence of hydroxyl radical scavengers (DMSO and EtOH), singlet oxygen quencher (NaN_3) and superoxide radical scavenger

(SOD). In spite of the fact that it is hard to propose correct reason however the outcome (Figure 4A.17) demonstrates that NaN_3 hinders more than other three scavengers in DNA cleaving experiment from SC form to NC form.

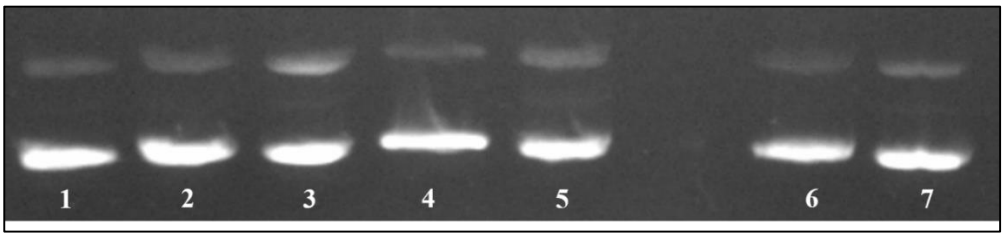

Figure 4A. 17*. Investigation the probable way of DNA cleavage.*
Lane 1 – DNA+ ***8****; Lane 2 – DNA +****8****+DMSO; Lane 3 – DNA +****8****+EtOH; Lane 4 – DNA +****8****+NaN_3; Lane 5– DNA +****8****+SOD; Lane 6 – DNA +****8****+ Methyl Green; Lane 7 – DNA +****8****+ DAPI*

This observation is in conformity with the fact that the DNA cleavage occurs by singlet molecular oxygen in presence of Cu(II) complexes.[52] The prediction of groove binding capacity of the complex **8** was tested using the minor groove binder DAPI and the major groove binder methyl green.[53] Figure 4A.17 demonstrates that major groove binder created a slight hindrance of the DNA damage intervened by the complex (Lane 6), recommending that the complex **8** specially connects through major groove of DNA helix.

4A.3.9 Cytotoxicity by MTT assay

The potential anti proliferative impacts of the compounds on cancer cell line (HeLa) were detected by the regular MTT assay. The ligand has shown no toxicity towards HeLa cell line upto 500 μM concentration range, while the complexes have shown considerable cytotoxic effect around 100 μM concentration. A sudden cytotoxic effect of these complexes were observed (Figure 4A.18) with increase in concentration in the range of 100 - 200 μM range. Relatively higher IC_{50} values have been observed for both the complexes (*i.e.*, 113 μM for complex **8** and 154 μM for complex **9**) with respect to the other reports available in literature.[54]

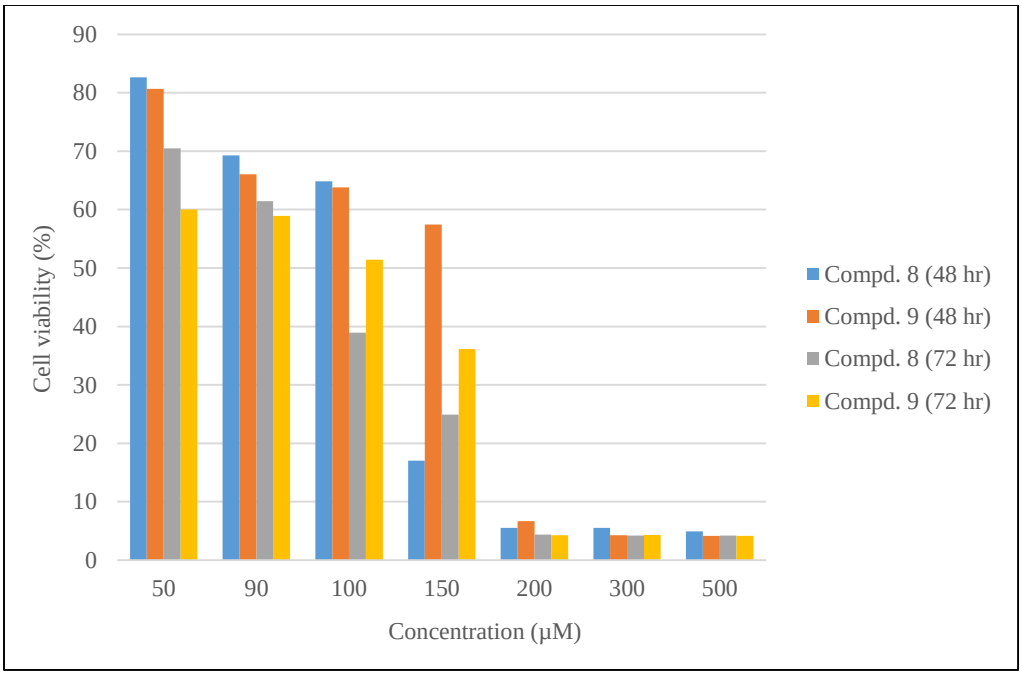

Figure 4A. 18*. Cell viability of HeLa cells after treatment with complexes* ***8*** *and* ***9*** *for 48 h and 72 h.*

4A.3.10 Confocal microscopy

A specific fluorescent dye 4´,6-diamidino-2-phenylindole (DAPI) and propidium iodide (PI) for HeLa cells which were applicable for dual staining analysis with the nucleic acid was used to gain insight into the apoptosis ability of the complex. DAPI can stain both living as well as dead cells *via* penetration through the cell membrane while PI penetrates only dead cells. The nuclei of the untreated cells were stained evenly with DAPI (blue) but very few with PI (red) (Figure 4A.19), which indicate that most of the untreated cells were alive. But after treatment with the copper complex **8** very few viable cells were found by confocal microscopic experiment.

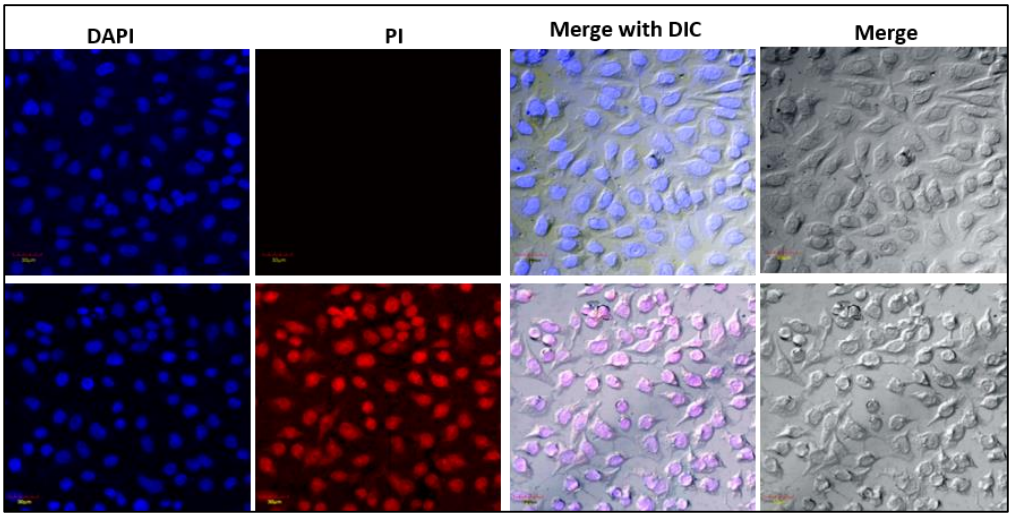

***Figure 4A. 19**. DAPI/PI staining of untreated and drug treated HeLa cells. Panel (a) corresponds to the untreated cells, panel (b) corresponds to cells treated with the Cu(II) complex.*

4A.3.11 Catecholase activity study

3,5-di-tert-butylcatechol (3,5-DTBC) in the presence of two bulky t-butyl substituent in the ring is used as the substrate to scrutinize the catecholase like activity of transition metal complexes.[22, 55] This substrate is also generally preferable due to its low quinone-catechol reduction potential.[22, 55] UV-Vis spectroscopic technique was employed to monitor the overall oxidation reaction under aerobic condition. To screen the response a 10^{-4} M methanolic solution of these two complexes were treated with 100 equivalent 3,5-BTDC. A new band starts to gradually appear near 400 nm with time due to the formation of the oxidized product 3,5-DTBQ upon addition of complex solution on catechol substrate (Figure 4A.20).

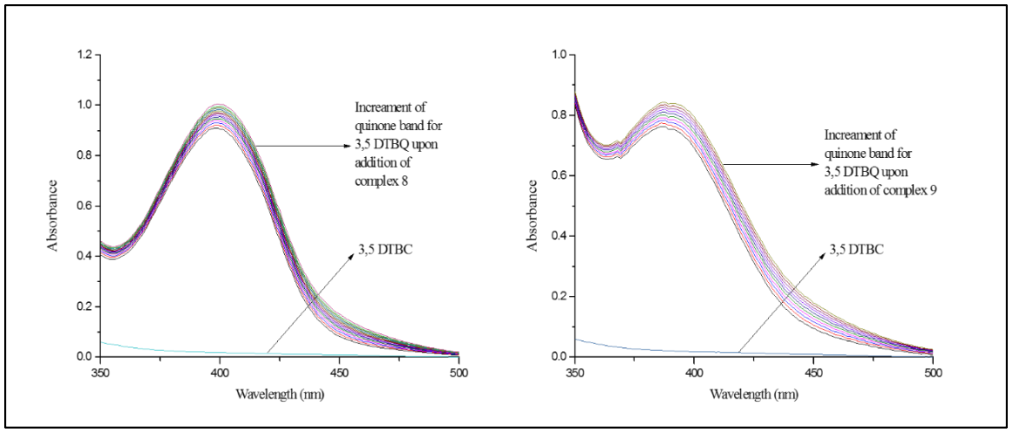

Figure 4A. 20. *Gradual increase of di-quinone band of catechol oxidation for complex* ***8*** *(left) and complex* ***9*** *(right).*

The rate constant for the catalytic reaction was calculated by traditional initial rate method to comprehend the kinetic feature of catalysis for complex **8** and **9**. The observed rate versus substrate concentration data were then analyzed on the basis of the Michaelis–Menten approach of enzymatic kinetics to determine the Michaelis−Menten constant (K_M) and maximum initial rate (V_{max}) using Michaelis−Menten plots (Figure 4A.21).[56]

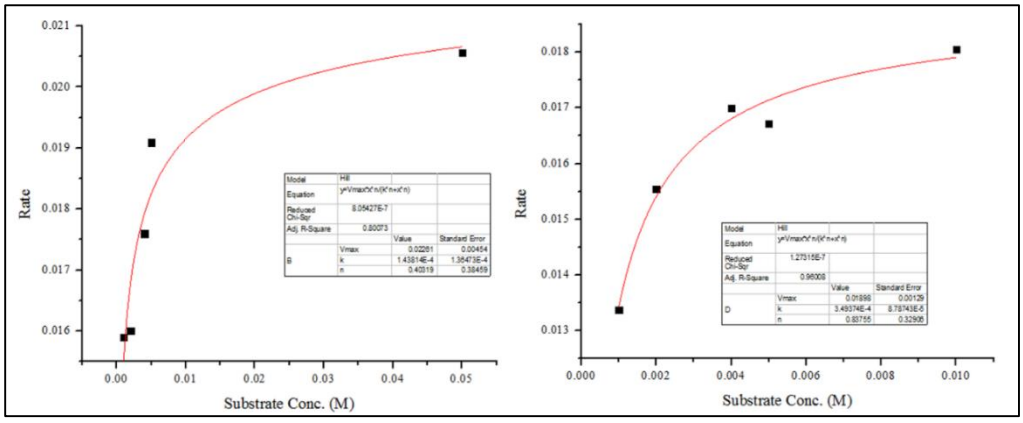

Figure 4A. 21*. Michaelis Menten plot for complex* ***8*** *(left) and* ***9*** *(right).*

The turnover frequency values (k_{cat}) were obtained by dividing the V_{max} values by the concentration of the corresponding complexes. The fact regarding the potential activity of both complexes is clearly represented in Table 4A.6.

Table 4A. 6*. Table for various kinetic parameters of catecholase activity.*

Complex	Complex Conc. (M)	V_{max} (M min^{-1})	Std. Error	K_M (M)	Std. Error	k_{cat} / T.O.N (h^{-1})
8	0.0001	0.02261	0.00454	1.4×10^{-4}	1.3×10^{-4}	13.5×10^{3}
9	0.0001	0.01898	0.00129	3.4×10^{-4}	8.7×10^{-5}	11.3×10^{3}

This activity may be due to the fact that the positive charge on the piperazinyl moiety may help the facilitation of catalyst-substrate interaction by forming a positive channel which might be a prerequisite for showing better catalytic activities.[26] A similar mechanism has been proposed to explain the activity of copper/zinc superoxide dismutase where positively charged arginine and lysine residue play a role to attract the anion and guiding them towards the catalytic center.[57] The turnover frequency (k_{cat}) of both the complexes is almost similar in range and are comparable with previous reports. [58-60]

The investigation was done to identify the formation of probable complex-substrate aggregate through ESI-MS spectrometry (Figure 4A.22).

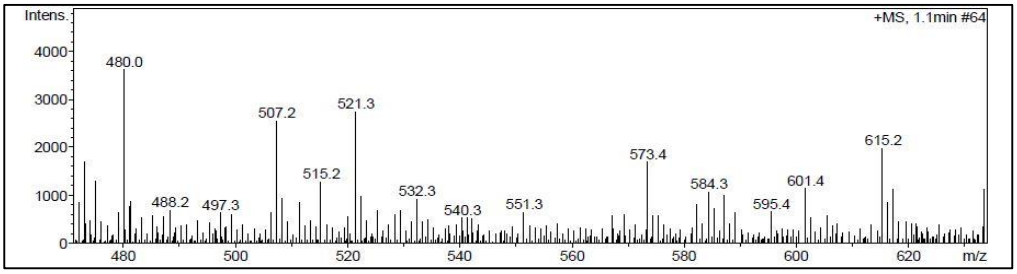

Figure 4A. 22*. Intermediate mass for catechol oxidation using Cu(II) complexes.*

In each case one molecular ion peak (*m/z*) at 480.0 is observed for $[Cu(HL^3)–DTBC–(HL^3)Cu]^{2+}$ with little bit of deviation which is in the range of earlier report. [7] This result suggests that two mononuclear units combine to form a dimeric specie to catalyze the catechol oxidation reaction for one substrate. The probable reaction mechanism for complexes **8** and **9** are represented in Scheme 4A.2.

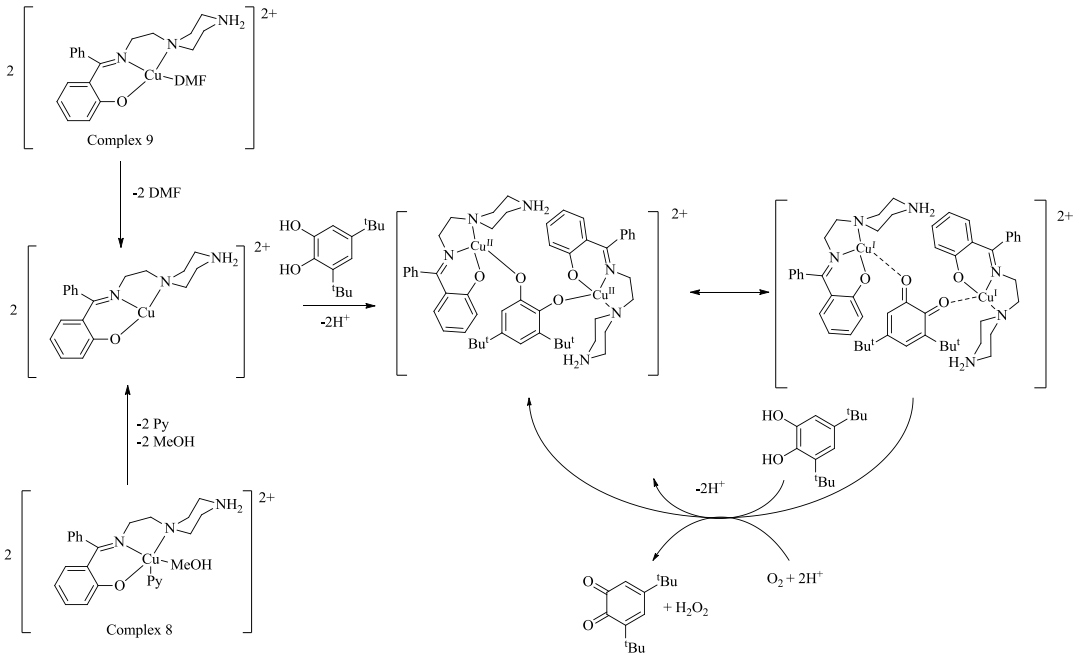

Scheme 4A. 2. *Probable mechanism for catechol oxidation by complex* ***8*** *and* ***9****.*

Formation of H_2O_2 during catalytic oxidation procedure gives some insight into the plausible mechanistic pathway for catechol oxidation. Taking complex **9** as a representative, positive result was found for quantitative detection of I_3^- band (~353nm.) (Figure 4A.23) by UV-Vis spectroscopy (applying reported methodology [61]) which is indicative for the formation of H_2O_2 during the process. It should be noted that the reports containing the studies aimed to definitely establish the mode of the dioxygen reduction to either water or dihydrogen peroxide are quite scarce and investigation report for probable formation of peroxide in reaction mixture is also limited.[62-65] The mode of oxidation can be rationalized as follows. In case of dicopper(II) complexes, the simultaneous reduction of two copper(II) centers to the copper(I) state results in the oxidation of one equivalent of catechol, leading to the release of one quinone molecule. In case of these copper (II) complexes only one electron transfer may occur, resulting in the formation of copper (I)-semiquinonate intermediate species.

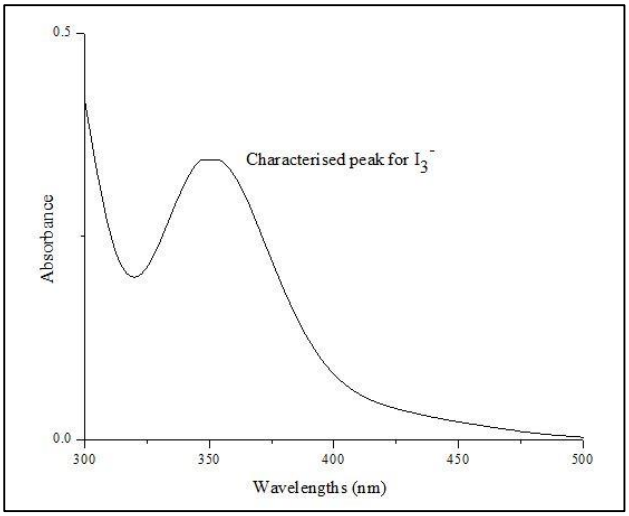

Figure 4A. 23. *UV-Vis spectra to show formation of peroxide during oxidation.*

The reaction of such species with dioxygen may result in the two electrons reduction of the latter, leading to the reoxidation of the copper (I) ion, a release of the quinone molecule and dihydrogen peroxide formation.

4A.4 Conclusions

In conclusion two new Cu(II) complexes $[Cu(HL^3)(MeOH)(Py)](ClO_4)_2$ **(8)** and $[Cu(HL^3)(DMF)]$ $(NO_3)_2$ **(9)** have been synthesized using a newly developed Schiff based ligand 2-(phenyl((2-(piperazin-1-yl)ethyl)imino)methyl)phenol (**HL^3**). ETBr displacement assay, agarose gel electrophoresis experiment, fluorescence quenching technique for BSA and SDS-Page electrophoresis technique clearly indicate that both complexes have potent nuclease and protease activity. MTT assay and confocal microscopic images also indicate the cytotoxic nature of these complexes towards cancer cell line. Apart from this, both the complexes are quite active towards catechol oxidation.

4A.5 References

[1]. Hartinger, C. G.,Dyson, P. J. (2009), Bioorganometallic chemistry-from teaching paradigms to medicinal applications, Chemical Society Reviews, 38, 391-401.(DOI: 10.1039/B707077M)

[2]. Jaouen, G.,Vessieres, A.,Butler, I. S. (1993), Bioorganometallic chemistry: a future direction for transition metal organometallic chemistry?, Accounts of Chemical Research, 26, 361-369.(DOI: 10.1021/ar00031a002)

[3]. Roy, S.,Roy, S.,Saha, S.,Majumdar, R.,Dighe, R. R.,Jemmis, E. D.,Chakravarty, A. R. (2011), Cobalt(II) complexes of terpyridine bases as photochemotherapeutic agents showing cellular uptake and photocytotoxicity in visible light, Dalton transactions (Cambridge, England : 2003), 40, 1233-42.(DOI: 10.1039/c0dt00223b)

[4]. Osório, R. E. H. M. B.,Peralta, R. a.,Bortoluzzi, A. J.,De Almeida, V. R.,Szpoganicz, B.,Fischer, F. L.,Terenzi, H.,Mangrich, A. S.,Mantovani, K. M.,Ferreira, D. E. C.,Rocha, W. R.,Haase, W.,Tomkowicz, Z.,Anjos, A. D.,Neves, A. (2012), Synthesis, magnetostructural correlation, and catalytic promiscuity of unsymmetric dinuclear copper(II) complexes: Models for catechol oxidases and hydrolases, Inorganic Chemistry, 51, 1569-1589.(DOI: 10.1021/ic201876k)

[5]. Das, M.,Nasani, R.,Saha, M.,Mobin, S. M.,Mukhopadhyay, S. (2015), Nickel(ii) complexes with a flexible piperazinyl moiety: studies on DNA and protein binding and catecholase like properties, Dalton Transactions, 44, 2299-2310.(DOI: 10.1039/C4DT02675F)

[6]. Solomon, E. I.,Heppner, D. E.,Johnston, E. M.,Ginsbach, J. W.,Cirera, J.,Qayyum, M.,Kieber-Emmons, M. T.,Kjaergaard, C. H.,Hadt, R. G.,Tian, L. (2014), Copper active sites in biology, Chemical Reviews, 114, 3659-3853.(DOI: 10.1021/cr400327t)

[7]. Banu, K. S.,Chattopadhyay, T.,Banerjee, A.,Bhattacharya, S.,Suresh, E.,Nethaji, M.,Zangrando, E.,Das, D. (2008), Catechol Oxidase Activity of a Series of New Dinuclear Copper (II) Complexes with 3 , 5-DTBC and TCC as Substrates : Syntheses , X-ray Crystal Structures , Spectroscopic Characterization of the Adducts and Kinetic Studies, Inorganic Chemistry, 47, 7083-7093.(DOI: 10.1021/ic701332w)

[8]. Barone, G.,Terenzi, A.,Lauria, A.,Almerico, A. M.,Leal, J. M.,Busto, N.,García, B. (2013), DNA-binding of nickel(II), copper(II) and zinc(II)

complexes: Structure–affinity relationships, Coordination Chemistry Reviews, 257, 2848-2862.(DOI: 10.1016/j.ccr.2013.02.023)

[9]. Loganathan, R.,Ramakrishnan, S.,Suresh, E.,Riyasdeen, A.,Akbarsha, M. A.,Palaniandavar, M. (2012), Mixed Ligand Copper(II) Complexes of N,N-Bis(benzimidazol-2-ylmethyl)amine (BBA) with Diimine Co-Ligands: Efficient Chemical Nuclease and Protease Activities and Cytotoxicity, Inorganic Chemistry, 51, 5512-5532.(DOI: 10.1021/ic2017177)

[10]. Linder, M. C.,Goode, C. A., (1991), Biochemistry of Copper.Plenum: New York.

[11]. Kaim, W.,Rall, J. (1996), Copper—A "Modern" Bioelement, Angewandte Chemie International Edition in English, 35, 43-60.(DOI: 10.1002/anie.199600431)

[12]. Sorrell, T. N. (1989), Synthetic models for binuclear copper proteins, Tetrahedron, 45, 3-68.(DOI: 10.1016/0040-4020(89)80033-X)

[13]. Kitajima, N.,Moro-oka, Y. (1994), Copper-Dioxygen Complexes. Inorganic and Bioinorganic Perspectives, Chemical Reviews, 94, 737-757.(DOI: 10.1021/cr00027a010)

[14]. Bhat, S. S.,Kumbhar, A. A.,Heptullah, H.,Khan, A. A.,Gobre, V. V.,Gejji, S. P.,Puranik, V. G. (2011), Synthesis, Electronic Structure, DNA and Protein Binding, DNA Cleavage, and Anticancer Activity of Fluorophore-Labeled Copper(II) Complexes, Inorganic Chemistry, 50, 545-558.(DOI: 10.1021/ic101534n)

[15]. Tanimoto, S.,Matsumura, S.,Toshima, K. (2008), Target-selective degradation of proteins by porphyrins upon visible photo-irradiation, Chemical Communications, 3678-3680.(DOI: 10.1039/B806961A)

[16]. Kumar, C. V.,Buranaprapuk, A.,Sze, H. C.,Jockusch, S.,Turro, N. J. (2002), Chiral protein scissors: High enantiomeric selectivity for binding and its effect on protein photocleavage efficiency and specificity, Proceedings of the National Academy of Sciences, 99, 5810-5815.(DOI: 10.1073/pnas.082119599)

[17]. Kahne, D.,Still, W. C. (1988), Hydrolysis of a peptide bond in neutral water, Journal of the American Chemical Society, 110, 7529-7534.(DOI: 10.1021/ja00230a041)

[18]. Fife, T. H.,Przystas, T. J. (1986), Divalent metal ion catalysis in amide hydrolysis. The hydrolysis of N-acylimidazoles, Journal of the American Chemical Society, 108, 4631-4636.(DOI: 10.1021/ja00275a059)

[19]. Hegg, E. L.,Burstyn, J. N. (1998), Toward the development of metal-based synthetic nucleases and peptidases: a rationale and progress report in applying the principles of coordination chemistry, Coordination Chemistry Reviews, 173, 133-165.(DOI: S0010-8545(98)00157-X)

[20]. Pratviel, G.,Bernadou, J.,Meunier, B. (1995), Carbon—Hydrogen Bonds of DNA Sugar Units as Targets for Chemical Nucleases and Drugs, Angewandte Chemie International Edition in English, 34, 746-769.(DOI: 10.1002/anie.199507461)

[21]. Patra, A. K.,Bhowmick, T.,Roy, S.,Ramakumar, S.,Chakravarty, A. R. (2009), Copper(II) complexes of L-arginine as netropsin mimics showing DNA cleavage activity in red light, Inorganic chemistry, 48, 2932-43.(DOI: 10.1021/ic8017425)

[22]. Dey, S. K.,Mukherjee, A. (2013), Zero-Order Catechol Oxidase Activity by a Mononuclear Manganese(III) Complex Showing High Turnover Comparable to Catechol Oxidase Enzyme, ChemCatChem, 5, 3533-3537.(DOI: 10.1002/cctc.201300596)

[23]. Fernandes, C.,Neves, A.,Bortoluzzi, A. J.,Mangrich, A. S.,Rentschler, E.,Szpoganicz, B.,Schwingel, E. (2001), A new dinuclear unsymmetric copper(II) complex as model for the active site of catechol oxidase, Inorganica Chimica Acta, 320, 12-21.(DOI: 10.1016/S0020-1693(01)00470-4)

[24]. Moura, E.,Afonso, J.,Hein, L.,Vieira-Coelho, M. A. (2006), Br. J. Pharmacol., 149, 1049.

[25]. Burstyn, J. N.,Deal, K. A. (1993), Selective catalytic hydrolysis of a simple phosphodiester by a macrocyclic copper(II) complex, Inorganic Chemistry, 32, 3585-3586.(DOI: 10.1021/ic00069a005)

[26]. Das, M.,Mandal, P.,Malviya, N.,Choudhuri, I.,Charmier, M. A. J.,Morgado, S.,Mobin, S. M.,Pathak, B.,Mukhopadhyay, S. (2016), Copper complexes with a flexible piperazinyl arm: nuclearity driven catecholase activity and interactions with biomolecules, Journal of Coordination Chemistry, 69, 3619-3637.(DOI: 10.1080/00958972.2016.1236193)

[27]. SAINT (2013), , V8.34A, Bruker AXS Inc: Madison, WI, USA.

[28]. Sheldrick, G. (1996), Sadabs, University of Göttingen, Germany Program for Empirical Absorption Correction of Area Detector Data.

[29]. SHELXTL-2014/7 (2014), Bruker AXS Inc.: Madison, WI, USA.

[30]. Nakamoto, K., (2009), Infrared and Raman Spectra of Inorganic and Coordination Compounds, Theory and Applications in Inorganic Chemistry.6th ed. John Wiley & Sons, Inc.: Hoboken, New Jersey.

[31]. Lever, A. B. P., (1984), Inorganic Electronic Spectroscopy.2nd ed. Elsevier Science, New York.

[32]. Addison, A. W.,Rao, T. N.,Reedijk, J.,van Rijn, J.,Verschoor, G. C. (1984), Synthesis, structure, and spectroscopic properties of copper(II) compounds containing nitrogen-sulphur donor ligands; the crystal and molecular structure of aqua[1,7-bis(N-methylbenzimidazol-2[prime or minute]-yl)-2,6-dithiaheptane]copper(II) perchlorate, Journal of the Chemical Society, Dalton Transactions, 1349-1356.(DOI: 10.1039/DT9840001349)

[33]. Yang, L.,Powell, D. R.,Houser, R. P. (2007), Structural variation in copper(i) complexes with pyridylmethylamide ligands: structural analysis with a new four-coordinate geometry index, τ_4, Dalton Transactions, 955-964.(DOI: 10.1039/B617136B)

[34]. Sandhya, B.,Hegde, A. H.,Kalanur, S. S.,Katrahalli, U.,Seetharamappa, J. (2011), Interaction of triprolidine hydrochloride with serum albumins: Thermodynamic and binding characteristics, and influence of site probes, Journal of Pharmaceutical and Biomedical Analysis, 54, 1180-1186.(DOI: 10.1016/j.jpba.2010.12.012)

[35]. Li, D.,Wang, Y.,Chen, J.,Ji, B. (2011), Characterization of the interaction between farrerol and bovine serum albumin by fluorescence and circular

dichroism, Spectrochimica Acta Part A: Molecular and Biomolecular Spectroscopy, 79, 680-686.(DOI: 0.1016/j.saa.2011.04.005)

[36]. Roy, A. S.,Samanta, S. K.,Ghosh, P.,Tripathy, D. R.,Ghosh, S. K.,Dasgupta, S. (2016), Cell cytotoxicity and serum albumin binding capacity of the morin-Cu(II) complex and its effect on deoxyribonucleic acid, Molecular BioSystems, 12, 2818-2833.(DOI: 10.1039/C6MB00344C)

[37]. Azzellini, M. A. A.,Abbott, M. P.,Machado, A.,Miranda, M. T. M.,Garcia, L. C.,Caramori, G. F.,Gonçalves, M. B.,Petrilli, H. M.,Ferreira, A. M. C. (2010), Interactions of di-imine copper(II) complexes with albumin: competitive equilibria, promoted oxidative damage and DFT studies, Journal of the Brazilian Chemical Society, 21, 1303-1317.(DOI: 10.1590/S0103-50532010000700018)

[38]. Ifa, D. R.,Wu, C.,Ouyang, Z.,Cooks, R. G. (2010), Desorption electrospray ionization and other ambient ionization methods: current progress and preview, Analyst, 135, 669-681.(DOI: 10.1039/B925257F)

[39]. Gökçe, C.,Gup, R. (2013), Synthesis, characterization and DNA interaction of new copper(II) complexes of Schiff base-aroylhydrazones bearing naphthalene ring, Journal of Photochemistry and Photobiology B: Biology, 122, 15-23.(DOI: 10.1016/j.jphotobiol.2013.02.014)

[40]. Yang, X.-B.,Huang, Y.,Zhang, J.-S.,Yuan, S.-K.,Zeng, R.-Q. (2010), Synthesis, characterization and DNA interaction of copper (II) complexes with Schiff base ligands derived from 2-pyridinecarboxaldehyde and polyamines, Inorganic Chemistry Communications, 13, 1421-1424.(DOI: 10.1016/j.inoche.2010.08.006)

[41]. Duan, R.-R.,Wang, L.,Huo, W.-Q.,Chen, S.,Zhou, X.-H. (2014), Synthesis, characterization, and DNA binding of two copper(II) complexes as DNA fluorescent probes, Journal of Coordination Chemistry, 67, 2765-2782.(DOI: 10.1080/00958972.2014.946918)

[42]. Gao, C.,Ma, X.,Lu, J.,Wang, Z.,Tian, J.,Yan, S. (2011), Synthesis, structure, DNA binding, and cleavage activity of two copper(II) complexes, Journal of Coordination Chemistry, 64, 2157-2169.(DOI: 10.1080/00958972.2011.587514)

[43]. Meyer-Almes, F. J.,Porschke, D. (1993), Mechanism of intercalation into the DNA double helix by ethidium, Biochemistry, 32, 4246-4253.(DOI: 10.1021/bi00067a012)

[44]. li, P.,Niu, M.,Hong, M.,Cheng, S.,Dou, J. (2014), Effect of structure and composition of nickel(II) complexes with salicylidene Schiff base ligands on their DNA/protein interaction and cytotoxicity, Journal of Inorganic Biochemistry, 137, 101-108.(DOI: 10.1016/j.jinorgbio.2014.04.005)

[45]. Lakshmipraba, J.,Arunachalam, S.,Vijay Solomon, R.,Venuvanalingam, P. (2015), Synthesis, DNA binding and docking studies of copper(II) complexes containing modified phenanthroline ligands, Journal of Coordination Chemistry, 68, 1374-1386.(DOI: 10.1080/00958972.2015.1014349)

[46]. Ou, Z. B.,Lu, Y. H.,Lu, Y. M.,Chen, S.,Xiong, Y. H.,Zhou, X. H.,Mao, Z. W.,Le, X. Y. (2013), A copper(II) complex with 2-(2′-pyridyl)benzimidazole and l-arginine: synthesis, structure, antibacterial activities, and DNA interaction, Journal of Coordination Chemistry, 66, 2152-2165.(DOI: 10.1080/00958972.2013.800195)

[47]. Sun, J.,Deng, S.-Y.,Zhang, L.,He, J.,Jiang, L.,Mao, Z.-W.,Ji, L.-N. (2009), DNA affinity and cleavage by naphthalene-based mononuclear and dinuclear copper(II) complexes, Journal of Coordination Chemistry, 62, 3284-3295.(DOI: 10.1080/00958970903055875)

[48]. Raman, N.,Sakthivel, A.,Jeyamurugan, R. (2010), Synthesis, structural characterization, antimicrobial, DNA-binding, and photo-induced DNA cleavage activity of some bio-sensitive Schiff base copper(II) complexes, Journal of Coordination Chemistry, 63, 4380-4397.(DOI: 10.1080/00958972.2010.539212)

[49]. Sun, Y.-G.,Li, K.-L.,Xu, Z.-H.,Lv, T.-Y.,Wang, S.-J.,You, L.-X.,Ding, F. (2013), Synthesis, characterization, and interaction with DNA of Cu(II) and Zn(II) complexes with 2,2′-bipyridyl-6,6′-dicarboxylic acid, Journal of Coordination Chemistry, 66, 2455-2464.(DOI: 10.1080/00958972.2013.806655)

[50]. Patra, A. K.,Roy, S.,Chakravarty, A. R. (2009), Synthesis, crystal structures, DNA binding and cleavage activity of l-glutamine copper(II) complexes of heterocyclic bases, Inorganica Chimica Acta, 362, 1591-1599.(DOI: 10.1016/j.ica.2008.08.003)

[51]. Louie, A. Y.,Meade, T. J. (1999), Metal Complexes as Enzyme Inhibitors, Chemical Reviews, 99, 2711-2734.(DOI: 10.1021/cr9804285)

[52]. Kawanishi, S.,Inoue, S.,Yamamoto, K. (1989), Hydroxyl radical and singlet oxygen production and DNA damage induced by carcinogenic metal compounds and hydrogen peroxide, Biological Trace Element Research, 21, 367-372.(DOI: 10.1007/bf02917277)

[53]. Ahmad, M.,Afzal, M.,Tabassum, S.,Kalińska, B.,Mrozinski, J.,Bharadwaj, P. K. (2014), Synthesis and structure elucidation of a cobalt(II) complex as topoisomerase I inhibitor: In vitro DNA binding, nuclease and RBC hemolysis, European Journal of Medicinal Chemistry, 74, 683-693.(DOI: 10.1016/j.ejmech.2013.10.025)

[54]. Krishnamoorthy, P.,Sathyadevi, P.,Cowley, A. H.,Butorac, R. R.,Dharmaraj, N. (2011), Evaluation of DNA binding, DNA cleavage, protein binding and in vitro cytotoxic activities of bivalent transition metal hydrazone complexes, European Journal of Medicinal Chemistry, 46, 3376-3387.(DOI: 10.1016/j.ejmech.2011.05.001)

[55]. Merkel, M.,Möller, N.,Piacenza, M.,Grimme, S.,Rompel, A.,Krebs, B. (2005), Less Symmetrical Dicopper(II) Complexes as Catechol Oxidase Models—An Adjacent Thioether Group Increases Catecholase Activity, Chemistry – A European Journal, 11, 1201-1209.(DOI: 10.1002/chem.200400768)

[56]. Jana, A.,Ruiz, E.,Mohanta, S. (2013), Structures, Magnetochemistry, Spectroscopy, Theoretical Study, and Catechol Oxidase Activity of Dinuclear and Dimer-of-Dinuclear Mixed-Valence Mn, Inorganic Chemistry, 52, 7732-7746.(DOI: 10.1021/ic400916h)

[57]. Chattopadhyay, T.,Mukherjee, M.,Mondal, A.,Maiti, P.,Banerjee, A.,Nethaji, M.,Zangrando, E.,Das, D. (2010), A Unique Nickel System having

Versatile Catalytic Activity of Biological Significance, 3121-3129.(DOI: 10.1021/ic901546t)

[58]. Banu, K. S.,Chattopadhyay, T.,Banerjee, A.,Bhattacharya, S.,Zangrando, E.,Das, D. (2009), Catechol oxidase activity of dinuclear copper(II) complexes of Robson type macrocyclic ligands: Syntheses, X-ray crystal structure, spectroscopic characterization of the adducts and kinetic studies, Journal of Molecular Catalysis A: Chemical, 310, 34-41.(DOI: 10.1016/j.molcata.2009.05.016)

[59]. Chakraborty, P.,Adhikary, J.,Ghosh, B.,Sanyal, R.,Chattopadhyay, S. K.,Bauzá, A.,Frontera, A.,Zangrando, E.,Das, D. (2014), Relation between the Catalytic Efficiency of the Synthetic Analogues of Catechol Oxidase with Their Electrochemical Property in the Free State and Substrate-Bound State, Inorganic chemistry, 53, 8257-8269.(DOI: 10.1021/ic5005177)

[60]. Majumder, S.,Sarkar, S.,Sasmal, S.,Sañudo, E. C.,Mohanta, S. (2011), Heterobridged dinuclear, tetranuclear, dinuclear-based 1-D, and heptanuclear-based 1-D complexes of copper(II) derived from a dinucleating ligand: Syntheses, structures, magnetochemistry, spectroscopy, and catecholase activity, Inorganic Chemistry, 50, 7540-7554.(DOI: 10.1021/ic200409d)

[61]. Biswas, A.,Das, L. K.,Drew, M. G. B.,Aromí, G.,Gamez, P.,Ghosh, A. (2012), Synthesis, Crystal Structures, Magnetic Properties and Catecholase Activity of Double Phenoxido-Bridged Penta-Coordinated Dinuclear Nickel(II) Complexes Derived from Reduced Schiff-Base Ligands: Mechanistic Inference of Catecholase Activity, Inorganic Chemistry, 51, 7993-8001.(DOI: 10.1021/ic202748m)

[62]. Chyn, J.-P.,Urbach, F. L. (1991), Autoxidation of 3,5-di-t-butylcatechol catalyzed by two pyrazolatebridged dicopper complexes with different structural features, Inorganica Chimica Acta, 189, 157-163.(DOI: 10.1016/S0020-1693(00)80184-X)

[63]. Balla, J.,Kiss, T.,Jameson, R. F. (1992), Copper(II)-catalyzed oxidation of catechol by molecular oxygen in aqueous solution, Inorganic Chemistry, 31, 58-62.(DOI: 10.1021/ic00027a012)

[64]. Selmeczi, K.,Réglier, M.,Giorgi, M.,Speier, G. (2003), Catechol oxidase activity of dicopper complexes with N-donor ligands, Coordination Chemistry Reviews, 245, 191-201.(DOI: 10.1016/j.cct.2003.08.002)

[65]. Ackermann, J.,Meyer, F.,Kaifer, E.,Pritzkow, H. (2002), Tuning the Activity of Catechol Oxidase Model Complexes by Geometric Changes of the Dicopper Core, Chemistry – A European Journal, 8, 247-258.(DOI: 10.1002/1521-3765)

Chapter 4B

Counter anion directed flexibility of Ni(II) Schiff base complexes: Lysozyme binding and glycosidase activity

4B.1 Introduction

Studies on the coordination behaviors of transition metal complexes along with their intriguing topologies, have received considerable attention in recent years for their versatile physical and chemical properties. Small inorganic molecules, particularly the metal coordination complexes have been gaining importance to investigate the phenomena at interface between inorganic chemistry and biology. It assist to discover the mechanism of the activities of naturally occurring metalloenzymes, the entry of metal ions into cells as well as in active sites of proteins, metal-induced conformational signaling, drug–protein interactions and biomimicry.[1-4] It is now recognized that metal complexes are particularly suited for the optimization of non-covalent interactions, since they can combine the advantage of flexibility in ligand design with access to a variety of coordination geometries, geometrical and optical isomers, oxidation states and electronic configurations.[5] Currently, much of the information regarding the role of metals in natural systems is gained through comparative studies on metalloenzymes and model metal complexes.[6] Thus, use of transition metals by nature in different biological processes drives the quest of the scientist to understand the underlying principles of its functionality, which eventually helps to develop different structural and more importantly functional model systems.[7]

Lysozyme was selected here as a model for probing the structural interactions of Ni(II) complexes with proteins due to its stability, relative propensity to crystallize under different range of conditions, and previous use in similar studies utilizing medicinal metal complexes.[8-11] The scaffold of hen

egg white lysozyme (HEWL), a relatively small globular protein, is particularly suitable to probe the fundamental interactions of proteins with metal complexes.[12] Moreover the fluorescence quantum yield of HEWL is quite high. Literature study reports that HEWL had been frequently used to study the interaction of proteins with metal ions and metal based drugs which proved that it is able to bind with different metal ions like Fe^{2+}, Mn^{2+}, Cu^{2+}, Co^{2+}, Gd^{3+}, Ag^{+}, Ni^{2+}, Au^{+} and some of their complexes.[13] Therefore HEWL has been selected in this chapter as a model protein to study its interaction with different substituted complexes through bio-physical approach using some spectroscopic techniques.

On the other side Glycoside hydrolases involve a large class of enzymes that catalyze the hydrolysis of glycosidic bond.[14, 15] These enzymes which are dominant in carbohydrate metabolism can be categorized into a number of subfamilies based on the structural resemblances. Numerous artificial enzymes mimic the glycoside hydrolysis to model the glycosyl transfer reactions perceived in nature and hence, these reactions are greatly important in the biological systems.[16] Although using various metal ions such as Cu^{II}, Ni^{II}, Co^{II}, and Al^{III}, the efficient cleavage of some glycosides and disaccharides has been investigated but still the other catalytic systems with wider applicability are essentially required.[17]

However ligand design [18] is an important part of synthesis to develop such kind molecule which can mimic glycosidase as well as can be able to bind with Hen Egg White Lysozyme Protein. Schiff bases with flexible piperazinyl arm has shown remarkable possibilities with such kind of activities of enzyme mimic and protein binding as discussed in previous three chapters. There were some difficulties to tune the flexibility of Schiff base ligands [**HL^1** = 1-phenyl-3-((2-(piperidin-4-yl)ethyl)imino)but-1-en-1-ol and **HL^2** = 4-((2-(piperazin-1-yl)ethyl)imino)pent-2-en-2-ol] with a specific metal ions. That means with Ni(II), the piperazinyl arm of those ligands are always lying in boat conformation and with Cu(II), this arm is showing chair conformation. In this regard in last chapter 4A, a ligand **HL^3** [(E)-2-(phenyl((2-(piperazin-1-

yl)ethyl)imino)methyl)phenol] have employed and the formed Cu(II) complexes after reacting with Cu(II) salts has shown only chair confirmation of piperazinyl arm. Thus it was a challenge to prepare structurally diverse compound playing with same metal ion. For this purpose in this chapter ligand **HL^3** was reacted with two different Ni(II) salts and finally, structurally two different complexes $[Ni(L^3)(MeOH)]$ $(ClO_4)_2$ **(10)** and $[Ni_2(HL^3)_2(H_2O)_2(MeOH)_2]Cl_3.3MeOH$ **(11)** were formed. Among these two Ni(II) complexes **10** and **11**, the piperazinyl arm is in boat conformation in Ni(II) complex **10** and in chair conformation in Ni(II) complex **11**.which is a chloro-bridged dimeric molecule. Apart from structural point of view, the lysozyme binding activities of these two complexes were determined. As, di-nuclear metal complexes have been recognized at the active sites of many metalloenzymes [19] thus here dinuclear complex **11** was employed towards glucosidase enzyme mimic.

4B.2 Experimental section

4B.2.1 Materials and methods

All the chemical reagents required were purchased from sigma and used without further purification. The specifications of all the instruments used for analysis purpose were same as described in the section 2.2.1 of the previous chapter 2. The ligand 2-(phenyl((2-(piperazin-1-yl)ethyl)imino)methyl)phenol (**HL^3**) was synthesized applying the same procedure as described in chapter 4A.

4B.2.2 X-ray crystallography

Single crystal X-ray structural studies of **10** and **11** were performed following the similar protocol as mentioned in the section 4A.2.2 of previous chapter 4A. Intensity data were reduced using SAINT.[20] Empirical absorption corrections were performed with SADABS package.[21] The structures were solved using direct methods and refined by fullmatrix least-square methods based on $|F|^2$ using SHELXL-97.[22] All non-hydrogen atoms were refined with anisotropic thermal parameters. Hydrogen atoms were placed in calculated positions and constrained to ride on their parent atoms. All the calculations were carried out

using SHELXS-97, SHELXL-97 and SHELXTL [22] programs. Crystal data and structural parameters are provided in Table 4B.1.

***Table 4B. 1**. Crystallographic data and structure refinement parameters for **10** and **11**.*

Complex	**10**	**11**
Empirical Formula	$C_{19}H_{22}ClN_3NiO_5$	$C_{40}H_{58}Cl_4N_6NiO_6$
Crystal system	Triclinic	Monoclinic
Space group	*P 1*	*P121*
a (Å)	9.1868(3)	14.4375(9)
b (Å)	10.5804(4)	24.4105(14)
c (Å)	10.6803(4)	16.0739(9)
α (°)	111.496(2)	90
β (°)	90.757(2)	103.8546(12)
γ(°)	95.694(2)	90
V (Å^3)	959.77(6)	5500.06
ρ_{calcd} (mg m^{-3})	1.614	1.268
Z	2	1
T (K)	153(2)	153(2)
F(0 0 0)	484	2198
Crystal size (mm^3)	0.24 × 0.18 × 0.16	0.34 × 0.28 × 0.24
θ ranges (°)	2.87 – 28.54	2.68 – 30.39
h/k/l	-13,13/-15,15/-15,15	-20,20/-35,35/-23,21
Reflections collected	5854	17452
Independent reflections	4746	10081
T_{max} and T_{min}	0.74 and 0.83	0.74 and 0.81
GOF	1.057	1.025
Final R indices	R1=0.0364,wR2 = 0.0924	R1 = 0.0736, wR2 = 0.2118
R indices (all data)	R1=0.0503,wR2 = 0.0865	R1 = 0.1382, wR2 = 0.2663

4B.2.3 Synthesis of [Ni(L^3)(MeOH)] $(ClO_4)_2$ (10)

15 mL of methanolic solution containing **HL**^{3} (0.15 g, 0.5 mmol) and $Ni(ClO_4)_2.6H_2O$ (0.18 g, 0.5 mmol) was stirred at room temp for 2 h. The orange colored precipitate was further dissolved in DMF and layered with MeOH. Finally, after 2 or 3 days red needle-shaped crystals were obtained. Yield: 85%.

Anal Calcd (%):$C_{19}H_{21}ClN_3NiO_5$ C, 49.02; H, 4.55; N, 9.03. Found (%): C, 49.04; H, 4.73; N, 8.92. $[C_{19}H_{21}N_3NiO]^+$ (m/z) calculated – 365.10 $[M]^+$; obtained – 366.11 $(M + H)^+$. Selected IR on KBr (ν/cm^{-1}): 1597 (–C=N), 1097(ClO_4^-).

4B.2.4 Synthesis of $[Ni_2Cl(HL^3)_2(H_2O)_2(MeOH)_2]Cl_3.3MeOH$ (11)

15 mL of methanolic solution containing **HL^3** (0.15 g, 0.5 mmol) was added drop wise to a 10 mL solution of $NiCl_2.6H_2O$ (0.12 g, 0.5 mmol) and the resultant mixture was stirred at room temp for 1hr and then the solution was concentrated by evaporating the solvent. Layering of the reaction mixture with diethyl ether furnished suitable crystals after few days. Yield: 72%. Anal. Calcd. (%) : $C_{40}H_{58}Cl_4N_6Ni_2O_6$ C, 49.12; H, 5.98; N, 8.59. Found (%): C, 49.20; H, 5.72; N, 8.45. $[C_{40}H_{58}ClNi_2N_6O_6]^{3+}$ (m/z) calculated – 289.7 $(M)^{3+}$; obtained – 289.1 $(M)^{3+}$. Selected IR on KBr (ν/cm^{-1}): 1605 (–C=N)

4B.2.5 Lysozyme binding study

The binding capacity experiments of complexes **10** and **11** with Hen Egg White Lysozyme were carried out using standard Trp fluorescence with excitation at 295 nm and the corresponding emission at 335 nm, using a Fluoromax-4p spectrofluorometer [from Horiba JobinYvon (Model: FM-100)] with a rectangular quartz cuvette of 1 cm path length. A stock solution of HEW Lysozyme was prepared in TRIS-HCl buffer (pH ~ 7.4). Concentrated stock solutions of complexes **10** and **11** was prepared by dissolving them separately in TRIS-HCl buffer and diluted suitably with TRIS-HCl buffer to get the required concentrations. An aqueous solution (2 mL) of HEWL protein (10 µM) was treated by successive additions of the respective complexes (0 to 100 µM).

4B.2.6 Glucoside hydrolysis activity

Glucosidase activity of the complexes was measured taking the solution of Ni(II) complexes in water at pH≈10.5 (50 mM CAPS buffer) which was treated separatey with 100 eqivalents of *p*-nitrophenyl-*α*-D-glucopyranoside and *p*-nitrophenyl-*β*-D-glucopyranoside under aerobic condition at room temperature. Absorbance *vs*. wavelength plots were recorded for these solutions at a regular time interval of 10 min. The reaction was monitored over the time by formation of *p*-nitrophenolate using UV-vis spectroscopy at 410 nm. The dependence of rate on substrate concentration and various kinetic parameters were determined by treating different concentartion of substrate with a fixed molar concentration of catalyst.

4B.2.7 Supplementary materials

CCDC 1421490, and 1421491 contain the supplementary crystallographic data for complex **10** and **11**, respectively. These data can be obtained free of charge via http://www.ccdc.cam.ac.uk/conts/retrieving.html, or from the Cambridge Crystallographic Data Centre, 12 Union Road, Cambridge CB2 1EZ, UK; fax: (+44) 1223-336-033; or e-mail: deposit@ccdc.cam.ac.uk.

4B.3 Results and discussion

4B.3.1 Synthesis and characterization

Synthesis of ligand (**HL^3**) and its nickel complexes are depicted in the scheme 4B.1. The characterization of ligand (**HL^3**) is well depicted in the previous chapter.

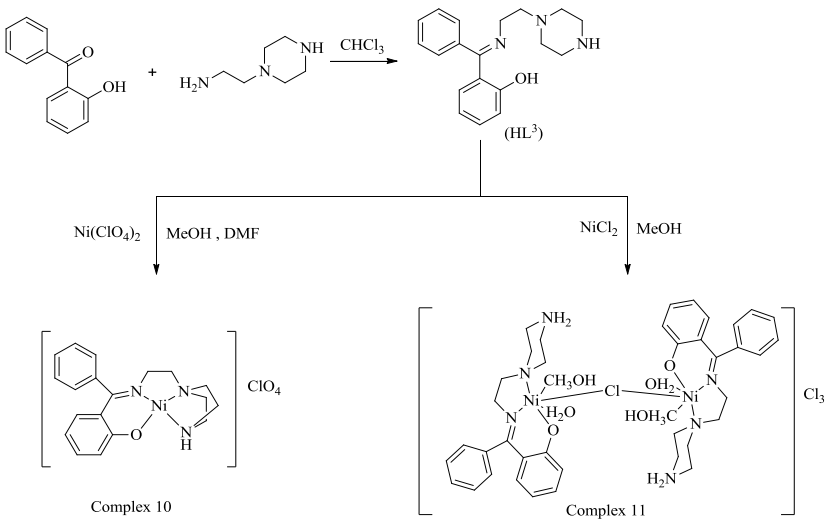

Scheme 4B. 1. *Formation of two Ni(II) Schiff base complexes (**10** & **11**)*

Both the complexes have been characterized by IR and ESI-MS spectroscopy, elemental analysis and single crystal X-ray crystallography. The IR spectra of ligand and complexes have shown characteristic band for -C=N in the region 1590-1610 cm^{-1}.[23] FTIR signals for non-coordinated ClO_4^- was also observed at 1042 cm^{-1}.[23] The electronic spectra of complex **10** and **11** (Figure 4B.1) have been studied in the solution state using CH_3OH as a solvent. The broad peaks in between 200-500 nm indicate the intramolecular LMCT transition.[24] The d-d transition band for octahedral complex was observed in between 1100 – 1200 nm.

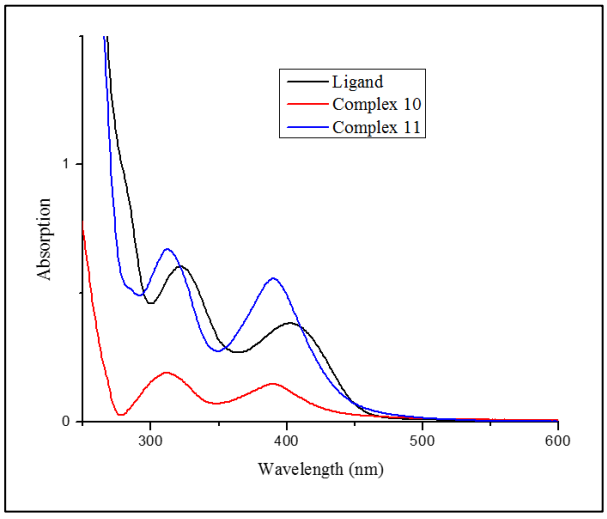

Figure 4B. 1*. Electronic spectra of Nickel complexes **10**&**11***

4B.3.2 Crystal structure of complex 10 and 11

Crystal structures of these two complexes depict two different types of Ni (II) centered coordination geometry where complex **10** exhibits square planar geometry and complex **11** exhibits octahedral geometry. In these two complexes, the major coordination bond lengths between Ni atom and N/O-donor centers are within the range of 1.801(1) to 2.292(7) Å (Table 4B.2), matches perfectly to an earlier report. [25]

Table 4B. 2. *Selected bond lengths (Å) and bond angles (°) for* ***10*** *and* ***11***

Complex	**10**	**11**
Ni(1)-N(1)	1.839(1)	2.012(3)
Ni(1)-N(2)	1.879(1)	2.248(3)
Ni(1)-N(3)	1.920(1)	.....
Ni(1)-O(1)	1.801(1)	2.002(3
Ni(1)-O(2)	.....	2.083(4)
Ni(1)-O(3)	.....	2.080(3)
Ni(2)-O(4)	.....	1.987(4)
Ni(2)-O(5)	.....	2.120(3)
Ni(2)-O(6)	.....	2.074(4)
Ni(1)-N(4)	.....	2.022(4)
Ni(1)-N(5)	.....	2.292(7)
Ni(1)-Cl(1)	.....	2.429(1)
Ni(2)-Cl(1)	.....	2.420(1)
N(1)-Ni(1)-N(2)	89.99(7)	83.9(1)
N(1)-Ni(1)-N(3)	164.69(7)	.....
N(1)-Ni(1)-O(1)	97.62(7)	90.2(1)
N(2)-Ni(1)-O(1)	172.3(7)	173.6(1)
Cl(1)-Ni(1)-N(1)	.....	177.3(1)
Cl(1)-Ni(2)-N(4)	.....	178.0(1)

The mono-metallic complex **10** crystalizes in the space group *P1*. The central metal atom is coordinated to the tetradentate Schiff base ligand L in a square planar fashion (Figure 4B.2). The average co-ordination bond angle around the Ni center of square planar geometry is around 90° whereas the least bond angle

was observed for N(2)–Ni(1)–N(3) (~76°) due to the formation of a chelated five membered ring piperazinyl moiety in a boat conformation. Furthermore, the independent molecules get connected with each other *via* disordered perchlorate ion through hydrogen bonding *viz*. N3–H1N···O2, N3–H1N···O5 and C11–H11···O4 to form a 1D chain (Figure 4B.2). Two such 1D strands are additionally joined by the same interconnecting perchlorate ion *via* C15–H15B···O5, C16–H16B···O4 and C19–H19A···O3 (Figure 4B.2).

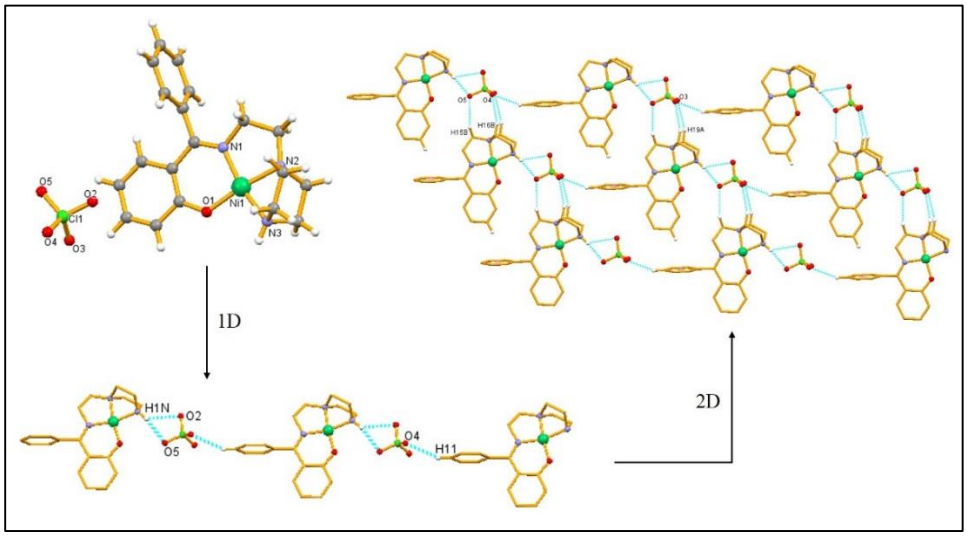

Figure 4B. 2. *Supramolecular interactions of complex* ***10***

The binuclear complex **11** with space group *P21/c* is a chloro bridged dinuclear complex where each Ni atom is in octahedral geometry and two axial positions are occupied by one methanol and one water molecule. The interesting features are that here the piperazinyl moiety has taken the chair confirmation. The nonbonding chloride ion is participated in non-covalent hydrogen bonding interactions (like N6–H6B···Cl2, O2–H10···Cl2, N3–H3B···Cl2, C17–H17A···Cl2, C15–H15B···Cl2 and C9–H9···Cl2) to connect neighboring three molecule. (Figure 4B.3)

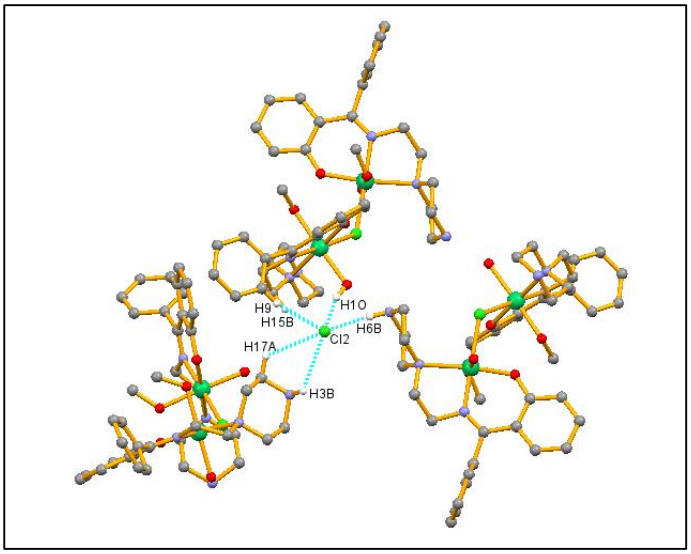

Figure 4B. 3. *Non covalent hydrogen bonding interactions in complex* ***11***

Furthermore, two individual molecules get interconnected *via* C31–H31···Π hydrogen bonding interaction to build a 1D chain and each 1D chain is further joined through N6–H6B···Cl2 and N3–H3B···Cl2 hydrogen bonding to make a 2D sheet type of network (Figure 4B.4).

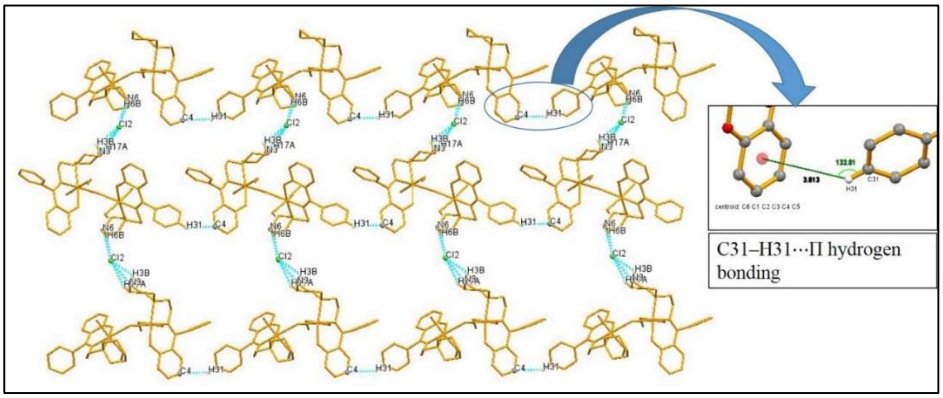

Figure 4B. 4. *2D Supramolecular networks in complex* ***11***

From the structural analyses of complex **10** and **11** it is evident that Ni(II) center of complex **10** is square planar in nature while complex **11** shows octahedral geometric feature around the metal center. Tuning of the flexibility of piperazine moiety in both the complexes is also a noticeable feature. The piperazine moiety of ligand $\mathbf{HL^3}$ of complex **10** is in boat conformation while for complex **11**, it is in a chair conformation. It may be assumed that counter anion of nickel salts play a significant role in this change of conformation. ClO_4^- anion has less ligation capacity than Cl^-. Therefore, in complex **11**, chloride ion

makes a bridge to form the dinuclear complex **11**. Thus it may be predicted that after coordination of chloride ion with Ni(II) center in complex **11,** it released the excess strain and the piperazine ring become in chair conformation which is thermodynamically more stable.

4B.3.3 Lysozyme binding study

The fluorescence spectra of these two complexes are exceptionally weak contrasted with the intrinsic fluorescence of tryptophan residues in HEWL. Henceforth, the quenching of intrinsic fluorescence of tryptophan residues present in HEWL has been utilized to understand the interaction between lysozyme and the complexes. The gradual decrease in the intrinsic fluorescence intensity of HEWL on addition of individual complex solutions, shown in Figure 4B.5 and Figure 4B.6, depict the changes in the local environment to tryptophan residues of the protein due to its binding to the complex. [26] HEWL contains six tryptophan moieties (28,62,63,108,111,and 123) with Trp-62, Trp-63, and Trp-108 located in the active site.[27] Although the six tryptophans are not independent emitters, the bulk of the fluorescence of lysozyme is located in Trp-62 and Trp-108. Subsequently, the quenching of fluorescence intensity of the protein in the presence of the metal complexes shows the probability of the changing the microenvironment of these two tryptophan residues. Figure 4B.5 and Figure 4B.6 indicate that the steady-state fluorescence quenching is related with blue shifts ($\Delta\lambda$ = 2 nm for complex **11**) of the wavelength of maximum fluorescence intensity (λ_{max}). The blue shifts of λ_{max} associated with complex **11** indicate the presence of non-polar environment favoring hydrophobic interactions between complex and the protein.

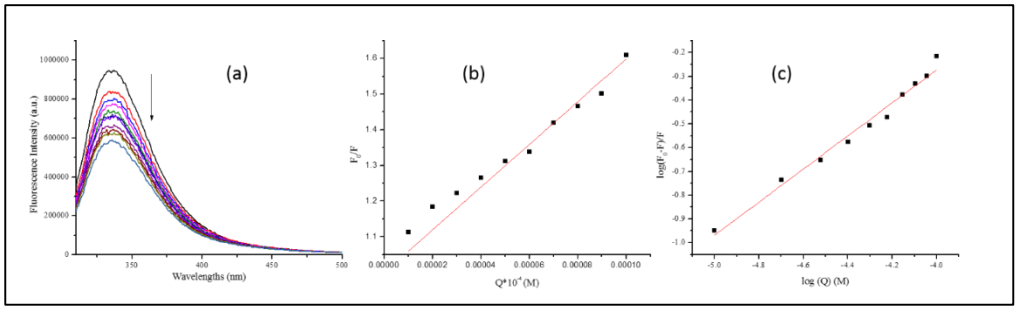

Figure 4B. 5. *(a) Fluorescence quenching of Lysozyme by complex* ***10*** *(0-100 µM). (b) & (c) Corresponding Stern Volmer Plot and Scatchard plot.*

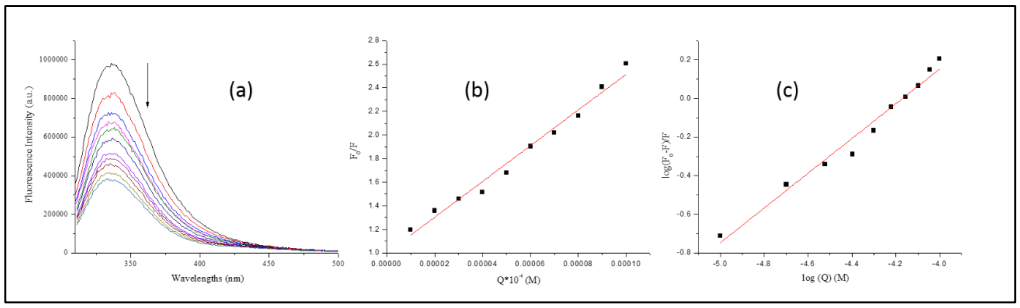

Figure 4B. 6. (a) Fluorescence quenching of Lysozyme by complex ***11*** *(0-100 µM). (b) & (c) Corresponding Stern Volmer Plot and Scatchard plot.*

Further, the apparent binding constants (K_a) of the order of 10^2 as obtained from Scatchard plot (Figure 4B.5 and Figure 4B.6) suggest that both the complexes possess moderate binding affinity towards HEWL. It was also a noticeable feature that chloro bridged dinuclear Ni(II) complex **11** has shown greater binding affinity than the complex **10.** As the number of the binding site of the protein towards each complex is almost one, thus it indicates the formation of 1:1 complex between HEWL and individual complex. All the parameters are tabulated in the Table 4B.3

Table 4B. 3. *Various parameters obtained from lysozyme binding study.*

System	K_{sv} (M^{-1})	K_a (M^{-1})	N
Complex 10	$5.9*10^4$	$3.1*10^2$	0.6
Complex 11	$1.5*10^5$	$5.6*10^3$	0.9

4B.3.4 Glycosidase activity study

Glycosidic bond cleavage by glucoside hydrolysis is presented in the Scheme 4B.2. In sequence to evaluate the ability of two complexes towards the cleavage of glucoside bonds, the hydrolysis of *p*-nitrophenyl-*α*-D-glucopyranoside and *p*-nitrophenyl-*β*-D-glucopyranoside was examined in aqueous solution in 50 mM CAPS buffer at pH≈10.5.

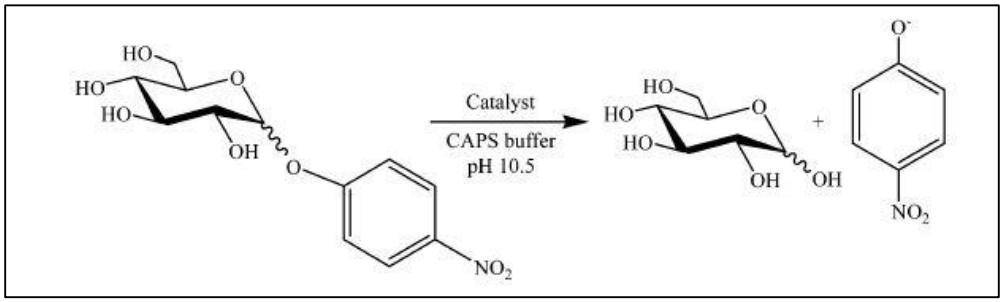

Scheme 4B. 2. *Schematic representation of hydrolysis of glucosidic linkage.*

For this purpose, 1.0×10^{-5} M solutions of these complexes were treated with 2.0×10^{-4} M solutions of glycoside substrates separately, at room temperature under aerobic conditions. The course of the reaction was monitored by UV-vis spectroscopic technique. From the outcome it was observed that only dinuclear complex **11** is showing effective glucosidase activity (Figure 4B.7). This result was quite similar with that of previously predicted as natural glycosidase is the dinuclear copper based enzyme.

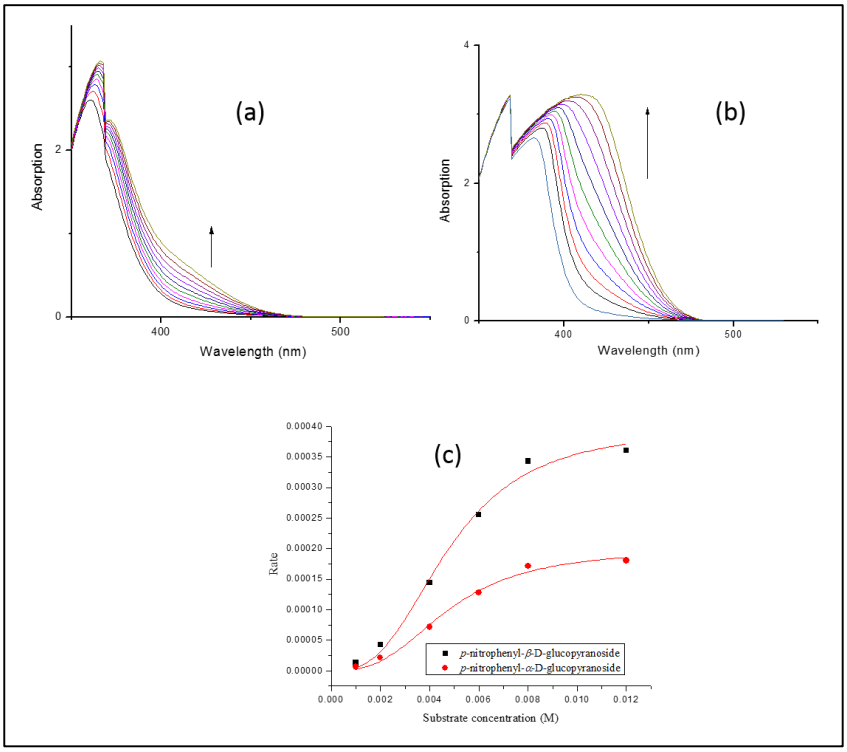

Figure 4B. 7. *Glucoside bond hydrolysis of (a) p-nitrophenyl-α-D-glucopyranoside (b) p-nitrophenyl-β-D-glucopyranoside (c) Corresponding Michaelis-menten plot.*

The kinetics of the hydrolysis *p*-nitrophenyl-*α*-D-glucopyranoside and *p*-nitrophenyl-*β*-D-glucopyranoside were determined by the Michaelis-Menten approach of enzyme kinetics by monitoring the *p*-nitrophenolate band at 410 nm as a function of time. The concentration of each of the glycoside substrates were kept constant at 10 times higher than that of the catalyst to maintain the pseudo-first-arrange reaction condition. The dependence of the initial rate on complex and substrate concentration was considered keeping in mind the end goal to explain the reactivity. The solutions of complex **11** were treated with different concentrations of each glycoside substrate to determine the dependence of rates on the substrate concentration and various kinetic parameters. The Michaelis-Menten approach has been applied to get the various kinetic parameters like K_{cat}, K_M and V_{max} which were shown in Table 4B.4.

Table 4B. 4. *Various parameters obtained from Michaleis-menten diagram.*

Substrate	**V_{max} (M min^{-1})**	**K_M (M)**	**k_{cat} / T.O.N (min^{-1})**
p-nitrophenyl-*α*-D-glucopyranoside	1.99×10^{-4}	4.0×10^{-3}	1.99
p-nitrophenyl-*β*-D-glucopyranoside	3.98×10^{-4}	4.6×10^{-3}	3.98

This hydrolysis of glucoside is directly dependent on the concentration of complex under the conditions employed. From literature, it was clear that influence of both metal centers in either natural glycosidase enzyme or artificial mimic enzyme is very effective towards hydrolysis of glucoside bond. Thus, finally it can be assumed that the observed catalytic activity of the complexes is associated with the electronic features of the ligand backbones as well as the influence of an overall geometry of two nickel (II) centers in complex **11.**

4B.4 Conclusions

In conclusion two new Ni(II) complexes $[Ni(L^3)(MeOH)]$ $(ClO_4)_2$ **(10)** and $[Ni_2(HL^3)_2(H_2O)_2(MeOH)_2]Cl_3.3MeOH$ **(11)** have been synthesized using a newly developed Schiff based ligand 2-(phenyl((2-(piperazin-1-yl)ethyl)imino)methyl)phenol **(HL^3)**. Structurally diverse geometry of two complexes were determined where one complex is square planar along with boat conformer piperazine moiety and other one is dinuclear chloro bridged octahedreal complex where piperazinyl arm is in chair conformer. Lysozyme binding activities of these complexes were also scrutinized and the result shows that dinuclear complex has higher binding capacity than the other mononuclear complex. Moreover dinuclear complex **11** shows potent glycosidase activity.

4B.5 References

[1]. David, S. S.,Meggers, E. (2008), Inorganic chemical biology: from small metal complexes in biological systems to metalloproteins, Current Opinion in Chemical Biology, 12, 194-196.(DOI: 10.1016/j.cbpa.2008.03.008)

[2]. Gray, H. B. (2003), Biological inorganic chemistry at the beginning of the 21st century, Proceedings of the National Academy of Sciences, 100, 3563-3568.(DOI: 10.1073/pnas.0730378100)

[3]. Broderick, J. B.,Coucouvanis, D. (2003), Bioinorganic chemistry, Current Opinion in Chemical Biology, 7, 157-159.(DOI: 10.1016/S1367-5931(03)00030-9)

[4]. Barondeau, D. P.,Getzoff, E. D. (2004), Structural insights into protein–metal ion partnerships, Current Opinion in Structural Biology, 14, 765-774.(DOI: 10.1016/j.sbi.2004.10.012)

[5]. Jena, H. S. (2014), Effect of non-covalent interaction on the diastereoselective self-assembly of Cu(II) complexes containing a racemic Schiff base in a chiral self-discriminating process, New Journal of Chemistry, 38, 2486-2499.(DOI: 10.1039/C3NJ01547E)

[6]. Osório, R. E. H. M. B.,Peralta, R. a.,Bortoluzzi, A. J.,De Almeida, V. R.,Szpoganicz, B.,Fischer, F. L.,Terenzi, H.,Mangrich, A. S.,Mantovani, K. M.,Ferreira, D. E. C.,Rocha, W. R.,Haase, W.,Tomkowicz, Z.,Anjos, A. D.,Neves, A. (2012), Synthesis, magnetostructural correlation, and catalytic promiscuity of unsymmetric dinuclear copper(II) complexes: Models for catechol oxidases and hydrolases, Inorganic Chemistry, 51, 1569-1589.(DOI: 10.1021/ic201876k)

[7]. Das, M.,Nasani, R.,Saha, M.,Mobin, S. M.,Mukhopadhyay, S. (2015), Nickel(II) complexes with a flexible piperazinyl moiety: studies on DNA and protein binding and catecholase like properties, Dalton Transactions, 44, 2299-2310.(DOI: 10.1039/C4DT02675F)

[8]. Razavet, M.,Artero, V.,Cavazza, C.,Oudart, Y.,Lebrun, C.,Fontecilla-Camps, J. C.,Fontecave, M. (2007), Tricarbonylmanganese(I)-lysozyme complex: a structurally characterized organometallic protein, Chemical Communications, 27, 2805-2807.(DOI: 10.1039/B703887A)

[9]. Binkley, S. L.,Ziegler, C. J.,Herrick, R. S.,Rowlett, R. S. (2010), Specific derivatization of lysozyme in aqueous solution with $Re(CO)_3(H_2O)^{3+}$, Chemical Communications, 46, 1203-1205.(DOI: 10.1039/B923688K)

[10]. Casini, A.,Mastrobuoni, G.,Temperini, C.,Gabbiani, C.,Francese, S.,Moneti, G.,Supuran, C. T.,Scozzafava, A.,Messori, L. (2007), ESI mass spectrometry and X-ray diffraction studies of adducts between anticancer platinum drugs and hen egg white lysozyme, Chemical Communications, 2, 156-158.(DOI: 10.1039/B611122J)

[11]. Santos-Silva, T.,Mukhopadhyay, A.,Seixas, J. D.,Bernardes, G. J. L.,Romão, C. C.,Romão, M. J. (2011), CORM-3 Reactivity toward Proteins: The Crystal Structure of a Ru(II) Dicarbonyl−Lysozyme Complex, Journal of the American Chemical Society, 133, 1192-1195.(DOI: 10.1021/ja108820s)

[12]. Vergara, A.,D'Errico, G.,Montesarchio, D.,Mangiapia, G.,Paduano, L.,Merlino, A. (2013), Interaction of Anticancer Ruthenium Compounds with Proteins: High-Resolution X-ray Structures and Raman Microscopy Studies of the Adduct between Hen Egg White Lysozyme and AziRu, Inorganic Chemistry, 52, 4157-4159.(DOI: 10.1021/ic4004142)

[13]. Moreau, S.,Awade, A. C.,Molle, D.,Le Graet, Y. e.,Brule, G. (1995), Hen egg white lysozyme-metal ion interactions: investigation by electrospray Ionization Mass Spectrometry, Journal of Agricultural and Food Chemistry, 43, 883-889.(DOI: 10.1021/jf00052a007)

[14]. Henrissat, B.,Bairoch, A. (1996), Updating the sequence-based classification of glycosyl hydrolases, Biochemical Journal, 316, 695-696.

[15]. Henrissat, B.,Davies, G. (1997), Structural and sequence-based classification of glycoside hydrolases, Current Opinion in Structural Biology, 7, 637-644.(DOI: 10.1016/S0959-440X(97)80072-3)

[16]. Yip, V. L. Y.,Thompson, J.,Withers, S. G. (2007), Mechanism of GlvA from Bacillus subtilis: A Detailed Kinetic Analysis of a 6-Phospho-α-glucosidase from Glycoside Hydrolase Family 4, Biochemistry, 46, 9840-9852.(DOI: 10.1021/bi700536p)

[17]. Baty, J.,Sinnott, M. L. (2004), Efficient electrophilic catalysis of 1,5-anhydrocellobiitol hydrolysis by AlIII; implications for the conservation of "rosin-alum" sized paper, Chemical Communications, 866-867.(DOI: 10.1039/B316417A)

[18]. Vijayan, P.,Viswanathamurthi, P.,Velmurugan, K.,Nandhakumar, R.,Balakumaran, M. D.,Kalaichelvan, P. T.,Malecki, J. G. (2015), Nickel(II) and copper(II) complexes constructed with N2S2hybrid benzamidine–thiosemicarbazone ligand: synthesis, X-ray crystal structure, DFT, kinetico-catalytic and in vitro biological applications, RSC Adv., 5, 103321-103342.(DOI: 10.1039/c5ra18568h)

[19]. Karlin, K. (1993), Metalloenzymes, structural motifs, and inorganic models, Science, 261, 701-708.(DOI: 10.1126/science.7688141)

[20]. (1998), SAINT Plus, 6.01, Bruker AXS: Madison, Wisconsin, USA.

[21]. (1998), SADABS, 2.01, Bruker AXS.: Madison, Wisconsin, USA.

[22]. Sheldrick, G. (2008), A short history of SHELX, Acta Crystallographica Section A, 64, 112-122.(DOI: 10.1107/S0108767307043930)

[23]. Nakamoto, K., (2009), Infrared and Raman Spectra of Inorganic and Coordination Compounds, Theory and Applications in Inorganic Chemistry.6th ed. John Wiley & Sons, Inc.: Hoboken, New Jersey.

[24]. Lever, A. B. P., (1984), Inorganic Electronic Spectroscopy.2nd ed. Elsevier Science, New York.

[25]. Bullock, S. J.,Harding, L. P.,Moore, M. P.,Mills, A.,Piela, S. A. F.,Rice, C. R.,Towns-Andrews, L.,Whitehead, M. (2013), Synthesis of ligands containing N-oxide donor atoms and their assembly into metallosupramolecular structures, Dalton Transactions, 42, 5805-5811.(DOI: 10.1039/C3DT00090G)

[26]. Lakowicz, J. R., (2006), Principles of Fluorescence Spectroscopy.Kluwer Academic Plenum Publishers, New York, USA, pp. 205

[27]. Formoso, C.,Forster, L. S. (1975), Tryptophan fluorescence lifetimes in lysozyme, Journal of Biological Chemistry, 250, 3738-3745.

Chapter 5

A novel approach of pseudohalide promoted enhanced corrosion inhibition by antimicrobial zinc(II) Schiff base complexes

Chapter 5

A novel approach of pseudohalide promoted enhanced corrosion inhibition by antimicrobial zinc(II) Schiff base complexes

5.1 Introduction

Coordination chemistry of zinc has served an important role in the advancement of various fast developing fields of science and technology. [1-4] The strategic synthesis of the zinc complexes has received considerable attention, because of the potential application in diverse fields with wide variety of uses in the interfaces of the various subjects in science.

Among various different socio economic problems, corrosion of metal is one of the major problems faced by chemical and other industries over the years. Corrosion is defined as the harsh attack on metals by its surroundings. The spontaneous damage of metal due to heterogeneous chemical reaction is the main reason behind the chemical corrosion.[5] The effects of various micro-organisms on metal are known as microbial corrosion.[6] Thus corrosion inhibition is one of the challenging fields for chemists as well as engineers. Corrosion inhibition by different materials is a surface phenomenon where the adsorption of the organic and inorganic compounds on the metal surface serves as a means of achieving the aim.[7] It is fascinating to imagine the blend of organic–inorganic hybrid compounds which can be readily active with effective surface chemistry to inhibit the corrosion on metal surface.[8] Knowing the orientation of the molecule, favorable configurations, atomic charges, steric and electronic effects would be useful for better understanding of the inhibitor performance of inorganic complexes. Thus, the benefit of utilizing inorganic coordination complexes evolved numerous research attempts for fabrication and applicability of these compounds as chemical models for corrosion resistance.

Among large varieties of metal corrosion, mild steel corrosion are getting more attention as mild steel finds extensive application due to its easy availability, low cost and good mechanical properties.[9] The main disadvantage of steel as a structural material is that it is prone to corrosion in aggressive environment.

There are few reports so far in the literature, on the applications of the zinc complexes as an effective corrosion inhibitor of stainless steel,[10-15] Moreover, independent Schiff bases are studied extensively as corrosion inhibitor as the presence of >C=N– group allows the corresponding Schiff bases to get adsorbed on the surface of mild steel and to form a monolayer on the surface spontaneously. Therefore, it can act as an effective corrosion inhibitor for mild steel.[16-19]

Furthermore, the interaction of metal ions with Schiff base has recently been designed as an efficient target owing to the wide range of applications based on their numerous functionalities as anti-bactericide,[20] antivirus,[21] and fungicide agents.[22] Thus it can be presumed that if such kind of metal coordination systems will be used as corrosion inhibitor then if they released from the metal surface for some external effects, the effect on environment will be minimal or advantageous as they have lots of biological significance.

Like previous chapters, here also tuning flexibility in ligand design is one of the key interests for structure-activity relationship in this kind of application. Moreover as the increasing number of heteroatoms enhance the adsorbing capacity on metallic surface[23], thus the idea of using azide like pseudo-halides as co-ligands has been conceived to improve upon the corrosion inhibition through better adsorption on the surface.

Taking account of all these facts, herein six zinc Schiff base complexes have been synthesized and characterized and their corrosion inhibition properties have been explored on mild steel in 15 % HCl solution. The corrosion inhibition efficiency was studied by electrochemical methods and protection of metal surface by Zn(II) complexes has been investigated by FE-SEM and AFM images. Apart from these, the antimicrobial activity of synthesized Zn(II) Schiff base azido complexes have been scrutinized.

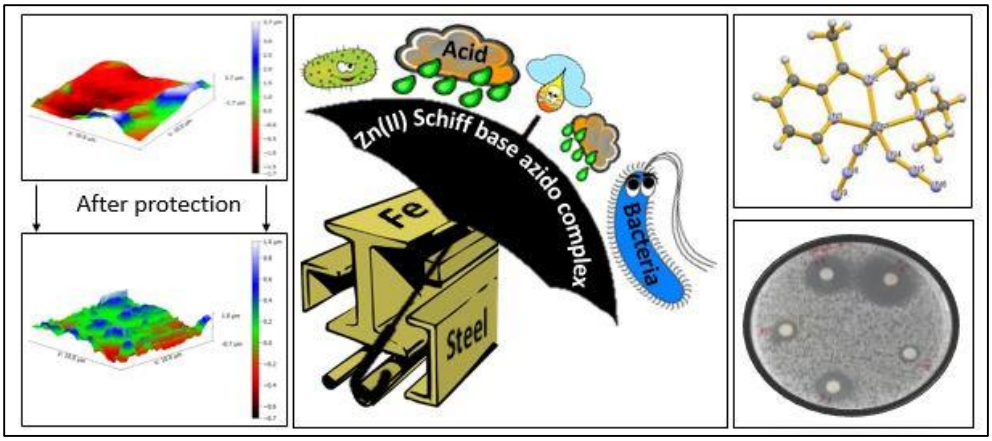

Figure 5. 1. *Pictorial representation of corrosion inhibition by zinc complexes.*

5.2 Experimental section

5.2.1 Materials and methods

All the chemical reagents required were purchased from Sigma, except HCl (purchased from Ranbaxy Fine Chemicals) and used without further purification. Infrared spectra (4000-500 cm^{-1}) were recorded with a BRUKER TENSOR 27 instrument in KBr pellets. Nuclear Magnetic Resonance (NMR) spectra were recorded in AVANCE III 400 Ascend Bruker BioSpin machine at ambient temperature. Mass spectrometric analyses were done on Bruker-Daltonics, micro TOF-Q II mass spectrometer and elemental analyses were carried out with a Thermo Flash 2000 elemental analyzer.

5.2.2 X-ray crystallography

Single crystal X-ray structural studies of **12-17** were performed on a CCD Agilent Technologies (Oxford Diffraction) SUPER NOVA diffractometer. Data for all the complexes were collected at 150(2) K except complex **16** which was taken 298(2) K using graphite-monochromated Mo Kα radiation (λ_α = 0.71073 Å). The strategy for the Data collection was evaluated by using the CrysAlisPro CCD software. The data were collected by the standard 'phi-omega scan techniques and were scaled and reduced using CrysAlisPro RED software. The structures were solved by direct methods using SHELXS-97 and refined by full

matrix least- squares with SHELXL-97, refining on F^2.[24] The positions of all the atoms were obtained by direct methods. All non-hydrogen atoms were refined anisotropically. The remaining hydrogen atoms were placed in geometrically constrained positions and refined with isotropic temperature factors, generally 1.2 U_{eq} of their parent atoms. The crystal and refinement data are summarized in Table 5.1.

Table 5. 1. *Crystallographic data and structure refinement parameters for* ***12-17.***

	12	**13**	**14**	**15**	**16**	**17**
Empirical formula	$C_{22}H_{34}Cl_2N_6O_8Zn$	$C_{30}H_{38}N_6O_{10}Zn_2$	$C_{11}H_{17}N_9Zn$	$C_{13}H_{21}N_9Zn$	$C_{13}H_{19}N_9OZn$	$C_{28}H_{42}N_{18}Zn_2$
Crystal system	Orthorhombic	Orthorhombic	Triclinic	Monoclinic	Triclinic	Monoclinic
Space group	*Pna2₁*	*Pcab*	*P-1*	*P 21/n*	*P-1*	*C1c1*
a [Å]	17.197(3)	13.4837(8)	9.302(2)	9.684(3)	9.9844(3)	10.1099(7)
b [Å]	13.955(3)	15.304(10)	9.636(10)	10.313(2)	13.108(4)	27.607(2)
c [Å]	12.194(2)	17.2599(8)	9.856(2)	17.237(4)	13.8180(4)	12.8065(8)
α [°]	90	90	69.82(13)	90	115.35(13)	90
β [°]	90	90	67.80	103.49	90.64	105.788
γ [°]	90	90	83.78(13)	90	92.82(15)	90
V [Å^3]	2926.67(9)	3561.8(4)	767.6(3)	1674.04	1631.25(9)	3439.5(4)
Z	4	4	2	4	4	4
D_{calcd} [mgm^{-3}]	1.468	1.442	1.474	1.463	1.558	1.471
F(000)	1344	1600	352	768	792	1584
GOF	1.059	1.133	1.096	1.019	1.086	1.018
Collected / unique	17933/5100	27941/3044	5494/2697	5349/4128	10488/7772	10005/8021
Final *R* indices	R1=0.054 wR2=0.142	R1=0.106 wR2=0.298	R1=0.034 wR2=0.08	R1=0.032 wR2=0.06	R1=0.035 wR2=0.102	R1=0.045, wR2=0.10
R indices (all data)	R1=0.069, wR2=0.161	R1=0.138, wR2=0.328	R1=0.039 wR2=0.09	R1=0.077, wR2=0.07	R1=0.0616, wR2=0.084	R1=0.063, wR2=0.11

5.2.3 Synthesis of Schiff base ligands (L^4, L^5, L^6 and L^7)

Four ligands **L^4** [N^1,N^1-dimethyl-N^2-(1-(pyridin-2-yl)ethylidene)ethane-1,2-diamine], **L^5** [N^1,N^1-diethyl-N^2-(1-(pyridin-2-yl)ethylidene)ethane-1,2-diamine], **L^6** [2-morpholino-N-(1-(pyridin-2-yl)ethylidene)ethanamine] and **L^7** [(2-(piperidin-1-yl)-N-(1-(pyridin-2-yl)ethylidene)ethanamine)] were prepared following the procedure reported in literature.[25, 26] These were used for the preparation of metal complexes without further purification.

5.2.4 Synthesis of $[Zn(L^4)_2](ClO_4)_2$ (12)

0.10 g (0.5 mmol) of Schiff base ligand **L^4** dissolved in 10 mL of methanol was added dropwise to a solution of 0.19 g of $Zn(ClO_4)_2.6H_2O$ (0.5 mmol) in 5 mL of methanol. The mixture was stirred for 1 hour at room temperature and filtered after that. Colorless block-shaped crystals of **12**, suitable for X-ray diffraction, were formed by slow evaporation of the filtrate in the air. Yield: 72%. Anal. Calcd. (%) $C_{22}H_{34}ZnCl_2N_6O_8$: C, 40.85; H, 5.30; N, 12.99. Found(%): C, 40.97; H, 5.21; N, 12.57. ESI-MS- 545.17 $([Zn(L^4)_2]ClO_4)^+$

5.2.5 Synthesis of $[Zn(\mu\text{-fumarate})(L^4)]_n$ (13)

A mixture of **L^4** (0.5 mmol, 0.010 g) and $Zn(OAc)_2.2H_2O$ (0.5 mmol, 0.11 g) was taken and stirred in methanol (15 mL) for 30 minutes at room temperature. After that, an aqueous solution (10 mL) of the sodium salt of the fumaric acid (1.2 mmol, 0.19 g) was added and stirring was continued for 1 hour more. The mixture was concentrated and filtered and the colorless block-shaped crystals of **13**, suitable for X-ray diffraction, were formed after two weeks on slow evaporation of the filtrate in air. Yield: 62% (based on metal salt). Anal. Calcd. (%) $C_{30}H_{40}Zn_2N_6O_{10}$: C, 46.59; H, 4.95; N, 10.87. Found(%): C, 45.77; H, 4.77; N, 10.32. ESI-MS- 314.00 $[ZnL^4(H\text{-fumarate})]^+$

5.2.6 Synthesisof $[ZnL^4(N_3)_2]$ (14)

Ligand **L^4** (0.5 mmol, 0.10 g) and $Zn(OAc)_2.2H_2O$ (0.5 mmol,0.11 g) were stirred in methanol (15 mL) for 30 min at room temperature. An aqueous solution (10 mL) of sodium azide (1 mmol, 0.07 g) was added into it thereafter and stirring was continued for 1 hour. The mixture was concentrated and filtered and the colourless block-shaped crystals of **14**, suitable for X-ray diffraction, were formed on slow evaporation of the filtrate in air. Yield: 85%. Anal. Calcd. (%) $C_{11}H_{17}Zn\ N_9$: C, 38.78; H, 5.03; N, 37.00. Found (%): C, 38.34; H, 4.94; N, 36.57. ESI-MS (*m/z*) - 297.00 $[ZnL^4(N_3)]^+$

5.2.7 Synthesis of $[ZnL^5(N_3)_2]$ (15)

Ligand **L^5** (0.5 mmol, 0.10 g) and $Zn(OAc)_2.2H_2O$ (0.5 mmol, 0.11 g) were taken in methanol (15 mL) and stirred for 30 min at room temperature. After that an aqueous solution (10 mL) of sodium azide (1 mmol, 0.06 g) was added drop wise into it with continuous stirring. The stirring was continued for 1 hour. Then the solvent was evaporated to concentrate the solution and it was filtered. Finally the colourless block-shaped crystals of **15**, suitable for X-ray diffraction, were formed after 4 days on slow evaporation of the filtrate in air. Yield: 82%. Anal. Calcd. (%) $C_{13}H_{21}ZnN_9$: C, 42.34; H, 5.74; N, 34.19. Found (%): C, 42.44; H, 5.28; N, 33.70. ESI-MS (*m/z*) - 325.1 $[ZnL^5N_3]^+$

5.2.8 Synthesis of $[ZnL^6(N_3)_2]$ (16)

0.12 g of ligand **L^6** (0.5 mmol) and 0.11 g of $Zn(OAc)_2.2H_2O$ (0.5 mmol,) were mixed in methanol (15 mL) and stirred for 30 min at room temperature. Then 10 mL aqueous sodium azide (1 mmol, 0.06 g) was added into it slowly. The solution was stirred for 1 hour more. After that the solvent was evaporated to make it concentrate and then it was filtered. Finally the colourless block-shaped crystals of **16**, suitable for X-ray diffraction, were formed after 6 days on slow evaporation of the filtrate in air. Yield: 76%. Anal. Calcd. (%) $C_{13}H_{19}ZnN_9O$: C,

40.80; H, 5.00; N, 32.94. Found (%): C, 40.10; H, 4.88; N, 31.70. ESI-MS (*m/z*) - 340.1 $[ZnL^6N_3]^+$

5.2.9 Synthesis of $[ZnL^7(N_3)_2]$ (17)

In 15 mL of methanol, ligand $\mathbf{L^7}$ (0.5 mmol, 0.12 g) and $Zn(OAc)_2.2H_2O$ (0.5 mmol, 0.11 g) were stirred for 30 min at room temperature. An aqueous solution (10 mL) of sodium azide (1 mmol, 0.06 g) was added into it thereafter and stirring was continued for 1 hour. The reaction mixture was concentrated and filtered and then colourless block-shaped crystals of **17**, suitable for X-ray diffraction, were formed after 7 days on slow evaporation of the filtrate in air. Yield: 74% (based on metal salt). Anal. Calcd. (%) $C_{14}H_{21}ZnN_9$: C, 44.16; H, 5.56; N, 33.11. Found (%): C, 44.81; H, 5.75; N, 32.60. ESI-MS (*m/z*) - 338.1 $[ZnL^7N_3]^+$

5.2.10 Electrochemical experiments

The mild steel sheets [Composition: 0.055 % C, 0.52 % Mn, 0.018 % P, 0.005 % S 0.052 % Si, 0.044 % Al, 0.021 % Cr, 0.006 % Cu, 0.001 % Nb, 0.001 % Ti and balance Fe; Thickness: 2mm] were collected from Tata Steel, Jamshedpur, India. Square shaped (1 cm^2) mild steel samples were cut from this and used for the electrochemical experiments. One face of this specimen was sealed using Araldite, after connecting it to a copper wire. This square specimen of mild steel having 1 cm^2 exposed area was used as working electrode. In every experiment, metal samples were polished with fine emery paper (grade upto 2000), washed with distilled water, rinsed with acetone, dried and then stored in desiccator prior to their use. All electrochemical experiments were performed in a three-electrode cell, consist of working, reference and the counter electrode. Here saturated calomel electrode and platinum electrode were used as reference and counter electrode respectively. The three electrodes were connected to the Electrochemical Workstation, CH Instruments model CH660C. All tests were performed in 15% HCl medium and unstirred condition at room temperature

(298 ± 1 K) in presence and absence of inhibitor (Blank). Prior to electrochemical study, the system was left undisturbed for an hour, which was sufficient to attain stable open circuit potential (OCP).

The potentiodynamic polarization curve was obtained at a scan rate of 0.5 mVs^{-1} in the potential range, + 250 mV to – 250 mV with respect to OCP. The corrosion current density (I_{corr}) values were obtained by the Tafel extrapolation method using the software provided with the equipment.

Electrochemical Impedance Spectroscopy (EIS) experiments were performed at open circuit potential at applied frequency range 100 kHz to 100 mHz at 298 ± 1 K by using AC amplitude signal of 5 mV peak-to-peak.

5.2.11 Surface analysis

The surface was characterized by Field Emission Scanning Electronic Microscope (FE-SEM) and Atomic Force Microscopy (AFM). Micrographs were taken at room temperature (298 ± 1 K) after 6 h immersion of polished metal coupon in 15 % HCl solution with and without inhibitor.

5.2.12 Antimicrobial study

Same experimental protocols as described in chapter no 3 was employed here to measure the antibacterial activity of the synthesized inhibitor metal complexes.

5.2.13 Supplementary materials

CCDC 958284, 958286, 958285, 1560645, 1421494 and 1560646 contain the supplementary crystallographic data for complex **12-17**, respectively. These data can be obtained free of charge via http://www.ccdc.cam.ac.uk/conts/retrieving.html, or from the Cambridge Crystallographic Data Centre, 12 Union Road, Cambridge CB2 1EZ, UK; fax: (+44) 1223-336-033; or e-mail: deposit@ccdc.cam.ac.uk.

5.3 Results and discussion

5.3.1 Synthesis and characterization

Ligands $\mathbf{L^4}$, $\mathbf{L^5}$, $\mathbf{L^6}$ and $\mathbf{L^7}$ were prepared by reported methods, respectively.[25, 26] In compound **12**, ligand to metal ratio was used in 2:1 and zinc perchlorate was used as a metal precursor. In case of compound **13**, sodium fumarate was used as a co-ligand. Compounds **14-17** have been prepared in a methanolic solution of zinc salt in presence of several ligands $\mathbf{L^4}$, $\mathbf{L^5}$, $\mathbf{L^6}$ and $\mathbf{L^7}$ aqueous NaN_3 maintaining 1:1:2 ratio (Scheme 5.1 and Scheme 5.2), where azide ion has been utilized as co-ligand.

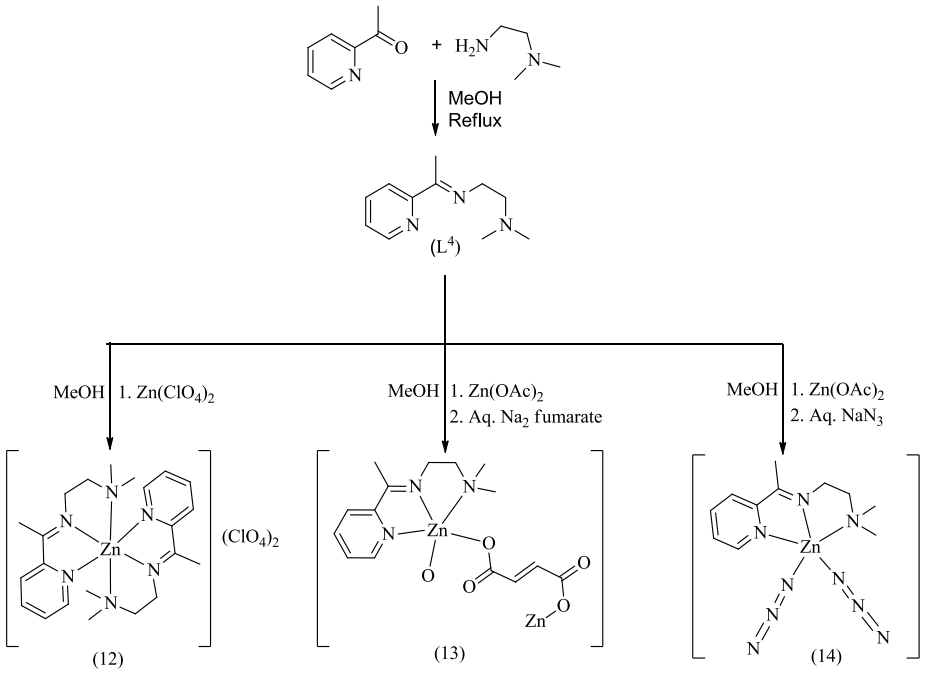

Scheme 5. 1. *Synthetic route of complexes* ***12-14***

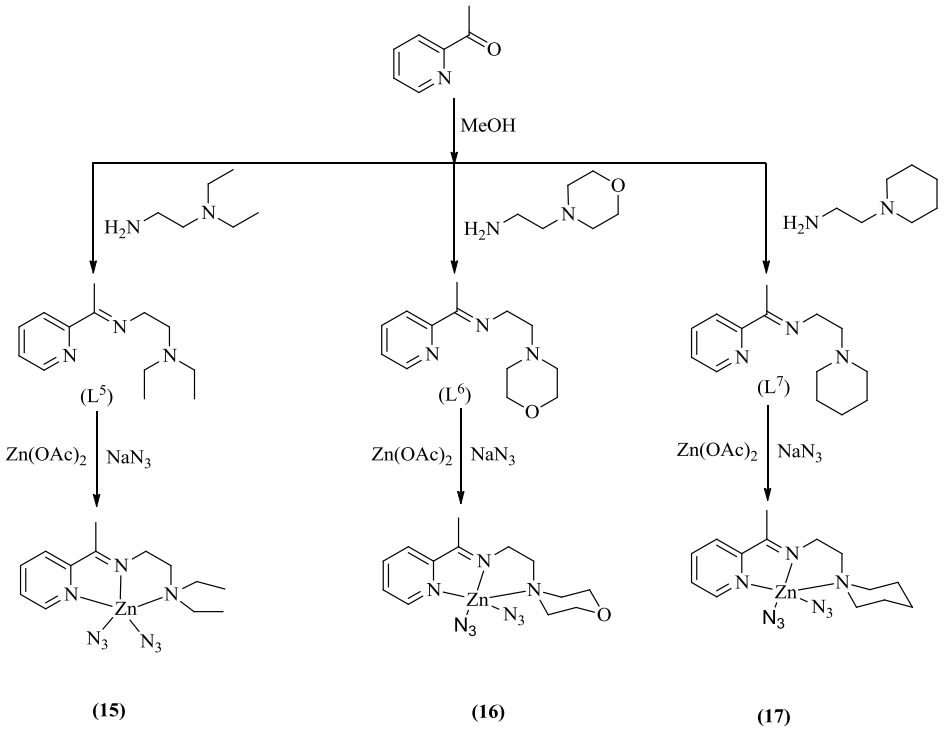

Scheme 5. 2. *Synthetic route of complexes* ***15-17***

All the compounds were characterized by different spectroscopic techniques apart from elemental analysis. The structures of the compounds were further determined by single crystal X-ray crystallography. The IR spectra of compound **12-17** show typical band for stretching vibration of C=N in the range of 1590-1600 cm^{-1}.[27] This indicates clearly that on complex formation C=N stretching frequency shifts in lower frequency region with respect to parent ligand. Compound **12** shows a strong band at 1091 cm^{-1} assigned to a non-coordinated ClO_4^- ion.[28] There a sharp band observed around 2036 cm^{-1} mainly due to the terminal azido stretching frequency in complex **12-17**. All the coordination bond lengths and bond angles of all complexes around the central zinc center are tabulated in Table 5.2.

Table 5. 2. *Selected bond lengths (Å) and bond angles (°) of five complexes* ***12-17.***

Complex	**12**	**13**	**14**	**15**	**16**	**17**
Zn(1)-N(1)	2.153(5)	2.224(9)	2.182(2)	2.193(1)	2.195(2)	2.270(5)
Zn(1)-N(2)	2.055(5)	2.319(10)	2.093(3)	2.082(1)	2.089(2)	2.049(3)
Zn(1)-N(3)	2.273(5)	2.227(9)	2.195(3)	2.249(1)	2.272(2)	2.249(4)

Zn(1)-N(4)	2.187(5)		1.995(3)	1.989(2)	1.973(2)	1.988(5)
Zn(1)-N(5)	2.052(5)					
Zn(1)-N(6)	2.481(6)					
Zn(1)-N(7)			2.008(4)	1.980(2)	2.013(2)	
Zn(1)-N(8)						2.004(5)
Zn(1)-O(1)		1.956(7)				
Zn(1)-O(3)		1.987(7)				
N(5)-Zn(1)-N(2)	168.1(2)					
N(5)-Zn(1)-N(1)	107.4(2)					
N(2)-Zn(1)-N(1)	76.2(2)	70.7(3)	74.88(10)	74.68(5)	74.99(7)	73.8(2)
N(5)-Zn(1)-N(4)	75.7(2)					
N(2)-Zn(1)-N(4)	116.1(2)		137.53(14)	128.81(6)	137.65(8)	
N(1)-Zn(1)-N(4)	86.3(2)		92.17(11)	89.33(6)	88.56(8)	
N(5)-Zn(1)-N(3)	100.9(2)					
N(2)-Zn(1)-N(3)	78.1(2)	80.6(4)	79.70(10)	80.14(5)	79.05(7)	79.9(1)
N(1)-Zn(1)-N(3)	150.1(2)	149.9(4)	153.02(11)	154.37(5)	153.82(7)	153.4(2)
N(4)-Zn(1)-N(3)	91.3(2)		100.66(12)	102.99(6)	108.86(8)	
N(5)-Zn(1)-N(6)	76.9(2)					
N(2)-Zn(1)-N(6)	91.8(2)					
N(1)-Zn(1)-N(6)	91.9(2)					
N(4)-Zn(1)-N(6)	150.6(2)					
N(3)-Zn(1)-N(6)	104.2(2)					
O(1)-Zn(1)-O(3)		81.1(3)				
O(1)-Zn(1)-N(1)		108.2(3)				
O(3)-Zn(1)-N(1)		105.3(3)				
O(1)-Zn(1)-N(3)		96.5(3)				
O(3)-Zn(1)-N(3)		95.2(4)				
O(1)-Zn(1)-N(2)		128.4(3)				
O(3)-Zn(1)-N(2)		150.4(3)				
N(4)-Zn(1)-N(7)			116.80(18)	118.32(6)	110.01(9)	
N(7)-Zn(1)-N(2)			105.20(15)	110.66(6)	109.37(8)	
N(7)-Zn(1)-N(1)			98.80(14)	91.90(6)	92.15(8)	
N(7)-Zn(1)-N(3)			96.43(15)	101.50(6)	99.60(7)	

5.3.2 Crystal structures of complexes

Compound **12** crystallized in orthorhombic space group $Pna2_1$. The zinc atom is in distorted octahedral environment and coordinated by two tridentate Schiff base ligands (**L^4**) (Figure 5.2). Though there are some coordination angles [N5-Zn1-N6 (76.87°) ; N5-Zn1-N4 (75.69°); N2-Zn1-N3 (78.13°); N1-Zn1-N2 (76.23°)] (Figure 5.2) deviating considerably from 90°, however this can be attributed for the chelating nature of Schiff base ligand. The bond lengths between Zn atom and N-donor centers are within the range of 2.052(5)–2.481(6)Å (Table 5.2), quite similar to those which have been reported earlier.[29] The two pyridine rings in the complex cation are approximately perpendicular to each other, making dihedral angle of 83.01°. The perchlorate anions are linked to the complex cation through C–H···O hydrogen bonds and these hydrogen bonds are mainly responsible for formation of supramolecular spiral chain like structures (Figure 5.2). The packing structure discloses the interaction of monomeric units to each other through C1–H1···O66 and C8–H8B···O66 hydrogen bonding, again another perchlorate unit get involved for formation of other spiral turn through C15–H15···O22 and C18–H18C···O33 hydrogen bonding.

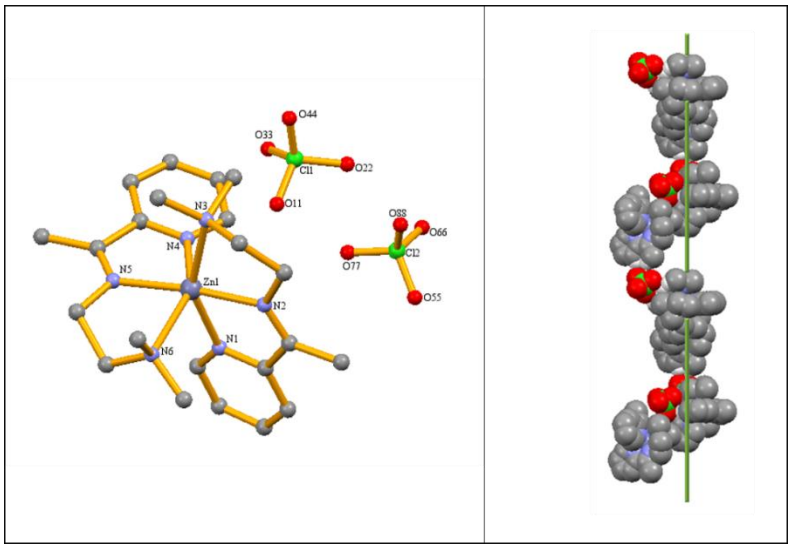

Figure 5. 2. *Crystal structure complex **12** (left); Packing diagram for the spiral chain in complex **12** (right).*

Compound **13** forms a 1D coordination polymeric *zig-zag* chain. Two crystallographically same zinc centers (Zn1) alternate along the chain (Figure 5.3). Each zinc atom is coordinated in distorted square pyramidal fashion by three nitrogen donors from tridentate chelating Schiff base ligand and two oxygen donors from two *bis*-bidentate bridging (crystallographically different) fumarate ligand. The distortion of the coordination geometry can be calculated by the τ value, a reference to describe the degree of distortion for square-pyramid and trigonal-bipyramid [square pyramid, $\tau = 0$; trigonal-bipyramid, $\tau = 1$; $\tau = (\beta - \alpha)/60°$, α and β are the two largest angles around the central atom [30]. The τ value for complex **13** is 0.147, indicating a distorted square-pyramidal geometry adopted by zinc center. The repeat unit along the chain encompasses three zinc centers (Figure 5.3). All chains are parallel to each other (Figure 5.3). Neighbouring chains can be thought of as stacked in planes coplanar with the *ac*-plane. Two adjacent linear polymeric chains are also interconnected through C8–H8B···O4 hydrogen bonding (Figure 5.3).

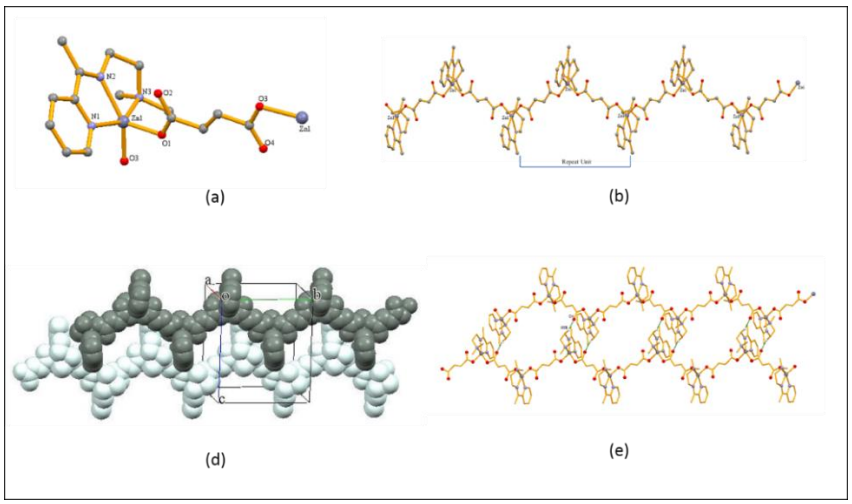

Figure 5. 3. *(a) Structure of complex **13**. (b) Longer chain segment of **13** (c) Packing diagram for the parallel chains in **13**. (d) Intermolecular hydrogen bonding between two adjacent chains of **13**.*

In the case of all the compounds **14** to **17** the zinc atom shows a distorted square pyramidal geometry. Five coordination site of zinc is fulfilled by one tridentate Schiff base ligand and two azide ions (Figure 5.4). In every case, The azide ions are not coaxial to the coordinative bond rather they are making angles 128.2° (N5-N4-Zn1) and 141.2° (N8-N7-Zn1) for compound **14;** 133.3° (N5-

N4-Zn1) and 134.38° (N8-N7-Zn1) for compound **15**; 141.91° (N5-N4-Zn1) and 128.46° (N8-N7-Zn1) for compound **16**; 126.10° (N6-N5-Zn1) and 122.59° (N9-N8-Zn1) for compound 17. The τ values for these four complexes are found to be near about 0.26, suggestive of a distorted square-pyramidal geometry.

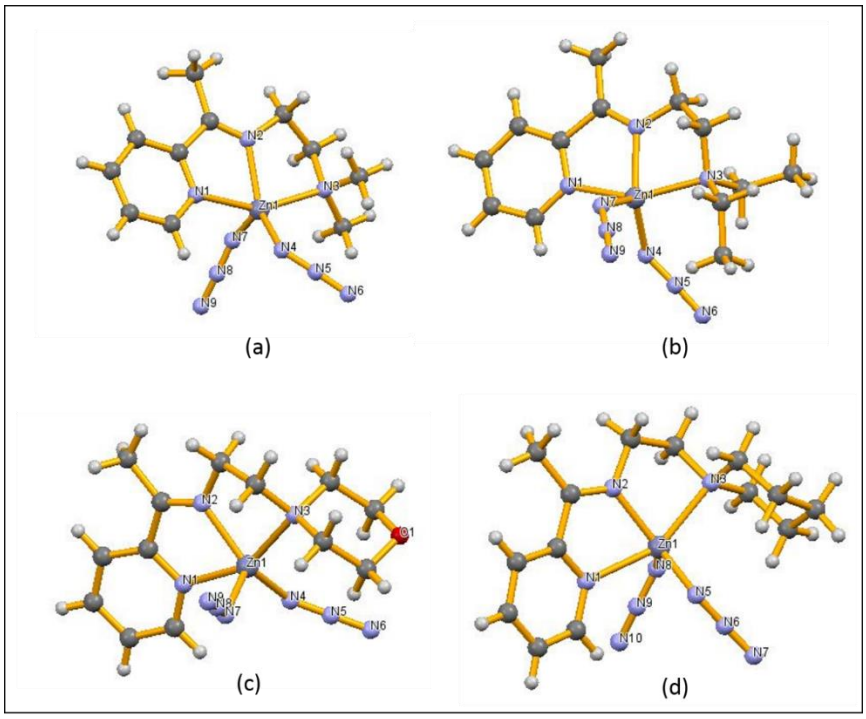

Figure 5. 4. *Crystal structure of complex* ***14****, (a), complex* ***15*** *(b), complex* ***16*** *(c) and complex* ***17*** *(d)*

For the compounds **2** the individual molecules are found to be forming 1D linear chain like structures when interconnected by C3–H3···N9 hydrogen bonding (Figure 5.5); and again such two simultaneous chains grown in opposite directions is further connected to other chains to form a 2D plane through C7–H7A···N6 and C11–H11A···N6 hydrogen bonding (Figure 5.5).

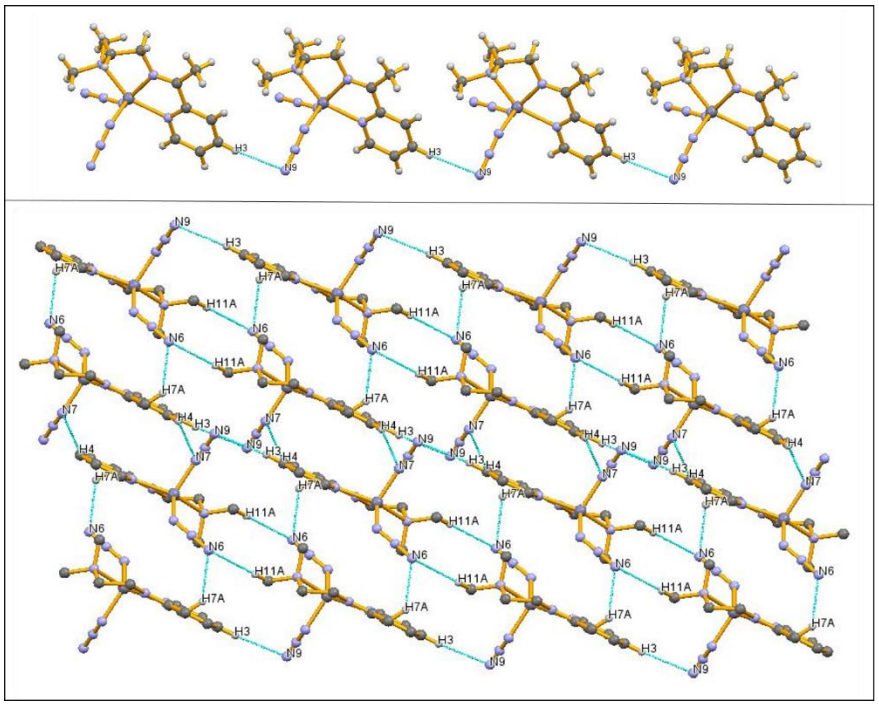

Figure 5. 5. *One dimensional (above) and two dimensional (below) supraamolecular polymeric network of complex* ***14.***

In case of compound **15**, each unit molecules are connected with each other by C3–H4···N9 and C3–H3···N9 hydrogen bonding to form a 1D supramolecular chain (Figure 5.6). Again each 1D chain is interconnected by C8–H8A···N6 hydrogen bonding to make a 2D sheet like polymeric structure. (Figure 5.6)

Each unit cell of **complex 16** possess two monomeric units and each units are connected by C20–H20C···N7 hydrogen bonding. There is several hydrogen bonding interactions (C1–H1···N6, C20–H20A···N6, C23–H23A···O1, C9–H9A···N17, C8–H8A···N13, C7–H7A···N13 and C7–H7A···N14) which are mainly responsible for the one dimensional chain like structure (Figure 5.7).

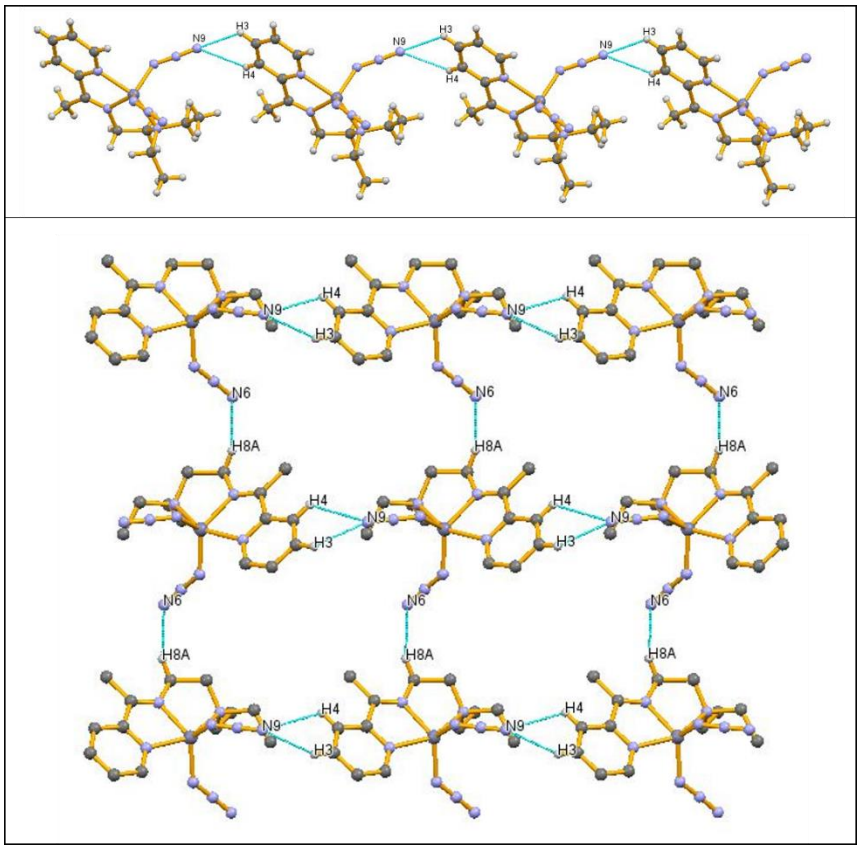

Figure 5. 6. *One dimensional (above) and two dimensional (below) supraamolecular polymeric network of complex* ***15****.*

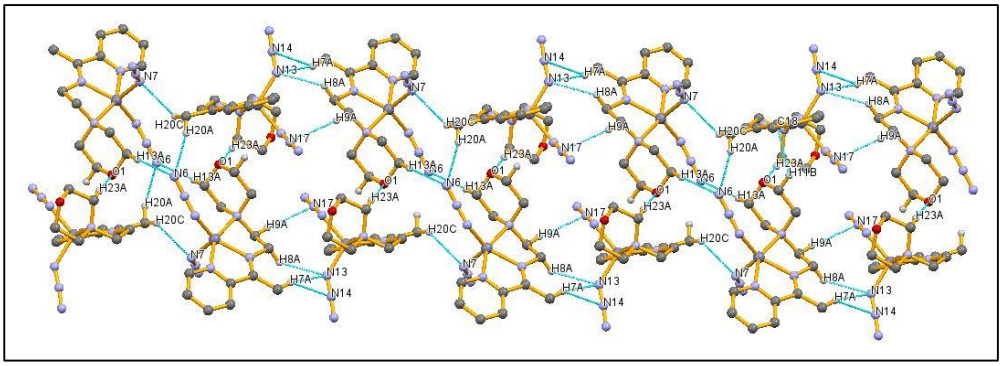

Figure 5. 7. *One dimensional chain line supramolecular polymeric network of complex* ***16***

In case of complex **17**, there are also two monomeric units are present in the unit cell of the crystal system. There are several hydrogen bonding interactions (like, C8–H8A···N20, C13–H13A···N20, C21–H21B···N5, C21–H21B···N6, C21–H21A···N10, C7–H7C···N15 and C7–H7C···N15) which

connect individual nearest molecules to make a 1D polymeric chain. (Figure 5.6) The other hydrogen bonding networks like C7–H7B···N20, C4–H4···N20 and C22–H22B···N7 are responsible for formation of 2D supramolecular sheet. (Figure 5.8).

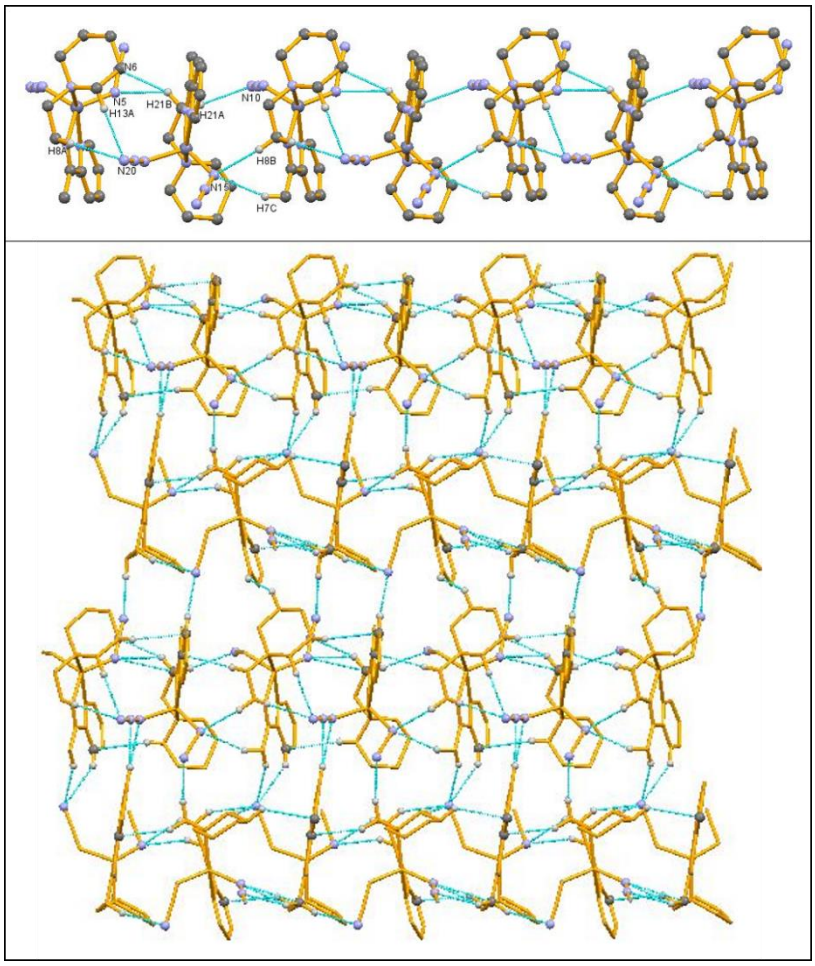

Figure 5. 8. *1D (above) and 2D (below) supramolecular network of complex* ***17.***

5.3.3 Electrochemical studies

Electrochemical studies have been carried out to measure the corrosion inhibition property of the above said complexes. Initially, the corrosion inhibition property of the four ligands at an optimum concentration of 200 ppm has been tested but all the ligands did not exhibit significant corrosion inhibition efficiency. However, much more interesting results have been obtained when the metal complexes have been subjected for similar properties. Interestingly

complex **12** has not shown much significant inhibition property with comparison of parental ligand $\mathbf{L^4}$ and other precursor moieties. Therefore it has been intended to introduce another co-ligand in metal Schiff base complex in the form of fumarate to study the corrosion inhibition property in complex **13**. However, it has been found that complex **13** is sparingly soluble in water and therefore electrochemical studies could not be performed. But due to the less solubility of complex **13** in water, the electrochemical studies were not performed. Therefore it has been planned to introduce azide as a coligand which is having many N atoms which can act as donor sites. Interestingly, in that case, the synthesized complex **14** has shown the considerable corrosion inhibition property. Encouraged by these results we tried to employ different Schiff base ligands to explore the best possible combination for this kind of activity. Ligand $\mathbf{L^5}$, $\mathbf{L^6}$ and $\mathbf{L^7}$ provided us complex **15**, **16** and **17** respectively, which have shown good corrosion inhibition in 15% HCl medium. The enhanced corrosion inhibition property in **14-17** may be due to the greater availability of N absorbing sites in azide molecules. Zn complexes diminish the corrosion process which was revealed by the polarization and impedance studies. These studies were performed after stabilization of open circuit potential (OCP).

5.3.4 Potentiodynamic polarization measurements

After optimizing the concentration of potentiodynamic polarization curve of all the ligands (Figure 5.9 and Table 5.3), the polarization curves for mild steel electrode in 15% HCl solution were performed without and with inhibitors (Zn(II) Schiff base azide complexes **14-17**) at various concentrations.

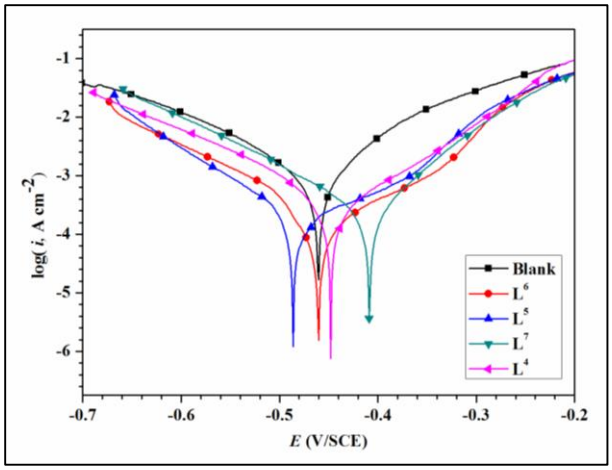

Figure 5. 9. *Polarization curves for mild steel in 15% HCl solution in absence and in presence of four ligands at an optimum concentration of 0.2 g/L.*

Table 5. 3. *Electrochemical parameters of potentiodynamic polarization studies in 15% HCl at 298 ±1 K in absence and in presence of four ligands at an optimum concentration of 0.2 g/L.*

Inhibitor	**Concentration (g/L)**	E_{corr} **(mV)**	β_a **(mV/dec)**	β_c **(mV/dec)**	I_{corr} **µA/cm²**	η **(%)**
Blank		– 468	248.4	– 274.4	1053.0	
L^4	0.2	– 432.3	225.65	– 291.77	353.7	66.41
L^5	0.2	– 473.5	307.84	– 229.06	261.8	75.13
L^6	0.2	– 442.4	286.94	– 288.56	180.8	82.83
L^7	0.2	– 412.6	179.16	– 245.62	284.4	72.99

The effect of different concentrations of Zn complexes in corrosion inhibition is shown in Figure 5.10.

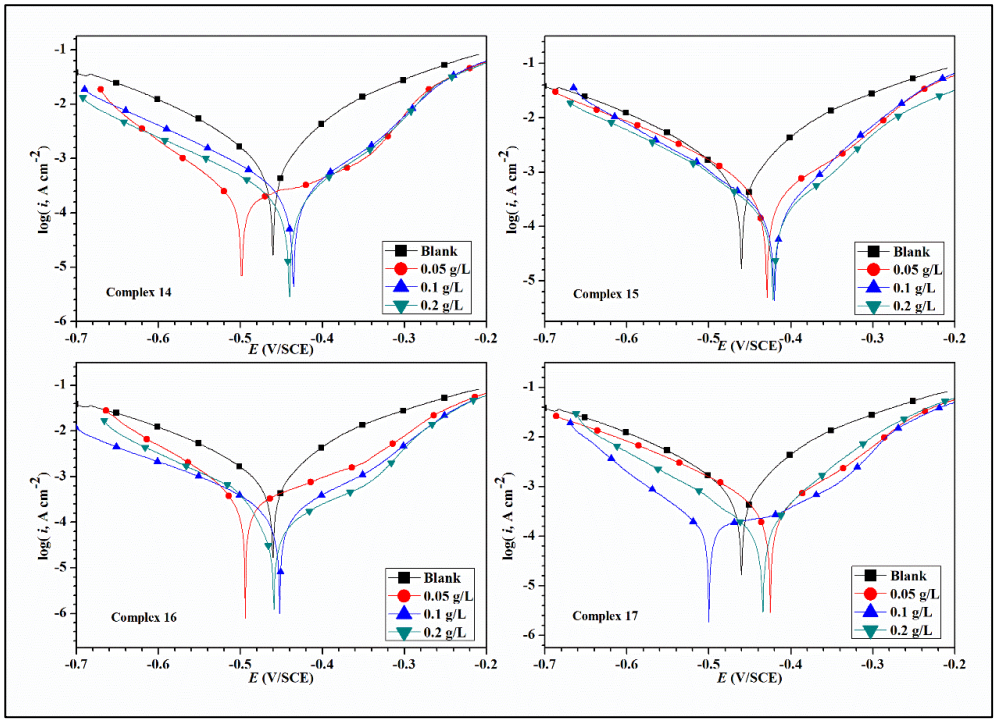

Figure 5. 10. *Polarization curves for mild steel in 15% HCl solution with and without various concentrations of inhibitors* ***14***, ***15***, ***16*** *and* ***17****.*

All potentiodynamic polarization parameters such as corrosion current density (i_{corr}), corrosion potential (E_{corr}), anodic (β_a) and cathodic (β_c) Tafel slopes acquired from these curves and the calculated inhibition efficiency ($\eta_{pol}(\%)$) values are listed in Table 5.4. The i_{corr} values were obtained by extrapolation of liner section of both Tafel curves. The following equation (1) has been used to calculate the efficiency ($\eta_{pol}(\%)$)

$$\eta_{pol}(\%) = \frac{i^0_{corr} - i_{corr}}{i^0_{corr}} \times 100 \quad \text{..... (1)}$$

where, i^0_{corr} and i_{corr} are corrosion current densities ($\mu A/cm^2$) without and with inhibitor.

Table 5. 4. *Electrochemical parameters of potentiodynamic polarization studies with and without inhibitor (Complex **14-17**) in 15% HCl at 298 ±1 K.*

Inhibitor	Concentration (g/L)	E_{corr} (mV)	β_a (mV/dec)	β_c (mV/dec)	I_{corr} µA/cm^2	η_{pol} (%)
Blank		– 468	248.4	– 274.4	1053.0	
Complex	0.05	– 486.1	394.01	– 215.33	338.4	67.86
14	0.1	– 427.2	213.36	– 302.86	256.8	75.61
	0.2	– 433.3	213.93	– 315.09	189.9	81.96
Complex	0.05	– 414.4	223.72	– 291.22	435.5	58.64
15	0.1	– 420.5	170.17	– 232.25	198.5	81.15
	0.2	– 408.9	159.10	– 245.02	169	83.95
Complex	0.05	– 480.7	339.52	– 222.94	415.7	60.52
16	0.1	– 442.7	248.30	– 308.54	187.3	82.21
	0.2	– 432.6	282.26	– 284.63	119.2	88.68
Complex	0.05	– 415.0	209.07	– 290.16	401.9	61.83
17	0.1	– 488.8	329.89	– 189.93	288.2	72.63
	0.2	– 439.4	176.84	– 244.11	179.5	82.95

There is no observable significant trend in the shift of E_{corr} values as well as β_a *&* β_c values on the addition of inhibitor with respect to that without inhibitor. In the present study, it was observed that all inhibitors in 15 % HCl solution exhibited anodic as well as cathodic inhibition effect *i.e.* 'mixed type with predominantly anodic inhibitor [31, 32] as the difference of E_{corr} values between blank and in presence of inhibitors lies within ± 85 mV v_s SCE with shifting of E_{corr} towards more anodic region. The corrosion inhibition efficiency was increased with the increasing concentration of inhibitor and the maximum efficiencies were shown at 0.1 g/L as listed in Table 5.4.

5.3.5 Impedance studies

Electrochemical impedance measurement technique was also employed to study the corrosion inhibition of mild steel. Initially the impedance studies for the all the four ligands were scrutinized at an optimum concentration of 0.2 g/L. The

results were documented in the form of the Nyquist diagram, Phase angle plot and Bode plot (Figure 5.11 and Table 5.5).

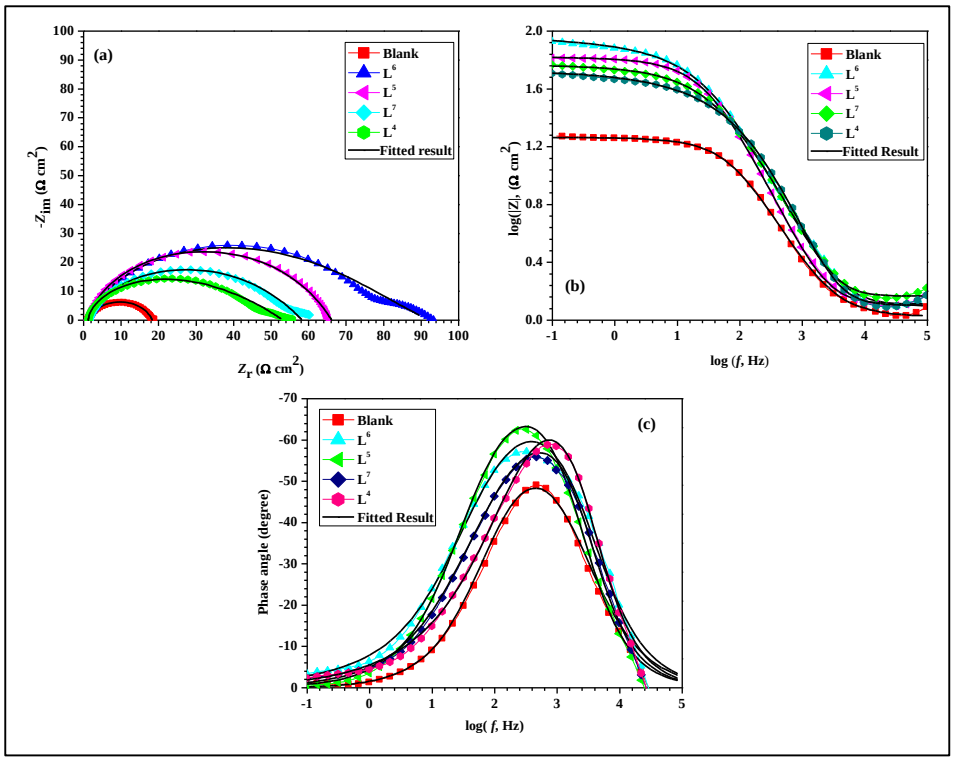

Figure 5. 11. *(a) Nyquist plot, (b) Bode plot and (c) Phase angle plot of mild steel in absence and presence of four ligands.*

Table 5. 5. *Electrochemical parameters of impedance studies in 15% HCl at 298 ±1 K in absence and in presence of four ligands at an optimum concentration of 0.2 g/L.*

Inhibitor	Concentration (g/L)	R_S (Ω cm^2)	R_p (=R_{ct} + R_f) (Ω cm^2)	n	Y_0 (μF/cm^2)	C_{dl} (μF/cm^2)	η_{imp} (%)
Blank		1.05	17.28	0.8047	405.9	121.79	
L^4	0.2	1.27	51.94	0.4687	1681.0	89.5	66.73
L^5	0.2	1.27	64.93	0.9999	43.6	43.7	73.38
L^6	0.2	1.24	90.85	0.3760	1119.0	25.2	80.98
L^7	0.2	1.46	56.86	0.5799	796.3	78.4	69.61

After this optimization the Nyquist plots for mild steel electrode in 15% HCl solution were performed without and with inhibitors (Zn(II) Schiff base azide

complexes **14-17**) at various concentrations and the results were depicted in the Figure. 5.12.

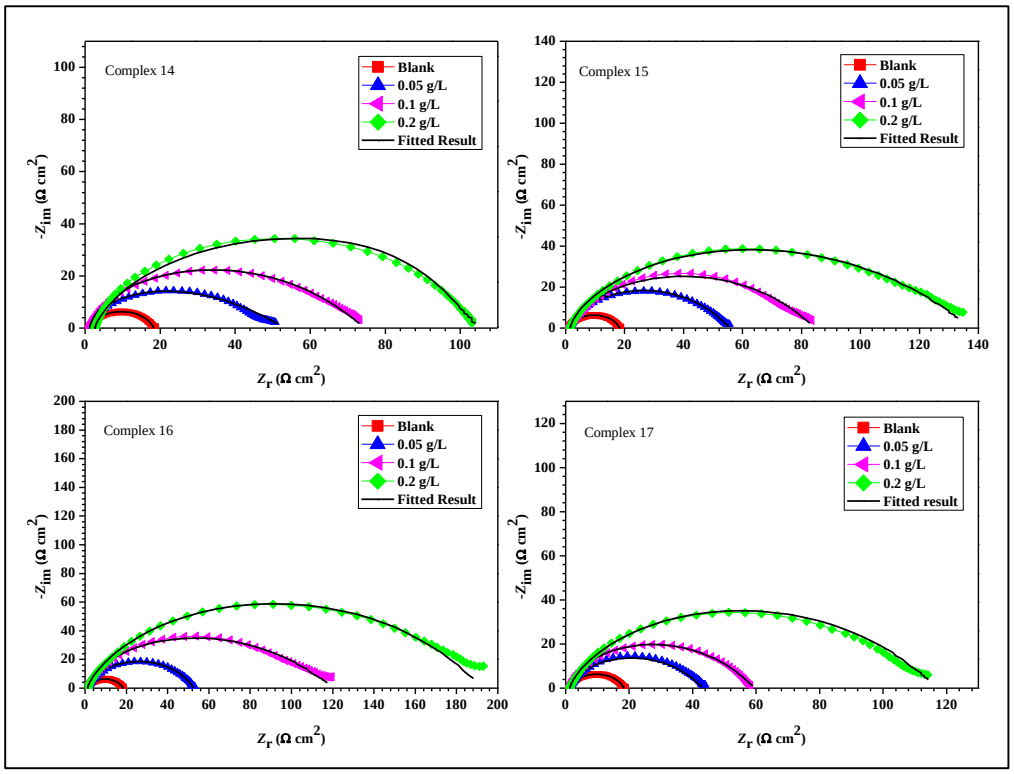

Figure 5. 12. *Nyquist plots for mild steel in 15% HCl in the absence and presence of different concentrations of all four inhibitors* ***14-17*** *at 298 ± 1 K.*

A single capacitive loop was observed in the frequency range 100 kHz to 100 mHz, which rises from the one time constant in impedance spectroscopy. In higher frequency range assigned with the charge transfer resistance and lower frequency was attributed to film resistance which was formed by inhibitor layer.[33, 34] Nyquist plots for mild steel in uninhibited solution are semi-circular in nature, but in the presence of inhibitors, the shape of the semicircle is depressed due to the frequency dispersion and microscopic roughness of the electrode surface.

The charge transfer resistance controlled the corrosion process of mild steel which is the reason for the semi-circular nature of Nyquist plot of uninhibited solution. But the depressed semi-circular Nyquist plot in the presence of inhibitors is considered as the polarization resistance (R_p) between

the metal and outer Helmholtz plane. In this case, polarization resistance (R_p) containing all the resistances between metal and solution interfaces were included. Those are mainly charge transfer resistance (R_{ct}), film resistance (R_f), accumulation resistance (R_a), diffuse layer resistance (R_d) *etc.*[35] It was observed from the Nyquist plot that the shape and size of depressed semicircle was gradually increased with respect to the concentration of inhibitors upto 0.2 g/L. This increase in the diameter of the semicircle shows that the R_p was increasing with increasing concentration of inhibitors. This phenomenon defined the protective layer formation on the metal surface and the consequent reduction in the metal dissolution. Furthermore, Bode plots can give more information in case of more intricate systems. The Bode plots of the synthesized inhibitors are presented in Figure 5.13. One important parameter *i.e.*, low-frequency impedance modulus Z_{mod} can be used to relate corrosion resistance of different samples.[36] Increase in Z_{mod} shows better protection ability as reported earlier.[37] Figure 5.13 showed that Z_{mod} increased as a function of the concentration for the synthesized inhibitor.

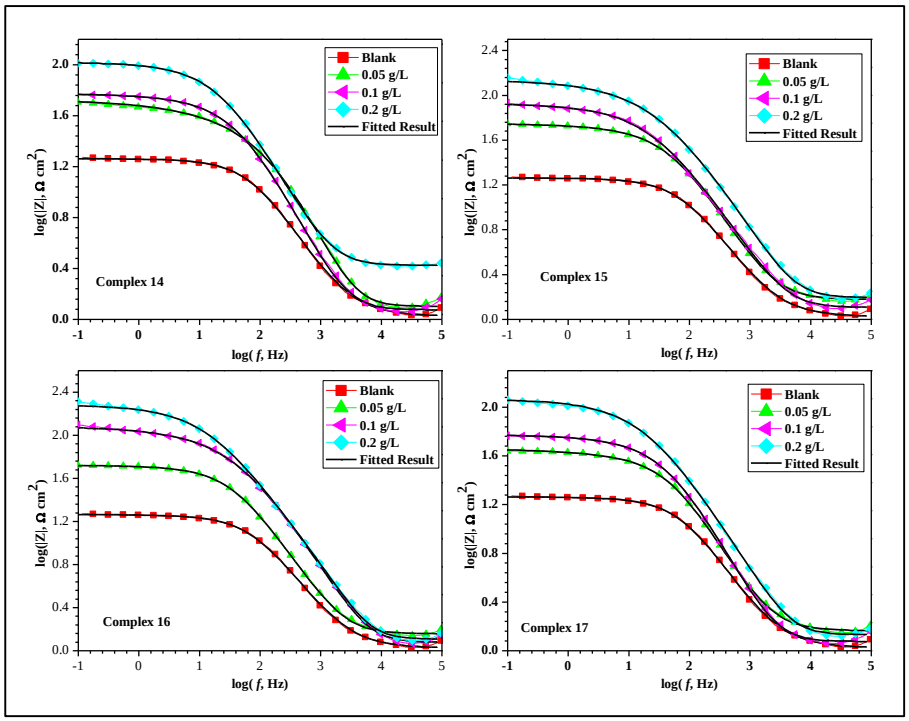

Figure 5. 13. *Bode plot of mild steel in 15% HCl without and with various concentrations of inhibitors* ***14-17****.*

The phase angle plots for the mild steel in the presence and absence of inhibitors in 15% HCl are given in Figure. 5.14. These also reinforce the inferences from Nyquist and Bode plots.

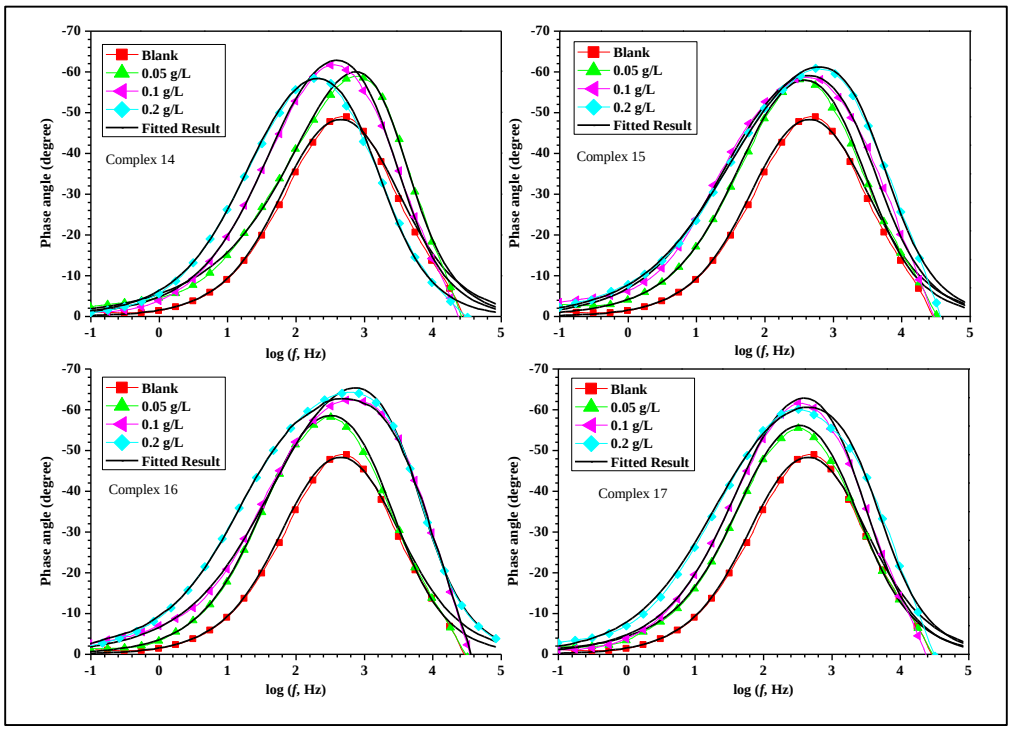

Figure 5. 14*.Phase angle plots of mild steel in 15% M HCl solutions without and with various concentrations of inhibitors* ***14-17.***

There is some deviation from ideal behavior in the impedance studies on double layer capacitance in inhibited solutions. This scattering has been endorsed to roughness and other in-homogeneities of the mild steel electrode and also due to anion adsorption. The uncharacteristic capacitance can be represented by a constant phase element (CPE),[16] and the impedance (Z_{CPE}) can be expressed by equation (2):

$$Z_{CPE} = \frac{1}{Y_0 (j.w)^n} \quad \text{..... (2)}$$

where, Y_0 is the quantity of CPE, j is the imaginary unit ($j^2 = -1$), n is the phase shift parameter that belongs to $0 < n < 1$, and w is the angular frequency in Hz. The depressed semicircle can be explained by this n value. The value in the range 0.5 to 1, implies that the semi-circle is depressed at higher frequency ranges. The n value is a measure of the in-homogeneity or roughness of the solid surface.[38]

The impedance parameter (R_s, R_{ct}, R_p, R_f, n, Y_0 & C_{dl}) are evaluated with the equivalent circuit fitting program. The EIS plots analyzed by software CHI instrument software and obtained the required data.[39] The corrosion inhibition efficiency was calculated using the polarization resistance (R_p) value using the following formula equation (3):

$$\eta_{imp}(\%) = \frac{R_p - R_p^0}{R_p} \times 100 \quad \text{..... (3)}$$

where, R^0_p and R_p are polarization resistances of mild steel in the absence and presence of the inhibitor respectively. The R_p values are observed to be linearly proportional to the concentrations of inhibitor molecules. All the obtained data was tabulated in Table 5.6. The double layer capacitance (C_{dl}) values were calculated from CPE parameter values Y_0 and n, using the equation (4),

$$C_{dl} = Y_0^{1/n} + R_{ct}^{(1-n)/n} \quad \text{..... (4)}$$

where, Y_0 and n are magnitudes of CPE and deviation parameter ($-1 \leq n \leq 1$, which is dependent on surface morphology)

The C_{dl} values, generally, are inversely proportional to the adsorbent concentration on the metal surface.

Table 5. 6. *Impedance data for corrosion of mild steel in 15% HCl in presence and absence of different concentration of different inhibitors* ***14-17*** *at 298 ±1 K.*

Inhibitor	Concentration (g/L)	R_S (Ω cm^2)	R_p (=R_{ct} + R_f) (Ω cm^2)	n	Y_0 (μF/cm^2)	C_{dl} (μF/cm^2)	η_{imp} (%)
Blank		1.05	17.28	0.8047	405.9	121.79	
Complex **14**	0.05	1.26	51.94	0.4687	1681.03	89.5	66.73
	0.1	1.28	73.25	0.5574	749.25	67.5	76.41
	0.2	2.63	102.47	0.9999	33.20	33.2	83.13
Complex **15**	0.05	1.48	54.50	0.9355	72.28	49.4	68.29
	0.1	1.23	83.25	0.9884	30.76	28.7	79.24
	0.2	1.50	135.58	0.9999	17.63	17.6	87.25
Complex **16**	0.05	1.42	51.20	0.9999	33.25	33.2	66.25
	0.1	1.12	119.27	0.9999	20.92	20.9	85.51
	0.2	1.28	191.23	0.6199	341.18	62.1	90.96
Complex **17**	0.05	1.43	44.70	0.8897	150.35	80.9	61.34
	0.1	1.19	58.43	0.5758	557.73	44.8	70.43
	0.2	1.35	115.38	0.6053	516.74	80.0	85.02

Although here all the complexes have almost similar kind of corrosion inhibition activities but complex **16** show relatively higher inhibition efficiency which arises may be due to the presence of an extra non-coordinated O atom in the complex structure.

5.3.6 Equivalent circuits

The equivalent circuit, in the absence of inhibitor, is shown in Figure. 5.15.

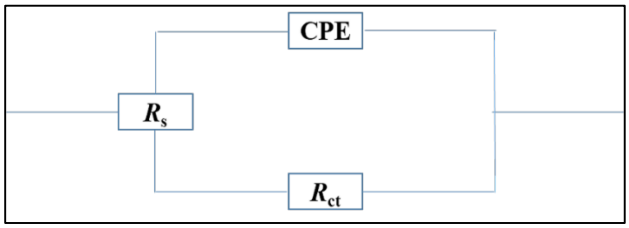

Figure 5. 15. *Equivalent circuits used to fit EIS data of mild steel in HCl medium without inhibitor.*

Here, the resistance is considered as charge transfer resistance and include all other ions or any kinds of corrosion product. The equivalent circuit is changed for the system in the presence of inhibitor as shown in Figure 5.16. In this behavior of metallic electrode, the parallel network: charge transfer resistance-double layer capacitance is established in presence of inhibitor.

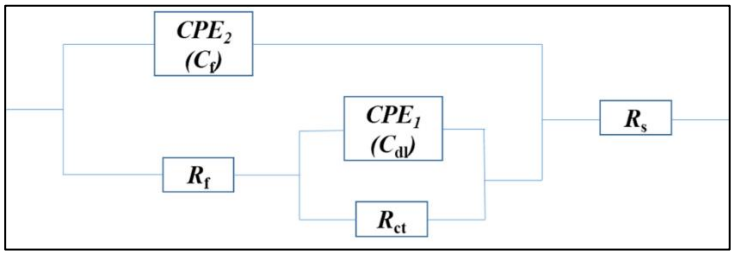

Figure 5. 16. *Equivalent circuits (with inhibitor) used to fit the EIS data of mild steel in HCl medium.*

5.3.7 Adsorption isotherm

The type of isotherm applicable for the adsorption of inhibitors on metal helps in understanding the nature of interaction of the inhibitors with the metal surface. In the present case, Langmuir adsorption isotherm gave the best fit to the

experimental data. The obtained data were tested for Langmuir adsorption isotherm, which can be represented by the equation (5),

$$\frac{C}{\theta} = \frac{1}{K_{ads}} + C \quad \text{..... (5)}$$

where, K_{ads} is the adsorption-desorption equilibrium constant and C is adsorbent concentration. For **14-17**, straight lines were obtained from the plots of C/θ $_{Vs}$ C with a high correlation coefficient (r^2) value of 0.998, 0.998 and 0.996 respectively at 298 ± 1 K (Figure 5.17).

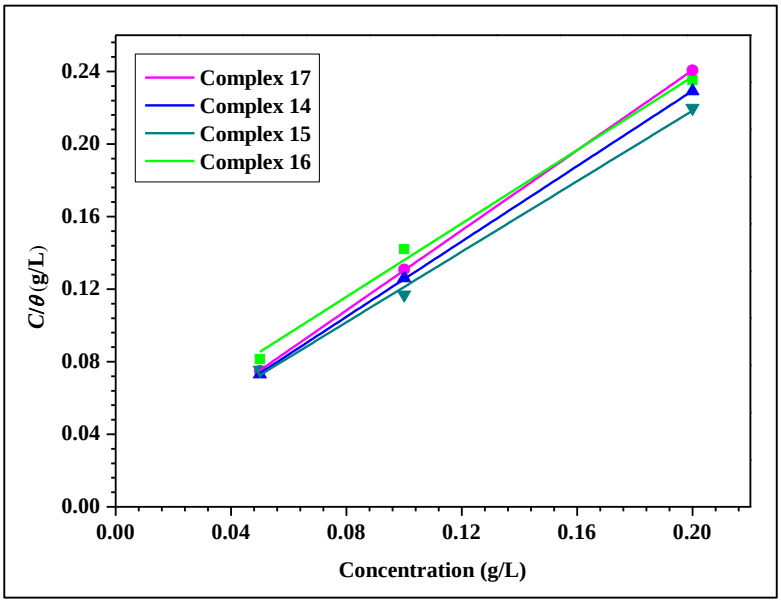

Figure 5. 17. *Langmuir adsorption isotherm of all inhibitors* ***14-17*** *on mild steel surface in 15% HCl medium.*

The values of K_{ads} in association with the standard Gibbs free energy of adsorption ΔG^0_{ads} was obtained from the Langmuir adsorption isotherm by the following equation (6),

$$K_{ads} = \frac{1}{C_{(sol.)}} \exp\left(\frac{\Delta G^0_{ads}}{RT}\right) \quad \text{..... (6)}$$

where, R is the universal gas constant, T is the absolute temperature and $C_{(sol.)}$ is the conc. of water (1000 g/L). The values of K_{ads} is represented here in $g^{-1}L$, thus in this equation the conc. of water is taken in g/L (1000 g/L) in place of 55.5 mole/L.[39, 40] The obtained ΔG^0_{ads} values of our synthesized inhibitors are -26.60 kJ/mol, -26.35 kJ/mol, -25.43 kJ/mol and -26.80 kJ/mol for complex **14**,

15, 16 and **17** respectively. The above range of ΔG^0_{ads} values designate the contribution of physisorption along with chemisorption as the ΔG^0_{ads} values around -40 kJ mol^{-1} or higher (more negative) are associated with chemisorption while ΔG^0_{ads} values of inhibitor lies in the order of -20 kJ mol^{-1} or even lower (more positive) satisfy the physisorption type mechanism. Thus it can be decided that inhibitor molecules were adsorbed on the metallic surface following a mixed type adsorption phenomenon.

5.3.8 Surface morphology study

5.3.8.1 FE-SEM and EDX study

The surfaces of mild steel samples exposed to 15% HCl without and with optimum concentration of inhibitors are shown in Figure 5.18. Critical corrosion damage can be watched when metal was presented to the corrosive medium for 6 h without inhibitor. However on addition of inhibitors, uniformity and smoothness of metal surface improved significantly, indicating a considerable decrease in corrosion damage.

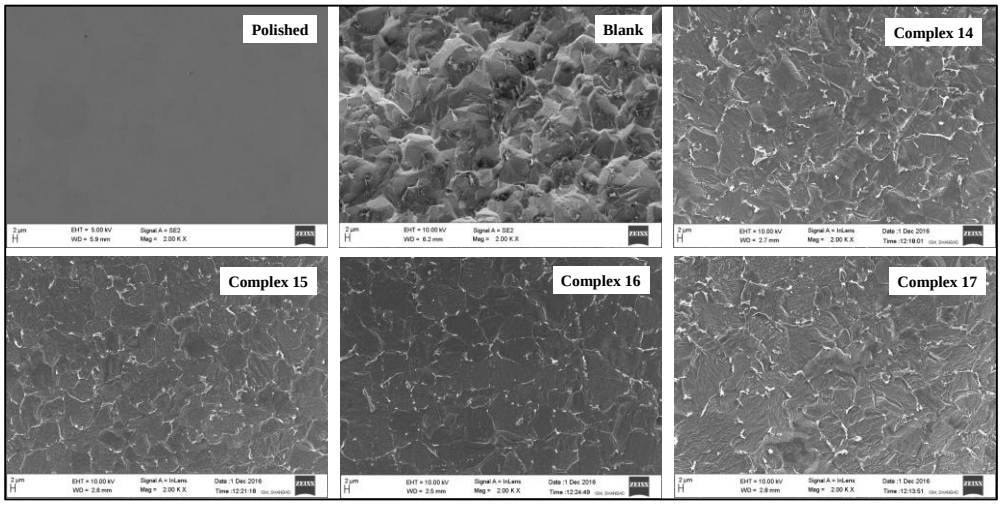

Figure 5. 18. *FE-SEM images of mild steel in 15% HCl solution at 298 ± 1 K, in the absence and presence of inhibitors* ***14-17*** *at 0.2 g/L after 6 h of immersion.*

Energy Dispersive X-ray Spectroscopy analysis was confirmed which elements were present in metal surface after inhibitor adsorption. (Figure. 5.19.) The EDX spectra of inhibitor complexes show the elemental peak for Fe, C and N atoms In case of complex **16**, one extra peak of O atom was observed which

arises due the morpholinium moiety in the complex structure. The relative proportional data obtained from EDX analysis were tabulated in the Table 5.7.

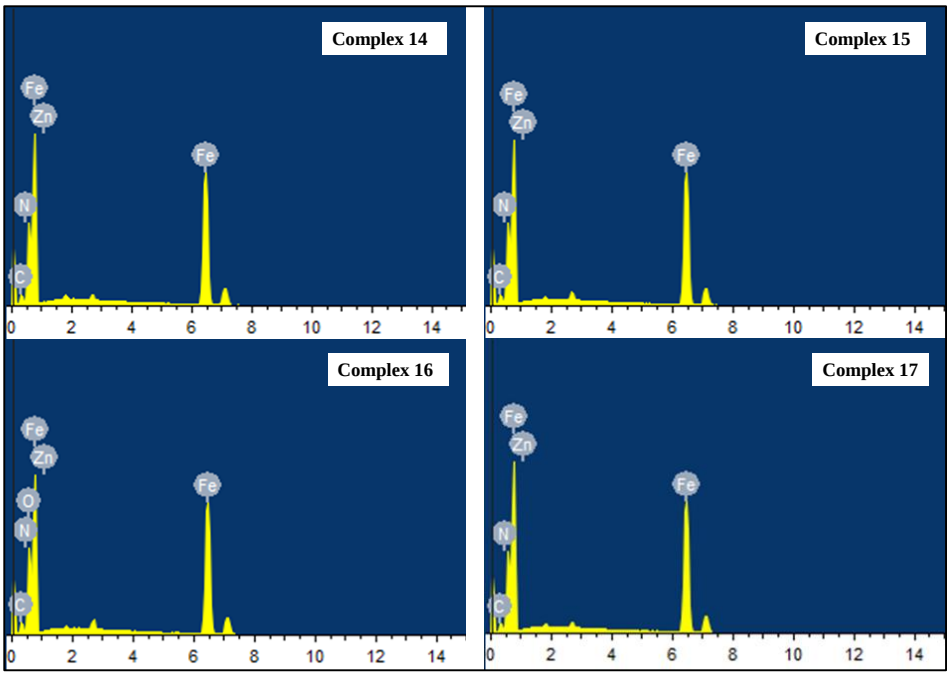

Figure 5. 19. *EDX spectra of mild steel surface after 6 h immersion in 15% HCl solution with 0.2 g/L of inhibitor complexes* ***14-17****.*

Table 5. 7. *EDX analysis results for surface characterization.*

Complexes	**Elements**	**Compositions**
Complex **14**	C, N, Fe, Zn	3.32, 1.40, 95.13, 0.15
Complex **15**	C, N, Fe, Zn	3.63, 1.01, 95.20, 0.15
Complex **16**	C, N, O, Fe, Zn	3.86, 0.22, 11.67, 83.82, 0.42
Complex **17**	C, N, Fe, Zn	3.85, 1.19, 94.75, 0.20

5.3.8.2 Atomic force microscopy

The surface roughness of mild steel sample was evaluated by the AFM 3D image. Figure 5.20 clearly show the surface roughness difference of metal specimens with and without inhibitors. AFM image indicate that the maximum roughness results in 15% HCl medium and the surface roughness of mild steel coupon decreases after adding inhibitor. The smoothest surface was obtained when Zn(II) Schiff base complexes **14-17** were used as an inhibitor.

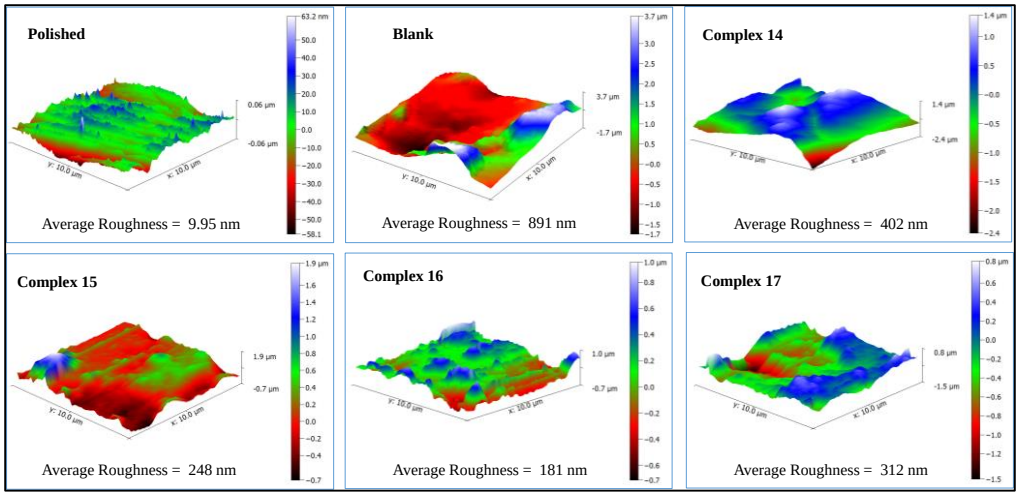

Figure 5. 20. *AFM micrograph of mild steel surface in different condition: Polished; without inhibitor (Blank); in presence of inhibitor (Complex **14-17**).*

5.3.9 Stability study in acidic media

Already from the results of EDX analysis it was observed that the entire elemental composition of Zn(II) Schiff base complexes **14-17** was present on the mild steel surface in acidic medium. And that result was quite significant to understand regarding no such prominent degradation of inhibitor molecule in corrosive medium. To get more insight view for this stability, the UV-Vis experiment and FTIR experiment were performed before and after immersion in HCl taking only the complex **16** (due to its relative higher inhibition efficiency). Solid state and solution state (in 15% HCl) UV-Vis spectra and FTIR spectra (Figure 5.21) clearly indicate that this inhibitor molecule is stable in presence of acid solution.

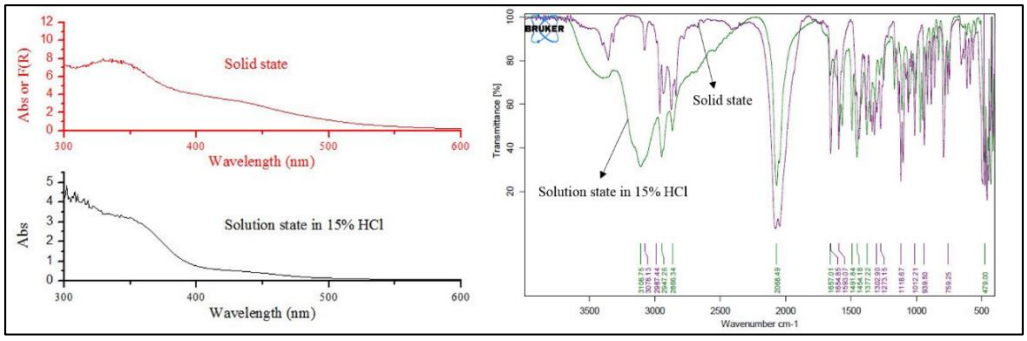

Figure 5. 21*. Solid and solution state (in 15% HCl) UV-Vis spectra (left) and FTIR spectra (right) of complex **16**.*

5.3.10 Inhibition mechanism

The adsorption process of any molecule on the surface is dependent on mainly few physicochemical criteria like; chemical nature of functional groups involved, electron density of donor atoms and aromaticity, molecular shape and size. [41] Electrostatic interaction, donor-acceptor interaction between aromatic π-electrons and vacant orbitals of Fe atoms and donor properties of hetero atom and vacant d-orbital of iron surface atom and other unsaturation remaining in the molecules are main driving forces of any organic molecules to get adsorbed on metallic surface. [42] When a particular organic molecule act as a ligand in a metal complex system, in the presence of other co-ligands like azide the tendency for adsorption may increase due to binding through available lone pairs of co-ligand and unused donating sites of ligands. The high inhibitory effect is also controlled by the large size and molecular weight. [43] To get more stringent physical insight of mechanism for adsorption process the free energy for adsorption was measured and described in the adsorption isotherm section **5.3.7**. From that results it was quite clear that adsorption of Zn(II) complexes on mild steel were taken place through physisorption along with chemisorption pathway.

5.3.11 Antimicrobial activity

Nosocomial infections or more commonly hospital-acquired infections are defined as an infection in a patient or health care professional not evident prior to accessing a hospital or health care facility. [44] The most frequent nosocomial infections reported are caused by bacteria as the Gram-positive Methicillin-Resistant *Staphylococcus aureus* (MRSA).Ten millions of medical devices are used each year and, in spite of many advances in biomaterials, a significant proportion of each type of device becomes colonized by bacteria and becomes the focus of an implant-related infection. [45] *Staphylococcus* comprises up to two-thirds of all pathogens in orthopaedic implant infections as well as infections from infected medical surgical instruments. Although mild steel is not largely used in health care industry but still for any kind of corrosion inhibition

antibacterial effect of same molecule give extra advantages because it pertained that if they released from the closed system it can act as an antibacterial agent. For these reasons, in this study the antibacterial activity of Zn(II) azido Schiff base complexes were evaluated and all these complexes have moderate anti-bacterial activity against MRSA. The corresponding MIC values are depicted in Table 5.8. Bacterial growth inhibition capability of the complexes is directly dependent on the concentration of the complexes. Just for representative purpose the dose dependent zone of inhibition of complex **14** was presented in Figure. 5.22.

Table 5. 8. *Tables for showing the results obtained from antibacterial activity test*

Compounds	Solvent	Disk diffusion test (mm)	MIC (µg/mL)	MBC (µg/mL)
Complex **14**	MeOH	10	8.3	8
Complex **15**	MeOH	09	7.9	7
Complex **16**	MeOH	14	8.6	8
Complex **17**	MeOH	12	7.2	6

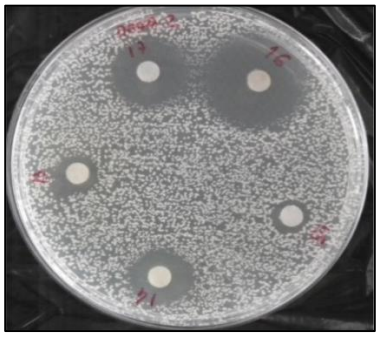

Figure 5. 22. *Concentration dependent disk diffusion susceptibility test for complex **16** against MRSA.*

5.4 Conclusions

The corrosion preventing performances and antibacterial activities of the synthesized Zn (II) Schiff base complexes were studied. All the complexes were structurally characterized by single crystal X-ray analysis. Initially two complexes **12** and **13** with lesser number of heteroatoms were tested to measure

the potential corrosion inhibition capacity. But these two complexes did not show significant corrosion inhibition with respect to the parent ligands. Thus the idea for the use of azide like pseudohalides as a co-ligand was planned and finally successfully implemented. Furthermore, the antibacterial activity of these inhibitor molecules was scrutinized which shows the good resistance capacity against *Staphylococcus aureus*.

Considering all of the above facts it can be concluded that this kind of pseudohalide promoted enhanced corrosion inhibition approach is one of the fruitful strategies to develop corrosion resistance metal complexes which are worth for further investigation.

5.5 References

[1]. Burgess, J.,Prince, R. H., (2006), Zinc: Inorganic & Coordination Chemistry. In: Encyclopedia of Inorganic Chemistry, John Wiley & Sons, Ltd.

[2]. Laitaoja, M.,Valjakka, J.,Jänis, J. (2013), Zinc Coordination Spheres in Protein Structures, Inorganic Chemistry, 52, 10983-10991.(DOI: 10.1021/ic401072d)

[3]. Mjos, K. D.,Orvig, C. (2014), Metallodrugs in Medicinal Inorganic Chemistry, Chemical Reviews, 114, 4540-4563.(DOI: 10.1021/cr400460s)

[4]. Evans, O. R.,Lin, W. (2002), Crystal Engineering of NLO Materials Based on Metal−Organic Coordination Networks, Accounts of Chemical Research, 35, 511-522.(DOI: 10.1021/ar0001012)

[5]. Steger, R. J. (1992), Plasma etch apparatus with conductive coating on inner metal surfaces of chamber to provide protection from chemical corrosion, Google Patents.

[6]. Rojas-Chapana, J.,Tributsch, H. (2001), Biochemistry of sulfur extraction in bio-corrosion of pyrite by Thiobacillus ferrooxidans, Hydrometallurgy, 59, 291-300.(DOI: 10.1016/S0304-386X(00)00185-7)

[7]. Shanmughan, S. K.,Kakkassery, J. T.,Raphael, V. P.,Kuriakose, N. (2015), Electrochemical and AFM studies on adsorption behavior of a Polynuclear

Schiff Base at carbon steel in HCl medium, Current Chemistry Letters, 4, 67-76.(DOI: 10.5267/j.ccl.2015.2.001)

[8]. El-Gamel, N. E. A.,Fekry, A. M. (2015), Antimicrobial ruthenium complex coating on the surface of titanium alloy. High efficiency anticorrosion protection of ruthenium complex, Bioelectrochemistry, 104, 35-43.(DOI: 10.1016/j.bioelechem.2015.02.005)

[9]. Biswas, A.,Pal, S.,Udayabhanu, G. (2017), Effect of chemical modification of a natural polysaccharide on its inhibitory action on mild steel in 15% HCl solution, Journal of Adhesion Science and Technology, 1-22.(DOI: 10.1080/01694243.2017.1306912)

[10]. Mahdavian, M.,Naderi, R. (2011), Corrosion inhibition of mild steel in sodium chloride solution by some zinc complexes, Corrosion Science, 53, 1194-1200.(DOI: 10.1016/j.corsci.2010.12.013)

[11]. Mahdavian, M.,Attar, M. M. (2009), Electrochemical behaviour of some transition metal acetylacetonate complexes as corrosion inhibitors for mild steel, Corrosion Science, 51, 409-414.(DOI: 10.1016/j.corsci.2008.11.010)

[12]. Rajendran, S.,Apparao, B. V.,Palaniswamy, N. (1998), Synergistic and antagonistic effects existing among polyacrylamide, phenyl phosphonate and Zn^{2+} on the inhibition of corrosion of mild steel in a neutral aqueous environment, Electrochimica Acta, 44, 533-537.(DOI: 10.1016/S0013-4686(98)00079-6)

[13]. Naderi, R.,Mahdavian, M.,Attar, M. M. (2009), Electrochemical behavior of organic and inorganic complexes of Zn(II) as corrosion inhibitors for mild steel: Solution phase study, Electrochimica Acta, 54, 6892-6895.(DOI: 10.1016/j.electacta.2009.06.073)

[14]. Gonzalez, Y.,Lafont, M. C.,Pebere, N.,Moran, F. (1996), A synergistic effect between zinc salt and phosphonic acid for corrosion inhibition of a carbon steel, Journal of Applied Electrochemistry, 26, 1259-1265.(DOI: 10.1007/bf00249928)

[15]. Ita, B. I.,Offiong, O. E. (1997), Inhibition of steel corrosion in hydrochloric acid by pyridoxal, 4-methylthiosemicarbazide, pyridoxal- (4-

methylthiosemicarbazone) and its Zn(II) complex, Materials Chemistry and Physics, 48, 164-169.(DOI: 10.1016/S0254-0584(97)80113-7)

[16]. Keleş, H.,Emir, D. M.,Keleş, M. (2015), A comparative study of the corrosion inhibition of low carbon steel in HCl solution by an imine compound and its cobalt complex, Corrosion Science, 101, 19-31.(DOI: 10.1016/j.corsci.2015.07.013)

[17]. Singh, P.,Singh, D. P.,Tiwari, K.,Mishra, M.,Singh, A. K.,Singh, V. P. (2015), Synthesis, structural investigations and corrosion inhibition studies on Mn(II), Co(II), Ni(II), Cu(II) and Zn(II) complexes with 2-amino-benzoic acid (phenyl-pyridin-2-yl-methylene)-hydrazide, RSC Adv., 5, 45217-45230.(DOI: 10.1039/c4ra11929k)

[18]. Ashassi-Sorkhabi, H.,Shaabani, B.,Seifzadeh, D. (2005), Corrosion inhibition of mild steel by some schiff base compounds in hydrochloric acid, Applied Surface Science, 239, 154-164.(DOI: 10.1016/j.apsusc.2004.05.143)

[19]. Singh, P.,Singh, A. K.,Singh, V. P. (2013), Synthesis, structural and corrosion inhibition properties of some transition metal(II) complexes with o-hydroxyacetophenone-2-thiophenoyl hydrazone, Polyhedron, 65, 73-81.(DOI: 10.1016/j.poly.2013.08.008)

[20]. Gülerman, N. N.,Rollas, S.,Erdeniz, H.,Kiraz, M. (2001), Antibacterial, antifungal and antimycobacterial activities of some substituted thiosemicarbazides and 2,5-disubstituted-1,3,4-thiadiazoles, Fabad Journal of Pharmaceutical Sciences, 26, 1-5.

[21]. Tarasconi, P.,Capacchi, S.,Pelosi, G.,Cornia, M.,Albertini, R.,Bonati, A.,Dall'Aglio, P. P.,Lunghi, P.,Pinelli, S. (2000), Synthesis, spectroscopic characterization and biological properties of new natural aldehydes thiosemicarbazones, Bioorganic & Medicinal Chemistry, 8, 157-162.(DOI: 10.1016/S0968-0896(99)00260-6)

[22]. Mangamamba, T.,Ganorkar, M. C.,Swarnabala, G. (2014), Characterization of Complexes Synthesized Using Schiff Base Ligands and Their Screening for Toxicity Two Fungal and One Bacterial Species on Rice

Pathogens, International Journal of Inorganic Chemistry, 2014, 22.(DOI: 10.1155/2014/736538)

[23]. Hu, Z.,Meng, Y.,Ma, X.,Zhu, H.,Li, J.,Li, C.,Cao, D. (2016), Experimental and theoretical studies of benzothiazole derivatives as corrosion inhibitors for carbon steel in 1 M HCl, Corrosion Science, 112, 563-575.(DOI: 10.1016/j.corsci.2016.08.012)

[24]. Sheldrick, G. (2008), A short history of SHELX, Acta Crystallographica Section A, 64, 112-122.(DOI: 10.1107/S0108767307043930)

[25]. Gwaram, N. S.,Ali, H. M.,Khaledi, H.,Abdulla, M. A.,Hadi, A. H. A.,Lin, T. K.,Ching, C. L.,Ooi, C. L. (2012), Antibacterial Evaluation of Some Schiff Bases Derived from 2-Acetylpyridine and Their Metal Complexes, Molecules, 17, 5952-5971.(DOI: 10.3390/molecules17055952)

[26]. Shi, D.-H.,Wang, X.-L.,Liu, W.-W.,Jin, H. (2012), Synthesis, Crystal Structures, and Biological Activity of Schiff Base Zinc(II) Complexes Derived From (2-piperidin-1-ylethyl)-(1-pyridin-2-ylethylidene)amine, Synthesis and Reactivity in Inorganic, Metal-Organic, and Nano-Metal Chemistry, 42, 480-484.(DOI: 10.1080/15533174.2011.613083)

[27]. Rahaman, S. H.,Chowdhury, H.,Bose, D.,Ghosh, R.,Hung, C.-H.,Ghosh, B. K. (2005), Synthesis, structure and properties of mononuclear cobalt(II) and cobalt(III) pseudohalide complexes containing N-donor Schiff bases: Synthetic control of metal oxidation levels, Polyhedron, 24, 1755-1763.(DOI: 10.1016/j.poly.2005.05.010)

[28]. Sarkar, S.,Majumder, S.,Sasmal, S.,Carrella, L.,Rentschler, E.,Mohanta, S. (2013), Triple bridged μ-phenoxo-bis(μ-carboxylate) and double bridged μ-phenoxo-μ1,1-azide/μ-methoxide dicopper(II) complexes: Syntheses, structures, magnetochemistry, spectroscopy and catecholase activity, Polyhedron, 50, 270-282.(DOI: 10.1016/j.poly.2012.10.050)

[29]. Wang, C.-Y. (2011), Bis{N-methyl-N'-[1-(pyridin-2-yl)ethylidene]ethane-1,2-diamine}zinc bis(perchlorate), Acta Crystallographica Section E, 67, m1038-m1039.(DOI: DOI:10.1107/S1600536811026079)

[30]. Aziz ur, R.,Hussain, M.,Zia ur, R.,Rauf, A.,Nasim, F.-u.-H.,Tahir, A. A.,Ali, S. (2010), New tetrahedral, square-pyramidal, trigonal-bipyramidal and octahedral organotin(IV) 4-ethoxycarbonylpiperazine-1-carbodithioates: Synthesis, structural properties and biological applications, Journal of Organometallic Chemistry, 695, 1526-1532.(DOI: 10.1016/j.jorganchem.2010.03.008)

[31]. Wahdan, M. H. (1997), The synergistic inhibition effect and thermodynamic properties of 2-mercaptobenzimidazol and some selected cations as a mixed inhibitor for pickling of mild steel in acid solution, Materials chemistry and physics, 49, 135-140.

[32]. Solomon, M. M.,Umoren, S. A.,Abai, E. J. (2015), Poly(methacrylic acid)/silver nanoparticles composites: In-situ preparation, characterization and anticorrosion property for mild steel in H2SO4 solution, Journal of Molecular Liquids, 212, 340-351.(DOI: 10.1016/j.molliq.2015.09.028)

[33]. Deng, S.,Li, X.,Fu, H. (2011), Alizarin violet 3B as a novel corrosion inhibitor for steel in HCl, H_2SO_4 solutions, Corrosion Science, 53, 3596-3602.(DOI: 10.1016/j.corsci.2011.07.003)

[34]. Solmaz, R. (2010), Investigation of the inhibition effect of 5-((E)-4-phenylbuta-1,3-dienylideneamino)-1,3,4-thiadiazole-2-thiol Schiff base on mild steel corrosion in hydrochloric acid, Corrosion Science, 52, 3321-3330.(DOI: 10.1016/j.corsci.2010.06.001)

[35]. Solmaz, R.,Kardaş, G.,Çulha, M.,Yazıcı, B.,Erbil, M. (2008), Investigation of adsorption and inhibitive effect of 2-mercaptothiazoline on corrosion of mild steel in hydrochloric acid media, Electrochimica Acta, 53, 5941-5952.(DOI: 10.1016/j.electacta.2008.03.055)

[36]. Hegazy, M. A.,Hasan, A. M.,Emara, M. M.,Bakr, M. F.,Youssef, A. H. (2012), Evaluating four synthesized Schiff bases as corrosion inhibitors on the carbon steel in 1 M hydrochloric acid, Corrosion Science, 65, 67-76.(DOI: 10.1016/j.corsci.2012.08.005)

[37]. Lamaka, S. V.,Zheludkevich, M. L.,Yasakau, K. A.,Serra, R.,Poznyak, S. K.,Ferreira, M. G. S. (2007), Nanoporous titania interlayer as reservoir of

corrosion inhibitors for coatings with self-healing ability, Progress in Organic Coatings, 58, 127-135.(DOI: 10.1016/j.porgcoat.2006.08.029)

[38]. Hussin, M. H.,Kassim, M. J. (2011), Electrochemical, Thermodynamic and Adsorption Studies of (+)-Catechin Hydrate as Natural Mild Steel Corrosion Inhibitor in 1 M HCl, Int. J. Electrochem. Sci., 6 1396 - 1414.(DOI:

[39]. Biswas, A.,Pal, S.,Udayabhanu, G. (2015), Experimental and theoretical studies of xanthan gum and its graft co-polymer as corrosion inhibitor for mild steel in 15% HCl, Applied Surface Science, 353, 173-183.(DOI: 10.1016/j.apsusc.2015.06.128)

[40]. Dohare, P.,Ansari, K. R.,Quraishi, M. A.,Obot, I. B. Pyranpyrazole derivatives as novel corrosion inhibitors for mild steel useful for industrial pickling process: Experimental and Quantum Chemical study, Journal of Industrial and Engineering Chemistry.(DOI: 10.1016/j.jiec.2017.03.044)

[41]. Hegazy, M. A.,Abdallah, M.,Awad, M. K.,Rezk, M. (2014), Three novel di-quaternary ammonium salts as corrosion inhibitors for API X65 steel pipeline in acidic solution. Part I: Experimental results, Corrosion Science, 81, 54-64.(DOI: 10.1016/j.corsci.2013.12.010)

[42]. Singh, A. K.,Singh, P. (2015), Adsorption behaviour of o-hydroxy acetophenone benzoyl hydrazone on mild steel/hydrochloric acid interface, Journal of Industrial and Engineering Chemistry, 21, 552-560.(DOI: 10.1016/j.jiec.2014.03.018)

[43]. Abd El-Lateef, H. M. (2015), Experimental and computational investigation on the corrosion inhibition characteristics of mild steel by some novel synthesized imines in hydrochloric acid solutions, Corrosion Science, 92, 104-117.(DOI: 10.1016/j.corsci.2014.11.040)

[44]. John V. Bennett,William Robert Jarvis,Brachman, P. S., (2007), Epidemiology of Healthcare-Assosiated Infections. In: Bennett & Brachman's Hospital Infections, 5th edn. Lippincott Williams & Wilkins, USA, pp. 5-7

[45]. Ribeiro, M.,Monteiro, F. J.,Ferraz, M. P. (2012), Infection of orthopedic implants with emphasis on bacterial adhesion process and techniques used in

studying bacterial-material interactions, Biomatter, 2, 176-194.(DOI: 10.4161/biom.22905)

Chapter 6

Targeted synthesis of cadmium(II) Schiff base complexes towards corrosion inhibition on mild steel

Chapter 6

Targeted synthesis of cadmium(II) Schiff base complexes towards corrosion inhibition on mild steel

6.1 Introduction

Metals find wide applications in several industries, such as chemical and petrochemical industries.[1, 2] In oil industries, corrosion in metals is a major problem and it is controlled by using different kinds of inhibitors. Several techniques (pipe line cleaning, acid pickling, *etc.*) are used in industries where the utilization of acids makes metals highly susceptible to corrosion.[3-5] Inhibitors are widely used to minimize the metal loss during such processes.[6] Corrosion inhibition is a surface phenomenon where the adsorption of the organic and inorganic compounds on the metal surface serves as the means of achieving the corrosion inhibiting environment.[7] There are various types of organic and inorganic compounds which have been studied as inhibitors for protecting metals against corrosion. In this scenario, Schiff bases are studied extensively due to the presence of >C=N– groups which allow the corresponding Schiff bases to get adsorbed on the surface of mild steel and to form a monolayer on the surface spontaneously. Therefore, it can act as an effective corrosion inhibitor [8, 9] for mild steel,[10-13] stainless steel,[14, 15] iron, nickel,[16] copper,[17] aluminum,[18] and alloy,[19] in various aggressive solutions. The Schiff base ligands form stable complexes closely packed in the coordination sphere of metal ion to generate another class of compounds for corrosion inhibition.[20-22] The inhibitors work on the metal surface through the adsorption mechanism. The adsorption of an organic compound depends on the number of functional groups taking part. The interaction of inhibitor molecules with the metal surface is influenced by several factors, such as electron charge

density, molecular size, geometry and number of hetero atoms, such as N, O, S present in the molecule.[23]

Being inspired from the outcome of result of previous chapter it was necessary to choose such metal ion which can be more efficient towards corrosion inhibition. In industry, cadmium plating offers an exceptional bonding on the surface and is being increasingly used in aircraft manufacturing and is a preferred coating for the salt water environment. Recently, Schiff bases are getting more attention in the field of corrosion inhibition of mild steel.[24-26] With this point of view researchers have been focusing on metal coordination complexes to quantify their corrosion inhibition property.[10, 27, 28] Apart from this the role of sodium azide as a corrosion inhibitor is also well described in literature [29] as well as in the previous chapter. However, to the best of our knowledge, there is only one report where mild steel corrosion inhibition using cadmium coordination complexes have been explored.[30] Although cadmium has toxic effects on biological systems but as mentioned earlier that cadmium based system can effectively inhibit corrosion on mild steel, therefore this metal ion was selected to explore the effectiveness of the cadmium based coordination complexes and to understand the underlying mechanism so that it can help to develop more fruitful inhibitory systems in future. Furthermore, although toxic, effective inhibitor may get utilized in closed systems with proper recovery of the toxic metal ion. Taking account of all these facts, herein five cadmium Schiff base complexes $[Cd(L^4)_2](ClO_4)_2$ **(18)**, $[Cd(L^4)(cyanoacetate)(OAc)]$ **(19),** $[Cd_2(L^4)_2(N_3)_4]$ **(20)**, $[Cd(L^6)(N_3)_2]n$ **(21)**, and $[Cd_2(L^7)_2(N_3)_4]n$ **(22)** are synthesized using the similar Schiff bases (**L^4**, **L^6** and **L^7**) used in previous chapter 5. The complexes were characterized and explored for their corrosion inhibition property on mild steel in 15% HCl solution. Most of the complexes show considerable corrosion inhibition property while one polymeric cadmium azide complex has shown the maximum inhibition efficiency, which is quite good in comparison with other metal complex inhibitors reported earlier.[10, 11, 13, 20, 27, 31] The corrosion inhibition efficiency was studied by electrochemical methods and protection of metal surface by Cd(II) complexes

was shown by FE-SEM images. Nuclearity driven corrosion inhibition trend of Cd(II) complexes was further corroborated by quantum chemical calculations.

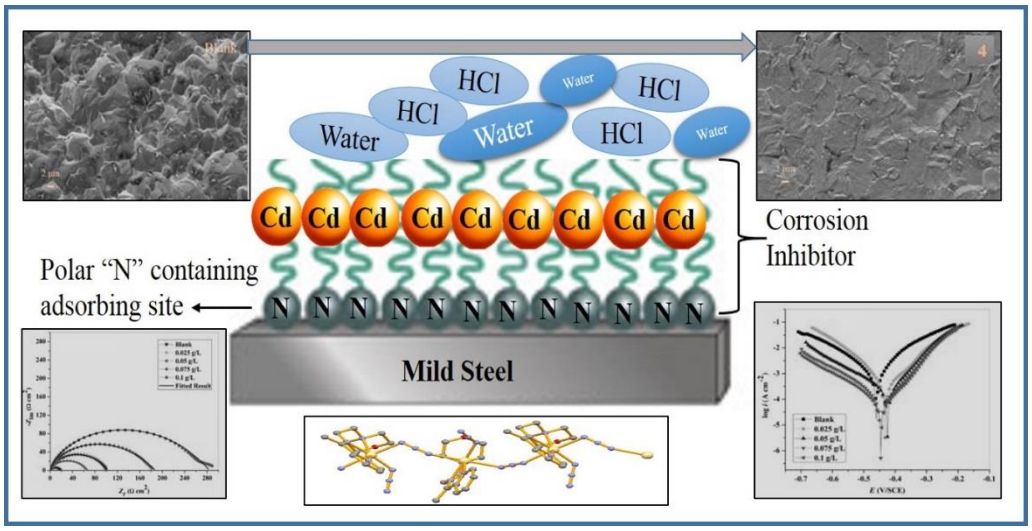

Figure 6. 1. *Pictorial representation of corrosion inhibition by cadmium complexes*

6.2 Experimental section

6.2.1 Materials and methods

All the chemical reagents required were purchased from Sigma, except HCl (purchased from Ranbaxy Fine Chemicals) and used without further purification. Infrared spectra (4000-500 cm^{-1}) were recorded with a BRUKER TENSOR 27 instrument in KBr pellets. Nuclear Magnetic Resonance (NMR) spectra were recorded in AVANCE III 400 Ascend Bruker BioSpin machine at ambient temperature. Mass spectrometric analyses were done on Bruker-Daltonics, micro TOF-Q II mass spectrometer and elemental analyses were carried out with a Thermo Flash 2000 elemental analyzer.

6.2.2 X-ray crystallography

Single crystal X-ray structural studies of **18-22** were performed on a CCD Agilent Technologies (Oxford Diffraction) SUPER NOVA diffractometer. Data for all the complexes were collected at 150(2) K except complex **21** which was taken 298(2) K using graphite-monochromated Mo Kα radiation (λ_α = 0.71073 Å). The strategy for the Data collection was evaluated by using the CrysAlisPro

CCD software. The data were collected by the standard 'phi-omega scan techniques and were scaled and reduced using CrysAlisPro RED software. The structures were solved by direct methods using SHELXS-97 and refined by full matrix least- squares with SHELXL-97, refining on F^2.[32] The positions of all the atoms were obtained by direct methods. All non-hydrogen atoms were refined anisotropically. The remaining hydrogen atoms were placed in geometrically constrained positions and refined with isotropic temperature factors, generally 1.2 U_{eq} of their parent atoms. The crystal and refinement data are summarized in Table 6.1.

Table 6. 1. *Crystallographic data and structure refinement parameters for* ***18****,* ***19****,* ***20****,* ***21*** *and* ***22****.*

Complex	**18**	**19**	**20**	**21**	**22**
Formula	$C_{22}H_{34}CdCl_2N_6O_8$	$C_{16}H_{22}CdN_4O_4$	$C_{22}H_{34}Cd_2N_{18}$	$C_{13}H_{19}CdN_9O$	$C_{28}H_{42}Cd_2N_{18}$
Crystal system	Orthorhombic	Triclinic	Monoclinic	Monoclinic	Monoclinic
Space group	*Pna2₁*	*P-1*	*P 21/n*	*P 21/c*	*P 21/c*
a (Å)	16.208(10)	8.438(10)	8.793(7)	11.520(2)	19.881(4)
b (Å)	14.134(10)	10.100(3)	15.677(13)	12.581(2)	10.893(2)
c (Å)	12.843(10)	11.303(2)	11.695(9)	11.804(2)	16.289(3)
α (°)	90	76.078(2)	90	90	90
β (°)	90	81.463(2)	107.422(9)	99.088(2)	100.828(2)
γ (°)	90	89.501(2)	90	90	90
Volume ($Å^3$)	2942.55(4)	924.30(3)	1538.3(2)	1689.45(5)	3465.10(12)
λ(Å)	0.71	0.71	0.71	0.71	0.71
ρ(mg m^{-3})	1.566	1.605	1.674	1.69	1.64
Z	4	2	4	4	4
T (K)	150(2)	150(2)	150(2)	298(2)	150(2)
Abs. Coeff (mm^{-1})	0.977	1.209	1.428	1.314	1.277
F(0 0 0)	1416	452	776	864	1728
Crystal size (mm^3)	0.23x0.16x0.13	0.23x0.16x0.13	0.33x0.26x0.18	0.23x0.18x0.14	0.33x0.26x0.21

θ ranges (°)	2.90-24.99	3.12-25.00	3.18 - 25.00	3.142-24.998	2.911- 25.00
Limiting Indices (h/k/l)	-19,19/-16,16/-15,15	-9,10/-12,9/-13,13	-10,10/-18,18/-13,13	-13,11/-14,13/-14,14	-23,23/-12,12/-19,18
Reflections collected	24292	6664	10003	11513	32482
Independent reflections	5171	3247	2712	2967	6087
Max & Min Transmission	0.883 and 0.806	0.858 and 0.768	0.7831and 0.650	1.000 and 0.435	1.000 and 0.799
Data/restraints/parameters	5171 / 1 / 358	3247 / 0 / 230	2712 / 0 / 193	2967 / 0 / 218	6087 / 0 / 435
GOF	1.055	1.124	1.081	1.056	1.055
Final R indices [I > 2σ(I)]	R1 = 0.023 wR2 =0.067	R1 = 0.017 wR2 =0.045	R1 = 0.082, wR2 = 0.222	R1 = 0.078, wR2 = 0.225	R1 = 0.022, wR2 = 0.055
R indices (all data)	R1 = 0.024, wR2 = 0.067	R1 = 0.018, wR2 = 0.045	R1 = 0.092, wR2 = 0.230	R1 = 0.083, wR2 = 0.232	R1 = 0.025, wR2 = 0.058
Largest peak and hole (e $Å^{-3}$)	0.687 and -0.267	0.409and -0.309	2.110 and -1.781	1.601 and -0.599	0.480 and -0.445

6.2.3 Synthesis of Schiff base ligands (L^4, L^6 and L^7)

Three ligands **L^4** **[**N,N-Dimethyl-N'-(1-pyridin-2-yl-ethylidene)-ethane-1,2-diamine], **L^6** **[**2-morpholino-N-(1-(pyridin-2-yl)ethylidene)ethanamine] and **L^7** [(2-(piperidin-1-yl)-N-(1-(pyridin-2-yl)ethylidene)ethanamine)] were prepared following the procedure reported in literature [33, 34] and previous chapter. These were used for preparation of metal complexes without further purification.

6.2.4 Synthesis of $[Cd(L^4)_2](ClO_4)_2$ (18)

0.19 g (1 mmol) of Schiff base ligand **L^4** dissolved in 10 mL of methanol was added drop wise into a solution of 0.15 g of $Cd(ClO_4)_2$ (0.5 mmol) in 5 mL of methanol. The mixture was stirred for 1 hour at room temperature and filtered thereafter. Colourless block-shaped crystals of **18**, suitable for X-ray diffraction, were formed after 15 days on slow evaporation of the filtrate in air. Yield: 78% (based on metal salt). Anal. Calcd. (%) $C_{22}H_{34}CdCl_2N_6O_8$: C, 38.08; H, 4.94; N, 12.11. Found(%): C, 37.98; H, 4.90; N, 11.77. ^{1}H NMR (400.13 MHz, 298 K, DMSO-d_6): δ 8.43-8.29 (m, 6H, aryl), 7.72 (d,2H, aryl), 3.95 (br. d, 4H, CH_{2alk}), 2.96 (br. d, 2H, CH_{2alk}), 2.70 (s, 6H, CH_{3alk} and 2H, CH_{2alk}), 2.17 (s, 12H, $N(CH_3)_2$). ^{13}C NMR (100.61 MHz, 293 K, DMSO-d_6): δ 169.7 (C_{imine}), 149.4 (C_{aryl}), 148.1 (C_{aryl}), 141.4 (C_{aryl}), 128.0 (C_{aryl}), 125.3 (C_{aryl}), 58.2 (NCH_2), 45.8 (NCH_2), 45.5 (NCH_3), 16.7 (CH_3*C*). ESI-MS (*m/z*) 248.10 $[Cd(L^4)_2]^{2+}$, 595.16 $[(Cd(L^4)_2)ClO_4]^+$

6.2.5 Synthesis of $[Cd(L^4)(cyanoacetate)(OAc)]$ (19)

Ligand **L^4** (0.5 mmol, 0.09 g) and $Cd(OAc)_2.2H_2O$ (0.5 mmol, 0.13 g) were stirred in methanol (15 mL) for 30 min at room temperature. A methanolic solution (10 mL) of piperadinium salt of cyanoacetic acid (1 mmol, 0.17 g) was added into it thereafter and stirring was continued for 1 hour. Then it was concentrated and filtered. The colourless block-shaped crystals of **19**, suitable for X-ray diffraction, were formed after 6 days on slow evaporation of the filtrate in air. Yield: 72% (based on metal salt). Anal. Calcd. (%) $C_{16}H_{22}CdN_4O_4$: C, 43.01; H, 4.96; N, 12.54. Found (%): C, 42.80; H, 5.04; N, 12.00.^{1}H NMR (400.13 MHz, 298 K, DMSO-d_6): δ 8.70 (d, J = 4Hz, 1H, aryl), 8.21 (m, 2H, aryl), 7.77 (m, 1H, aryl), 3.70 (s, 3H, CH_3 (acetate)), 2.73-2.50 (6H, CH_{2alk}), 2.33 (s, 6H, $N(CH_3)_2$), 1.79 (s, 3H, CH_{3alk}). ^{13}C NMR (100.61 MHz, 293 K, DMSO-d_6): δ 177.0 ($C_{cyano\text{-}acetate}$), 167.1 ($C_{acetate}$), 165.9 (C_{imine}), 149.5 (C_{aryl}), 148.1 (C_{aryl}), 140.1 (C_{aryl}), 127.2 (C_{aryl}), 124.0 (C_{aryl}), 117.8 ($C_{cyanide}$), 57.2 (NCH_2), 45.5 (NCH_2), 44.9 (CH_2*C*N), 25.5 (CH_3*C*), 21.8 (CH_3*C*), 15.7 (CH_3*C*). ESI-MS (*m/z*) 471.16 $[Cd(L^4)(Cyanoacetate)(OAc)]+Na^+$

6.2.6 Synthesis of $[Cd_2(L^4)_2(N_3)_4]$ (20)

Ligand **L^4** (0.5 mmol, 0.09 g) and $Cd(OAc)_2.2H_2O$ (0.5 mmol, 0.13 g) were taken in methanol (15 mL) and stirred for 30 min at room temperature. After that an aqueous solution (10 mL) of sodium azide (1 mmol, 0.06 g) was added drop wise into it with continuous stirring. The stirring was continued for 1 hour. Then the solvent was evaporated to concentrate the solution and it was filtered. Finally the colorless block-shaped crystals of **20**, suitable for X-ray diffraction, were formed after 4 days on slow evaporation of the filtrate in air. Yield: 82% (based on metal salt). Anal. Calcd. (%) $C_{22}H_{34}Cd_2N_{18}$: C, 34.08; H, 4.42; N, 32.51. Found (%): C, 33.31; H, 4.28; N, 31.70.^{1}H NMR (400.13 MHz, 298 K, DMSO-d_6): δ 8.38 (d, J = 4Hz, 2H, aryl), 8.08 (m, 4H, aryl), 7.69 (d, 2H, aryl), 3.54-3.42 (t, J = 12Hz, 8H, CH_{2alk}), 2.36 (s, 6H, CH_{3alk}), 2.17 (s, 12H, $N(CH_3)_2$). ^{13}C NMR (100.61 MHz, 293 K, DMSO-d_6): δ 169.1 (C_{imine}), 148.8 (C_{aryl}), 147.5 (C_{aryl}), 141.3 (C_{aryl}), 128.2 (C_{aryl}), 124.6 (C_{aryl}), 79.3 (NCH_2), 56.8 (NCH_2), 44.4 (NCH_3), 16.1 (CH_3C). ESI-MS (*m/z*) 347.07 $[Cd_2(L^4)_2(N_3)_2]^{2+}$, 734.15 $[Cd_2(L^4)_2(N_3)_3]^+$

6.2.7 Synthesis of $[Cd(L^6)(N_3)_2]_n$ (21)

0.11 g of ligand **L^6** (0.5 mmol) and 0.13 g of $Cd(OAc)_2.2H_2O$ (0.5 mmol,) were mixed in methanol (15 mL) and stirred for 30 min at room temperature. Then 10 mL aqueous sodium azide (1 mmol, 0.06 g) was added slowly into it. The solution was stirred for 1 hour more. After that the solvent was evaporated to make it concentrate and then it was filtered. Finally the colourless block-shaped crystals of **21**, suitable for X-ray diffraction, were formed after 6 days on slow evaporation of the filtrate in air. Yield: 76% (based on metal salt). Anal. Calcd. (%) $C_{13}H_{19}CdN_9O$: C, 36.33; H, 4.46; N, 29.33. Found (%): C, 37.10; H, 4.28; N, 30.70.^{1}H NMR (DMSO-d_6) 8.80 (d, J = 4Hz, 1H, Aryl), 8.29–8.24 (m, 2H, Aryl), 7.87–7.85 (m,1H, Aryl), 3.80, 3.76 (d, 4H, $2CH_2$), 3.69 (s, 4H, $2CH_2$), 2.79–2.77 (t, 4H, NCH_2), 2.69 (s, 3H, CH3) ^{13}C NMR (100.61 MHz, 293 K, DMSO-d_6): δ 165.8 (C_{imine}), 149.2 (C_{aryl}), 140.5 (C_{aryl}), 132.3 (C_{aryl}), 127.6

(C_{aryl}), 124.2 (C_{aryl}), 64.76-57.88 (4C, $2CH_{2morph}$), 53.44 - 44.36 (2C, $2CH_2$), 15.77 (1C, CH_3)

6.2.8 Synthesis of $[Cd_2(L^7)_2(N_3)_4]_n$ (22)

In 15 mL of methanol, ligand **L^7** (0.5 mmol, 0.12 g) and $Cd(OAc)_2.2H_2O$ (0.5 mmol, 0.13 g) were stirred for 30 min at room temperature. An aqueous solution (10 mL) of sodium azide (1 mmol, 0.06 g) was added into it thereafter and stirring was continued for 1 hour. The reaction mixture was concentrated and filtered and then colourless block-shaped crystals of **22**, suitable for X-ray diffraction, were formed after 7 days on slow evaporation of the filtrate in air. Yield: 74% (based on metal salt). Anal. Calcd. (%) $C_{28}H_{42}Cd_2N_{18}$: C, 39.31; H, 4.95; N, 29.47. Found (%): C, 39.81; H, 4.75; N, 30.60. ^{1}H NMR (400.13 MHz, 298 K, DMSO-d_6): δ 8.34 (d, J = 4Hz, 2H, aryl), 8.01 (m, 4H, aryl), 7.62 (d, 2H, aryl), 3.45-3.40 (t, J = 12Hz, 8H, CH_{2alk}), 2.32 (s, 6H, CH_{3alk}), 2.20-2.30 (m, 8H), 1.51-1.52 (m, 8H), 1.17-1.25 (m, 4H). ^{13}C NMR (100.61 MHz, 293 K, DMSO-d_6): δ 167.1 (C_{imine}), 146.8 (C_{aryl}), 145.5 (C_{aryl}), 140.3 (C_{aryl}), 126.2 (C_{aryl}), 122.6 (C_{aryl}), 45.3 (NCH_2), 35.8 (NCH_2), 24.0-30.0 (5C, $2CH_2$), 16.1 (CH_3*C*).

6.2.9 Electrochemical experiments

The detail procedures of electrochemical experiments were well described in the section 5.2.10 of chapter 5.

6.2.10 Weight loss measurement

The clean mild steel coupons were dipped in 400 mL 15% HCl taken in 500 mL beaker at 298 ± 1 K. Mild steel coupons after exposure to corrosive solution were cleaned by washing in running tap water and then by immersing in cleaning solution (solution of 50 g $SnCl_2$ and 20 g Sb_2O_3 per liter of conc. HCl). The difference of specimen weight before and after the immersion is the corrosion

weight loss. The corrosion rate (CR) and percent of inhibition efficiency (η_{wt}%) were calculated by following equations:

$$CR(mmpy) = \frac{87.6 \times \Delta W}{DAT} \quad \text{..... (1)}$$

$$\eta_{wt}(\%) = \frac{W^0 - W}{W^0} \times 100 \quad \text{..... (2)}$$

where, ΔW (mg) is the weight loss of mild steel (MS) specimens, A is the total surface area of MS specimen (in cm^2), T is the immersion time (6 h), D is the density of MS ($g\ cm^{-3}$), W^0 and W are the weight loss in the absence and presence of inhibitor.

6.2.11 Surface analysis

The surface was characterized by Field Emission Scanning Electronic Microscope (FE-SEM). Micrographs were taken at room temperature (298 ± 1 K) after 1 h and 6 h immersion of polished metal coupon in 15 % HCl solution with and without inhibitor.

6.2.12 Computational study

As per representative purpose, we have performed the density functional theory (DFT) calculations for complex **20** and complex **21** to understand the nuclearity assisted corrosion inhibition activity. All the calculations are carried out in gaseous phase[35] using RB3LYP level of theory as implemented in the Gaussians 09 package.[36] The 3-21G basis set is used for C, N, H, O and LANL2DZ for Cd was used for all the calculations.[37, 38] The Fukui functions were calculated using the $Dmol^3$ module. The Fukui function (f_k) is the first derivative of the electron density $\rho(r)$ with respect to the number of electrons N, in a constant external potential $\upsilon(r)$ and written as follows.[39]

$$f_k = \left(\frac{\partial \rho(\vec{r})}{\partial N} \right)_{\nu(\vec{r})} \quad \text{..... (3)}$$

Finite difference approximations have been used to get Fukui function in favor of nucleophilic and electrophilic attacks as,[39]

$f_k^+ = q_k(N+1) - q_k(N)$ ……. (4) [For nucleophilic attack]

$f_k^- = q_k(N) - q_k(N-1)$ ....……. (5) [For electrophilic attack]

Here, gross charge of the atom *k* is denoted by q_k. The q_k *(N+1),* q_k *(N)* and q_k *(N-1)* are the charges of the anionic, neutral and cationic species, respectively.

6.2.13 Supplementary materials

CCDC 958288, 958289, 958287, 1498769 and 1498770 contain the supplementary crystallographic data for **18**, **19**, **20**, **21** and **22** respectively. These data can be obtained free of charge *via* http://www.ccdc.cam.ac.uk/conts/retrieving.html, or from the Cambridge Crystallographic Data Centre, 12 Union Road, Cambridge CB2 1EZ, UK; fax: (+44) 1223-336-033; or e-mail: deposit@ccdc.cam.ac.uk.

6.3 Results and discussion

6.3.1 Synthesis

Ligands $\mathbf{L^4}$, $\mathbf{L^6}$ and $\mathbf{L^7}$ were prepared by reported methods, respectively.[33, 34] In compound **18**, ligand to metal ratio was used in 2:1 and cadmium perchlorate was used as a metal precursor. In the case of compound **19,** piperidinium salt of cyanoacetic acid is used where cyanoacetate ion act as co-ligand (Scheme 6.1). Compounds **20-22** have been prepared in a methanolic solution of cadmium salt in presence of several ligands $\mathbf{L^4}$, $\mathbf{L^6}$ and $\mathbf{L^7}$ and aqueous NaN_3 maintaining 1:1:2 ratio (Scheme 6.1), where azide ion has been utilized as co-ligand.

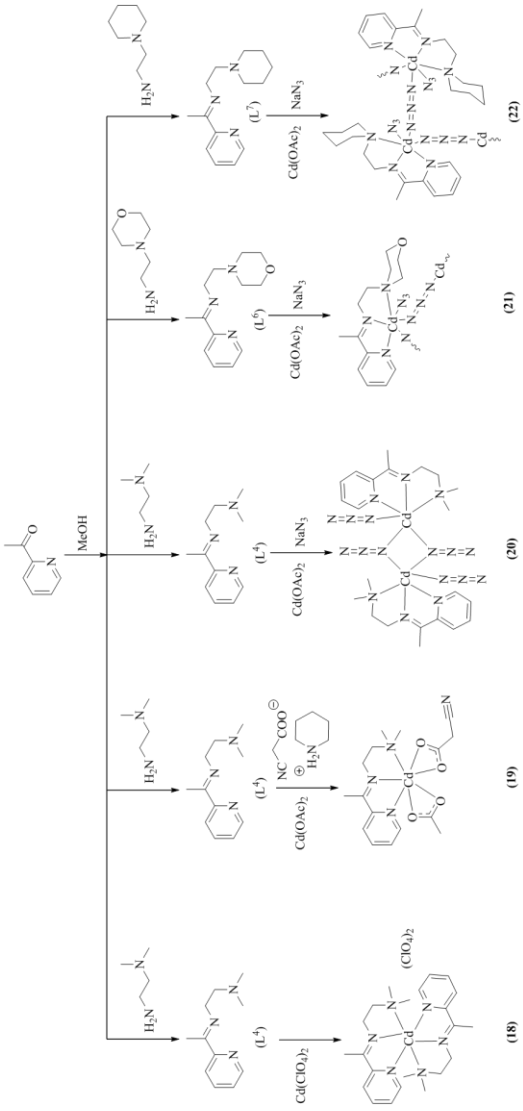

Scheme 6. 1. *Synthetic scheme for preparation of Cd(II) complexes.*

6.3.2 Characterization

All the compounds were characterized by different spectroscopic techniques apart from elemental analysis. The structures of the compounds were further determined by single crystal X-ray crystallography. The IR spectra of compound **18-22** show typical band for stretching vibration of C=N in the range of 1590-1600 cm^{-1}.[40] This clearly indicates that on complex formation C=N stretching frequency shifts in lower frequency region with respect to parent ligand. Compound **18** shows a strong band at 1091 cm^{-1} assigned to a non-coordinated ClO_4^- ion.[41] In the case of complex **19**, a relatively small band is observed at

2255 cm^{-1} which indicate the presence of nitrile stretching of cyanoacetate. There are two types of bands for azide ligands which have been observed around 2036 cm^{-1} and 2130 cm^{-1}, respectively for two types of stretching frequency *viz.*, terminal azido and bridging azido in complex **20**-**22**. For metal azido complexes **20**-**22** the azide ion coordinates to the metal center in different modes. Apart from the conventional terminal connection of azide ion, there are several other bridging modes exist (Figure. 6.2) [42] by which azide ion can get ligated between two metal centers.

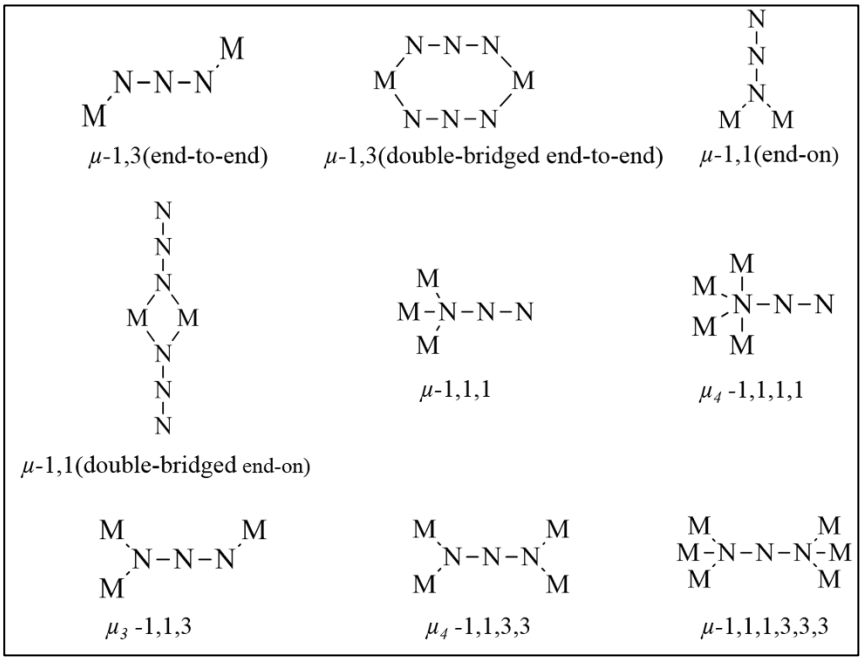

Figure 6. 2. *Various bridging fashion azide bonding.*

Among the above kind of existing bridging modes here we observed mainly the μ-1,3(end-to-end) and μ-1,1(double-bridged end-on) bridging coordination modes to generate polynuclear metal complexes.

6.3.3 Crystal structure of complex 18

Compound **18** crystallized in orthorhombic space group *Pna2₁*. The Cadmium atom is in the distorted octahedral environment and coordinated by two tridentate Schiff base ligands (**L^4**) (Fig 6.3). Though there are some coordination angles [N1-Cd1-N2 (70.39°); N2-Cd1-N3 (74.06°); N4-Cd1-N5 (73.70°); N5-Cd1-N6 (70.57°)] (Figure 6.3) deviating considerably from 90°, however, this

can be attributed to the chelating nature of Schiff base ligand. The bond lengths between Cd atom and N-donor centers are within the range of 2.284(3)–2.448(3) Å (Table 6.2), quite similar to those which have been reported earlier.[43]

Table 6. 2. *Selected bond lengths (Å) and bond angles (°) of Cd(II) complexes.*

Complex **18**			
Cd(1)-N(5)	2.284(3)	Cd(1)-N(2)	2.286(2)
Cd(1)-N(6)	2.359(3)	Cd(1)-N(1)	2.359(3)
Cd(1)-N(3)	2.380(2)	Cd(1)-N(4)	2.448(3)
N(5)-Cd(1)-N(6)	70.56(9)	N(1)-Cd(1)-N(2)	70.39(9)
N(1)-Cd(1)-N(6)	88.39(9)	N(2)-Cd(1)-N(3)	74.06(9)
N(3)-Cd(1)-N(6)	96.23(9)	N(4)-Cd(1)-N(5)	73.70(10)
N(2)-Cd(1)-N(4)	94.41(9)	N(1)-Cd(1)-N(4)	91.58(10)
Complex **19**			
Cd(1)-O(1)	2.238(14)	Cd(1)-O(4)	2.302(15)
Cd(1)-N(2)	2.329(17)	Cd(1)-N(1)	2.344(16)
Cd(1)-N(3)	2.431(16)	Cd(1)-O(3)	2.506(16)
O(4)-Cd(1)-N(2)	96.49(6)	N(1)-Cd(1)-N(2)	69.46(6)
O(1)-Cd(1)-N(3)	98.52(5)	O(4)-Cd(1)-N(3)	85.26(5)
N(2)-Cd(1)-N(3)	73.26(6)	O(1)-Cd(1)-O(3)	89.00(5)
Complex **20**			
Cd(1)-N(1)	2.231(12)	Cd(1)-N(4)	2.299(7)
Cd(1)-N(8)	2.325(8)	Cd(1)-N(4)#1	2.379(8)
Cd(1)-N(9)	2.380(9)	Cd(1)-N(7)	2.412(10)
N(1)-Cd(1)-N(4)	91.4(4)	N(1)-Cd(1)-N(7)	91.1(7)
N(4)-Cd(1)-N(4)#1	72.5(4)	N(8)-Cd(1)-N(4)#1	86.5(3)
N(1)-Cd(1)-N(9)	98.3(7)	N(4)-Cd(1)-N(9)	95.6(3)
N(8)-Cd(1)-N(9)	73.8(3)	N(4)#1-Cd(1)-N(9)	94.6(4)
N(7)-Cd(1)-N(8)	68.1(3)	N(4)#1-Cd(1)-N(7)	88.1(3)
Complex **21**			
Cd(1)-N(7)	2.228(15)	Cd(1)-N(2)	2.299(14)
Cd(1)-N(6)#1	2.391(16)	Cd(1)-N(4)	2.396(15)
Cd(1)-N(1)	2.404(15)	Cd(1)-N(3)	2.453(14)
N(2)-Cd(1)-N(6)#1	87.55(6)	N(7)-Cd(1)-N(6)#1	88.01(6)
N(6)#1-Cd(1)-N(3)	98.20(5)	N(4)-Cd(1)-N(7)	89.77(6)

N(2)-Cd(1)-N(4)	94.19(5)	N(2)-Cd(1)-N(3)	75.21(5)
N(6)#1-Cd(1)-N(1)	89.94(5)	N(1)-Cd(1)-N(2)	69.28(5)
N(1)-Cd(1)-N(4)	87.74(5)		
Complex **22**			
Cd(1)-N(10)	2.237(2)	Cd(1)-N(7)	2.299(2)
Cd(1)-N(2)	2.322(2)	Cd(1)-N(3)	2.404(2)
Cd(1)-N(1)	2.419(2)	Cd(1)-N(4)	2.483(2)
Cd(2)-N(16)	2.194(2)	Cd(2)-N(14)	2.317(2)
Cd(2)-N(6)#1	2.372(2)	Cd(2)-N(15)	2.377(2)
Cd(2)-N(13)	2.382(2)	Cd(2)-N(12)	2.578(2)
N(7)-Cd(1)-N(10)	95.48(10)	N(2)-Cd(1)-N(10)	160.82(8)
N(2)-Cd(1)-N(7)	95.82(9)	N(3)-Cd(1)-N(10)	119.86(8)
N(3)-Cd(1)-N(7)	91.34(8)	N(13)-Cd(2)-N(16)	93.49(9)
N(13)-Cd(2)-N(14)	69.18(7)	N(16)-Cd(2)-N(6)#1	96.48(10)

The two pyridine rings in the complex cation are approximately perpendicular to each other, making a dihedral angle of 88.57°. The perchlorate anions are linked to the complex cation through C–H···O hydrogen bonds and these hydrogen bonds are mainly responsible for the formation of a supramolecular spiral chain-like structure (Figure 6.3). The packing structure discloses that the monomeric units interacted with each other through C21–H21C···O5, C4–H4···O7 and C4–H4···O6 hydrogen bonding to make a 1D chain along *a* axis. Two such simultaneous 1D chains are further connected through C20–H20B···O8, C19–H19A···O6 and C9–H9A···O5 hydrogen bonding to make a 2D sheet-like structure in *ab* plane. (Figure 6.3)

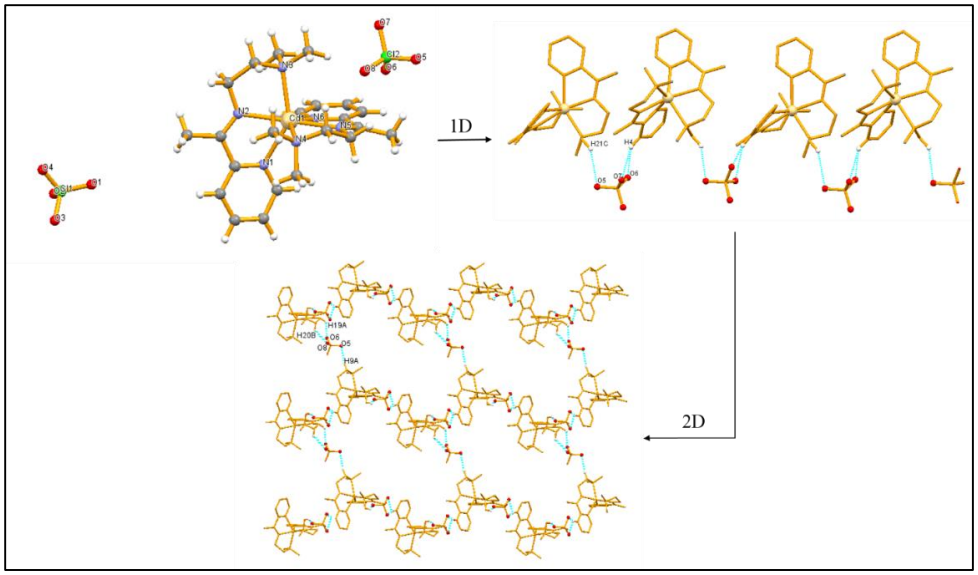

Figure 6. 3. *Monomer unit and the supramolecular network of complex* ***18.***

6.3.4 Crystal structure of complex 19

Compound **19** is a monomeric Cd(II) compound crystalized in the space group *P-1*. Here central cadmium ion is situated in a seven coordinated geometric environment which is relatively uncommon.[44] The seven coordination sites of Cd(II) ion is fulfilled by one tridentate Schiff base ligand (**L^4**), Two O-donor sites of one cyano-acetic acid and two O-donor sites of one acetate (Figure 6.4). The bond lengths between Cd atom and N-donor centers are within the range of 2.23(1)–2.50(2) Å (Table 6.2) and Cd-O distances are found to be in the range of 2.30-2.50 Å, quite similar to those which have been reported earlier. However, one particular Cd(1)-O(2) bond distance was found to be relatively longer *ca.* 2.73 Å. Each monomeric unit is linked with each other *via* C13–H13B···O3, C1–H1···O1 and C8–H8A···O4 hydrogen bonding (Figure 6.4) to make a 1D chain like structure. Two such simultaneous 1D chains are further connected through C8–H8B···N4 hydrogen bonding to make a 2D sheet-like structure (Figure 6.4).

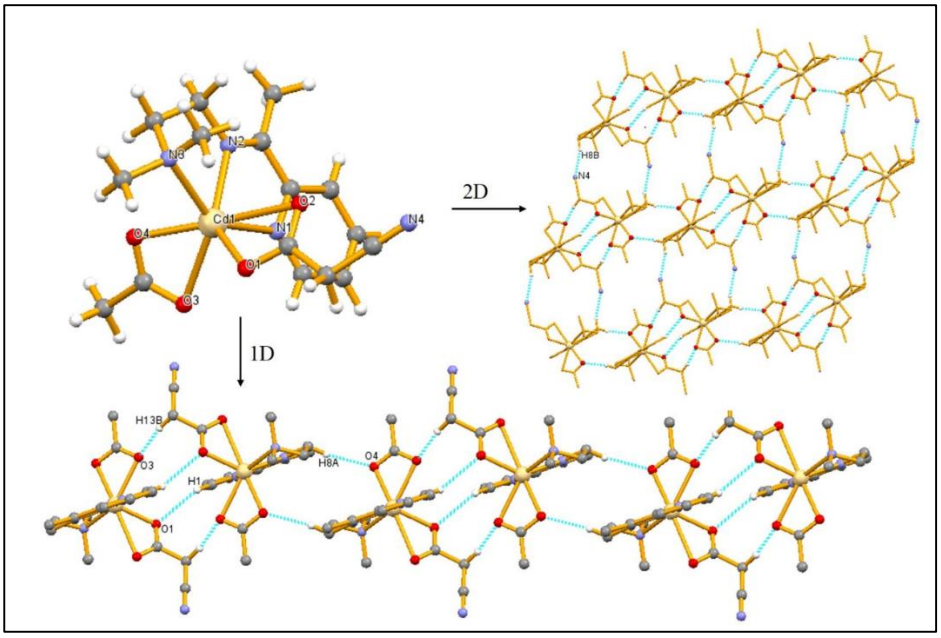

Figure 6. 4. *Monomer unit and the supramolecular network of complex* ***19****.*

6.3.5 Crystal structure of complex 20

Compound **20** is a symmetric dimeric Cd(II) compound crystalized in the space group $P2_1/n$. Each Cd^{2+} ion is located in an octahedral geometric environment. The octahedral geometry of each Cd(II) ion is fulfilled by one tridentate Schiff base ligand (**L^4**), one terminal azido ion and two bridging azido ions.(Figure 6.5). Two bridging azido ions make a bridge between two Cd(II) centers through a μ-1,1 double bridged end-on fashion. Though there are some coordination angles [N4-Cd1-N4 (72.5°); N7-Cd1-N8 (68.1°); N8-Cd1-N9 (73.8°)] deviating considerably from 90°, however, this can be attributed to the chelating nature of Schiff base ligand and bridging nature of azido ion. The bond lengths between Cd atom and N-donor centers are within the range of 2.23(2)–2.41(1) Å (Table 6.2), similar to earlier report.[43] Each dimeric unit is linked with each other *via* C4–H4···N3 hydrogen bonding (Figure 6.5) to make a 1D chain like structure along *c*-axis (Figure 6.5).

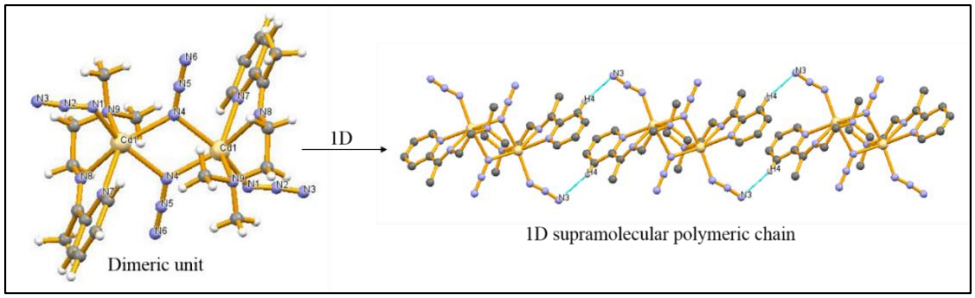

Figure 6. 5. *Dimeric structure and supramolecular network of complex* ***20****.*

6.3.6 Crystal structure of complex 21

Compound **21** forms a 1D coordination polymeric zig-zag chain along *c*-axis. Two crystallographically same cadmium centers (Cd1) alternate along the chain (Figure 6.6). Each cadmium atom is coordinated in distorted octahedral fashion by three nitrogen donors from tridentate chelating Schiff base ligand (**L^6**), one terminal azido ion and two nitrogen donors from two bridging (crystallographically different) azido ligand. These two azido ligands are responsible to make this coordination polymer making a bridge between two crystallographically same cadmium centers *via* a μ-1,3 end-end fashion. Two such 1D coordination polymeric chains are further connected *via* C2–H2···O1 hydrogen bonding to make a 2D sheet-like structure (Figure 6.6).

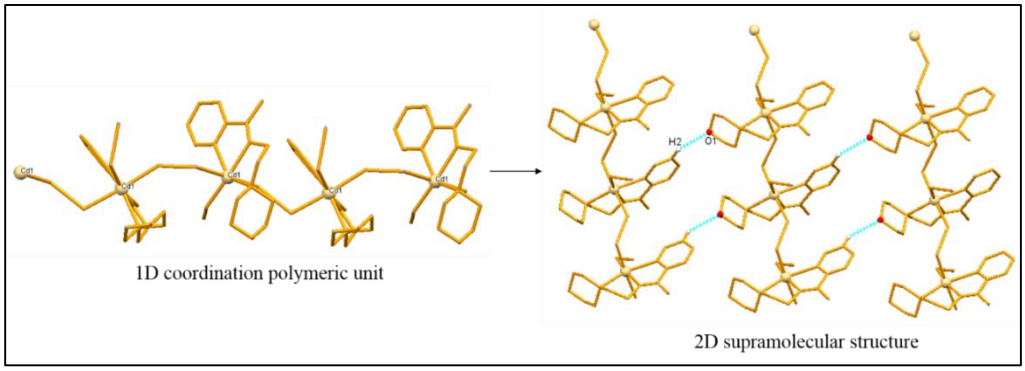

Figure 6. 6. *1D and 2D supramolecular network of complex* ***21****.*

6.3.7 Crystal structure of complex 22

Compound **22** forms again a 1D coordination polymeric *zig-zag* chain along *c*-axis. The smallest unit of this polymeric complex is a dimer unit which contains

crystallographically two different cadmium ions. Each cadmium atom is coordinated in distorted octahedral fashion by three nitrogen donors from tridentate chelating Schiff base ligand (**L**^{7}) and three azido ligand (Figure 6.7). Two different kind of azido ligand makes the bridge in μ-1,3 end to end fashion between two adjacent cadmium pairs to form the 1D-coordination polymeric structure.

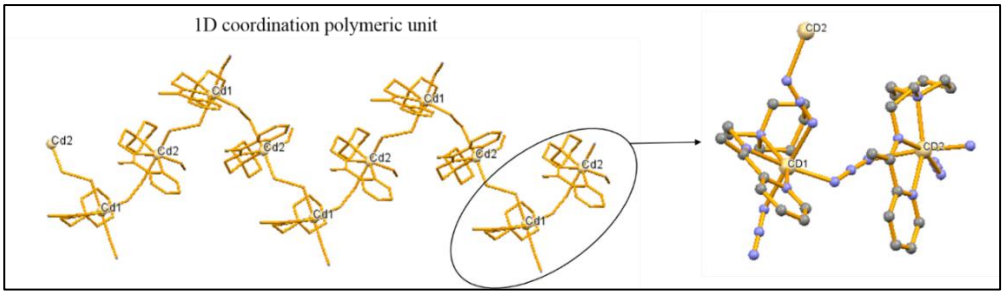

Figure 6. 7*. 1D Coordination polymeric structure of complex* ***22.***

6.3.8 Electrochemical studies

Electrochemical studies have been carried out to measure the corrosion inhibition property of the above said complexes. Initially, we have tested the corrosion inhibition property of complex **18** which was not showing significant inhibition property with comparison of parental ligand **L**^{4} and other precursor moieties. Therefore, we have introduced another coligand in metal Schiff base complex in the form of cyanoacetate to study the corrosion inhibition property in complex **19**. Unfortunately, this complex was also showing very little activity. Therefore it has been planned to introduce azide as a coligand which is having many N atoms which can act as donor sites. Interestingly, in that case, the synthesized complex **20** has shown considerable corrosion inhibition property. Encouraged by these results different Schiff base ligands have been employed to explore the best possible combination for this kind of activity. Ligand **L**^{6} and **L**^{7} provided us complex **21** and **22** respectively, which have shown good corrosion inhibition in 15% HCl medium. The enhanced corrosion inhibition property in **20 - 22** may be due to the greater availability of N absorbing sites in azide molecules. Cd complexes diminish the corrosion process which was

revealed by the polarization and impedance studies. These studies were performed after stabilization of open circuit potential (OCP).

6.3.9 Open circuit potential

The variation of open circuit potential (E_{ocp}) with time for mild steel in 15% HCl without and with the addition of different concentrations of Cd(II) complexes is shown in Figure. 6.8. The figures clearly indicate that stable OCP values were attained after 1 h of immersion, both in the absence and presence of the inhibitors. A concentration-dependent positive shift of corrosion potential with respect to the blank was observed on the addition of Cd(II) complexes into the corrosive medium. This indicates a probable impact on both anodic and cathodic polarization.[45]

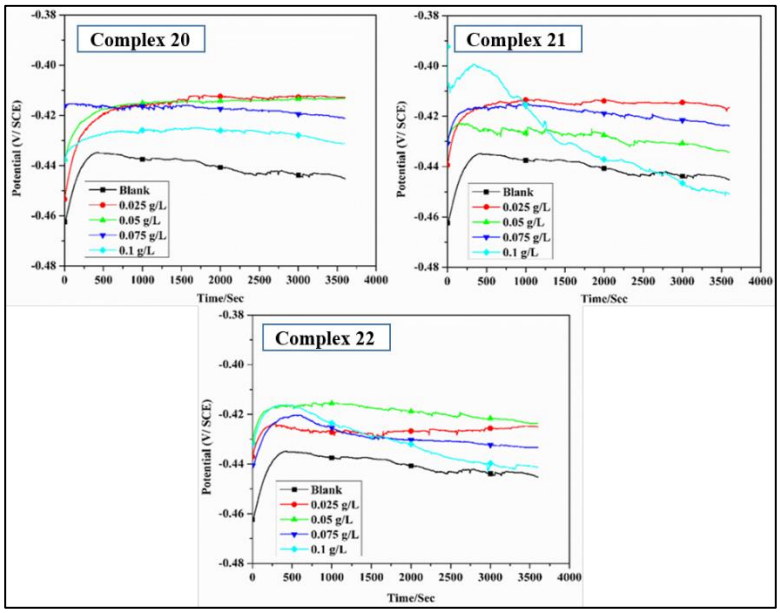

Figure 6. 8. *OCP plot for mild steel in 15% HCl in the absence and presence of different concentrations of Cd(II) complexes.*

6.3.10 Potentiodynamic polarization measurements

The polarization curves for mild steel electrode in 15% HCl solution were performed without and with inhibitors (Cd complex **20**, **21** & **22**) at various concentrations. The effect of different concentrations of Cd complexes in corrosion inhibition is shown in Figure 6.9. The Tafel curves were generated

after 1 hour of immersion in the test solution as a combination of anodic and cathodic polarization curves. All potentiodynamic polarization parameters such as corrosion current density (i_{corr}), corrosion potential (E_{corr}), anodic (β_a) and cathodic (β_c) Tafel slopes acquired from these curves and the calculated inhibition efficiency ($\eta_{pol}(\%)$) values are listed in Table 6.3. The i_{corr} values were obtained by extrapolation of liner section of both Tafel curves. The following equation (7) has been used to calculate the efficiency ($\eta_{pol}(\%)$)

$$\eta_{pol}(\%) = \frac{i^0_{corr} - i_{corr}}{i^0_{corr}} \times 100 \quad \text{..... (6)}$$

where, i^0_{corr} and i_{corr} are corrosion current densities ($\mu A/cm^2$) without and with inhibitor. The order of inhibition efficiency of those Cd complexes is **21**>**22**>**20**.

There is no significant trend observed in the shift of E_{corr} values as well as β_a & β_c values on the addition of inhibitor with respect to that without inhibitor. In the present study, it was observed that all inhibitors in 15% HCl solution exhibited anodic as well as cathodic inhibition effect *i.e.* 'mixed type with predominantly anodic inhibitor [46, 47] as the difference of E_{corr} values between blank and in presence of inhibitors lies within ± 85 mV v_s SCE with shifting of E_{corr} towards more anodic region. The inhibition efficiency depends on several aspects like interaction mode, adsorption center, structure and size. [31] The corrosion inhibition efficiency was increased with the increasing concentration of inhibitor and the maximum efficiencies were shown at 0.1 g/L as listed in Table 6.3.

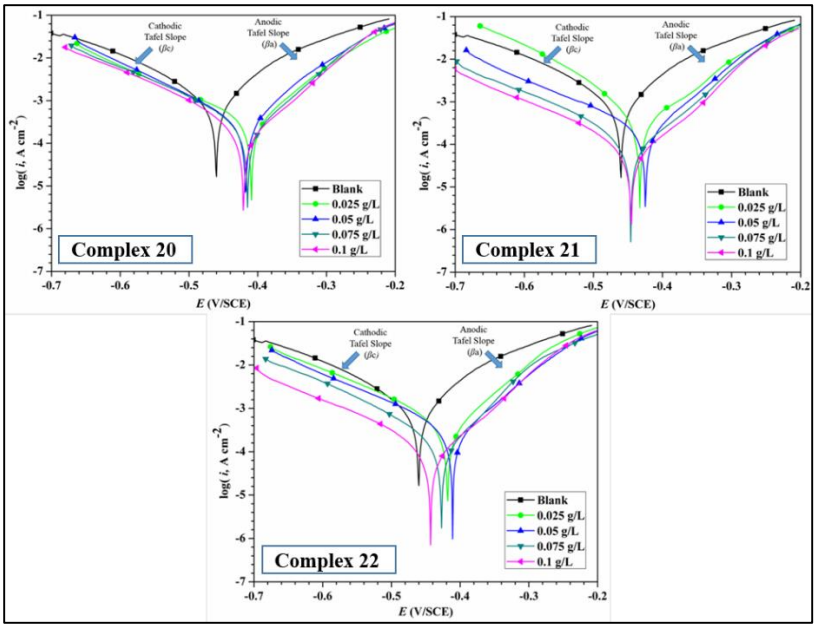

Figure 6. 9. *Polarization curves for mild steel in 15% HCl solution with and without various concentrations of inhibitors* ***20****,* ***21*** *and* ***22****.*

Table 6. 3. *Electrochemical parameters of potentiodynamic polarization studies with and without inhibitor in 15% HCl at 298 ±1 K.*

Inhibitor	Concentration (g/L)	E_{corr} (mV V_s SCE)	β_a (mV/dec)	β_c (mV/dec)	i_{corr} µA/cm^2	η_{pol}(%)
Blank		– 468.0	248.4	–274.4	1053	
Complex **20**	0.025	– 403.8	186.5	–367.6	394.8	62.5
	0.05	– 423.5	199.2	–281.8	329.3	68.72
	0.075	– 404.5	161.7	–284.6	221.2	78.99
	0.1	– 401.1	155.3	–286.9	161.6	84.65
Complex **21**	0.025	– 409.9	172.5	–224.3	333.3	68.34
	0.05	– 412.6	165.7	–358.4	235.7	77.61
	0.075	– 425.2	166.7	–301.4	91.2	91.34
	0.1	– 426.1	161.5	–310.2	65.2	93.8
Complex **22**	0.025	– 409.2	173	–312.5	374	64.48
	0.05	– 397.1	165.5	–329.3	279.2	73.48
	0.075	– 412.6	137	–272.7	127.9	87.85
	0.1	– 423.5	159.1	–313.0	92.3	91.23

6.3.11 Impedance studies

The corrosion of mild steel was also studied with the help of EIS technique. The Nyquist plots of mild steel sample with and without inhibitors (Cd(II) Schiff base complexes) in 15% hydrochloric acid medium are shown in Figure. 6.10. This shows a single capacitive loop in the frequency range 100 kHz to 10 mHz, which arises from the one time constant in impedance spectroscopy. In higher frequency range assigned with the charge transfer resistance and lower frequency was attributed to film resistance which was formed by inhibitor layer.[48, 49] In our case, in presence of inhibitor a very thin film was formed on the metallic surface throughout the adsorption process. Nyquist plots for mild steel in uninhibited solution are semi-circular in nature, but in the presence of inhibitors, the shape of the semicircle is depressed due to the frequency dispersion and microscopic roughness of the electrode surface.

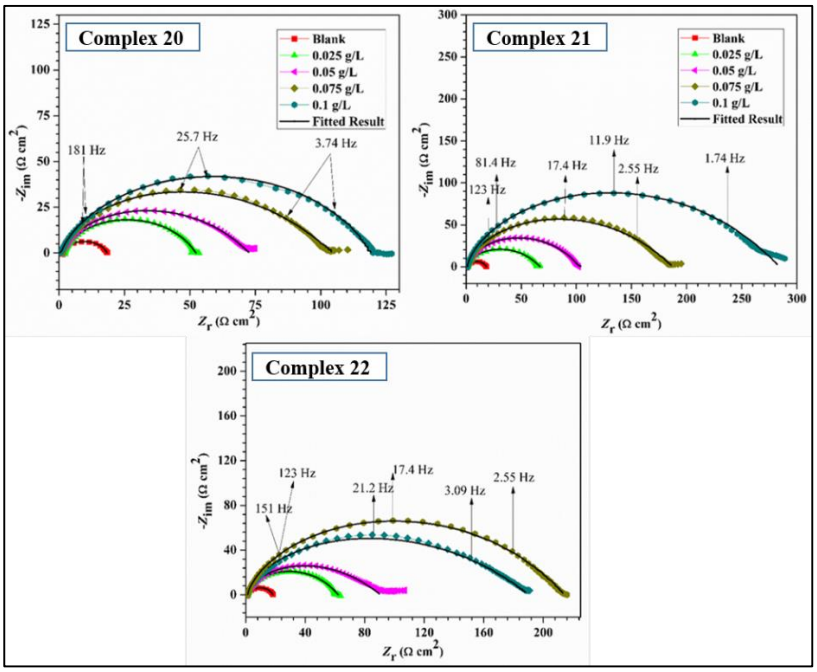

Figure 6. 10. *Nyquist plots for mild steel in 15% HCl in the absence and presence of different concentrations of all three inhibitors* ***20***, ***21*** *and* ***22*** *at 298 ± 1 K.*

The semi-circular Nyquist plot of uninhibited solution indicates that the corrosion process of mild steel was controlled by the charge transfer resistance. But the depressed semi-circular Nyquist plot in the presence of inhibitors is

considered as the polarization resistance (R_p) between the metal and outer Helmholtz plane. In this case, polarization resistance (R_p) containing all the resistances between metal and solution interfaces were included. Those are mainly charge transfer resistance (R_{ct}), film resistance (R_f), accumulation resistance (R_a), diffuse layer resistance (R_d) *etc.*[50] The shape and size of depressed semicircle was gradually increased with the addition of inhibitor up to 0.1 g/L concentrations. This increase in the diameter of the semicircle shows that the R_{ct} was increasing with increasing concentration of inhibitors. This phenomenon defined the protective layer formation on the metal surface and the consequent reduction in the metal dissolution. Furthermore, Bode plots can give more information in case of more intricate systems. The Bode plots of the synthesized inhibitors are presented in Figure 6.11. To compare corrosion resistance of different samples, one important parameter *i.e.*, low-frequency impedance modulus Z_{mod} can be used.[24] Increase in Z_{mod} demonstrates better protection performance as reported earlier.[51] Figure 6.11 showed that Z_{mod} increased as a function of the concentration for the synthesized inhibitor.

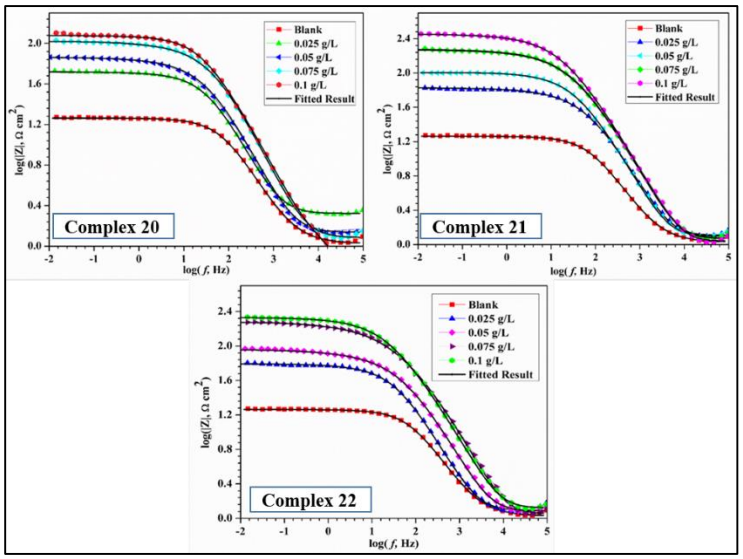

Figure 6. 11. *Bode plot of mild steel in 15% HCl without and with various concentrations of inhibitors (**20-22**)*

The phase angle plots for the mild steel in the presence and absence of inhibitors in 15% HCl are given in Figure. 6.12. These also reinforce the inferences from Nyquist and Bode plots.

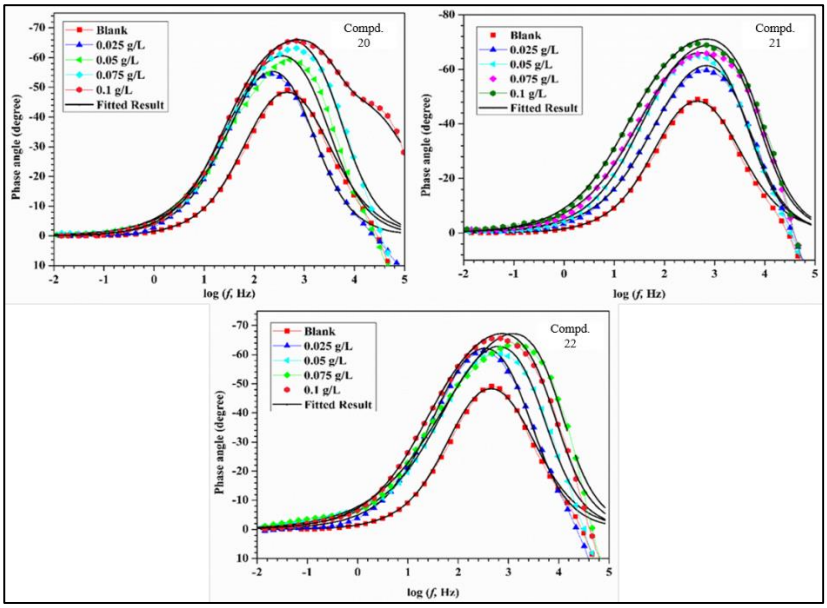

Figure 6. 12. *Phase angle plots of mild steel in 15% M HCl solutions without and with various concentrations of inhibitors* ***(20-22)***.

The Impedance studies on double layer capacitance in inhibited solutions have shown deviation from ideal behavior. This scattering has been attributed to roughness and other in-homogeneities of the mild steel electrode and also due to anion adsorption. The uncharacteristic capacitance can be represented by a constant phase element (CPE),[10] and the impedance (Z_{CPE}) can be expressed by equation (7):

$$Z_{CPE} = \frac{1}{Y_0 (j.w)^n} \quad \text{..... (7)}$$

where, Y_0 is the quantity of CPE, j is the imaginary unit ($j^2 = -1$), n is the phase shift parameter that belongs to $0 < n < 1$, and w is the angular frequency in Hz. The depressed semicircle can be explained by this n value. The value in the range 0.5 to 1, implies that the semi-circle is depressed at higher frequency ranges. The n value is a measure of the in-homogeneity or roughness of the solid surface.[52] The impedance parameter (R_s, R_{ct}, R_p, R_f, n, Y_0 & C_{dl}) are evaluated with the equivalent circuit fitting program. The EIS plots analyzed by software CHI instrument software and obtained the required data.[53] The equivalent circuit, in the absence of inhibitor, is shown in Figure. 6.13.

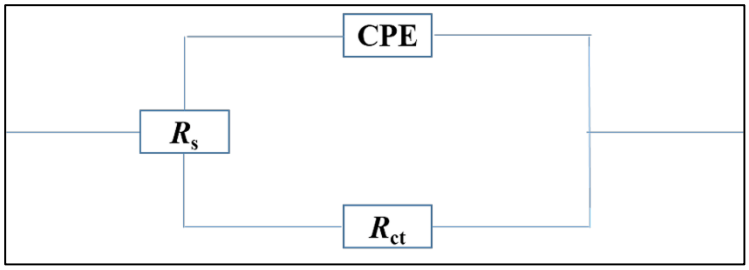

Figure 6. 13. *Equivalent circuits used to fit EIS data of mild steel in HCl medium without inhibitor.*

Here, the resistance is considered as charge transfer resistance and include all other ions or any kinds of corrosion product. The equivalent circuit is changed for the system in the presence of inhibitor as shown in Figure 6.14. In this behavior of metallic electrode, the parallel network: charge transfer resistance-double layer capacitance is established in presence of inhibitor.

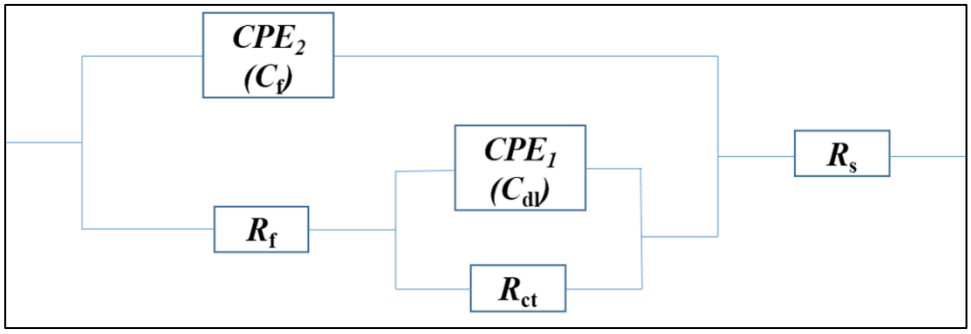

Figure 6. 14. *Equivalent circuits (with inhibitor) used to fit the EIS data of mild steel in HCl medium.*

The corrosion inhibition efficiency was calculated using the polarization resistance (R_p) value using the following formula equation (8):

$$\eta_{imp}(\%) = \frac{R_p - R_p^0}{R_p} \times 100 \quad \text{..... (8)}$$

where, R^0_p and R_p are polarization resistances of mild steel in the absence and presence of the inhibitor respectively. The R_p values are observed to be linearly proportional to the concentrations of inhibitor molecules. The maximum inhibition efficiency 93.89% was found for Cd complex **21** at 0.1 g/L concentration and other two Cd complexes **20** and **22** showed efficiency at this concentration of 84.95% and 91.88% respectively (Table 6.4). The double layer

capacitance (C_{dl}) values were calculated from CPE parameter values Y_0 and n, using the equation (9),

$$C_{dl} = Y_0^{1/n} + R_{ct}^{(1-n)/n} \quad \text{..... (9)}$$

where, Y_0 and n are magnitudes of CPE and deviation parameter ($-1 \leq n \leq 1$, which is dependent on surface morphology)

The C_{dl} values, generally, are inversely proportional to the adsorbent concentration on the metal surface.

Thus both the results obtained from PC and EIS methods are showing similar kind of efficiency trend among these three complexes. The higher efficiency of polymeric complexes (**21** and **22**) than dimeric complex **20** may be due to the higher availability of adsorbing N-donor sites as more number of azides were attached in the polymeric complexes. Among the two polymeric complexes, complex **21** is showing slightly higher inhibition efficiency, may be because of the presence of non-coordinated O donor adsorbing site.

Table 6. 4. Table 6.4. Impedance data for corrosion of mild steel in 15% HCl in presence and absence of different concentration of different inhibitor at 298 ±1 K.

Inhibitor	Conc. (g/L)	R_S (Ω cm^2)	R_{ct} (Ω cm^2)	R_f (Ω cm^2)	R_p (Ω cm^2)	χ^2	n	Y_0 (µF/cm^2)	C_{dl} (µF/cm^2)	n_f	Y_f (µF/cm^2)	C_f (µF/cm^2)	η_{imp}(%
Blank		1.05	17.28				0.8047	405.9	121.7				
Comp. **20**	0.025	2.07	50.23	0.03	50.26	3.56 x 10^{-3}	0.9999	43.2	43.2	0.6835	386.4	2.09	65.61
	0.05	1.32	71.43	0.04	71.47	1.09 x 10^{-2}	0.9635	55.5	45.1	0.5684	547.8	0.17	75.82
	0.075	1.13	103.81	0.08	103.89	9.43 x 10^{-3}	0.9606	37.0	29.4	0.5271	393.1	0.03	83.36
	0.1	0.28	114.84	3.80	118.64	4.71 x 10^{-4}	0.9999	7.35	7.3	0.7539	173.6	15.91	85.43
Comp. **21**	0.025	1.21	66.01	0.06	66.07	8.43 x 10^{-3}	0.9999	24.0	24.0	0.5723	465.3	0.20	73.84
	0.05	1.19	101.81	0.06	101.87	9.19 x 10^{-3}	0.9999	26.9	26.9	0.6052	311.4	0.25	83.03
	0.075	1.09	186.19	0.09	186.28	1.08 x 10^{-2}	0.9999	17.1	17.1	0.5655	294.0	0.09	90.72
	0.1	1.02	283.04	0.07	283.11	1.20 x 10^{-2}	0.9999	16.2	16.2	0.5925	221.2	0.11	93.89
Comp. **22**	0.025	1.18	61.10	0.04	61.14	1.56 x 10^{-2}	0.9659	66.7	54.9	0.5763	497.7	0.18	71.73
	0.05	1.15	89.49	0.06	89.55	1.52 x 10^{-2}	0.9765	32.8	28.5	0.5074	652.5	0.04	80.70
	0.075	0.99	189.00	0.14	189.14	1.32 x 10^{-2}	0.9999	12.0	12.0	0.5198	399.4	0.04	90.86
	0.1	1.23	213.02	0.09	213.11	7.30 x 10^{-3}	0.9999	13.4	13.4	0.6062	231.7	0.22	91.89

6.3.12 Adsorption isotherm

The adsorption isotherms give noteworthy information about the interaction happening between the inhibitors molecules and metal surfaces. In 15 % HCl medium, mild steel is surrounded by polar water molecules and other ions present. Therefore the adsorption of inhibitor molecules occur through substitution of water molecules which were previously attached to the metal surface *via* mainly two categories of adsorption processes. First one is chemisorption, where donor-acceptor type of irreversible interactions takes place *via* forming a coordinate bond between metal surface and inhibitor molecule. The second one is physisorption, here the inhibitor molecules adsorb on the concerned metallic surfaces by the electrostatic interaction. Adsorption of inhibitor molecules also indicates that the interaction force between metal-inhibitor is greater than that of metal-water. The surface coverage (θ) was calculated from the R^0_p and R_p values by the following equation (10):

$$\theta = \frac{R_p - R_p^0}{R_p} \quad \text{..... (10)}$$

The obtained data were tested for Langmuir adsorption isotherm, which can be represented by the equation (11),

$$\frac{C}{\theta} = \frac{1}{K_{ads}} + C \quad \text{..... (11)}$$

where, K_{ads} is the adsorption-desorption equilibrium constant and C is adsorbent concentration. For **20**, **21** and **22**, straight lines were obtained from the plots of C/θ $_{Vs}$ C with a high correlation coefficient (r^2) value of 0.998, 0.998 and 0.996 for **20**, **21** and **22** respectively at 298 ± 1 K (Figure 6.15). The values of K_{ads} in association with the standard Gibbs free energy of adsorption ΔG^0_{ads} was obtained from the Langmuir adsorption isotherm by the following equation (12),

$$K_{ads} = \frac{1}{C_{(sol.)}} \exp\left(\frac{\Delta G^0_{ads}}{RT}\right) \quad \text{..... (12)}$$

where, R is the universal gas constant, T is the absolute temperature and $C_{(sol.)}$ is the conc. of water (1000 g/L). The values of K_{ads} is represented here in $g^{-1}L$, thus in this equation the conc. of water is taken in g/L (1000 g/L) in place of 55.5 mole/L.[39, 53] In general when the obtained ΔG^0_{ads} values of inhibitor lies in the order of -20 kJ mol^{-1} or even lower (more positive), it satisfies the electrostatic interaction between inhibitor and metal surface (physisorption type). The ΔG^0_{ads} values around -40 kJ mol^{-1} or higher (more negative) are associated with coordinate bond formation (chemisorption type).[2] However, adsorption of the inhibitor molecules on the metallic surfaces cannot be considered as purely chemical or physical phenomenon.[2] Apart from chemisorption, inhibitor molecule is also adsorbed on the metallic surfaces *via* physisorption.[54, 55]

The obtained ΔG^0_{ads} values of our synthesized inhibitors are -27.96 kJ/mol, -28.35 kJ/mol and -28.20 kJ/mol for complex **20**, **21** and **22** respectively. The above range of ΔG^0_{ads} values designate the contribution of physisorption along with chemisorption. Thus it can be concluded that inhibitor molecules were adsorbed on the metallic surface following a mixed type adsorption phenomenon.

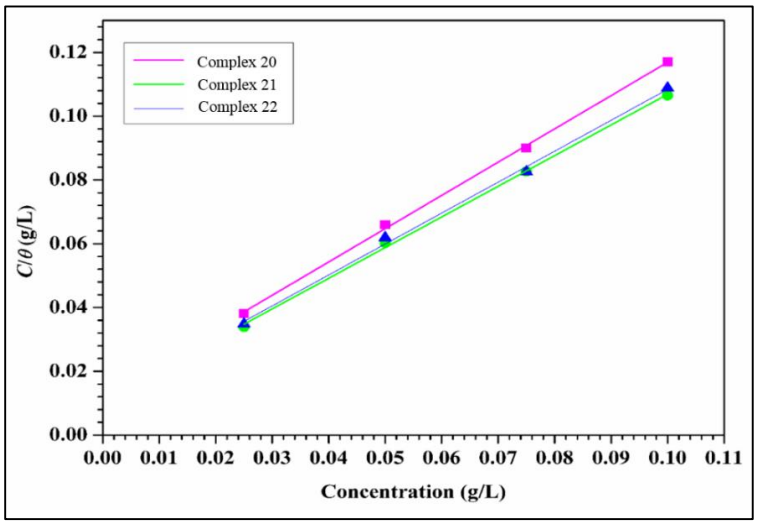

Figure 6. 15. *Langmuir adsorption isotherm of all inhibitors on mild steel surface in 15% HCl medium.*

6.3.13 Weight loss measurement

The results obtained from different electrochemical measurements are verified by the weight loss measurement. The effect of inhibitors at various concentrations is shown in Figure. 6.16 and Table 6.5. The inhibition efficiency (η_{wt}%) increased with increase in inhibitor concentrations. Table 6.5 shows that at 0.1 g/L complex **21** shows maximum inhibition efficiency. All the trends of inhibition efficiencies obtained from weight loss measurement are quite comparable with the results obtained from other electrochemical experiments. The higher efficiency of complex **21** may be due to the fact that it covered the metal surface efficiently and thus retarded the dissolution of mild steel.[53]

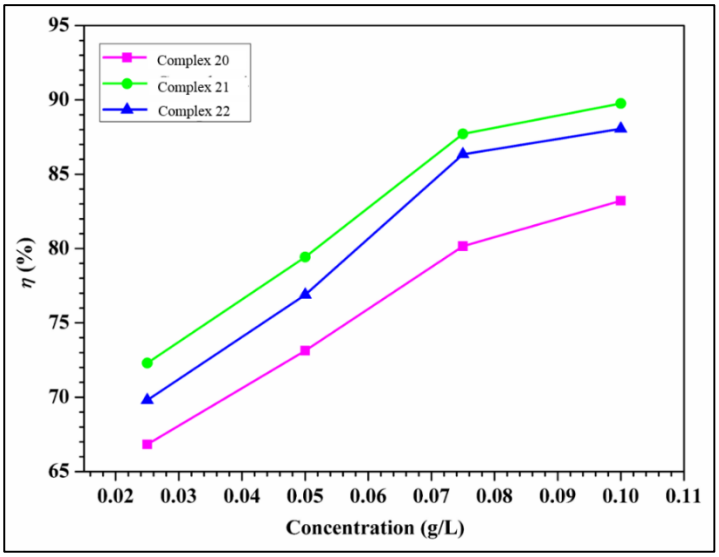

Figure 6. 16. *Variation of efficiency of inhibitors with concentration.*

Table 6. 5. *Calculated values of corrosion rate (CR) and inhibition efficiency (η %) for mild steel dissolution in 15% HCl in the absence and presence of different inhibitors for weight loss experiment at 298 ± 1K*

Inhibitor	Concentration (g/L)	Weight Loss (mg)	Corrosion rate (mmpy)	η (%)
Blank		541.5	35.97	
Complex **20**	0.025	179.62	11.93	66.83
	0.05	145.46	9.66	73.13
	0.075	107.42	7.13	80.16
	0.1	90.83	6.03	83.22
Complex **21**	0.025	149.97	9.96	72.30
	0.05	111.21	7.38	79.46
	0.075	66.53	4.42	87.71
	0.1	55.44	3.68	89.76
Complex **22**	0.025	163.49	10.86	69.80
	0.05	125.13	8.31	76.89
	0.075	73.92	4.91	86.35
	0.1	64.64	4.29	88.06

6.3.14 Surface morphology study

The surface morphology of the mild steel sample in 15% HCl solution in the absence and presence of inhibitors of optimum concentration (0.1 g/L) is shown in Fig. 16. Significant corrosion damage can be clearly observed when metal was kept immersed in 15% HCl solution for 1 h and 6 h respectively without inhibitor (Figure. 6.17 and Figure. 6.18). From both the images it was quite clearly visible that the surface roughness of mild steel increases in acidic medium with time in absence of inhibitor molecule. However, in the presence of inhibitors, uniformity and smoothness of metal surface improved remarkably with time. (Figure. 6.17 and Figure. 6.18). So it can be concluded that corrosive attack is considerably reduced by the inhibitor molecules in comparison with blank, indicating high-efficiency protective film on the mild steel surface are formed by these cadmium Schiff base complexes.

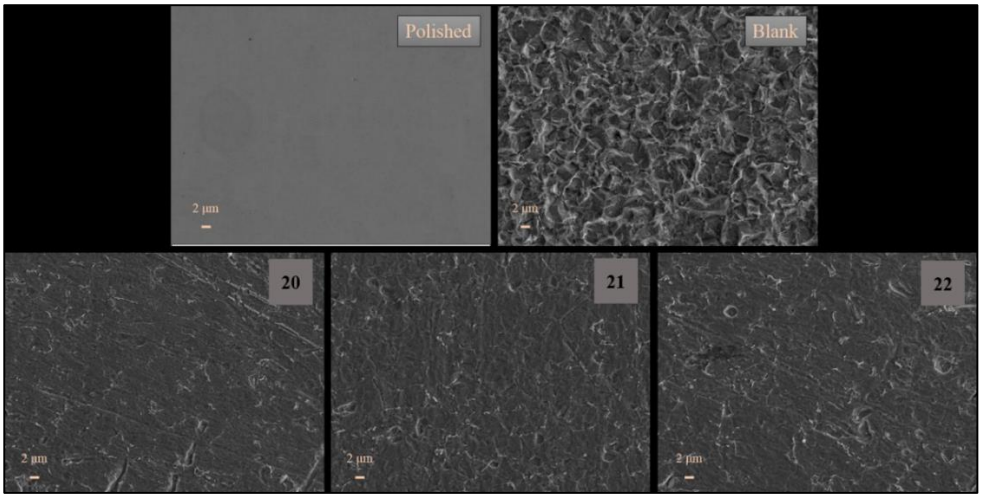

Figure 6. 17. *FE-SEM images of mild steel in 15% HCl solution at 298 ± 1 K, Polished: Before immersion; Blank: in the absence of inhibitors and presence of inhibitor* ***20****,* ***21****, &* ***22*** *at 0.1 g/L after 1 h of immersion.*

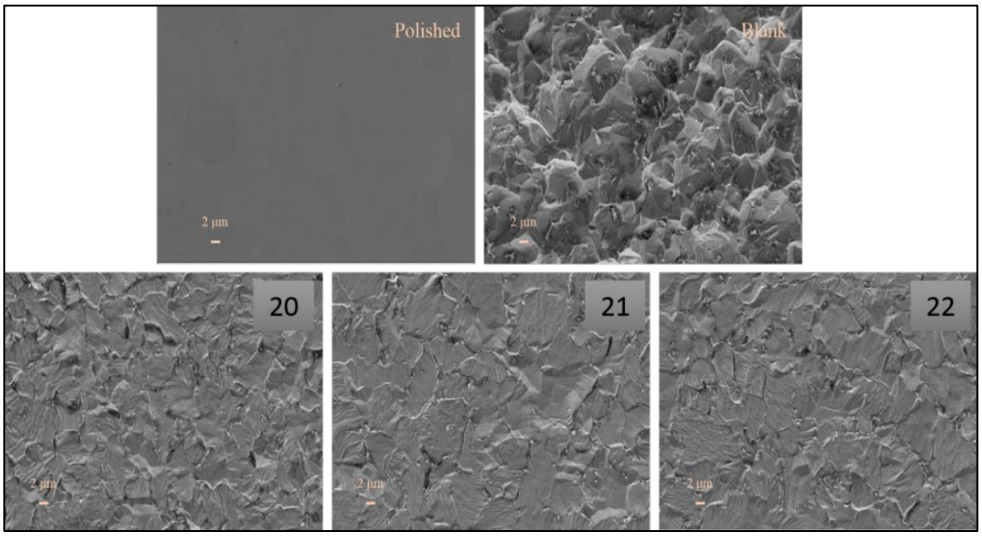

Figure 6. 18. *FE-SEM images of mild steel in 15% HCl solution at 298 ± 1 K, Polished: Before immersion; Blank: in the absence of inhibitors and presence of inhibitor* ***20****,* ***21****, &* ***22*** *at 0.1 g/L after 6 h of immersion.*

6.3.15 Stability study in acidic media and on steel surface

There are several examples of corrosion inhibition of mild steel in acidic medium using coordination complexes including metal Schiff base complexes.[27, 28, 56, 57] In spite of previous reports which support the intactness of entire coordination complexes in the application medium,

dissimilarities in the inhibition efficiency of our synthesized complexes indirectly indicate that this inhibition is not due to the formation of fragmented species of complexes in the medium. Furthermore, ESI-MS, UV-Vis and FTIR results in case of complex **20** before and after treatment with 15% HCl also clearly show the integrity of the complex in 15% HCl medium. Complex **20** was chosen for this study due to its fixed molar mass because of its dimeric nature. If complex **20** (0.1 g/L) get destroyed in the acidic medium then it may form new species like free ligands (0.04 g/L), azide ions (0.02 g/L), cadmium chloride (0.04 g/L) or precursor of ligands *i.e,* ketone (0.03 g/L) and amine (0.02 g/L). Thus, this fixed molar mass of complex **20** is an essential tool to understand about the species which is responsible factor for corrosion inhibition in acidic medium.

ESI-MS spectra of a single crystal of complex **20** in water had *m/z* peak at 347.07 for $[Cd_2(L^4)_2(N_3)_2]^{2+}$. After addition of 15% HCl, the *m/z* peak was observed at 347.1 which demonstrate the stability of complex in acidic medium (Figure. 6.19).

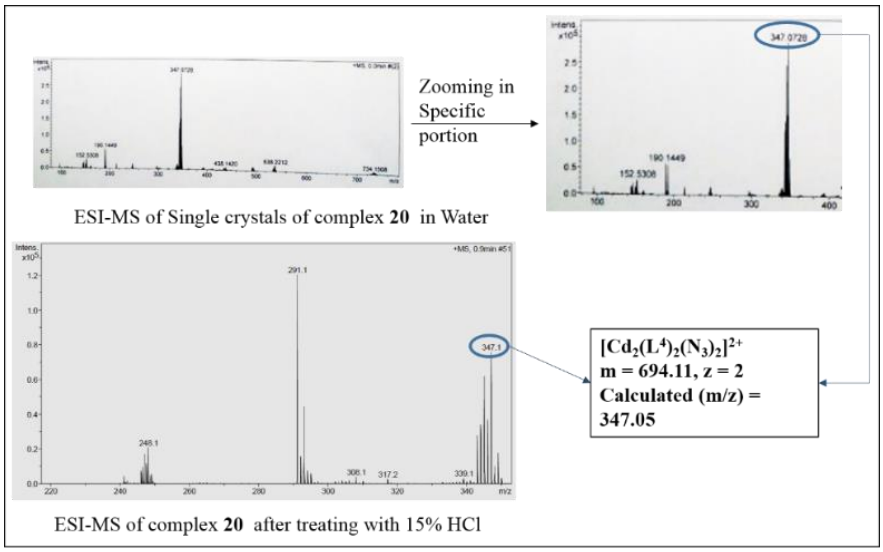

Figure 6. 19. *ESI-MS spectra of Complex **20** before and after treatment with 15% HCl*

Furthermore, solid state and solution (15% HCl) state UV-Vis spectra, as well as IR spectra, indicate the stability of the complex in acidic medium (Figure. 6.20 and Fig. 6.21).

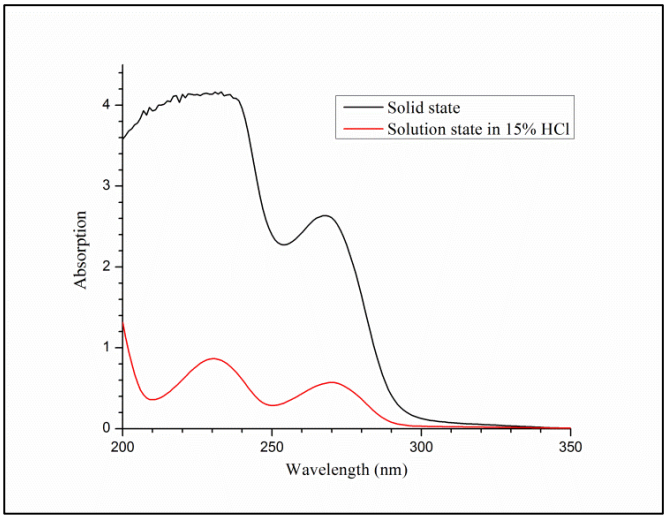

Figure 6. 20. *Solid and solution state (in 15% HCl) UV-Vis spectra of complex* ***20****.*

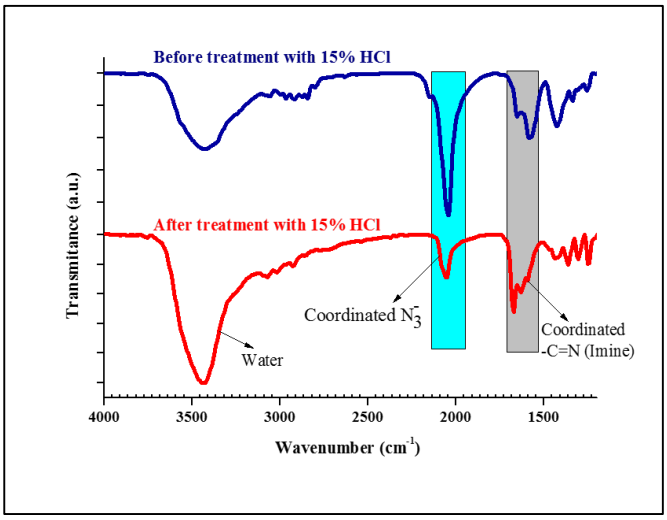

Figure 6. 21. *Overlapping IR spectra of complex* ***20*** *in solid and solution state (15% HCl).*

Almost similar XRD pattern obtained for the powder form of complex **20** and the thin film made after treatment with 15% HCl indicate the intactness of crystalline structure of the complex in the medium (Figure. 6.22). The deviation in peak intensity ratio arises may be due to the temperature effect on preparation of thin films.

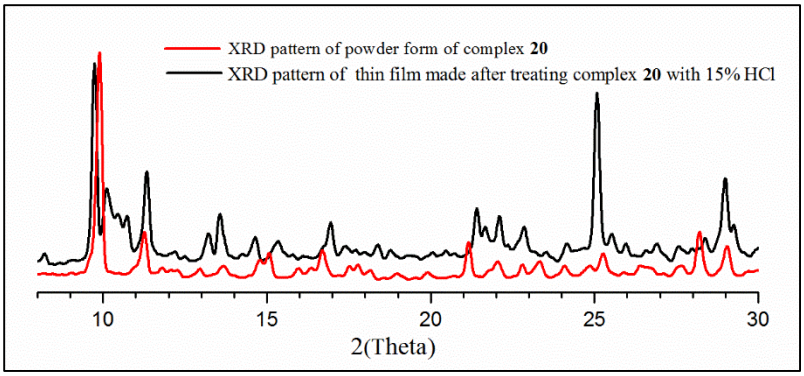

Figure 6. 22. *Overlapping XRD pattern of powder form of complex **20** and thin layer of complex **20** in 15% HCl.*

Still, electrochemical studies of ligand **L^4**, azide (NaN_3), cadmium chloride, 2-acetyl pyridine and N, N-dimethyl ethylene diamine were preformed taking the same concentration (0.1 g/L) of all to quantify the effect on corrosion inhibition to compare with the metal complex **20** to verify if decomposition of complex **20** occurs in acidic medium. All the data (Table 6.6 and 6.7; Figure. 6.23) show less inhibition efficiency for the constituents compared to complex **20**. Furthermore cadmium chloride salt is corrosive in nature which was reported in an earlier report.[58]

Table 6. 6. *Electrochemical parameters of potentiodynamic polarization studies in absence and presence of Ligand **L^4** (0.1g/L), 2-Acetyl pyridine (0.1g/L), N,N-dimethyl ethylene diamine (0.1g/L), Sodium azide (0.1g/L) and $CdCl_2$ (0.1g/L)*

Inhibitor	Concentration (g/L)	E_{corr} (mV/SCE)	β_a (mV/dec)	β_c (mV/dec)	I_{corr} µA/cm^2	η (%)
Blank		– 468.0	248.4	–274.4	1053.0	
N,N dimethyl ethylene diamine	0.1 g/L	– 454.6	335.3	–276.6	660.2	37.30
2-Acetyl pyridine	0.1/g/L	– 400.4	198.1	–291.1	420.0	60.11
$CdCl_2$	0.1g/L	– 443.8	436.6	–299.2	2514.0	Nil
Ligand **L^4**	0.1g/L	– 405.2	212.2	–304.4	371.1	64.75
Sodium azide	0.1g/L	– 409.2	219.9	–306.2	441.9	58.03

Table 6. 7. Impedance data for corrosion of mild steel in 15% HCl in absence and presence of Ligand L4 (0.1g/L), 2-Acetyl pyridine (0.1g/L), N,N-dimethyl ethylene diamine (0.1g/L), Sodium azide (0.1g/L) and $CdCl_2$ (0.1g/L)

Inhibitor	Conc (g/L)	R_S (Ω cm^2)	R_{ct} (Ω cm^2)	R_f (Ω cm^2)	$R_p = R_{ct} + R_f$	N	Y^0 (µF/cm^2)	C_{dl} (µF/cm^2)	n_f	Y^0_f	C_f (µF/cm^2)	η (%)
Blank		1.05	17.28			0.8047	405.9	121.7				
N,N dimethyl ethylene diamine	0.1 g/L	1.13	30.42	0.019	30.43	0.9999	83.4	83.4	0.5916	714.1	0.31	43.23
2-Acetyl pyridine	0.1 g/L	1.49	44.58	0.028	44.60	0.9999	45.3	45.3	0.6306	448.8	0.61	61.26
$CdCl_2$	0.1 g/L	1.65	12.65	0.015	12.66	0.9813	177.6	158.0	0.5516	1725.9		Nil
Ligand L^4	0.1 g/L	1.52	43.88	5.507	49.38	0.6807	364.8	52.5	0.9999	51.4	51.39	65.01
Sodium azide	0.1 g/L	1.38	61.15	0.027	61.17	0.9999	46.7	46.7	0.6654	351.7	1.05	71.75

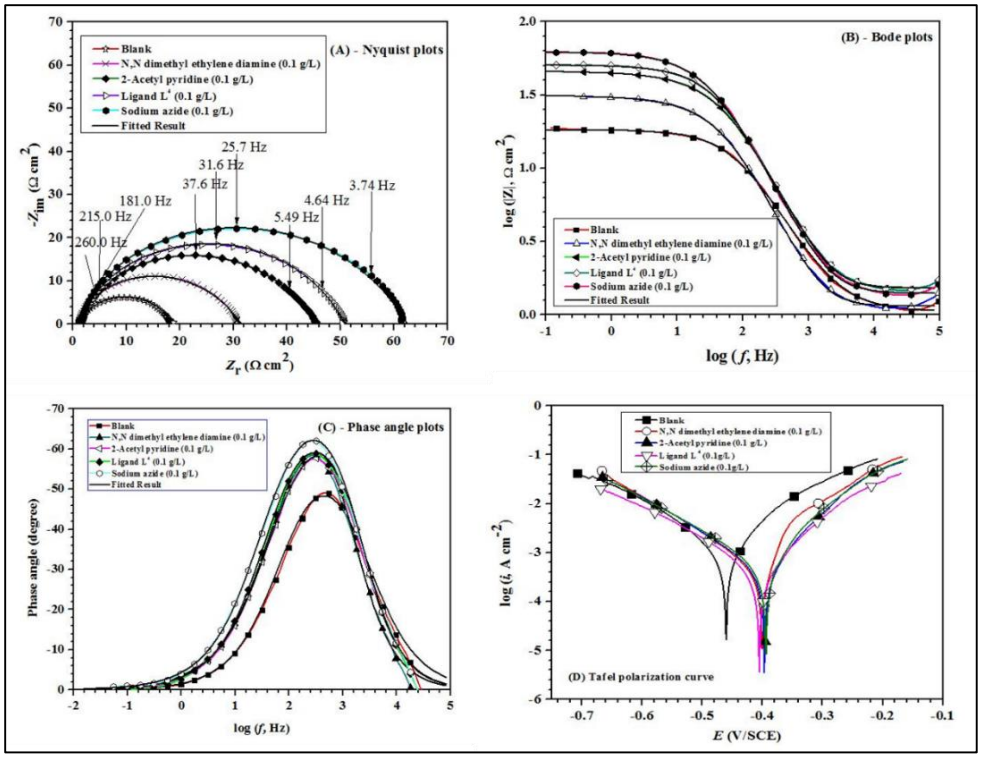

Figure 6. 23*. (A)-Nyquist plots, (B)-Bode plots and (C)-Phase angle plots (D)-Tafel polarization plots for mild steel in 15% HCl in the absence and presence of Ligand* ***L*** ^{4} *(0.1g/L), 2-Acetyl pyridine (0.1g/L), N,N-dimethyl ethylene diamine (0.1g/L),Sodium azide (0.1)*

Furthermore to scrutinize the composition of adsorbed inhibitor molecule, the EDX analysis of the metal surface was performed after 1 h of immersion in the acidic medium containing complex **20** (representative purpose). From the Figure. 6.24 it is clearly evident the presence of all elements of the inhibitor molecule on the mild steel surface. Thus it may be concluded that the whole metal complex is responsible for anti-corrosive film formation on the iron surface.

These phenomena clearly indicate the potential role of the Cd complexes in corrosion inhibition.

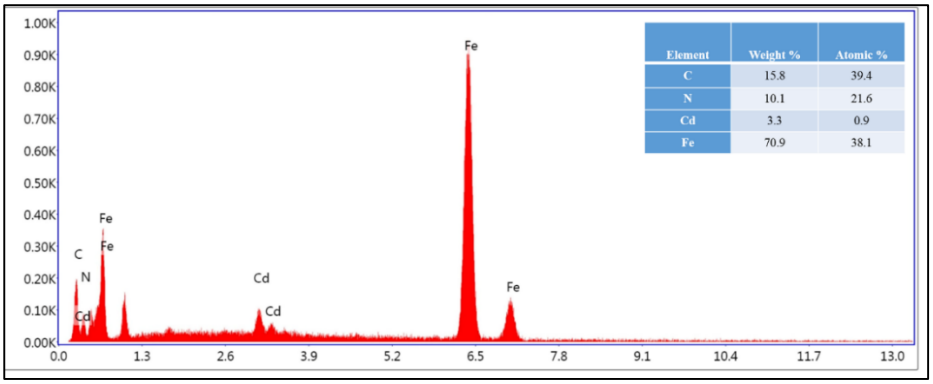

Figure 6. 24. *EDX spectra of complex* ***20*** *after adsorption on mild steel.*

6.3.16 Quantum chemical calculations

On the basis of the HSAB (hard–soft–acid–base) [59, 60] and the frontier-controlled interaction concepts,[60, 61] the bonding capabilities of the inhibitors towards the metal atom, Fe, can be well explained. According to HSAB principle, hard acids prefer to co-ordinate to hard bases and soft acids prefer to co-ordinate to soft bases. Metal atoms like Fe which are known as soft acids when binds with hard molecules it provides a larger HOMO–LUMO gap compared to binding a soft molecule where a smaller HOMO–LUMO gap is expected.[62-64] For representative purpose to compare inhibitory activity between polymeric complexes and dimeric complex only one polymeric complex **21** and one dimeric complex **20** have been taken for quantum chemical calculations and that suggests that the HOMO–LUMO gap for Complex **21** is smaller than that of Complex **20** which indicates that complex **21** is softer than Complex **20** (Table 6.8).

Table 6. 8. *Calculated quantum chemical parameters of the inhibitor molecules.*

Inhibitor	Comp. **20**	Comp. **21**
E_{HOMO} (eV)	-4.445	-2.465
E_{LUMO} (eV)	-2.07	-0.242
ΔE (eV)	2.375	2.223
$E_{LUMO(Fe)}$-$E_{HOMO(inh)}$ (eV)	4.322	2.342
I (eV)	4.445	2.465
A (eV)	2.07	0.242
χ (eV)	3.257	1.353
η (eV)	1.187	1.111
σ (eV^{-1})	0.842	0.9
ΔN	0.658	1.56

The order of this band gap values is similar with the optical band gap values obtained from UV/Vis experiment. Hence complex **21** has higher binding tendency than complex **20** towards Fe. Similarly using the concept of MO (molecular orbital) theory: since the cadmium complexes (inhibitor) is the electron pair donor and the Fe atom is the electron pair acceptor, the energy difference of the HOMO (LUMO is nothing special) of the complexes and the LUMO (HOMO is nothing special) of the Fe (*i.e.* -0.12376 eV reported in literature [65]) must be considered. The theory proposes that the overlap between the LUMO (Fe) and the HOMO (complex) is a foremost feature in bonding; the lower the HOMO–LUMO energy difference the higher the HOMO–LUMO overlap and the stronger the inhibitor-Fe interaction.[65] Another way to compare inhibition competence with constraints of molecular structure is to compute the fraction of electrons transferred from inhibitor to metal surface. According to Koopman's theorem,[66] E_{HOMO} and E_{LUMO} of the inhibitor molecule are related to the ionization potential (I) and the electron affinity (A), respectively. The ionization potential and the electron affinity are defined as $I = - E_{HOMO}$ and $A = - E_{LUMO}$. The absolute electronegativity (χ), global hardness (η) and softness (σ) of the inhibitors molecule are approximated as [$\chi = (I+A)/2$], [$\eta = (I-A)/2$] and [$\sigma = 1/\eta$].[67, 68] From the calculated result

(Table 6.8) it was very clear that softness of complex **21** is higher than complex **20** which supports the previous explanation. Pearson method [69] was utilized to calculate the fraction of electrons transfer (ΔN) from the inhibitor to metallic surface using the following equation (13).[70]

$$\Delta N = \frac{\chi_{Fe} - \chi_{inh}}{2(\eta_{Fe} + \eta_{inh})} \quad \text{..... (13)}$$

There are random use of the theoretical value of χ_{Fe} = 7 eV and of η_{Fe} = 0 eV to calculate ΔN in many literature in recent time.[60, 71] However, the use of this (χ_{Fe} = 7 eV) is conceptually wrong as it is only accompanying with the free electron gas Fermi energy of iron without considering the electron- electron interaction.[72] Thus in recent times researchers have used work function (ϕ) for the correct measure of electronegativity of iron.[73] Thus to measure ΔN more convincingly χ_{Fe} is replaced by ϕ in the equation (14).

$$\Delta N = \frac{\phi - \chi_{inh}}{2(\eta_{Fe} + \eta_{inh})} \quad \text{..... (14)}$$

DFT derived ϕ values for the Fe (1 0 0), Fe (1 1 0) and Fe (1 1 1) planes are 3.91 eV, 4.82 eV and 3.88 eV. Herein only Fe (1 1 0) surface has chosen because of its packed surface and higher stabilization energy. When $\Delta N > 0$ or vice versa if $\Delta N < 0$, the electron transfer from the inhibitor molecule to the metal surface will occur.[2] It was also well-known that electron donating ability of inhibitor molecule increases if $\Delta N < 3.6$.[74] The tabulated data (Table 6.8) shows that the ΔN values for both the inhibitors are positive and less than 3.6 which means both have capability to donate its electron to the metallic surface. It was also observed that the order of electron transfer is higher in the case of polymeric complex **21** than dimeric complex **20** which also confirms that complex **21** has the greater tendency to donate electrons and therefore the higher affinity to bind onto the metal surface.

As it was proposed that due to more heteroatom availability the polymeric complexes have greater tendency to interact with Fe surface, thus to investigate this phenomenon theoretically, molecular electrostatic potential (MEP) mapping was employed which provides a visual method to comprehend the location of the electrophilic attack, nucleophilic attack and the electrostatic potential zero regions.[75] The HOMO- LUMO orbital, total electron density surface mapped with molecular electrostatic potential (MEP) and contour representation of the electrostatic potential of complex **20** and complex **21** are represented in Figure. 6.25.

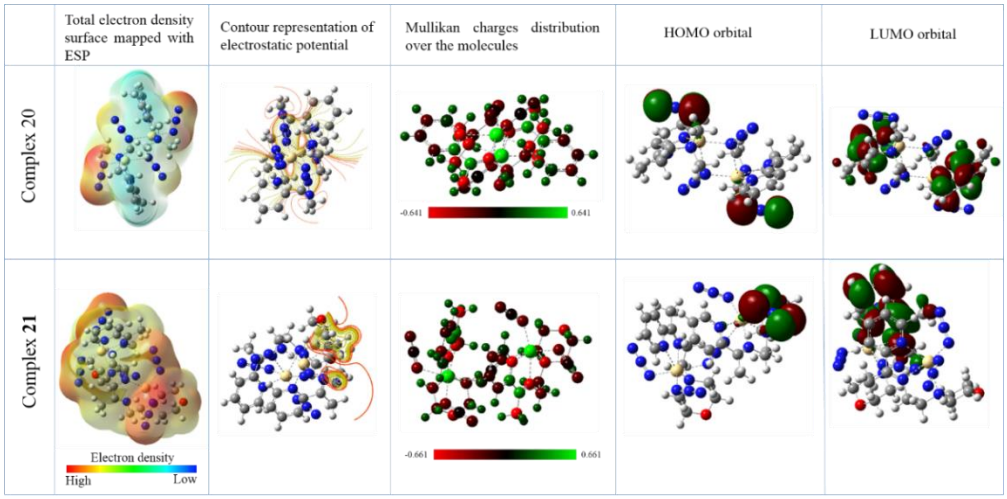

Figure 6. 25. *Molecular ESP map, Mulliken charge distribution diagram and HOMO-LUMO orbital electron density diagram for complex* ***20*** *and complex* ***21***.

In these maps, different values of the MEP were demonstrated with the help of different colors, which are red, yellow, green, light blue and blue. The red and yellow colors, appropriate for the negative parts of the MEP, are associated to electrophilic reactivity, blue colors appropriate for the positive parts to the nucleophilic reactivity and the green color signifies the ESP zero region. From this figure, it is clear that here red or yellow sites are mainly observed over azido N atoms. Thus Azido N atoms are a main responsible factor to interact with the metal surface. These remarks further confirmed by Mulliken charges on the reactive N atoms. The Mulliken charges on azido N atoms are more negative in

complex **21** than complex **20** which is also a supportive indication of greater inhibition efficiency of polymeric complexes.

This phenomenon is further corroborated with the Fukui indices analysis which is an important strategy to find out which atoms in the molecule mainly participate in this donor acceptor type of interactions. Fukui indices analysis. Fukui indices analysis can sensibly determine the local reactivity as well as the corresponding nucleophilic and electrophilic behavior of the molecule.[39] The higher value of f_k^+ suggests acceptance of electron from the metal surface and higher value of f_k^- suggests higher donation ability of inhibitor molecules.[39] The calculated Fukui indices are presented in Table 6.9. And the results indicate that N and C atoms of azide and acetyl pyridine moiety are the most susceptible sites for electron acceptance or donation. It was observed a relatively high f_k^- values which was observed for the atoms like N(4), N(42), N(2), N(40), N(3), N(41), N(7) and N(45) indicate that N atoms of azide has higher affinity to donate electrons to the steel surface. Besides this a relatively higher f_k^+ values associated with N(4), N(42), C(13), C(51), C(15) and C(53) atoms in complex **20** indicate terminal N atoms of azide and C atoms lies in the pyridine ring are responsible for accepting electron from the mild steel surface. From the table it was also clearly seen that Cd(1) and Cd(39) have tendency to accept electron from steel surface. Similarly the N atoms located in the azide part of complex **21** are more capable to donate electron while the C atoms lies on the acetyl pyridine ring favors more acceptance of electron from metallic surface. The presence of more number of heteroatoms in complex **21** than complex **20** gives more preference towards nucleophilic as well as electrophilic attack[2] and this observation indirectly supports the higher inhibition efficiency of complex **21** than complex **20.** So overall the expected prediction of localized attack is quite comparable with the observable results obtained from Fukui indices calculation.

***Table 6. 9**. Calculated Fukui functions for the complex **20** and complex **21**.*

Complex **20**				Complex **21**			
Atoms	f_k^+	f_k^-	f_k^0	Atoms	f_k^+	f_k^-	f_k^0
Cd(1)	0.005	0.02	0.013	Cd(1)	0.002	0.022	0.012
N (2)	0.031	0.108	0.069	O (2)	0.008	0.012	0.01
N (3)	0.014	0.033	0.024	N (3)	0.018	-0.005	0.006
N (4)	0.042	0.116	0.079	N (4)	0.025	-0.005	0.01
N (5)	-0.001	-0.003	-0.002	N (5)	-0.003	-0.004	-0.003
N (6)	0.004	0.001	0.002	N (6)	0.014	0.006	0.01
N (7)	0.016	0.024	0.02	N (7)	-0.002	0.002	0
N (8)	0.02	0	0.01	N (8)	-0.001	0.004	0.001
N (9)	0.03	0.004	0.017	N (9)	0.017	0.04	0.029
N (10)	-0.002	-0.003	-0.003	N (10)	0.002	0.016	0.009
C (11)	0.015	0.004	0.009	N (11)	-0.001	0.056	0.027
C (13)	0.042	0.023	0.033	C (12)	0.008	0	0.004
C (15)	0.033	0.021	0.027	C (14)	0.018	0.009	0.013
C (17)	0.022	0.014	0.018	C (16)	0.016	0.009	0.013
C (19)	0.03	0.008	0.019	C (18)	0.015	0.006	0.01
C (20)	0.026	0.009	0.017	C (20)	0.024	0	0.012
C (21)	0.007	0.005	0.006	C (21)	0.016	0.006	0.011
C (25)	0.007	0.003	0.005	C (22)	0.005	0.004	0.005
C (28)	0.003	0.002	0.002	C (26)	0.006	0.001	0.004
C (31)	0.002	0.003	0.003	C (29)	0.002	0.001	0.002
C (35)	0	0.002	0.001	C (32)	0	0.002	0.001
Cd(39)	0.006	0.02	0.013	C (35)	0.001	0.002	0.001
N (40)	0.031	0.108	0.069	C (38)	0.002	0.001	0.001
N (41)	0.014	0.033	0.024	C (41)	0.001	0	0.001
N (42)	0.042	0.116	0.079	Cd(44)	0.002	0.013	0.008
N (43)	-0.001	-0.003	-0.002	N (45)	0.015	0.12	0.067
N (44)	0.004	0.001	0.002	N (46)	0.033	0	0.016
N (45)	0.016	0.024	0.02	N (47)	0.044	0.006	0.025
N (46)	0.02	0	0.01	N (48)	-0.003	-0.003	-0.003
N (47)	0.03	0.004	0.017	N (49)	0.041	0.064	0.053
N (48)	-0.002	-0.003	-0.003	N (50)	0.004	0.042	0.023
C (49)	0.015	0.004	0.009	O (51)	0.009	0.008	0.008
C (51)	0.042	0.023	0.033	C (52)	0.002	0.002	0.002

C (53)	0.033	0.021	0.027	C (53)	0.001	0.001	0.001
C (55)	0.022	0.014	0.018	C (54)	0.024	0.003	0.013
C (57)	0.03	0.008	0.019	C (55)	0.046	0.002	0.024
C (58)	0.026	0.009	0.017	C (56)	0.03	0.005	0.018
C (59)	0.007	0.005	0.006	C (57)	0.009	0.002	0.005
C (63)	0.007	0.003	0.005	C (58)	0.003	0.002	0.003
C (66)	0.003	0.002	0.002	C (59)	0.002	0.002	0.002
C (69)	0.002	0.003	0.003	C (60)	0	0.001	0
C (73)	0	0.002	0.001	N (61)	0.007	0.022	0.015
				N (62)	0.031	0.073	0.052
				N (63)	0.004	0.016	0.01
				N (64)	0.019	0.051	0.035
				C (66)	0.059	0.017	0.038
				C (68)	0.043	0.014	0.029
				C (70)	0.028	0.007	0.017
				C (72)	0.008	0.004	0.006
				N (88)	0.03	0.136	0.083
				N (89)	0.006	0.042	0.024

6.3.17 Inhibition mechanism

There are certain physicochemical criteria which dictate the adsorption process of any molecule on the surface like; chemical nature of functional groups, the electron density of donor atoms and aromaticity, molecular shape, and size.[76, 77] Any inhibitor molecule may get adsorbed on the metal surface *via* electrostatic type interactions, donor-acceptor interactions, coordinate bonding interaction or combination of all.[10, 78, 79] When a particular organic molecule act as a ligand in a metal complex system, in the presence of other co-ligands like azide the tendency for adsorption may increase due to binding through available lone pairs of co-ligand and unused donating sites of ligands. The large size and molecular weight also play a part towards greater inhibitory efficiency.[35] Considering these information and ΔG^0_{ads} values obtained from experimental results, it can be predictable that adsorption was taken place through physisorption along with chemisorption pathway. Although there is no

such huge difference in the ΔG^0_{ads} values (– 27.96 kJ/mol, – 28.35 kJ/mol and – 28.20 kJ/mol for complex **20**, **21** and **22** respectively) between different substances but still from the observed valued it can be presumed that more negative ΔG^0_{ads} values were obtained with increase of the availability of heteroatoms in case of cooordination polymeric substances (complex **21** and **22**). Complex **21** posses most negative ΔG^0_{ads} value which may be due to presence of more number of heteroatom including one non coordinated O-donor atom. Presence of these hetero atoms facilitate both electrostatic as well as coordinate bonding type interactions with the surface. Thus combination of both physisorption along with chemisorption was observed in the synthesized systems. Theoretical observation also indicate the overall higher efficiency of polymeric substances and Fukui indices value corelate the active participation of N aoms of azide towards interaction with mild steel surface.

6.4 Conclusions

The corrosion averting capabilities of the prepared cadmium Schiff base complexes were studied towards mild steel corrosion in HCl solution. For target-oriented synthesis, firstly Schiff base ligand **L^4 [**N,N-Dimethyl-N'-(1-pyridin-2-yl-ethylidene)-ethane-1,2-diamine] has been taken as of prime importance where three cadmium complexes have been synthesized. The corrosion inhibition property of cadmium (II) complexes has been scrutinized in step by step manner. Complex **18** where no co-ligand is involved was not found to be significantly active towards corrosion inhibition. Also after employing cyanoacetic acid as a co-ligand in complex **19**, no such improvement has been observed in corrosion inhibition property which may be due to its monomeric nature and a lesser number of adsorbing site. Then to improve adsorbing site azide ion as a co-ligand has been introduced in complex **20** and structurally adsorbing site has been increased along with the nuclearity of the compound due to bridging nature of the co-ligand. The results are that the azido bridge dimeric complex **20** has shown remarkable corrosion inhibition property towards mild

steel. After discovering the utility of azide ion as co-ligand towards inhibition property it was contemplated to use the other Schiff base ligands **L^6 [**2-morpholino-N-(1-(pyridin-2-yl)ethylidene)ethanamine] and **L^7** [(2-(piperidin-1-yl)-N-(1-(pyridin-2-yl)ethylidene)ethanamine)] to prepare well designed polymeric complex **21** and **22** which have shown very high corrosion inhibition properties due to the presence of increased number of adsorbing sites and this high inhibition efficiency is quite good with respect to the other inorganic systems[13, 27] as well as organic inhibitors.[80]

Although a quantitative comparison of differences between substances is not reasonably possible as the experimental values are very close to each other but still considering the similar trend of activity among different substances obtained from different experimental as well as theoretical results, it can be concluded that increasing adsorbing sites by increasing nuclearity could be one of the key factors to develop corrosion resistance polymeric metal complexes which are worth for further investigation.

6.5 References

[1]. Ofoegbu, S. U.,Galvao, T. L. P.,Gomes, J. R. B.,Tedim, J.,Nogueira, H. I. S.,Ferreira, M. G. S.,Zheludkevich, M. L. (2017), Corrosion inhibition of copper in aqueous chloride solution by 1H-1,2,3-triazole and 1,2,4-triazole and their combinations: electrochemical, Raman and theoretical studies, Physical Chemistry Chemical Physics, 19, 6113-6129.(DOI: 10.1039/C7CP00241F)

[2]. Saha, S. K.,Dutta, A.,Ghosh, P.,Sukul, D.,Banerjee, P. (2016), Novel Schiff-base molecules as efficient corrosion inhibitors for mild steel surface in 1 M HCl medium: experimental and theoretical approach, Physical Chemistry Chemical Physics, 18, 17898-17911.(DOI: 10.1039/C6CP01993E)

[3]. Abiola, O. K.,James, A. O. (2010), The effects of Aloe vera extract on corrosion and kinetics of corrosion process of zinc in HCl solution, Corrosion Science, 52, 661-664.(DOI: 10.1016/j.corsci.2009.10.026)

[4]. Hegazy, M. A.,Aiad, I. (2015), 1-Dodecyl-4-(((3-morpholinopropyl)imino)methyl)pyridin-1-ium bromide as a novel corrosion

inhibitor for carbon steel during phosphoric acid production, Journal of Industrial and Engineering Chemistry, 31, 91-99.(DOI: 10.1016/j.jiec.2015.06.012)

[5]. Farag, A. A.,Ali, T. A. (2015), The enhancing of 2-pyrazinecarboxamide inhibition effect on the acid corrosion of carbon steel in presence of iodide ions, Journal of Industrial and Engineering Chemistry, 21, 627-634.(DOI: 10.1016/j.jiec.2014.03.030)

[6]. Ahamad, I.,Prasad, R.,Quraishi, M. A. (2010), Thermodynamic, electrochemical and quantum chemical investigation of some Schiff bases as corrosion inhibitors for mild steel in hydrochloric acid solutions, Corrosion Science, 52, 933-942.(DOI: 10.1016/j.corsci.2009.11.016)

[7]. Shanmughan, S. K.,Kakkassery, J. T.,Raphael, V. P.,Kuriakose, N. (2015), Electrochemical and AFM studies on adsorption behavior of a Polynuclear Schiff Base at carbon steel in HCl medium, Current Chemistry Letters, 4, 67-76.(DOI: 10.5267/j.ccl.2015.2.001)

[8]. Gupta, N. K.,Quraishi, M. A.,Verma, C.,Mukherjee, A. K. (2016), Green Schiff's bases as corrosion inhibitors for mild steel in 1 M HCl solution: experimental and theoretical approach, RSC Advances, 6, 102076-102087.(DOI: 10.1039/C6RA22116E)

[9]. Ansari, K. R.,Quraishi, M. A.,Singh, A. (2014), Schiff's base of pyridyl substituted triazoles as new and effective corrosion inhibitors for mild steel in hydrochloric acid solution, Corrosion Science, 79, 5-15.(DOI: 10.1016/j.corsci.2013.10.009)

[10]. Keleş, H.,Emir, D. M.,Keleş, M. (2015), A comparative study of the corrosion inhibition of low carbon steel in HCl solution by an imine compound and its cobalt complex, Corrosion Science, 101, 19-31.(DOI: 10.1016/j.corsci.2015.07.013)

[11]. Singh, P.,Singh, D. P.,Tiwari, K.,Mishra, M.,Singh, A. K.,Singh, V. P. (2015), Synthesis, structural investigations and corrosion inhibition studies on Mn(II), Co(II), Ni(II), Cu(II) and Zn(II) complexes with 2-amino-benzoic acid

(phenyl-pyridin-2-yl-methylene)-hydrazide, RSC Adv., 5, 45217-45230.(DOI: 10.1039/c4ra11929k)

[12]. Ashassi-Sorkhabi, H.,Shaabani, B.,Seifzadeh, D. (2005), Corrosion inhibition of mild steel by some schiff base compounds in hydrochloric acid, Applied Surface Science, 239, 154-164.(DOI: 10.1016/j.apsusc.2004.05.143)

[13]. Singh, P.,Singh, A. K.,Singh, V. P. (2013), Synthesis, structural and corrosion inhibition properties of some transition metal(II) complexes with o-hydroxyacetophenone-2-thiophenoyl hydrazone, Polyhedron, 65, 73-81.(DOI: 10.1016/j.poly.2013.08.008)

[14]. Hosseini, S. M. A.,Azimi, A.,Sheikhshoaei, I.,Salari, M. (2010), Corrosion Inhibition of 302 Stainless Steel with Schiff Base Compounds, J. Iran. Chem. Soc., 7, 799-806.

[15]. Shabani-Nooshabadi, M.,Ghandchi, M. S. (2015), Santolina chamaecyparissus extract as a natural source inhibitor for 304 stainless steel corrosion in 3.5% NaCl, Journal of Industrial and Engineering Chemistry, 31, 231-237.(DOI: 10.1016/j.jiec.2015.06.028)

[16]. BİlgİÇ, S.,Çaliskan, N. (2001), An investigation of some Schiff bases as corrosion inhibitors for austenitic chromium–nickel steel in H2SO4, Journal of Applied Electrochemistry, 31, 79-83.(DOI: 10.1023/a:1004182329826)

[17]. Ehteshamzade, M.,Shahrabi, T.,Hosseini, M. G. (2006), Inhibition of copper corrosion by self-assembled films of new Schiff bases and their modification with alkanethiols in aqueous medium, Applied Surface Science, 252, 2949-2959.(DOI: 10.1016/j.apsusc.2005.05.003)

[18]. Şafak, S.,Duran, B.,Yurt, A.,Türkoğlu, G. (2012), Schiff bases as corrosion inhibitor for aluminium in HCl solution, Corrosion Science, 54, 251-259.(DOI: 10.1016/j.corsci.2011.09.026)

[19]. Thirugnanaselvi, S.,Kuttirani, S.,Emelda, A. R. (2014), Effect of Schiff base as corrosion inhibitor on AZ31 magnesium alloy in hydrochloric acid solution, Transactions of Nonferrous Metals Society of China, 24, 1969-1977.(DOI: 10.1016/S1003-6326(14)63278-7)

[20]. Mishra, M.,Tiwari, K.,Singh, A. K.,Singh, V. P. (2015), Versatile coordination behaviour of a multi-dentate Schiff base with manganese(II), copper(II) and zinc(II) ions and their corrosion inhibition study, Inorganica Chimica Acta, 425, 36-45.(DOI: 10.1016/j.ica.2014.10.026)

[21]. Soliman, S. A.,Metwally, M. S.,Selim, S. R.,Bedair, M. A.,Abbas, M. A. (2014), Corrosion inhibition and adsorption behavior of new Schiff base surfactant on steel in acidic environment: Experimental and theoretical studies, Journal of Industrial and Engineering Chemistry, 20, 4311-4320.(DOI: 10.1016/j.jiec.2014.01.038)

[22]. Ansari, K. R.,Quraishi, M. A. (2014), Bis-Schiff bases of isatin as new and environmentally benign corrosion inhibitor for mild steel, Journal of Industrial and Engineering Chemistry, 20, 2819-2829.(DOI: 10.1016/j.jiec.2013.11.014)

[23]. Aytaç, A.,Özmen, Ü.,Kabasakaloğlu, M. (2005), Investigation of some Schiff bases as acidic corrosion of alloy AA3102, Materials Chemistry and Physics, 89, 176-181.(DOI: 10.1016/j.matchemphys.2004.09.003)

[24]. Hegazy, M. A.,Hasan, A. M.,Emara, M. M.,Bakr, M. F.,Youssef, A. H. (2012), Evaluating four synthesized Schiff bases as corrosion inhibitors on the carbon steel in 1 M hydrochloric acid, Corrosion Science, 65, 67-76.(DOI: 10.1016/j.corsci.2012.08.005)

[25]. Hu, Z.,Meng, Y.,Ma, X.,Zhu, H.,Li, J.,Li, C.,Cao, D. (2016), Experimental and theoretical studies of benzothiazole derivatives as corrosion inhibitors for carbon steel in 1 M HCl, Corrosion Science, 112, 563-575.(DOI: 10.1016/j.corsci.2016.08.012)

[26]. Yilmaz, N.,Fitoz, A.,Ergun, Ü.,Emregül, K. C. (2016), A combined electrochemical and theoretical study into the effect of 2-((thiazole-2-ylimino)methyl)phenol as a corrosion inhibitor for mild steel in a highly acidic environment, Corrosion Science, 111, 110-120.(DOI: 10.1016/j.corsci.2016.05.002)

[27]. Mahdavian, M.,Naderi, R. (2011), Corrosion inhibition of mild steel in sodium chloride solution by some zinc complexes, Corrosion Science, 53, 1194-1200.(DOI: 10.1016/j.corsci.2010.12.013)

[28]. Mahdavian, M.,Attar, M. M. (2009), Electrochemical behaviour of some transition metal acetylacetonate complexes as corrosion inhibitors for mild steel, Corrosion Science, 51, 409-414.(DOI: 10.1016/j.corsci.2008.11.010)

[29]. Hersch, P. (1961), Localization of Ferrous Corrosion by Azide, Nature, 190, 163-164.

[30]. Ade, S. B.,Deshpande, M. N.,Kolhatkar, D. G. (2012), Corrosion a universal environmental Problem: a role of Schiff base metal complexes as inhibitors Journal of Chemical and Pharmaceutical Research, 4(2), 1033-1035.

[31]. Aytaç, A. (2010), Cu(II), Co(II) and Ni(II) complexes of –Br and –OCH2CH3 substituted Schiff bases as corrosion inhibitors for aluminium in acidic media, Journal of Materials Science, 45, 6812-6818.(DOI: 10.1007/s10853-010-4779-7)

[32]. Sheldrick, G. (2008), A short history of SHELX, Acta Crystallographica Section A, 64, 112-122.(DOI: 10.1107/S0108767307043930)

[33]. Gwaram, N. S.,Ali, H. M.,Khaledi, H.,Abdulla, M. A.,Hadi, A. H. A.,Lin, T. K.,Ching, C. L.,Ooi, C. L. (2012), Antibacterial Evaluation of Some Schiff Bases Derived from 2-Acetylpyridine and Their Metal Complexes, Molecules, 17, 5952-5971.(DOI: 10.3390/molecules17055952)

[34]. Shi, D.-H.,Wang, X.-L.,Liu, W.-W.,Jin, H. (2012), Synthesis, Crystal Structures, and Biological Activity of Schiff Base Zinc(II) Complexes Derived From (2-piperidin-1-ylethyl)-(1-pyridin-2-ylethylidene)amine, Synthesis and Reactivity in Inorganic, Metal-Organic, and Nano-Metal Chemistry, 42, 480-484.(DOI: 10.1080/15533174.2011.613083)

[35]. Abd El-Lateef, H. M. (2015), Experimental and computational investigation on the corrosion inhibition characteristics of mild steel by some novel synthesized imines in hydrochloric acid solutions, Corrosion Science, 92, 104-117.(DOI: 10.1016/j.corsci.2014.11.040)

[36]. Becke, A. D. (1988), Density-functional exchange-energy approximation with correct asymptotic behavior, Physical Review A, 38, 3098-3100.

[37]. Kidambi, S.,Ramamoorthy, A. (2002), Quantum Chemical Calculations of Cadmium Chemical Shifts in Inorganic Complexes, The Journal of Physical Chemistry A, 106, 10363-10369.(DOI: 10.1021/jp0265891)

[38]. Frisch, M. J.,Trucks, G. W.,Schlegel, H. B.,Scuseria, G. E.,Robb, M. A.,Cheeseman, J. R.,Scalmani, G.,Barone, V.,Mennucci, B.,Petersson, G. A.,Nakatsuji, H.,Caricato, M.,Li, X.,Hratchian, H. P.,Izmaylov, A. F.,Bloino, J.,Zheng, G.,Sonnenberg, J. L.,Hada, M.,Ehara, M.,Toyota, K.,Fukuda, R.,Hasegawa, J.,Ishida, M.,Nakajima, T.,Honda, Y.,Kitao, O.,Nakai, H.,Vreven, T.,Montgomery Jr., J. A.,Peralta, J. E.,Ogliaro, F.,Bearpark, M. J.,Heyd, J.,Brothers, E. N.,Kudin, K. N.,Staroverov, V. N.,Kobayashi, R.,Normand, J.,Raghavachari, K.,Rendell, A. P.,Burant, J. C.,Iyengar, S. S.,Tomasi, J.,Cossi, M.,Rega, N.,Millam, N. J.,Klene, M.,Knox, J. E.,Cross, J. B.,Bakken, V.,Adamo, C.,Jaramillo, J.,Gomperts, R.,Stratmann, R. E.,Yazyev, O.,Austin, A. J.,Cammi, R.,Pomelli, C.,Ochterski, J. W.,Martin, R. L.,Morokuma, K.,Zakrzewski, V. G.,Voth, G. A.,Salvador, P.,Dannenberg, J. J.,Dapprich, S.,Daniels, A. D.,Farkas, Ö.,Foresman, J. B.,Ortiz, J. V.,Cioslowski, J.,Fox, D. J. (2009), Gaussian 09, Gaussian, Inc.: Wallingford, CT, USA.

[39]. Dohare, P.,Ansari, K. R.,Quraishi, M. A.,Obot, I. B. Pyranpyrazole derivatives as novel corrosion inhibitors for mild steel useful for industrial pickling process: Experimental and Quantum Chemical study, Journal of Industrial and Engineering Chemistry.(DOI: 10.1016/j.jiec.2017.03.044)

[40]. Rahaman, S. H.,Chowdhury, H.,Bose, D.,Ghosh, R.,Hung, C.-H.,Ghosh, B. K. (2005), Synthesis, structure and properties of mononuclear cobalt(II) and cobalt(III) pseudohalide complexes containing N-donor Schiff bases: Synthetic control of metal oxidation levels, Polyhedron, 24, 1755-1763.(DOI: 10.1016/j.poly.2005.05.010)

[41]. Sarkar, S.,Majumder, S.,Sasmal, S.,Carrella, L.,Rentschler, E.,Mohanta, S. (2013), Triple bridged μ-phenoxo-bis(μ-carboxylate) and double bridged μ-phenoxo-μ1,1-azide/μ-methoxide dicopper(II) complexes: Syntheses, structures, magnetochemistry, spectroscopy and catecholase activity, Polyhedron, 50, 270-282.(DOI: 10.1016/j.poly.2012.10.050)

[42]. Trivedi, M.,Singh, G.,Kumar, A.,Rath, N. P. (2014), A cyano and end-to-end azido bridged 3D copper(II)-copper(I) mixed-valence coordination polymer and its transformation to copper nitride nanoparticles, RSC Advances, 4, 34110-34116.(DOI: 10.1039/C4RA05980H)

[43]. Afkhami, F. A.,Khandar, A. A.,Mahmoudi, G.,Maniukiewicz, W.,Lipkowski, J.,White, J. M.,Waterman, R.,Garcia-Granda, S.,Zangrando, E.,Bauza, A.,Frontera, A. (2016), Synthesis, X-ray characterization, DFT calculations and Hirshfeld surface analysis of Zn(II) and Cd(II) complexes based on isonicotinoylhydrazone ligand, CrystEngComm, 18, 4587-4596.(DOI: 10.1039/C6CE00877A)

[44]. Jäntti, A.,Wagner, M.,Wagner, M.,Suontamo, R.,Kolehmainen, E.,Rissanen, K. (1998), Schiff-Base Podates – X-ray, NMR and Ab Initio Molecular-Orbital Studies of the Cadmium(II) Complexes of Linear and Three-Armed Podands in Solution and Solid State, European Journal of Inorganic Chemistry, 1998, 1555--1562.(DOI: 10.1002/(SICI)1099-0682(199810)1998:10<1555::AID-EJIC1555>3.0.CO;2-F)

[45]. Odewunmi, N. A.,Umoren, S. A.,Gasem, Z. M. (2015), Utilization of watermelon rind extract as a green corrosion inhibitor for mild steel in acidic media, Journal of Industrial and Engineering Chemistry, 21, 239-247.(DOI: 10.1016/j.jiec.2014.02.030)

[46]. Wahdan, M. H. (1997), The synergistic inhibition effect and thermodynamic properties of 2-mercaptobenzimidazol and some selected cations as a mixed inhibitor for pickling of mild steel in acid solution, Materials chemistry and physics, 49, 135-140.

[47]. Solomon, M. M.,Umoren, S. A.,Abai, E. J. (2015), Poly(methacrylic acid)/silver nanoparticles composites: In-situ preparation, characterization and anticorrosion property for mild steel in H2SO4 solution, Journal of Molecular Liquids, 212, 340-351.(DOI: 10.1016/j.molliq.2015.09.028)

[48]. Deng, S.,Li, X.,Fu, H. (2011), Alizarin violet 3B as a novel corrosion inhibitor for steel in HCl, H2SO4 solutions, Corrosion Science, 53, 3596-3602.(DOI: 10.1016/j.corsci.2011.07.003)

[49]. Solmaz, R. (2010), Investigation of the inhibition effect of 5-((E)-4-phenylbuta-1,3-dienylideneamino)-1,3,4-thiadiazole-2-thiol Schiff base on mild steel corrosion in hydrochloric acid, Corrosion Science, 52, 3321-3330.(DOI: 10.1016/j.corsci.2010.06.001)

[50]. Solmaz, R.,Kardaş, G.,Çulha, M.,Yazıcı, B.,Erbil, M. (2008), Investigation of adsorption and inhibitive effect of 2-mercaptothiazoline on corrosion of mild steel in hydrochloric acid media, Electrochimica Acta, 53, 5941-5952.(DOI: 10.1016/j.electacta.2008.03.055)

[51]. Lamaka, S. V.,Zheludkevich, M. L.,Yasakau, K. A.,Serra, R.,Poznyak, S. K.,Ferreira, M. G. S. (2007), Nanoporous titania interlayer as reservoir of corrosion inhibitors for coatings with self-healing ability, Progress in Organic Coatings, 58, 127-135.(DOI: 10.1016/j.porgcoat.2006.08.029)

[52]. Hussin, M. H.,Kassim, M. J. (2011), Electrochemical, Thermodynamic and Adsorption Studies of (+)-Catechin Hydrate as Natural Mild Steel Corrosion Inhibitor in 1 M HCl, Int. J. Electrochem. Sci., 6 1396 - 1414.(DOI:

[53]. Biswas, A.,Pal, S.,Udayabhanu, G. (2015), Experimental and theoretical studies of xanthan gum and its graft co-polymer as corrosion inhibitor for mild steel in 15% HCl, Applied Surface Science, 353, 173-183.(DOI: 10.1016/j.apsusc.2015.06.128)

[54]. Solmaz, R. (2014), Investigation of corrosion inhibition mechanism and stability of Vitamin B1 on mild steel in 0.5 M HCl solution, Corrosion Science, 81, 75-84.(DOI: 10.1016/j.corsci.2013.12.006)

[55]. Solmaz, R. (2014), Investigation of adsorption and corrosion inhibition of mild steel in hydrochloric acid solution by 5-(4-Dimethylaminobenzylidene)rhodanine, Corrosion Science, 79, 169-176.(DOI: 10.1016/j.corsci.2013.11.001)

[56]. Khaled, K. F.,Babić-Samardžija, K.,Hackerman, N. (2006), Cobalt(III) complexes of macrocyclic-bidentate type as a new group of corrosion inhibitors for iron in perchloric acid, Corrosion Science, 48, 3014-3034.(DOI: 10.1016/j.corsci.2005.11.011)

[57]. Mishra, M.,Tiwari, K.,Mourya, P.,Singh, M. M.,Singh, V. P. (2015), Synthesis, characterization and corrosion inhibition property of nickel(II) and copper(II) complexes with some acylhydrazine Schiff bases, Polyhedron, 89, 29-38.(DOI: 10.1016/j.poly.2015.01.003)

[58]. Borgmann, C. W. (1937), Initial Corrosion Rate of Mild Steel Influence of the cation, Industrial & Engineering Chemistry, 29, 814-821.(DOI: 10.1021/ie50331a018)

[59]. Pearson, R. G. (1988), Absolute electronegativity and hardness: application to inorganic chemistry, Inorganic Chemistry, 27, 734-740.(DOI: 10.1021/ic00277a030)

[60]. Koch, E.-C. (2005), Acid-Base Interactions in Energetic Materials: I. The Hard and Soft Acids and Bases (HSAB) Principle–Insights to Reactivity and Sensitivity of Energetic Materials, Propellants, Explosives, Pyrotechnics, 30, 5-16.(DOI: 10.1002/prep.200400080)

[61]. Klopman, G. (1968), Chemical reactivity and the concept of charge- and frontier-controlled reactions, Journal of the American Chemical Society, 90, 223-234.(DOI: 10.1021/ja01004a002)

[62]. Karzazi, Y.,Belghiti, M. E. A.,Dafali, A.,Hammouti, B. (2014), A theoretical investigation on the corrosion inhibition of mild steel by piperidine derivatives in hydrochloric acid solution, Journal of Chemical and Pharmaceutical Research, 6, 689-696.

[63]. Kaya, S.,Banerjee, P.,Saha, S. K.,Tuzun, B.,Kaya, C. (2016), Theoretical evaluation of some benzotriazole and phospono derivatives as aluminum corrosion inhibitors: DFT and molecular dynamics simulation approaches, RSC Advances, 6, 74550-74559.(DOI: 10.1039/C6RA14548E)

[64]. Ansari, K. R.,Quraishi, M. A.,Singh, A. (2015), Corrosion inhibition of mild steel in hydrochloric acid by some pyridine derivatives: An experimental and quantum chemical study, Journal of Industrial and Engineering Chemistry, 25, 89-98.(DOI: 10.1016/j.jiec.2014.10.017)

[65]. Hasanov, R.,Sadıkoğlu, M.,Bilgiç, S. (2007), Electrochemical and quantum chemical studies of some Schiff bases on the corrosion of steel in

H_2SO_4 solution, Applied Surface Science, 253, 3913-3921.(DOI: 10.1016/j.apsusc.2006.08.025)

[66]. Koopmans, T. (1934), Über die Zuordnung von Wellenfunktionen und Eigenwerten zu den Einzelnen Elektronen Eines Atoms, Physica, 1, 104-113.(DOI: 10.1016/S0031-8914(34)90011-2)

[67]. Lukovits, I.,Kálmán, E.,Zucchi, F. (2001), Corrosion Inhibitors—Correlation between Electronic Structure and Efficiency, CORROSION, 57, 3-8.(DOI: 10.5006/1.3290328)

[68]. Rodríguez-Valdez, L. M.,Villamisar, W.,Casales, M.,González-Rodriguez, J. G.,Martínez-Villafañe, A.,Martinez, L.,Glossman-Mitnik, D. (2006), Computational simulations of the molecular structure and corrosion properties of amidoethyl, aminoethyl and hydroxyethyl imidazolines inhibitors, Corrosion Science, 48, 4053-4064.(DOI: 10.1016/j.corsci.2006.05.036)

[69]. Martinez, S. (2003), Inhibitory mechanism of mimosa tannin using molecular modeling and substitutional adsorption isotherms, Materials Chemistry and Physics, 77, 97-102.(DOI: 10.1016/S0254-0584(01)00569-7)

[70]. Li, X.,Deng, S.,Fu, H.,Li, T. (2009), Adsorption and inhibition effect of 6-benzylaminopurine on cold rolled steel in 1.0 M HCl, Electrochimica Acta, 54, 4089-4098.(DOI: 10.1016/j.electacta.2009.02.084)

[71]. Pearson, R. G. (1988), Chemical hardness and bond dissociation energies, Journal of the American Chemical Society, 110, 7684-7690.(DOI: 10.1021/ja00231a017)

[72]. Cao, Z.,Tang, Y.,Cang, H.,Xu, J.,Lu, G.,Jing, W. (2014), Novel benzimidazole derivatives as corrosion inhibitors of mild steel in the acidic media. Part II: Theoretical studies, Corrosion Science, 83, 292-298.(DOI: 10.1016/j.corsci.2014.02.025)

[73]. Obot, I. B.,Macdonald, D. D.,Gasem, Z. M. (2015), Density functional theory (DFT) as a powerful tool for designing new organic corrosion inhibitors. Part 1: An overview, Corrosion Science, 99, 1-30.(DOI: 10.1016/j.corsci.2015.01.037)

[74]. Awad, M. K.,Mustafa, M. R.,Elnga, M. M. A. (2010), Computational simulation of the molecular structure of some triazoles as inhibitors for the corrosion of metal surface, Journal of Molecular Structure: THEOCHEM, 959, 66-74.(DOI: 10.1016/j.theochem.2010.08.008)

[75]. Contreras, R. R.,Fuentealba, P.,Galván, M.,Pérez, P. (1999), A direct evaluation of regional Fukui functions in molecules, Chemical Physics Letters, 304, 405-413.(DOI: 10.1016/S0009-2614(99)00325-5)

[76]. Hegazy, M. A.,Abdallah, M.,Awad, M. K.,Rezk, M. (2014), Three novel di-quaternary ammonium salts as corrosion inhibitors for API X65 steel pipeline in acidic solution. Part I: Experimental results, Corrosion Science, 81, 54-64.(DOI: 10.1016/j.corsci.2013.12.010)

[77]. Parkins, R. N., (1981), Corrosion Inhibition. In: Electrochemical Materials Science, Springer US, Boston, MA, pp. 307-331.

[78]. Singh, A. K.,Singh, P. (2015), Adsorption behaviour of o-hydroxy acetophenone benzoyl hydrazone on mild steel/hydrochloric acid interface, Journal of Industrial and Engineering Chemistry, 21, 552-560.(DOI: 10.1016/j.jiec.2014.03.018)

[79]. Sastri, V. S., (2011), Corrosion Inhibition: Theory and Practice. In: Green Corrosion Inhibitors, John Wiley & Sons, Inc., pp. 139-166 (9781118015438).

[80]. Negm, N. A.,Kandile, N. G.,Aiad, I. A.,Mohammad, M. A. (2011), New eco-friendly cationic surfactants: Synthesis, characterization and applicability as corrosion inhibitors for carbon steel in 1 N HCl, Colloids and Surfaces A: Physicochemical and Engineering Aspects, 391, 224-233.(DOI: 10.1016/j.colsurfa.2011.09.032)

Chapter 7

General conclusions and future scope

Chapter 7

General conclusions and future scope

The attempts to design new metal complexes based on flexidentate Schiff base moieties for better understanding of the structure-activity relationship between several kinds of biological, chemical as well as material properties and various complex structures tuned by flexibility as well as flexibility controlled nuclearity are the main goals of this work.

In this regard this thesis is mainly focused on total twenty two newly synthesized metal complexes of four metal ions (Ni^{2+}, Cu^{2+}, Zn^{2+}, and Cd^{2+}).

In case of copper and nickel complexes (Complex **1-11**) it has been observed (Chapter **2-4**) that ligand flexibility and nuclearity take important role towards different kind of application like biomacromolecular interaction, catecholase and antimicrobial activity and other biological activities. The role of counter anion as well as metal ion towards tuning the ligand flexibility inside the metal complexes has been also explored here. Thus this work could be the stepping stone for further tuning of the ligand using the flexibility to develop polynuclear compounds which can show more efficacy in terms of biological and biomimetic catalytic applications.

Apart from this, the approach of using pseudohalide (azide) as a co-ligand along with other Schiff base ligands has been successfully implemented in chapter **5** for synthesis of zinc complexes (Complex **12-17**) with high efficiency towards corrosion inhibition of mild steel. Being inspired by this result more robust cadmium salts were introduced in chapter **6** to design new complexes (Complex **18-22**) in a well-planned way for getting very high corrosion inhibition efficiency. The outcome has shown that polynuclear cadmium complexes with flexible ligand can demonstrate excellent corrosion inhibition property. Therefore, this approach can be extended for other systems with different metal ions with minimum toxicity.